PREDICTION OF SHOCK / TURBULENT BOUNDARY LAYER SEPARATED FLOWS USING THE NAVIER - STOKES EQUATIONS

Da Chun Jiang, M.Eng.Sc.

March, 1986

A thesis submitted for the Degree of Doctor of Philosophy
in the Faculty of Engineering of the University of Glasgow

ProQuest LLC.
789 East Eisenhower Parkway
P.O. Box 1346
Ann Arbor, MI 48106 – 1346

A B S T R A C T

Progress made in computational method in fluid mechanics will allow the increasing use of numerical solutions of the compressible Navier-Stokes equations to determine flows of increasing complexity. Much attention is now given in computational aerodynamics to viscous-inviscid interaction phenomena which are frequently encountered in real flows.

This present work concentrates on numerically solving complete, compressible Reynolds-averaged Navier-Stokes equations for a turbulent interaction problem. The original MacCormack's implicit method has been developed and improved in the present research work to enable it to be used for calculations using complex multi-equation turbulent models and to increase its ability to control nonlinear instability. These extensions retain second order accuracy and the block bidiagonal form of the original MacCormack's implicit scheme (1981) which constitute its main advantage. The computed results and validation of them through comparison with experiments, as follows, showed that these developments are feasible.

The scheme developed was mainly tested on the calculations for an interaction between an incident shock wave and a laminar boundary layer on a flat plate and an isothermal wall supersonic turbulent flow over a ramp set at various angles. The computed results for the laminar interaction problem provided very good agreement with experimental data. For turbulent interacting problems, three different turbulence models, the original Cebeci-Smith (C-S) model, the C-S model with a relaxation modification and the K-ϵ model are

investigated as was the influence of Reynolds number on the flow. The results have been compared with experimental data obtained by Princeton University. These comparisons showed that the solution strongly depends on the turbulence model. Generally, all the models can predict the overall pressure rise, but fail to predict the flow field near to and downstream of the reattachment point. Comparatively, the K-ϵ model gives the best results.

ACKNOWLEDGEMENTS

The author wishes to express his gratitude for the unfailing guidance and encouragement given by his supervisor, Professor B.E.Richards and to Dr. H.Y.Wong for his invaluable help and criticism regarding preparation of this thesis.

The author would like to thank the University of Glasgow's computing service centre staff and the Engineering faculty computer service staff who gave their assistance enthusiastically. The author is especially grateful to Mrs. Effie Murray-Smith whose valuable advice and enthusiatic assistance during his computing work. Thanks are also due to Miss M.B.Simpson and Miss K.M.Houston, the secretaries of Aeronautics & Fluid Mechanics Department, for their excellent service and effective help.

The author wishes to express his appreciation for the supporting scholarship given by the University of Glasgow and Department of Aeronautical & Fluid Mechanics and the ORS award scheme.

Finally, the author is gratefully indebted to his wife, Gong Ming-rui, who typed this thesis and gave considerable support and encouragement.

C O N T E N T S

NOTATION

Symbols.

A,B	Jacobian Matrix of the inviscid part of flux vector F and G
B_i	intermittency factor
C	sound speed
C_f	skin friction coefficient $2\tau_w/(\rho_\infty u_\infty^2)$
C_h	heat transfer coefficient
C_p, C_v	specific heats at constant pressure & constant volume
D	Van Driest damping factor
E	total energy per unit volume
e	specific internal energy
F	flux vector in X direction
$\vec{f}_e$	the external force per unit volue
G	flux vector in Y direction
$\hat{G}$	flux vector in η direction
H	column vector of source term
I_{CON}	the number of the grid point just before corner
II	grid points numbers in X direction
JJ	grid points numbers in Y direction
J_1	the highest grid point number in fine mesh
K	turbulent kinetic energy
$\bar{K}$	thermal conductivity coefficient
k	Von Karman's Constant
L_t	turbulent length scale
M	Mach number
$\vec{n}$	unit normal vector (outward)

P	static pressure
Pr	Prandtl number
Pr_t	turbulent Prandtl number
P_t	effective pressure, $P + 2\rho K / 3$
Q	source or sink of energy
$\vec{q}$	heat flux vector
q_x	X direction heat flux
q_y	Y direction heat flux
R	gas constant
Re_L	free stream Reynolds number based on reference length L
R_t	turbulent Reynolds number
T	temperature
U	column vector of dependent variables
u_e	the velocity on the edge of boundary layer
u,v,w	velocity components in X, Y, and Z directions respectively
u_τ	friction velocity $\sqrt{(\tau_w/\rho_w)}$
$\vec{V}$	velocity vector in Cartesian coordinate
V_t	turbulent velocity scale
W	flux vector in Z direction
X,Y,Z	axes of Cartesian coordinate
Y^+	Yu_τ/ν_w
α	ramp angle
γ	ratio of specific heats
δ	boundary layer thickness
δ^*	displacement thickness
δ_o^*	displacement thickness on the incoming boundary
δ_o	boundary layer thickness on the incoming boundary
δ_{ij}	Kronecker delta

ϵ	turbulent energy dissipation
Λ_A, Λ_B	diagonal matrix of A and B
λ	the bulk viscosity
μ	viscosity coefficient
μ_t	turbulent eddy viscosity
ν	dynamic viscosity or effective viscosity in MacCormack's scheme
ξ, η	axes in transformed coordinates
ρ	density
$-\rho\overline{u_i'' u_j''}$	Reynolds stress
$\vec{\vec{\sigma}}$	stress tensor
σ_{ij}	viscous stress
τ_w	shear stress on the wall
ΔX	mesh spacing in X direction
$\Delta\eta$	mesh spacing in η direction

Superscripts.

n	the value at $n \cdot \Delta t$ time
''	the fluctuating quantity in mass-weighted average form
'	the fluctuating quantity in Reynolds decomposition method

Subscripts.

i,j	the value on the grid point (i, j)
o	stationary condition
w	wall value
∞	free stream value

CHAPTER 1

INTRODUCTION

The branch of study of computational fluid dynamics (C.F.D.) is directed towards the simulation of flow fields by numerical solution of the relevant flow equations. The Navier-Stokes flow equations are considered to provide an exact description of a continuum fluid in motion. Hence the numerical simulation of these particular equations play a very important role in C.F.D. Although C.F.D. is a relatively new discipline, it has received special attention and rapid development of techniques have been obtained in recent years. This can be attributed to three compelling reasons. First, the rapid development of computer speed and capacity and computer architecture makes it possible to calculate a complicated and practical configuration with less computer cost and higher efficiency. Secondly, progress made in devising numerical algorithms allows the determination of flows of increasing complexity by solving complete, compressible Navier-Stokes equations rather than more simplified modelling equations. Third, because of these technological advances it is becoming recognised that numerical simulation can provide important new technological capabilities that cannot be obtained from experimental facilities, e.g., the simulation of high Reynolds number flow at real flight conditions and the high temperature behaviour on the surface of an aerospace vehicle. Chapman[1] and Kutler[2] in their excellent reviews outlined the positive results being achieved in C.F.D. and the future developments required. Recently, Shang[3] in

his literature survey provided an assessment of the state of art of the numerical solution of the compressible Navier-Stokes equations. Whilst it is expected that C.F.D. would provide a new means to supplement the data base available for atmospheric vehicle design, there remains the need for further development before this methodology is used as a design tool. The main developments needed to achieve success concern, i) the efficiency and accuracy of numerical procedures, ii) turbulence modelling, iii) computational mesh generation.

The inviscid/viscous interaction phenomenon frequently encountered in real flows is now given much attention in computational aerodynamics. The solution of the inviscid/viscous-interaction problem using the Navier-Stokes equations for flow configurations when the size of the viscous region is substantial is regarded as a cornerstone of fluid dynamic research, and a building block for realising the ultimate goal in configurational design and relates to all the difficulties mentioned above.

This thesis presents the development and results of a numerical solution of the time-dependent, Reynolds-averaged, compressible Navier-Stokes equations for a supersonic turbulent flow over a ramp at various angles using as a starting point MacCormack's implicit finite difference algorithm. Three turbulence models, the original Cebeci-Smith (C-S) algebraic model, the C-S model with a relaxation modification and the K-ϵ model, are examined in this investigation.

In order to sustain computational stability at large Courant number and to match the source term produced by turbulence, it was found necessary to inject some new treatments to the original algorithm.

1.1. Outline of Research Work on the Two-Dimensional Interaction Between a Shock Wave and a Boundary Layer.

The interaction of a shock wave and a boundary layer, particularly the turbulent boundary layer, is a configuration that is frequently present in practical flight at transonic and supersonic speeds. Some typical interactions are sketched in Fig 1. This particular type of interaction can result in large effects on wall pressure distribution and if the interaction is strong enough can produce flow separation, which itself may lead to undesirable unsteady flow effects such as flutter, buzz etc. Since the first systematic investigations into this problem were carried out by Liepmann (1946), it has remained a subject of considerable research, because of its complexity.

Pearcey (1961)[4], Green (1970)[5], Hankey and Holden (1975)[6], MacCormack and Lomax[7] (1979), Adamson and Messiter[8] (1980) have reviewed a wide variety of related theoretical and experimental studies. According to these reviews, the numerical solution of the laminar interaction has been satisfactorily achieved. For a large class of laminar free-interaction problems where the asymptotic theory yields detailed structure of the interacting boundary layer, the application of Navier-Stokes equations is not even necessary. For turbulent flow, however, the basic structure of the solution is vastly different and this case cannot be treated with methods that are simply extensions of those used for laminar interactions. To date, there exists no solution of the turbulent interaction case of reasonably large strengths which is as satisfactory as the laminar situation.

In a turbulent flow field, many length and velocity scales coexist. So, it is difficult to prescribe suitable initial and boundary conditions for resolving the Navier-Stokes equations. Even

if this problem is correctly solved, it is not reasonable to use N-S equations directly for strong turbulent flow, since the broad continuous spectrum of turbulent fluctuations requires very fine mesh sizes for any numerical process. This degree of detail is not compatible with the power of present computers[1] [9]. Solving the Reynolds-averaged Navier-Stokes equations, which are obtained by statistical averaging the original equations can avoid these difficulties. But, it will introduce new unknown turbulent field variables and hence the problem of closure will require to be overcome through appropriate turbulence modelling. Some new equations, of either algebraic or partial differential form, along with their corresponding initial and boundary conditions must be included to close the system. The stiffness of this nonlinear system will increase and the type of solution will greatly depend on the turbulence model chosen. Turbulence modelling will remain for some time a critical issue to be resolved because of the slow rate of progress in understanding the phenomenon. The need to obtain a suitable turbulence model which can suit engineering applications, however, is urgent. Further testing of existing turbulence models in numerical schemes and comparison with experimental results are thus necessary.

This technology to simulate turbulent flows with Reynolds-averaged Navier-Stokes equations is relatively young, and most emphases to date still focus on two-dimensional flows.

A detailed discussion on turbulence modelling methods will be presented in Chapter 4.

There are essentially two numerical approaches to study this interaction problem, a global approach and a coupling approach. In

the present study, the global approach is used. However a simple introduction to these two approaches are given in the following sections.

1.2. Coupling Approach.

It is a fact that whilst viscous effects are only important in a small part of the flow field their influence is felt in a considerably larger region. Hence, it is natural and reasonable to decompose the flow field into two parts, a thin viscous layer and an inviscid flow region. The approach is then to solve them separately by using different governing equations and to join the solutions through a so called coupling condition or coupling equation in order to take their mutual effects into account. In the high Reynolds number situation only a set of boundary layer equations is needed for the thin viscous layer and the Euler equations for inviscid flow. Compared with the solution of complete N-S equations, the reduction in the stiffness of the equation solution and in the computer cost are obvious. The failure of using the classical boundary-layer theory for solving the viscous-inviscid interaction problems is not always a consequence of Prandtl's equations but actually to the resulting simplified matching which relates the viscous boundary condition to some given external inviscid flow. If the coupling between both flow regions can be correctly achieved, this approach will give satisfactory results. It remains still a difficult problem to achieve matching, particularly in regions of separated flow. Hankey[6] and Le Balleur and Viviand[10] gave an excellent review of recent applications of this approach. The results in this area have been successful following considerable refinement, but there exist problems in developing schemes to tackle general configurations. This approach will not be discussed further.

1.3. Global Approach.

In this approach, the flow field of interest is determined as the solution of a single system of equations valid everywhere. Generally the time-dependent Navier-Stokes equations (Reynolds-averaged Navier-Stokes are needed when turbulence is present) are used. However, it is a characteristic feature of the global approach that all the non-dissipative terms of N-S equations, i.e., as described by the full Euler equations, should be included in the equations used, so that a continuous transition is automatically insured between the inviscid flow and the viscous layers. This technique needs no a priori knowledge of the location and the extent of the viscous zones. This is the reason for the preference in using this approach.

1.3.1. Numerical Method.

Two types of methods are used at the present time for the numerical solution of the full N-S equations.

(1). The finite element methods are based on the principle of variations or the method of weighted residuals. These methods can flexibly represent arbitrary complicated boundaries. However, an important shortcoming of the methods is for it to describe flow problems with strong gradients, particularly these generated by shock waves[11]. Some special processes have been devised to present the finite element application to deal with the shock wave. For example the so called 'Element Discontinuity' method is commonly used but it requires some parameters to be known in advance, such as the position and strength of the shock wave. This is not always realistic for the prediction of complex flows. In addition it will further increase programming complexity and storage requirements. Although finite element methods have received increasing attention in fluid mechanics,

particularly in their application to the solution of incompressible N-S equations, they have not yet been widely used in compressible flows. Up to now there has been no practical application to the research problem confronted in the present work.

(2). The finite difference method is based on the principle of Taylor's expansion. Its important ability to automatically capture shock waves and the development more recently of a technique to transform coordinates in order to fit the body thus allowing accurate presentation of boundary conditions on an arbitrary configuration make it to be far the most widely used. A short review on the development of finite difference algorithms is given below.

1.3.2. The Development of Finite Difference Numerical Algorithms.

Historically, MacCormack[12] (in 1969) is considered the first fluid dynamicist to have solved practically the complete Navier-Stokes equations by using his second-order two-step explicit scheme. Carter[13] however was the first to obtain the solution of the N-S equations for a supersonic laminar flow over a 10° corner by means of Brailovskaya's[14] scheme. Peyret and Viviand[15] have widely reviewed extensively finite difference algorithms that appeared before 1975. Since then, a number of different numerical algorithms and results have been reported. Following an extensive literature search available numerical solutions of N-S equations that have been directed towards the interaction of a shock wave and a boundary layer are listed in Table 1. The conclusions resulting from this literature search are as follows:

(1). The main efforts in improving numerical algorithms are concentrated in the following topics:

a. The reduction of the restriction on the marching time step

size, Δt.

b. The improvement of matrix inversion methods to deal with the left side of implicit schemes.

c. The control of nonlinear oscillations which usually concern the treatment of regions of steep flow gradient.

d. The numerical and code compatibility.

A short discussion of each item follows.

The severe restriction on time step size is considered the main obstacle to enhance computational efficiency, particularly in the calculation for high Reynolds number turbulent flows. Until the mid 1970's the numerical methods used were predominantly explicit procedures subject to the limitation of the C.F.L. condition. An example is the MacCormack's second order, two-step explicit scheme. In the middle of the 1970's, hybrid schemes appeared. Hybrid schemes are based on the time split concept. The numerical operator in the direction along which a fine mesh is needed is chosen to have less restriction on Δt whilst for other directions, an ordinary explicit scheme is used. Since Shang[16] and MacCormack[17] proposed their hybrid schemes respectively an order of magnitude of enhancement in efficiency was achieved, but further enhancement is restricted by the explicit operator. After 1975, the implicit scheme, which removed the C.F.L. condition, gradually became predominant. The now very popular implicit numerical procedures include those developed separately by Briley and McDonald[18], Beam and Warming[19], and MacCormack[20].

In an implicit numerical procedure the major effort of the overall scheme is expended in inverting the left side matrix. Special techniques are used to improve the matrix inversion. These include: the ADI (alternating-direction implicit)[21] [18] scheme which results

in the need only to solve a simple block-tridiagonal system; the ADI technology plus diagonal approximation[22] which further reduce the block system to a tridiagonal form; and the line Gauss-Seidel iteration scheme etc.

The presence of steep gradients in the flow, typified by shock waves caused considerable speculation as to the proper numerical treatment. In the late 1960's shock fitting procedures[23] were used. Then in the 1970's the addition of an additional artificial viscosity term, such as MacCormack's fourth order product term and Beam and Warming's fourth order term, become much used and has attained great success. But the determination of the value of the coefficient of artificial viscosity is hard to achieve. In the late 1970's Steger and Warming presented flux splitting procedures[35] to take advantage of the natural directions of information travel to treat steep flow gradients and in the early 1980's TVD (total variation diminishing) schemes[24][25] appeared to describe flow gradients with precision.

Problems about numerical and code compatibility are particularly caused by those turbulent models using complex equations for turbulent field variables. Numerical compatibility concerns whether the addition of the complex turbulent modelling equations will introduce further difficulties in numerical calculation. Code compatibility concerns the ease of incorporating them into the numerical algorithm for N-S equations. By referring to Table 1, it can be seen that there are few results from calculations using two-equation models for the complex flows presented. Part of the reason is the large increase in stiffness of numerical solutions resulting from the use of these models. Coakley[81] has pointed out that the Reynolds-Stress model and some of the two-equation models, such as Jones-Launder's K-ϵ model

and Wilcox-Rubesin's K-ω^2 model, possess lower numerical compatibility than others. Typical difficulties that occur in calculations are the need to run at reduced time marching size and the occurrence of instabilities in the start-up phase, regardless of the size of the time step. In one reference [68] it has been reported that for some flow problems the use of K-ϵ (J-L) model failed to give converged results.

Other than choice of unsuitable initial values, numerical instability may be attributed to the inappropriate numerical treatment for turbulent field variable equations. For example, the MacCormack's hybrid scheme was popularly used for calculations using multi-equation turbulence models[64][65][68]. The source terms caused by turbulent field variables appear in the implicit operator of this scheme, but they are treated explicitly due to the difficulties otherwise encountered. In the complex flow to be studied, the computed values of K and L_t using the K-ϵ model are very small in a region close to the wall, particularly near the reattachment point. This makes the calculation very sensitive to small changes in K and L_t. The explicit treatment of a source term usually produces a large value which can cause calculation instabilities. In their calculations mentioned above, the authors have needed to introduce some additional conditions into the program to artificially restrict the unfavourable development of K and ϵ. Thus, it is essential to successful numerical implementation of multi-equation models to remove these artificial conditions and to provide an appropriate treatment of the source term.

Another failing is that many conventional numerical schemes run into difficulty when incorporated with turbulent models using the turbulent field equation. These include the majority of the

conventional schemes, including the MacCormack's hybrid scheme, which are difficult to code for Reynolds stress models because of the difficulty of dealing with the Reynolds stress term. The Warming and Beam's scheme even has difficulty in using multi-equationed eddy-viscosity models because of the lack of an accurate Jacobian of the source terms. In order to promote the calculation of turbulent flow using higher-order models it is a pressing matter to develop an effective numerical scheme. Part of the present research work is attempting to modify and to extend MacCormack's new implicit scheme (1981) to meet with the requirements mentioned above. This approach was taken rather than to construct a new numerical scheme.

(2). The use of the fully conservative form of the finite difference equation is necessary to prevent numerical losses in mass, momentum and energy, particularly in the shock wave capture method.

(3). At minimum, second order accurate schemes are needed in the finite difference method. The first-order accurate methods tend to be highly dissipative, which often smears flow features that should be crisp and competes with the physically relevant dissipative processes in the flow. Paradoxically, however, the use of first order flux split procedures at isolated discontinuities in the flow can improve numerical precision locally, but their use throughout the flow field calculation will in general artificially increase dissipation and losses in conserved quantities.

(4). The difficulties caused by turbulence modelling lead to the lack of success in turbulence calculation using high order closure models .

CHAPTER 2

MATHEMATICAL MODEL

It is well established that the complete, time-dependent Navier-Stokes equations provide the exact description of the motion of a continuous medium. The derivation of the Navier-Stokes equations can be found expounded in many text books on fluid mechanics[26] [27]. Here, only the general formulation of the Navier-Stokes equations and a simple discussion about its validity and general property are given.

2.1. The Conservation Equations in Integral Form.

Based on the Eulerian approach, the application of the fundamental conservation principles of mass, momentum and energy in a Galilean frame of reference lead to the following conservation equations in integral form relative to a control volume ∇ enclosed by a fixed bounding surface, S:

$$\frac{\partial}{\partial t}\iiint_{\nabla}\rho d\nabla + \iint_{S}\rho\vec{V}.\vec{n}\ dS = 0 \qquad (2.1)$$

$$\frac{\partial}{\partial t}\iiint_{\nabla}\rho\vec{V}d\nabla + \iint_{S}(\vec{n}.\vec{V}\rho\vec{V} - \vec{n}.\vec{\sigma})\ dS = \iiint_{\nabla}\vec{f}_e\ d\nabla \qquad (2.2)$$

$$\frac{\partial}{\partial t}\iiint_{\nabla}E d\nabla + \iint_{S}\vec{n}.[E\vec{V} - \vec{\sigma}\vec{V} + \vec{q}]\ dS = \iiint_{\nabla}(\vec{f}_e.\vec{V} + Q)\ d\nabla \qquad (2.3)$$

In these equations, t is the time, ρ is the density, $\vec{V}$ is the velocity in the frame of reference, and E is the total energy per unit volume:

$$E = (e + 1/2\ \vec{V}^2)\ \rho \qquad (2.4)$$

where e is the specific internal energy.

And $\vec{\sigma}$ is the stress tensor, $\vec{q}$ the heat-flux vector, $\vec{f}_e$ the external force per unit volume, Q the source or sink of energy in the control volume (∇) and n is the unit vector outward and normal to the boundary

surface (S).

In most situations the appearance of $\vec{f}_e$ represents only the body force which is usually negligibly small. Thus in the absence of a source or sink of energy, the right side of equations (2.2), (2.3) become zero.

The integral equations hold for any volume element contained in the flow field. They are the foundation for the finite-volume algorithm and are frequently used in checking the overall validity of approximate numerical solutions.

2.2. The Conservation Equations in Differential Form.

If the properties of the medium are continuous and sufficiently differentiable in some domain of space and time, then the conservation equations in integral form can be transformed into an equivalent set of partial differential equations by means of Gauss' divergence theorem. They are:

$$\frac{\partial \rho}{\partial t} + \text{div}\,(\rho\vec{V}) = 0 \tag{2.5}$$

$$\frac{\partial}{\partial t}(\rho\vec{V}) + \text{div}\,(\rho\vec{V}\vec{V} - \vec{\vec{\sigma}}) = \vec{f}_e \tag{2.6}$$

$$\frac{\partial E}{\partial t} + \text{div}\,(E\vec{V} - \vec{\vec{V}}\vec{\vec{\sigma}} + \vec{q}) = \vec{f}_e \cdot \vec{V} + Q \tag{2.7}$$

Similar to the arguments given in Section 2.1., if there is not any source or sink of energy in the flow field then the $\vec{f}_e$ is negligibly small and the right side of (2.6) and (2.7) again become zero.

2.3. The Navier-Stokes Equations.

In the above equations, ρ, $\vec{V}$ and E (or e) are the basic dependent variables. Some constitutive relationships for the stress tensor $\vec{\vec{\sigma}}$ and the heat-flux vector $\vec{q}$ must be added to these equations to obtain a closed system. For the motion of a continuous medium, the stress tensor obeys the Newton's law and the heat-flux vector follows

Fourier's law of heat conduction, i.e., the stress tensor and the heat-flux vector are respectively the linear functions of the velocity and temperature gradients.

From their definition we have:

$$\vec{\vec{\sigma}} = -P\vec{\vec{I}} + \vec{\vec{\tau}} \tag{2.8}$$

$$\vec{\vec{\tau}} = \lambda \operatorname{div} \vec{\vec{V}}\vec{\vec{I}} + \mu \cdot \operatorname{def} \vec{V}^{**} \tag{2.9}$$

$$\vec{q} = -\bar{K} \cdot \operatorname{grad} T \tag{2.10}$$

where P is the pressure

$\vec{\vec{\tau}}$ is the viscous stress tensor

μ is the viscosity coefficient

λ is the bulk viscosity and from Stokes' hypothesis $\lambda = -2\mu/3$

$\vec{\vec{I}}$ is the unit tensor $\quad (\vec{\vec{I}}) = \begin{bmatrix} 1 & 0 & 0 \\ 0 & 1 & 0 \\ 0 & 0 & 1 \end{bmatrix}$

T is the absolute temperature

$\bar{K}$ is the thermal conductivity coefficient.

$(\operatorname{def} \vec{V})/2$ is the tensor of rates of deformation.

** $$\operatorname{def} \vec{V} = \mu \left(\frac{\partial U_i}{\partial X_j} + \frac{\partial U_j}{\partial Y_i} \right) \vec{I}_i \cdot \vec{I}_j$$

where

i, j = x, y, z

and $\vec{I}_i$ is the unit vector along the i direction.

or $$(\operatorname{def} \vec{V}) = \begin{bmatrix} \tau_{xx} & \tau_{xy} & \tau_{xz} \\ \tau_{xy} & \tau_{yy} & \tau_{yz} \\ \tau_{xz} & \tau_{yz} & \tau_{zz} \end{bmatrix}$$

$$\tau_{ij} = \mu \left[\frac{\partial U_i}{\partial X_j} + \frac{\partial U_j}{\partial X_i} \right]$$

Equations (2.8), (2.9) and (2.10) introduce new unknown variables, P, T, λ, μ and K, and hence some new relations have to be introduced. The state variables ρ, e, T, and P are connected together by thermodynamic relations. An important special case is that of perfect gas, for which:

$$e = C_v T \tag{2.11}$$

$$P = \rho RT \qquad (R = \text{gas constant}) \tag{2.12}$$

$$\text{or } P = (\gamma-1)\,\rho\,(E - 1/2\,\vec{V}^2) \tag{2.13}$$

C_v specific heats at constant volume

γ ratio of specific heats

And the viscosity and thermal conductivity coefficients depend on the local thermodynamic state. In normal conditions they depend only on the temperature:

$$\mu = \mu(T),\ \bar{K} = \bar{K}(T) \tag{2.14}$$

As an example, for air, the μ can be approximated accurately by the Sutherland law:

$$\mu = 1.45809 \times 10^{-6}\ T^{1.5} / (T + 110.4^{\circ}K) \qquad N\cdot sec/m^2 \tag{2.15}$$

With these additions the set of partial differential equations (2.5), (2.6), (2.7) become a complete closed system.

Although the appellation 'Navier-Stokes equation' seems to have been used originally for the momentum equation, it is now customary to refer to the complete set of the partial differential equations. For simplicity, we shall call them in the short form, N-S equations.

2.4. The Validity of the Navier-Stokes Equations.

As it has been pointed out in Section **2.3.**, the N-S equations are the combination of the universal conservative laws, respectively for mass, momentum and energy, and the Newton's and Fourier's laws. Thus, the title question is equivalent to the discussion of the validity of

the Newton's law and the Fourier's law. For fluid gas flows, from the kinetic theory of molecular motion, the two laws can be derived from the solution of the Boltzman equation in the limit of small Knudsen number[28]. This number K_n is defined locally as the ratio of a characteristic mean free path to a macroscopic length characteristic of local flow gradients, i.e., $K_n = \ell/L$ where ℓ is the mean free path and L is a local characteristic length. In other words, the N-S equations apply when flow properties do not vary appreciably over a distance of the order of the mean free path. The reasonable condition for their validity is considered as $K_n < 10^{-1}$. For atmospheric air, ℓ is roughly in the magnitude of 10^{-5} cm. In laminar flow, since L is of the same magnitude of the radius of curvature of the body surface, then there is little doubt of the validity of N-S equations for this flow condition.

Turbulent flow includes comprehensive scales from micro to macro levels. The smallest scale of motion is commonly referred to as the Kolmogorov microscale[29], which can be expressed as:

$$\eta = 3\ell \, (R_{e\delta})^{1/4} \, / \, (u_e / C) \qquad (2.16)$$

where $R_{e\delta}$ is the Reynolds number based on the thickness of the boundary layer.

u_e is the velocity of flow at the edge of the boundary layer.

C is the mean molecular velocity and equal to 500m/sec for air at 0° C.

The smallest $R_{e\delta}$ for the existence of turbulence is about 3000. It is obvious that, except when the Mach number reaches very high values, even the finest scales of the turbulence remain much larger than the mean free path. So, there is no contradiction to the fact

that the Navier-Stokes equations contain the necessary information for turbulence.

2.5. General Properties of the N-S Equations.

2.5.1. Well Posed Problem.

The mathematical problem concerning the proper initial and boundary condition to ensure existence and uniqueness of solutions of the Navier-Stokes equations have not yet been solved for the differential form let alone for the analogous finite difference form. However, the experience in solving this system of equations tells us to impose conditions that take into account the physical meaning of the problem as well as the mathematical nature of the system of equations. This physical requirement of a mathematical formulation is referred to as the well-posed problem. A well-posed problem can be achieved only if the boundary conditions are properly specified. The solutions of the differential equations then vary continuously with respect to perturbation of the initial and boundary conditions.

2.5.2. The Type of the N-S Equations.

In order to develop a well-posed problem, a definition of the type of partial differential equations being considered is essential.

In the asymptotic limit of the Reynolds number approaching infinity, the time-dependent N-S equations must reduce to a quasi-linear hyperbolic system. Unfortunately our knowledge of classification of coupled, partial differential equations is very limited when the value of the Reynolds number is finite.

However, we can examine each equation separately from others. Because of the time derivative term and furthermore the explict appearance of the corresponding substantial derivative in their nonconservative form, each equation can be naturally associated with

one basic variable assuming all the other variables to be known quantities.

The continuity equation is always of hyperbolic character for steady as well as for unsteady flows. This first order equation in which the characteristic curves are the trajectories of fluid particles is used to determine the unknown ρ.

The time dependent momentum equations are of parabolic type with respect to time. In the limit of steady state, they are of elliptic nature since the highest order space derivatives can be clustered into an elliptic operator. The energy equation has the same property as the momentum equations.

If the system of the Navier-Stokes equations retains the mathematical properties of each of the equations considered separately, the system can be qualified as of hybrid parabolic-hyperbolic type in general and of hybrid elliptic-hyperbolic type in the case of steady flow. Following earlier statements, all the interesting problems in fluid dynamics are of a mixed initial and boundary value nature. The initial value of all variables are required by the parabolic-hyperbolic character, while the boundary condition are imposed by a solid surface or an artificial boundary.

The parabolic or elliptic character of the N-S equations results from the dissipative effects (viscosity, thermal conductivity). In flow regions where these effects are very small, the solution will tend to exhibit the properties of solution of Euler's equations for inviscid flow, and the parabolic or elliptic nature of the equations will be of secondary significance, at least for the local properties of the solution.

Discussion on how to impose a proper boundary condition will be

left to the next chapter and follows on from the present conclusions.

2.6. The Flux-Vector Form of the N-S Equations.

In most practical uses, equations (2.5) - (2.7) are frequently rewritten in flux vector form for Cartesian coordinates. In the absence of a heat source (or sink) and neglecting body forces, we have

$$\frac{\partial U}{\partial t} + \frac{\partial F}{\partial x} + \frac{\partial G}{\partial y} + \frac{\partial W}{\partial z} = 0 \qquad (2.17)$$

where

$$U = \begin{bmatrix} \rho \\ \rho u \\ \rho v \\ \rho w \\ E \end{bmatrix} \quad \text{is the dependent variable}$$

$$F = \begin{bmatrix} \rho u \\ \rho u^2 + P - \sigma_{xx} \\ \rho uv - \sigma_{xy} \\ \rho uw - \sigma_{xw} \\ (E + P - \sigma_{xx})\, u - v\sigma_{xy} - w\sigma_{xw} - K\dfrac{\partial T}{\partial x} \end{bmatrix}$$

$$G = \begin{bmatrix} \rho v \\ \rho uv - \sigma_{xy} \\ \rho v^2 + P - \sigma_{yy} \\ \rho vw - \sigma_{yw} \\ (E + P - \sigma_{yy})\, v - u\sigma_{xy} - w\sigma_{yw} - K\dfrac{\partial T}{\partial y} \end{bmatrix}$$

$$W = \begin{bmatrix} \rho w \\ \rho uw - \sigma_{xw} \\ \rho vw - \sigma_{yw} \\ \rho w^2 + P - \sigma_{ww} \\ (E + P - \sigma_{ww})\, w - u\sigma_{xw} - v\sigma_{yw} - K\dfrac{\partial T}{\partial z} \end{bmatrix}$$

and

$$\sigma_{ij} = \lambda \left(\frac{\partial u_k}{\partial x_k} \right) \delta_{ij} + \mu \left(\frac{\partial u_i}{\partial x_j} + \frac{\partial u_j}{\partial x_i} \right) \qquad (2.18)$$

$$K = \frac{C_p \mu}{Pr} \qquad (2.19)$$

Here C_p is the specific heat at constant pressure, Pr the Prandtl number, u, v, w the velocity components in Cartesian coordinates, σ_{ij} viscous stress and δ_{ij} is the Kronecker delta ($\delta_{ij} = 1$ for $i = j$; $\delta_{ij} = 0$ for $i \neq j$). In equation (2.18) and in later sections the repeated indices are used, which can be understood as a summation, e.g., for 2-D flow

$$\frac{\partial u_k}{\partial x_k} = \frac{\partial u}{\partial x} + \frac{\partial v}{\partial y}, \quad u_i u_i = u^2 + v^2, \text{ etc..}$$

Equations (2.17) - (2.19) together with the state equation (2.12) or (2.13) and Sutherlands law are used as the governing equations in the later calculations.

In order to impose accurate boundary conditions, a coordinate transformation is often necessary. The general form of N-S equations with transformed coordinates (ξ, η, ζ) are given in Appendix A-1.

CHAPTER 3

THE DISCRETIZATION OF THE TIME-DEPENDENT N-S EQUATIONS

From Section **2.5.2.**, it has been established that the momentum equations and energy equations of the steady N-S equations have elliptical properties. Their resolution is a boundary value problem. On all boundaries enclosing the calculation region, the boundary condition must be correctly given in advance. In most of the practical calculations, only a finite computational region will be treated such that it is almost impossible to specify all boundary conditions beforehand. Earlier research work[30] showed that the uniqueness and existence of steady incompressible N-S equations are related to the Reynolds number. If the Reynolds number based on the free stream parameters is above a particular value there exists no solution. However the resolution of the unsteady N-S equations in all interesting problems of fluid dynamics is a mixed initial and boundary value problem. This raises less problems in establishing the existence of the solution and in assigning boundary conditions. That is the reason why most methods used use the time-dependent N-S equations. The solution to steady state, if it exists, is obtained when t tends to infinity. Another advantage is that if the initial value given is physically reasonable, the procedure to solve the unsteady system will really reflect the development of the physical flow and will give the solution of the transient behaviour.

Recently a so called parabolized method of steady N-S equations has been presented[31]. It also depends on the scheme of solving an

initial-boundary value problem.

In this chapter, only a finite-difference method of time-dependent N-S equations will be discussed.

3.1 The Discretization and Its Related Problem.

3.1.1. The Approximation of a Derivative.

Based on the Taylor expansion principle, a differential quotient can be approximated by a difference quotient which is calculated on discretized nodes. Texts describing the difference method[30] [32], give a full range of approaches. Here, the approximation of a first-order derivative is taken as an example.

Assuming there are some discretized nodes in a space (length or time) as shown, the difference approximations might have the following forms.

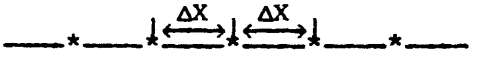

1. Forward difference:

$$\frac{\partial U}{\partial X} = (U_{i+1}-U_i)/\Delta X - \frac{1}{2}\frac{\partial^2 U}{\partial X^2}\Delta X - \cdots\cdots \equiv (U_{i+1}-U_i)/\Delta X - O(\Delta X)$$

$$\text{or} \quad \frac{\partial U}{\partial X} \cong (U_{i+1} - U_i) \;/\; \Delta X \qquad (3.1)$$

2. Backward difference:

$$\frac{\partial U}{\partial X} = (U_i-U_{i-1})/\Delta X + \frac{1}{2}\frac{\partial^2 U}{\partial X^2}\Delta X - \cdots\cdots \equiv (U_i-U_{i-1})/\Delta X + O(\Delta X)$$

$$\text{or} \quad \frac{\partial U}{\partial X} \cong (U_i - U_{i-1}) \;/\; \Delta X \qquad (3.2)$$

3. Central difference:

$$\frac{\partial U}{\partial X} = (U_{i+1}-U_{i-1})/2\Delta X + \frac{1}{3}\frac{\partial^3 U}{\partial X^3}\Delta X^2 - \cdots \equiv (U_{i+1}-U_{i-1})/2\Delta X + O(\Delta X^2)$$

$$\text{or} \quad \frac{\partial U}{\partial X} \cong (U_{i+1} - U_{i-1}) \;/\; 2\Delta X \qquad (3.3)$$

If all the terms in the differential equation are replaced by proper difference approximations, the differential equation becomes an algebraic equation. This approximated equation is called a difference equation. It does not follow, however, that any arbitrary form of approximating difference equation has a physically realistic solution. It must have characteristics of convergence, consistence and

stability. Conversely, if a linear partial differential equation does have a physical solution and its approximating difference equation also has these characteristics, then the finite-difference equation would have a physically reasonable solution. In the following sections, these problems will be discussed.

3.1.2. Accuracy of the Finite-Difference Method.

The accuracy expresses the degree of approximation of the finite difference equation to the differential equation. It is commonly accepted that the lowest order of discretized length, both in space and time, in the truncated error is taken as the order of accuracy of the finite difference approximation equation. For example, the difference approximations, (3.1) and (3.2) are of first-order accuracy and that in (3.3), second-order accuracy. In finite-difference methods second-order or higher accuracy is usually required.

3.1.3. Convergence.

If the solution of a finite difference equation continuously approaches the exact solution of the differential equation on each point of the computational region when the discretized length (both in the space and time) tends to zero then this finite difference equation is considered to be convergent.

Assuming U_j^* is the physical solution of a differential equation and U_j the actual solution of the corresponding difference equation at the position j ΔX. The convergent property can be expressed as:

$$\text{when } \Delta X, \Delta t \longrightarrow 0, \quad U_j \longrightarrow U_j^* \tag{3.4}$$

3.1.4. Consistence.

If in difference equations all unknown variables are expanded around U_j^n by means of a Taylor expansion, one can obtain an approximating differential equation which has the same form as the

original differential equation and a truncated error term. If the truncated error tends towards zero when the discretized lengths ΔX, Δt approach zero, the difference equation is considered to be consistent with the original differential equation. Consistence is a necessary condition for convergence.

3.1.5. Stability.

Stability of a finite difference equation is another very important property. The essence of stability is that there should be a limit to the extent to which any component of an initial function and a round-off error can be amplified in the numerical procedure. In appendix A-2, the solution of a one-dimension heat diffusion difference equation is solved at $S = 1/2$ and $S = 1$ respectively. It can be seen clearly that when $S = 1/2$ the difference equation is stable and has a convergent solution, however, the other calculation is divergent.

For linear difference equation one can apply Lax's Equivalence theorem[32] which indicates that for a properly posed initial-value problem and a finite difference approximation to it that satisfies the consistency condition, stability is the necessary and sufficient condition for convergence. Unfortunately, to date there is no a rigorous mathematical theorem for the nonlinear systems which usually describe practical fluid dynamic problems. Nevertheless, it is evident that at least stability is necessary for convergence so that it is very important to undertake a stability analysis.

For initial value problems, a so called Von Neumann method is the most widely used in this analysis. This method is based on the Fourier series expansion. Suppose a difference equation is expressed as:

$$U_j^{n+1} = L\, U_j^n \tag{3.5}$$

where L is a difference operator

If the kth Fourier component of U_j^n is $U_j^n(k) = V^n(k) \exp(ikX_j)$, after the operation of equation (3.5) the kth Fourier component at n+1 is

$$U_j^{n+1}(k) = V^{n+1}(k) \exp(ikX_j) \equiv G\, U_j^n(k) \tag{3.6}$$

Where $G = V^{n+1} / V^n$, which is usually a complex function of Δt, ΔX and k and is called the amplification matrix, and $i = \sqrt{-1}$. Clearly, it is necessary for stability that G has a bounded value. The necessary condition for stability by Von Neumann (see reference [32], page 70) is given by the mathematical expression:

$$|\lambda_n| \leq 1 + O(\Delta t) \quad \text{for} \begin{cases} 0 < \Delta t < \tau \\ \text{all } k \text{ in } \Omega \\ n = 1, \ldots, N \end{cases} \tag{3.7}$$

where λ_n are the eigenvalues of amplification matrix G

τ is an arbitrary positive number

Ω is the calculation region

N is the number of dependent variables in U

It has been proved that if the matrix G is a normal matrix, the Von Neumann condition is sufficient as well as necessary for stability.

The Von Neumann analysis only offers a method for linear initial value problems. It does not give any information concerning the effects of boundary conditions. In numerical analyses, the implementation of stable numerical boundary conditions is also a major issue and one that has not been completely resolved.

For nonlinear problems there exists no complete method for numerical analysis of stability. A method of overcoming this

difficulty is to analyse the locally linearized form of this equation by using the Von Neumann method and then to use the results as the reference of stability.

For the hyperbolic problem, the well known C.F.L. (Courant-Friedrichs-Lewy) condition is usually used as the criterion of stability. The C.F.L. condition is a necessary condition for the solution of difference equations to converge to differential equations. It requires that the dependent region of the difference problem should be smaller than that of the differential problem. It can be expressed as

Courant Number ≤ 1

In spite of these formidable obstacles, wide-ranging numerical solutions of the Navier-Stokes equations have been obtained. These results usually compare favourably with the accompanying experimental observations. This criterion of validation is fully justified based upon the fact that the Navier-Stokes equations were developed to describe physical phenomena.

3.1.6. Nonlinear Oscillation.

In finite-difference method the Fourier component of shortest resolved wavelength is $\lambda_{min} = 2\Delta X$, where ΔX is the mesh-spacing.

In some practical flow fields, however, there exist steep flow gradients e.g. shock waves, which cover a distance much shorter than any practical mesh size. It is impossible to achieve an exact solution of this phenomenon numerically. If the numerical scheme has insufficient dissipation to smooth it, these physically short wave phenomena would produce numerical oscillations, which often lead to the failure of calculation. Let us consider the numerical amplification. The amplification matrix can be expressed as $G = |G|$

$e^{i\Phi}$. For the approximation to be a exact $|G|$ should be a unit matrix and Φ should have the value of $\Phi_e = -k\,\Delta t$. Because the $|G|$ expresses the change of amplitude and Φ reflects the change of phase angle, the $|G|$ is used to represent the dissipative property of scheme and Φ/Φ_e to represent the dispersive error[33]. In practice, for numerical robustness, $|G| < 1$ and $\Phi/\Phi_e \cong 1$ is needed. Warming and Beam[34] have reported that in their trapezoidal scheme, $|G| = 1$ and $\Phi/\Phi_e < 1$. This is the reason why their second-order scheme is more sensitive to nonlinear instability. For the MacCormack two step scheme we can come to the same conclusion. In order to improve these schemes it is necessary to append an additional dissipation term to ensure nonlinear stability. MacCormack used a fourth-order product term which takes the following form:

$$C\,\Delta X^4\,\frac{\partial^2 P}{\partial X^2}\,\frac{\partial^2 U}{\partial X^2}$$

where coefficient C is usually called an artificial viscosity coefficient.

In the present calculation a fourth order damping term is used. It controlled the nonlinear oscillation effectively.

3.2. Difference Method Schemes.

3.2.1. Explicit Scheme.

In this scheme the solution at $(n+1)\Delta t$ on any mesh point of the computational region can be expressed by the function of the known value on this region.

Its common form is

$$U^{n+1} = L\,U^n \tag{3.8}$$

Among the large number of explicit schemes one of the most well known is the MacCormack two step scheme which was successfully used in the calculation of the interaction between a shock wave and a boundary

layer.

In two dimensions, this scheme can be written as:

predictor step:

$$\overline{U^{n+1}_{i,j}} = U^{n}_{i,j} - \frac{\Delta t}{\Delta X}(F^{n}_{i+1,j}-F^{n}_{i,j}) - \frac{\Delta t}{\Delta Y}(G^{n}_{i,j+1}-G^{n}_{i,j}) \qquad (3.9)$$

corrector step:

$$U^{n+1}_{i,j} = \frac{1}{2}[U^{n}_{i,j}+\overline{U^{n+1}_{i,j}} - \frac{\Delta t}{\Delta X}(\overline{F^{n+1}_{i,j}}-\overline{F^{n+1}_{i-1,j}}) - \frac{\Delta t}{\Delta Y}(\overline{G^{n+1}_{i,j}}-\overline{G^{n+1}_{i,j-1}})] \qquad (3.10)$$

The stability condition demanded is

$$\Delta t \leq \frac{1}{\frac{|U|}{\Delta X} + \frac{|V|}{\Delta Y} + C\sqrt{\frac{1}{\Delta X^2} + \frac{1}{\Delta Y^2}} + \Theta} \qquad (3.11)$$

where C is the sound speed and Θ is related to the viscous effect.

The advantage of explicit schemes are their ease of programming, even for the modern vector computer. Its time marching step, however, is severely restricted by the stability condition. This is particularly true in solutions which need very fine mesh. For example calculations of turbulence, using this approach will only achieve very low computational efficiency. It is imperative to overcome this restriction on step size. An initial improvement can be obtained from the use of time split technology. Thus, the equation (3.7) can be rewritten as

$$U^{n+1}_{i,j} = L_y\,(\Delta t/2)\; L_x\,(\Delta t)\; L^{n}_{y}\,(\Delta t/2)\; U^{n} \qquad (3.12)$$

where the operators L_x and L_y are corresponding to the discretized forms of two one-dimensional equations respectively. Namely

$$L_x \longrightarrow \frac{\partial U}{\partial t} + \frac{\partial F}{\partial X} = 0 \qquad (3.13)$$

$$L_y \longrightarrow \frac{\partial U}{\partial t} + \frac{\partial G}{\partial Y} = 0 \qquad (3.14)$$

3.2.2. Implicit Scheme.

In this scheme, the solutions at $(n+1)\Delta t$ on all mesh points of the computational region are conjoint, requiring the solution of a set of algebraic equations to obtain a local solution. Modern implicit

schemes are of following common form

$$[\text{Numerical}]\ \delta U_{i,j} = [\text{Physical}] \tag{3.15}$$

To illustrate the method, Beam and Warming's implicit scheme is described.

The 2-D N-S equation is

$$\frac{\partial U}{\partial t} + \frac{\partial F}{\partial X} + \frac{\partial G}{\partial Y} = 0 \tag{3.16}$$

The local Taylor expansion yields:

$$U^{n+1} = U^n + \frac{\Delta t}{2}\left[\left(\frac{\partial U}{\partial t}\right)^n + \left(\frac{\partial U}{\partial t}\right)^{n+1}\right] + O(\Delta t^3) \tag{3.17}$$

$$\left.\begin{aligned} F^{n+1} &= F^n + A^n(U^{n+1} - U^n) + O(\Delta t^2) \\ G^{n+1} &= G^n + B^n(U^{n+1} - U^n) + O(\Delta t^2) \end{aligned}\right\} \tag{3.18}$$

where $A = \frac{\partial F}{\partial U}$, $B = \frac{\partial G}{\partial U}$ are the Jacobians.

By substituting (3.16), (3.18) into (3.17), we obtain a new system

$$\left[I + \frac{\Delta t}{2}\left(\frac{\partial A^{\cdot}}{\partial X} + \frac{\partial B^{\cdot}}{\partial Y}\right)\right] \delta U_{i,j}^{n+1} = \Delta U_{i,j}^{n} + O(\Delta t^3) \tag{3.19}$$

where $\delta U_{i,j}^{n+1} = U^{n+1} - U^n$

$$\Delta U_{i,j}^{n} = -\Delta t \left(\frac{\partial F}{\partial X} + \frac{\partial G}{\partial Y}\right)^n$$

and the dot in the equation (3.19) indicate that the derivatives operator also on $\delta U_{i,j}^{n+1}$.

After introducing a suitable space difference approximation in (3.19), a complete implicit scheme can be obtained.

It can be seen clearly that the 'physical' change part of equation (3.15) is $\left(-\Delta t \left(\frac{\partial F}{\partial X} + \frac{\partial G}{\partial Y}\right)\right)$ which expresses the local approximated change of governing equation in Δt, and the 'Numerical part' is an implicit operator, $\left[I + \frac{\Delta t}{2}\left(\frac{\partial A}{\partial X} + \frac{\partial B}{\partial Y}\right)\right]$, which conveys the local changes globally in stable manner. This gives an explanation as to why the implicit scheme is unconditionally stable. The unbounded size of time step is favourable for the enhancement of the computational effiency. This has become the predominant approach in recent years.

The implicit scheme, however, requires the inversion of the implicit operator which uses much computer time. To reduce this, particular techniques have been used. The alternating direction (ADI) technique is one of them. According to this technique equation (3.19) can be rewritten as

$$(I + \Delta t \frac{\partial A}{\partial X}) \delta U^{n+1} = \Delta U^{*} \tag{3.20}$$

$$(I + \Delta t \frac{\partial B}{\partial Y}) \Delta U^{*} = \Delta U \tag{3.21}$$

If the central difference approximation is used for the space derivative, the implicit operators in equations (3.20) and (3.21) result in two block tri-diagonal matrixes. This simplifies the inversion.

MacCormack devised an implicit scheme in 1981 the result of which needed only the solution of a block bidiagonal system. This will be introduced in Chapter 5.

3.2.3. Hybrid Scheme.

As pointed out in Section 3.2.1., the difference operator can be replaced by sub-operators, each corresponding to a single dimension equation. Hence, their stability conditions need only be met in their corresponding one-dimensional approximated equation. It has been proved[16] that if each sub-operator is of second-order accuracy then the symmetric operator

$$L = \cdots L_y (\Delta t/2) L_x (\Delta t) L_y (\Delta t/2) \cdots$$

will retain second-order accuracy. Thus, the difference operator in the direction along which a fine mesh is necessary is represented by an algorithm that has less restriction in Δt. Compared with the explicit scheme, the gain in computational efficiency is obvious.

3.2.4. Flux Vector Splitting.

Steger and Warming[35] devised a Flux Vector Splitting scheme from

the idea that the upwind scheme is of dissipative property ($|G| < 1$). They divided the Jacobian matrix into two parts, one is related to a positive eigenvalue, called A^+, another to a negative eigenvalue, A^-. Then the derivative of A^+ part is approximated by a forward difference operator, and the A^- part by a backward difference. It is evident that this difference scheme strictly follows the physical behaviour. Coakley[78][81] developed a new scheme based on Flux Vector Splitting. He found that artificial viscosity is not needed for transonic calculation, although other workers have reported that some artificial viscosity is still necessary.

3.3. Boundary Condition.

In the numerical analysis, the implementation of stable numerical boundary conditions is also a major issue and one that is not completely resolved. Here, based on the property of N-S equations and practical physical flows the explicit aspects of boundary conditions are given.

3.3.1. Viscous Part.

In the boundary layer region, the flow is parabolic in character and no special considerations are required for subsonic flow. The boundary conditions usually used are as follows:

Incoming Boundary:

U, V, T or E are prescribed and $\frac{\partial P}{\partial Y} = 0$ is assumed.

Outer Boundary:

the assumptions, $\frac{\partial T}{\partial X} = \frac{\partial u}{\partial X} = \frac{\partial v}{\partial X} = 0$ and $\frac{\partial P}{\partial Y} = 0$ are used.

Body Surface:

No slip condition is used, i.e., $U = 0$, $V = 0$ on an impermeable wall and $U = 0$, $V = V_m$ if there is mass transfer through surface.

$\frac{\partial T}{\partial Y} = 0$ for adiabatic wall

$T = T_w$ for isothermal wall

An approximating normal momentum equation is used to determine P or ρ.

3.3.2. Inviscid Part.

In this region the N-S equations simplify to Euler equations.

Incoming Boundary:

If Mach number M > 1, all the eigenvalues of the Jacobian matrix are positive. The flow parameters will not be affected by downstream flow. Thus, all the parameters on this boundary are prescribed.

If M < 1, one of the eigenvalues of the Jacobian matrix $\partial F/\partial U$ is negative. The flow on this boundary is affected by downstream flow. The boundary condition can be set by characteristic relations plus an additional functional relation.

These characteristic relations can be derived from an approximate one-dimensional equation because in many cases the tangential derivatives on these boundary conditions are of minor importance . They are

$$\frac{\partial P^n}{\partial X} - (C^n)^2 \frac{\partial \rho^n}{\partial X} = 0 \qquad (3.22)$$

$$\frac{\partial v^n}{\partial X} = 0 \qquad (3.23)$$

$$\frac{\partial P^n}{\partial X} - \rho^n C^n \frac{\partial u^n}{\partial X} = 0 \qquad (3.24)$$

It is often possible to replace (3.22) by constant mass flow and (3.23) by V = 0.

The additional functional equation can have the following forms:

1) Setting static pressure P fixed

2) Setting total pressure P_o = constant

3) Letting total temperature (or enthalpy) equal a constant

4) Keeping the Mach number fixed

The choice of any one of these relations depends on the problem posed.

Out-flow Boundary:

For $M > 1$, $\frac{\partial U}{\partial X} = 0$ is used since in supersonic flow downstream disturbances do not propagate upstream. As long as this boundary is set far away from the main computational region of interest, the effects of a poorly defined boundary condition will be negligibly small.

For $M < 1$, then the flow on this boundary and the flow in the inner region will influence each other. A similar treatment can be applied as used for the incoming boundary when $M < 1$.

Upper Boundary:

For $M > 1$

All the parameters in this boundary are prescribed. The simple wave condition can also be used.

For $M < 1$

It is necessary to place this boundary as far as possible away from the disturbing source, when infinite conditions can be used.

3.4. Computational Mesh.

The appropriate selection of an optimal grid system for a given problem is paramount. It has been found that the success or failure of a solution hinges on this choice. There exist conflicting factors. From consideration of the accuracy of the solution, more mesh points and a coordinate transform are necessary. However for computational efficiency fewer points and a rectangular mesh are required. Thus the computational mesh chosen is a compromise of these factors.

In general, current technology in grid generation can be classified into two major groups. One is through the use of differential equations to generate the grid[36]. Another follows an algebraic interpolation approach. In this research the second approach is used.

CHAPTER 4

TURBULENCE MODELLING

As it has been pointed out in Section 1.1., it is not a realistic task, neither now nor in the future, to use the N-S equations directly to obtain the instantaneous behaviour of a turbulent flow field. Nevertheless, many approximate numerical methods have been developed for the numerical study of turbulent flow. In general, these methods can be divided into two types.

(1) Turbulent Eddy Simulations.

The main physical concepts of this approach arise from the properties that large eddies extract energy from the mean flow, are highly anisotropic, variable from flow to flow and transport the greater part of the turbulent momentum and energy, whereas small eddies dissipate energy, tend towards isotropy, are nearly 'universal' in character, and transport relatively little turbulent energy or momentum. Thus, the large eddies are directly simulated numerically from complete time-dependent Navier-Stokes equations, while the small subgrid scale eddies are modelled. It is evident that, this approach can yield fine details of all relevant quantities characterizing turbulence. Such simulations, however, can be extremely demanding on computer memory and speed, particularly for high Reynolds number flows. Although some successful calculations for simple turbulent flow have been reported, there is still a lot of work to do before the method can be used practically to solve engineering problems. This method will not be used and further discussed in the present research work. More information can be obtained from reference [1] and [37].

(2) Solution of the Reynolds-averaged N-S Equations.

For most engineering problems, it is unnecessary to know the instantaneous values of flow parameters at every time step. Even though turbulence is a random, continuum and strictly three-dimensional phenomenon it can be assumed to be a property of the flow and not the flow medium. It is possible to develop this approach to solve statistically averaged N-S equations rather than the original ones. Then, only statistical averaged variables are concerned, and the requirements on mesh nodes will obviously be much less than the full simulation approach. However, it gives rise to a new problem. Due to the nonlinear convective term, any statistical process would lead to new unknown quantities which must be complemented with closure conditions, the definition of which is termed a turbulent model. This approach is amenable to modern computers, recognizing their limitations. At the present stage it constitutes the main approach to the solution of turbulent flow and is used in this research. In this chapter, there will be provided only a simple introduction to modelling methods of unknowns in Reynolds-averaged N-S equations and an outline of models which will be used in the present research. More details of a variety of models and complete reviews of turbulence modelling methods can be found from several excellent books and articles[29][38-41].

4.1. Reynolds-averaged N-S Equations.

4.1.1. Statistical Average.

One can get a statistical average of any physical quantity of a turbulent flow field by taking the time average over a time interval which is long compared to turbulent eddy fluctuations yet small compared to macroscopic flow changes. This can be expressed as

$$\bar{\Phi} = \frac{1}{T}\int_0^T \Phi \, dt \qquad (4.1)$$

where Φ represents an arbitrary random variable

T is the time interval

In some cases, when the period over which a change of macroscopic flow occurs is very short, one can use an ensemble average method[42].

In the following sections, regardless of the kind of averaging method used all quantities with a bar will be considered as statistically averaged.

4.1.2. The Decomposition of Turbulent Quantities.

Following section 4.1.1, a turbulent quantity can be decomposed into a statistical mean quantity plus a fluctuating quantity, e.g., in the classical Reynolds decomposition method a physical quantity can be expressed as $\Phi = \bar{\Phi} + \Phi'$, where $\bar{\Phi}$ is the statistical averaged quantity and Φ' is the fluctuating quantity. From (4.1), it is apparent that $\bar{\Phi'} = 0$. This method will lead to too large a number of unknown quantities, particularly in compressible flows. For example, a flux $\rho U\Phi$ is considered. By using Reynolds decomposition and after the statistical averaging, we get

$$\overline{\rho U\Phi} = \bar{\rho}\bar{U}\bar{\Phi} + \overline{\rho' U'}\bar{\Phi} + \overline{\rho'\Phi'}\bar{U} + \overline{\rho' U'\Phi'} + \bar{\rho}\overline{U'\Phi'} \qquad (4.2)$$

In incompressible flow, only the first and the last terms exist, whereas in compressible flow, all of these terms have to be kept. Obviously this problem is caused by the density fluctuation. In order to avoid too many unknowns to be introduced, a so called Favre or Mass-Weighted decomposition method is used. In this method, the turbulent quantity is first multiplied by density, and the statistical averaging then taken. Accordingly, we get

$\Phi = \tilde{\Phi} + \Phi''$, where $\tilde{\Phi} = \frac{\overline{\rho\Phi}}{\bar{\rho}}$, $\overline{\rho\Phi''} = 0$, however, $\overline{\Phi''} \neq 0$.

The quantity with tildes is referred to as mass-weighted averaged

mean quantity. Thus the equation (4.2) can be rewritten as

$$\overline{\rho U\Phi} = \bar{\rho}\tilde{U}\tilde{\Phi} + \overline{\rho U''\Phi''} \tag{4.3}$$

It is evident that this decomposition method can produce the same form both for incompressible flow and compressible flows.

4.1.3. Reynolds-averaged N-S Equations.

In equations (2.17) the dependent variables u, v, w, E use the Mass-Weighted decomposition and the P, σ and q use classical Reynolds decomposition. A statistical average is then made over the whole set of equations resulting in Reynolds-averaged equations to give:

Continuity equation

$$\frac{\partial \bar{\rho}}{\partial t} + \frac{\partial}{\partial X_j}(\bar{\rho}\tilde{u}_j) = 0 \tag{4.4}$$

Momentum equation

$$\frac{\partial}{\partial t}(\bar{\rho}\tilde{u}_i) + \frac{\partial}{\partial X_j}(\bar{\rho}\tilde{u}_i\tilde{u}_j + \bar{P}\delta_{ij} - \overline{\sigma_{ij}} + \overline{\rho u_i'' u_j''}) = 0 \tag{4.5}$$

Energy equation

$$\frac{\partial}{\partial t}\tilde{E} + \frac{\partial}{\partial X_j}(\tilde{E}\tilde{u}_j + \bar{P}\tilde{u}_j - \overline{\sigma_{ij}}\tilde{u}_i + q_j + \overline{\rho h'' u_j''} + \tilde{u}_i\,\overline{\rho u_i'' u_j''}) = 0 \tag{4.6}$$

where i = X, Y, Z for 3-D, and i = X, Y, for 2-D

$$\bar{\sigma}_{ij} = -\frac{2}{3}\bar{\mu}\left(\frac{\partial \tilde{u}_k}{\partial X_k}\right)\delta_{ij} + \bar{\mu}\left(\frac{\partial \tilde{u}_i}{\partial X_j} + \frac{\partial \tilde{u}_j}{\partial X_i}\right) \tag{4.7}$$

$$\bar{q}_j = -\frac{C_p\bar{\mu}}{Pr}\frac{\partial \tilde{T}}{\partial Y} \tag{4.8}$$

This set of equations is the base of the present research work. Equations (4.4) to (4.8) are suitable both for incompressible and compressible flow. Comparing with the original N-S equations the new unknowns introduced are $\overline{\rho u_i'' u_j''}$ and $\overline{\rho h'' u_j''}$ and hence some new relations have to be added to make this system closure. The correlation relation, $-\overline{\rho u_i'' u_j''}$ is usually referred to as Reynolds stress.

4.2. The Modelling of Unknown Variables.

4.2.1. The Modelling of $\overline{\rho h'' u_j''}$.

Except when the Mach number is very high, this correlation

relation has less importance than the term $\overline{\rho u_i'' u_j''}$. To date, in most existing models, it uses a simple algebraic expression[29]:

$$\overline{\rho h'' u_j''} = - C_p \frac{\mu_t}{Pr_t} \frac{\partial T}{\partial X_j} \qquad (4.9)$$

where C_p is the specific heat at constant pressure

and Pr_t is the turbulent Prandtl number

4.2.2. The Modelling of Reynolds Stress $-\overline{\rho u_i'' u_j''}$.

Because the behaviour of the Reynolds stress $-\overline{\rho u_i'' u_j''}$ governs the velocity field through (4.5), its modelling is the central feature of the calculation for turbulence. The accuracy of numerical simulations depends principally upon the accuracy of Reynolds stress modelling.

Essentially, there are two ways to model the term $\overline{\rho u_i'' u_j''}$. One is directly to solve Reynolds stress transport equations which are listed in Appendix A-3. This method takes the transport process of turbulent stress into account. Therefore, this modelling method should more relate to physical actuality, but it also gives rise to mathematical complexity in the solution of this system. This has been borne out since this method has not been successfully used in calculations for the complex flow problem considered in the present research work[41]. Further details about this method are given in the literature[43][44]. The other makes use of Boussinesq's Eddy-Viscosity concepts (1877). The Reynolds-Stress is replaced by a product of an effective viscosity called 'Eddy-Viscosity' and the rate of strain of mean-velocity as follows

$$- \overline{\rho u_i'' u_j''} = \mu_t \left[- \frac{2}{3} \frac{\partial \tilde{u}_k}{\partial X_k} \delta_{ij} + \frac{\partial \tilde{u}_i}{\partial X_j} + \frac{\partial \tilde{u}_j}{\partial X_i} \right] \qquad (4.10)$$

An analogy from the representation of molecular viscosity leads to an expression of eddy viscosity:

$$\mu_t = C_\mu \bar{\rho} V_t L_t \qquad (4.11)$$

where V_t is the turbulence velocity scale

L_t is the turbulence length scale

Thus the problem is transformed into the modelling of V_t and L_t. This is referred to as the eddy-viscosity model. In the following section the eddy-viscosity modelling method will be discussed.

4.3. Eddy-Viscosity Model.

According to the numbers of partial differential equations used to determine the two turbulent scales, the Eddy-Viscosity model can be further classified to zero- (or algebraic), one- and two-equation models. For convenience of discussion later, the normalized form of the additional turbulent field differential equation is given as follws:

$$\left.\begin{aligned} &(\bar{\rho} S_\ell)_{,t} + (\bar{\rho} S_\ell u_j + Q_{\ell,j})_{,j} = H_\ell \\ &Q_{\ell,j} = -((\bar{\mu} + \mu_t) / Pr_\ell)(S_{\ell,j}) \\ &\ell = 1, 2 \end{aligned}\right\} \qquad (4.12)$$

where S_ℓ represent a variable of turbulent field

$$(\ )_{,t} = \partial(\ )/\partial t$$

$$(\ )_{,j} = \partial(\ )/\partial X_j$$

Referring to Appendix A-3, it is easily seen that the term $Q_{\ell,j}$ in equation (4.12) corresponds to the modelling of terms IV of equation (A-3-1) where an assumption of the gradient diffusion is used. H_ℓ is called the source or sink term which contains the modelling of the production and dissipation of the turbulent flow field variables (corresponding to term II and III of equation (A-3-1) respectively). The term V in equation (A-3-1) is the most difficult to model. Fortunately, this term is negligibly small as long as the Mach number is not very high, say not larger than 5. To date, in the mean flow field modelling method this term is neglected.

In the ensuing paragraphs, some typical models are listed.

1) Cebeci-Smith (C-S) zero order or algebraic Model.

In this model, the turbulent velocity and length scales are specified by different algebraic relations in two layers. It is expressed as:

In the inner layer:

$$
\left.
\begin{aligned}
&V_t = \ell \left| \left(\left(\frac{\partial \tilde{u}}{\partial Y}\right)^2 + \left(\frac{\partial \tilde{v}}{\partial X}\right)^2 \right)^{1/2} \right| \\
&L_t \equiv \ell = kYD \\
&C_\mu = 1 \\
&\mu_{tin} = \bar{\rho} \ell^2 \left| \left(\left(\frac{\partial \tilde{u}}{\partial Y}\right)^2 + \left(\frac{\partial \tilde{v}}{\partial X}\right)^2 \right)^{1/2} \right| \\
&\text{In the outer layer} \\
&V_t = \tilde{u}_e \\
&L_t = \delta^* B_i \\
&C_\mu = 0.0168 \\
&\mu_{tou} = 0.0168\, \bar{\rho} \tilde{u}_e \delta^* B_i \\
&\mu_t = \begin{cases} \mu_{tin} & Y \leq Y_\ell \\ \mu_{tou} & Y > Y_\ell \end{cases}
\end{aligned}
\right\} \qquad (4.13)
$$

where

$D = [1 - \exp(- Y^+/A^+)]$ is called Van-Driest damping factor

$Y^+ = Y u_\tau \bar{\rho}_w / \bar{\mu}_w$

$u_\tau = \sqrt{\tau_w / \bar{\rho}_w}$

$k = 0.4$ is the Von Karman constant

u_e is the velocity on the edge of boundary layer

δ^* is the displacement thickness. $\delta^* = \int_0^\delta (1 - \tilde{u} / \tilde{u}_e)\, dY$

$B_i = [1 + 5.5(Y / \delta)^6]^{-1}$ is called the intermittency factor.

δ is the thickness of boundary layer

Y_ℓ is the Y value, where $\mu_{tou} \leq \mu_{tin}$

the subscript w indicates the value will be taken on the solid

wall

2) The Relaxation of Turbulence Eddy Viscosity:

The measurements and some theoretical analyses have indicated that the Reynolds stress approaches a new equilibrium state exponentially[56]. In order to take the effects of upstream history into account, a relaxation of turbulence viscosity is introduced[56] [60]. It is formulated as follows:

$$(\mu_t)_{local} = (\mu_t)_{eq} - [(\mu_t)_{eq} - (\mu_t)_o]\, e^{-\frac{X-X_o}{\lambda\delta_o}} \qquad (4.14)$$

where $(\mu_t)_{eq}$ is the turbulence eddy viscosity calculated at the local position by using an algebraic model.

$(\mu_t)_o$ is the value at presetting position X_o.

δ_o is the boundary layer thickness at X_o.

λ is the coefficient of relaxation.

X_o is the position from which the relaxation procedure of eddy viscosity starts.

3) Rubesin-Glushko one-equation model

The turbulent velocity scale is obtained from the solution of turbulent kinetic energy equation and the length scale is obtained from an algebraic relation. For details one can see References 68 and 78.

4) Jones-Launder (K-ϵ) two-equation model[45].

In this model the turbulent velocity scale is obtained from the turbulent kinetic energy (K) equation and the length scale is determined by the turbulence energy dissipation (ϵ) in conjunction with (K).

Following equation (4.11), this model can be expressed as

$$S_1 = K \equiv 1/2\ \overline{u_i'' u_i''}, \quad S_2 = \epsilon$$

$$H_K = \bar{\rho}\,[AK - \epsilon(1 + \frac{2\bar{u}}{\bar{\sigma}\epsilon}\,(\frac{\partial K^{1/2}}{\partial Y})^2)] \qquad (4.15)$$

$$H_\epsilon = \bar{\rho}\ [C_1 A\epsilon + \frac{2C_\mu \bar{\mu} K^2}{\bar{\rho}\epsilon} (\frac{\partial^2 u}{\partial Y^2})^2 - C_2 f_2 \epsilon^2/K] \tag{4.16}$$

$$V_t = \sqrt{K}$$

$$L_t = K^{1.5} / \epsilon$$

$$\mu_t = C_\mu \bar{\rho} K^2 / \epsilon \tag{4.17}$$

where

$A = C_\mu \phi K / \epsilon - 2/3\ \Psi$ which is related to the production of turbulence field variable S

$$\phi = (\frac{\partial \tilde{u}_i}{\partial X_j} + \frac{\partial \tilde{u}_j}{\partial X_i} - \frac{2}{3}\delta_{ij} \frac{\partial \tilde{u}_k}{\partial X_k}) \frac{\partial \tilde{u}_i}{\partial X_j} \tag{4.18}$$

$$\Psi = \frac{\partial \tilde{u}_k}{\partial X_k} \tag{4.19}$$

$$f_2 = 1 - C_{e1} \exp(- R_t^2 / C_{e2}) \tag{4.20}$$

$$C_\mu = C\ f_\mu \tag{4.21}$$

$$f_\mu = \exp(-C_d / (1 + 0.02\ R_t)) \tag{4.22}$$

$$Pr_K = 1.0$$

$$Pr_\epsilon = 1.3$$

$$R_t = \bar{\rho} V_t L_t / \bar{\mu} = \bar{\rho} K^2 / (\epsilon \mu) \tag{4.23}$$

In the original J-L model, the values of coefficients are

$C_1 = 1.55$, $C_2 = 2.0$, $C = 0.09$, $C_d = 2.5$, $C_{e1} = 0.3$, $C_{e2} = 1.0$.

Although the turbulent kinetic energy , K, is negligibly small in most parts of the flow field , it becomes comparable to the mean kinetic energy in regions with high shear and low mean velocity, such as in the vicinity of the solid wall or in the recirculation zone. In the K-ϵ model, the pressure due to the kinetic energy of turbulence, $2/3\bar{\rho}K$, has to be considered. This can be done through replacing the static pressure $\bar{P}$ by an effective pressure $\bar{P}_t = \bar{P} + 2/3\bar{\rho}K$. And the total energy $\tilde{E}$ should furthermore include K, i.e. $\tilde{E} = \bar{\rho}(C_v\tilde{T} + 0.5\tilde{u}_i\tilde{u}_i + K)$.

CHAPTER 5

THE NUMERICAL METHOD

Following the discussion given in previous sections, the numerical method of prediction of the two-dimensional flow interaction between a shock wave and a turbulent boundary layer is developed in the following sections.

5.1. Coordinate Transformation.

The specific configuration to be investigated is the supersonic flow over a ramp or a flat plate. Accordingly the following coordinate transformation is introduced:

$$\left.\begin{aligned} \xi &= X \sec \alpha \\ \eta &= Y - X \tan \alpha \end{aligned}\right\} \qquad (5.1)$$

$$\left.\begin{aligned} \text{where } \alpha &= 0 \qquad \text{for flat plate} \\ \alpha &= \text{ramp angle} \qquad \text{on the ramp} \end{aligned}\right\} \qquad (5.2)$$

5.2. Governing Equation.

The governing equations are the two-dimensional form of the Reynolds averaged equations (4.4)-(4.8) plus the turbulent modelling equations under the transformed coordinate system (ξ,η). In practice, their nondimensional form is used. The velocity components (u,v), density (ρ), total energy (E) and pressure (P), length (X,Y), viscosities (μ,μ_t), time (t) temperature (T) and the turbulent field variables K and ϵ are nondimensionalized by u_∞, ρ_∞, $\rho_\infty u_\infty^2$, L, μ_∞, L/u_∞, u_∞^2/R, u_∞^2, u_∞^2/L respectively where the subscript ∞ indicates the incoming condition, R is a gas constant and L is a characteristic length. Thus, the governing equation can be rewritten as

$$\frac{\partial U}{\partial t} + \frac{\partial F}{\partial \xi} \sec \alpha + \frac{\partial \hat{G}}{\partial n} = H \tag{5.3}$$

where

$$U = \begin{bmatrix} \rho \\ \rho u \\ \rho v \\ E \\ \rho S_1 \\ \rho S_2 \end{bmatrix}, \quad F = \begin{bmatrix} \rho u \\ \rho u^2 + P_t - \sigma_{txx} \\ \rho uv - \sigma_{txy} \\ (E + P_t - \sigma_{txx})u - \sigma_{txy}v + q_{tx} \\ \rho S_1 u + Q_{1x} \\ \rho S_2 u + Q_{2x} \end{bmatrix}, \quad H = \begin{bmatrix} 0 \\ 0 \\ 0 \\ 0 \\ H_1 \\ H_2 \end{bmatrix}$$

$$\hat{G} = \begin{bmatrix} \rho v' \\ \rho uv' - \sigma_{txy} - (P_t - \sigma_{txx}) \tan\alpha \\ \rho vv' + P_t - \sigma_{tyy} - \sigma_{txy} \tan\alpha \\ (E + P_t)v' - \sigma_{tyy}v - \sigma_{txy}(u - v\tan\alpha) + q_{ty} - (q_{tx} - \sigma_{txx})\tan\alpha \\ \rho S_1 v' + Q_{1y} - Q_{1x} \tan\alpha \\ \rho S_2 v' + Q_{2y} - Q_{2x} \tan\alpha \end{bmatrix}$$

$$v' = v - u \tan\alpha \tag{5.4}$$

$$P_t = P + 2/3\ \rho K \tag{5.5}$$

$$E = \rho \left[\gamma / (\gamma - 1)\ T + 0.5(u^2 + v^2) + K\right] \tag{5.6}$$

$$\sigma_{tij} = (\mu + \mu_t) / Re_L \left[-\frac{2}{3} \frac{\partial u_k}{\partial X_k} \delta_{ij} + \left(\frac{\partial u_j}{\partial X_i} + \frac{\partial u_i}{\partial X_j}\right)\right] \tag{5.7}$$

$$q_{ti} = -\frac{\gamma}{(\gamma - 1)\ Re_L} \left(\frac{\mu_t}{Pr_t} + \frac{\mu}{Pr}\right) \frac{\partial T}{\partial X_i} \tag{5.8}$$

Q_{1i}, Q_{2i}, H_1 and H_2 are respectively corresponding to the nondimensional form of equation (4.12) (4.15) and (4.16).

And the state equation becomes

$$P = \rho T \quad \text{or} \quad P = (\gamma - 1)[E - \rho/2\ (u^2 + v^2) - \rho k] \tag{5.9}$$

If an algebraic turbulence model is used, the equations related to S_1, S_2 and the terms related to turbulence kinetic energy in equations (5.5), (5.6) and (5.9) vanish. Here and in later sections for

convenience the tilde and bar over the dependent variables are omitted, however, it has to be understood that all of the physical quantities are the statistical mean quantities.

5.3. Computational Mesh.

Although there is no fixed rule to determine the computational grid point distribution, some general considerations have to be taken in to account. They are

1) To reflect sufficiently the properties of the flow field.

2) Under the presupposition of ensuring accuracy, the numbers of grid points should be decreased to the utmost to raise the computational efficiency.

In the viscous boundary layer in order to arrange that the viscous diffusion has the same order as the inviscid convection, the Reynolds number based on the mesh spacing should have a value equal to 1. This extreme demand is unrealistic, particularly in high Reynolds number cases, and also is unnecessary. In fact, in the boundary layer the viscous diffusion in the stream direction has less importance than that in the normal direction so that the spacing ΔX has less restriction up to the value at which it will cause too large a truncated error. In contrast, the spacing ΔY should be taken as small as possible. Arising from practical experience in this study, the position of the first point above wall can be determined in the following way:

$\Delta Y_{min} \approx \delta / 10$ for laminar flow

$Y^+ < 10$ for turbulent flow

For the two-equation model, however, usually $Y^+ \leqslant 4$ was found necessary for achieving a convergent solution.

In the present research work an algebraic method to generate the

computational grid was used. In the computational region, the grid point distribution along the X direction is as shown in Figue 2, and the spacing ΔX is uniform in as far as $\Delta\xi = \Delta X$ on the flat plate part and $\Delta\xi = \Delta X \sec\alpha$ on the ramp. However in the η direction the grid is composed of two meshes. One is a coarse mesh which locates far away from the wall and has a uniform spacing, and the other is a fine mesh which is near the wall and has a varying mesh spacing. Here, the following algebraic formula is used to determine the mesh spacing:

for the fine mesh

$$\eta(1) = 0 \tag{5.10}$$

$$\Delta\eta_j = \eta(j) - \eta(j-1) = \Delta\eta_{max}(\Delta\eta_{min}/\Delta\eta_{max})^{\frac{J1-j}{J1-2}} \tag{5.11}$$

$j = 2, 3, \cdots\cdots J1$

$\eta(j) = \eta(j-1) + \Delta\eta_j$

for the coarse mesh

$$\Delta\eta = (H - H_{J1}) / (JJ - J1) \tag{5.12}$$

where J1 is the number of the highest node in fine mesh.

H_{J1} is the height of fine mesh.

JJ is the number of the highest node in η direction.

H is the height of the computational region.

$\Delta\eta_{min}$ is a specified minimum mesh spacing.

$\Delta\eta_{max}$ is a specified maximum mesh spacing in fine mesh.

In the calculation for the flat plate, the plate is placed in the middle of the first two points, while for ramp calculation, the first point is on the solid wall.

5.4. Numerical Method.

As it has been pointed out in Section **1.3.2.**. The computational efficiency and the numerical and the code compatibility of a numerical scheme are very important for turbulent flow calculations using

complex turbulent field variable equations. Usually, implicit schemes are unconditionally stable, however, difficulties arise when incorporating multi-turbulent modelling equations as mentioned in Chapter 1.

The MacCormack's new implicit scheme (1981), which is of second order accuracy and can use unbounded time step as long as $\nu\Delta t/\rho\Delta X^2$ and $\nu\Delta t/\rho\Delta Y^2$ remain bounded as Δt, ΔX and ΔY approach zero, possesses three advantages over conventional fully implicit methods. First, the method uses two-point, one-sided differences in the implicit part of the algorithm. Thus, block bidiagonal systems of the algebraic equations are resultant, which are less costly to invert and more easy to program than the block tridiagonal systems found in conventional methods. Second, the method employs inviscid Jacobians and corrects them using effective viscous terms added to the Eulerian eigenvalues based on the weighted idea. This maintains stability while avoiding the expensive use of the complete viscous Jacobians in the calculation and is an important characteristic to make it easy to be extended into the calculations using high order turbulent models including Reynolds stress models, if the source term is well dealt with. Finally, the algorithm allows the implicit step to be dropped in regions where the explicit stability restriction is satisfied, such as found in the region away from the boundary layer where the mesh spacing is large. For these reasons this method is chosen as a base for this study.

The new developments presented in this research include, the implicit treatment of source term, the derivation of new Jacobians A and B (equation (5.24) and (5.25)) to conform with the new coordinate system and added requirements for the calculation of the two-equation turbulent model, and the enhancement in the numerical nonlinear

stability at large Courant numbers and the calculations of two equation models .

5.4.1. MacCormack's Implicit Scheme.

The final form of the numerical algorithm used in the present research work is as follows

Predictor step

$$\begin{cases} \Delta U^n_{i,j} = -\frac{\Delta t}{\Delta X}\left(F(U^n_{i+1,j}) - F(U^n_{i,j})\right) - \frac{\Delta t}{\Delta n_+}\left(\hat{G}(U^n_{i,j+1}) - \hat{G}(U^n_{i,j})\right) \\ \qquad + \Delta t H(U^n_{i,j}) + \text{Artificial damping term} & (5.13) \\ \left(I + \frac{\Delta t}{\Delta X}|A^n_{i,j}| + \Delta t\lambda_x I\right)\delta U^{*n}_{i,j} = \Delta U^n_{i,j} + \frac{\Delta t}{\Delta X}|A^n_{i+1,j}|\delta U^{*n}_{i+1,j} & (5.14) \\ \left(I + \frac{\Delta t}{\Delta n_+}|B^n_{i,j}| + \Delta t\lambda_y I\right)\delta \bar{U}^{n+1}_{i,j} = \delta U^{*n}_{i,j} + \frac{\Delta t}{\Delta n_+}|B^n_{i,j+1}|\delta \bar{U}^{n+1}_{i,j+1} & (5.15) \\ \Delta n_+ = n(j+1) - n(j) & (5.16) \\ \bar{U}^{n+1}_{i,j} = U^n_{i,j} + \delta \bar{U}^{n+1}_{i,j} & (5.17) \end{cases}$$

Corrector step

$$\begin{cases} \Delta \bar{U}^{n+1}_{i,j} = -\frac{\Delta t}{\Delta x}\left(F(\bar{U}^{n+1}_{i,j}) - F(\bar{U}^{n+1}_{i-1,j})\right) - \frac{\Delta t}{\Delta n_-}\left(\hat{G}(\bar{U}^{n+1}_{i,j}) - \hat{G}(\bar{U}^{n+1}_{i,j-1})\right) \\ \qquad + \Delta t H(\bar{U}^{n+1}_{i,j}) + \text{Artificial damping term} & (5.18) \\ \left(I + \frac{\Delta t}{\Delta X}|\bar{A}^{n+1}_{i,j}| + \Delta t\lambda_x I\right)\delta \bar{U}^{*n+1}_{i,j} = \Delta \bar{U}^{n+1}_{i,j} + \frac{\Delta t}{\Delta X}|\bar{A}^{n+1}_{i-1,j}|\delta \bar{U}^{*n+1}_{i-1,j} & (5.19) \\ \left(I + \frac{\Delta t}{\Delta n_-}|\bar{B}^{n+1}_{i,j}| + \Delta t\lambda_y I\right)\delta U^{n+1}_{i,j} = \delta \bar{U}^{*n+1}_{i,j} + \frac{\Delta t}{\Delta X}|\bar{B}^{n+1}_{i,j-1}|\delta U^{n+1}_{i,j-1} & (5.20) \\ \Delta n_- = n(j) - n(j-1) & (5.21) \\ U^{n+1}_{i,j} = 0.5(U^n_{i,j} + \bar{U}^{n+1}_{i,j} + \delta U^{n+1}_{i,j}) & (5.22) \end{cases}$$

The derivatives caused by viscous stress and heat diffusion in F and $\hat{G}$ are dealt with as the following way. The n direction derivative in F flux and the ξ direction derivative in $\hat{G}$ flux are always approximated by central differences. Then, the derivative along ξ direction in F and the derivative along n direction in $\hat{G}$ use a backward difference approximation in the predictor step and a forward difference approximation in the corrector step.

In equation (5.13) and (5.18) the artifical damping terms are considered necessary to control the nonlinear numerical instability

encountered in the present tests. The terms, λ_x, λ_y in equations (5.14), (5.15), (5.19) and (5.20) are concerned with the simplified implicit treatment of the source term. These will be discussed later.

The equations (5.14), (5.15) and (5.19), (5.20) result from the factorization approximation. They form a block bidiagonal system which is more easy to invert than the original upper- or lower- block tridiagonal system. The price paid by this approximation, however, is a limited time step Δt to be used in practical calculations. The reason can be explained as follows. The standard factorization approximation of $\left\{ I + \Delta t \frac{\Delta A}{\Delta X} + \Delta t \frac{\Delta B}{\Delta Y} \right\}$ is $\left\{ I + \Delta t \frac{\Delta A}{\Delta X} \right\} \cdot \left\{ I + \Delta t \frac{\Delta B}{\Delta Y} \right\}$ which can simply be inverted one factor at a time. A multiplication of the above two factors, however, yields in addition to the original factor the term $\Delta t^2 \cdot \frac{\Delta A}{\Delta X} \cdot \frac{\Delta B}{\Delta Y}$. This term represents an error introduced by approximate factorization, whose norm is proportional to $\frac{\Delta t||A||}{\Delta X} \cdot \frac{\Delta t||B||}{\Delta Y}$, the product of the CFL numbers in the X and Y directions. It is seen that even though the factorization approximation can remain second-order accurate, too large a CFL number (i.e too large a Δt) will cause error.

5.4.2. <u>The Jacobians A and B & Their Diagonalization</u>.

The matrices $|A|$ and $|B|$ are related to the Jacobians of the flux vectors F and $\hat{G}$. It has been deduced[20] that $|A|$ and $|B|$ have positive eigenvalues and are defined as

$$|A| = S_x^{-1} D_A S_x \qquad \text{and} \qquad |B| = S_y^{-1} D_B S_y \tag{5.23}$$

where S_x, S_y and their inverses denote the matrices that diagonalize the Jacobians of the inviscid part of F and $\hat{G}$. Namely

$$A = \frac{\partial F_{inviscid}}{\partial U} = S_x^{-1} \Lambda_A S_x \tag{5.24}$$

$$B = \frac{\partial \hat{G}_{inviscid}}{\partial U} = S_y^{-1} \Lambda_B S_y \tag{5.25}$$

From equation (5.24), (5.25), A, B, S_x^{-1}, Λ_A, S_x, S_y^{-1}, Λ_B, S_y can be

derived. If the K-ϵ turbulence model is used under the new coordinate system (ξ, η) we have

$$S_x = \begin{bmatrix} 1-a\beta/c^{*2} & \beta u/c^{*2} & \beta v/c^{*2} & -\beta/c^{*2} & \beta/c^{*2} & 0 \\ -v & 0 & 1 & 0 & 0 & 0 \\ -uc^{*}+a\beta & c^{*}-\beta u & -\beta v & \beta & -\beta & 0 \\ uc^{*}+a\beta & -c^{*}-\beta u & -\beta v & \beta & -\beta & 0 \\ -k & 0 & 0 & 0 & 1 & 0 \\ -\epsilon & 0 & 0 & 0 & 0 & 1 \end{bmatrix}$$

$$\Lambda_A = \begin{bmatrix} u & & & & & \\ & u & & & & \\ & & u+c & & & \\ & & & u-c & & \\ & & & & u & \\ & & & & & u \end{bmatrix}$$

$$S_y = \begin{bmatrix} 1-a\beta/c^{*2} & \beta u/c_{*2} & \beta v/c^{*2} & -\beta/c^{*2} & \beta/c^{*2} & 0 \\ -(u\cos\alpha+v\sin\alpha) & \cos\alpha & \sin\alpha & 0 & 0 & 0 \\ a\beta-c^{*}(v\cos\alpha-u\sin\alpha) & -\beta u-c^{*}\sin\alpha & c^{*}\cos\alpha-\beta v & \beta & -\beta & 0 \\ a\beta+c^{*}(v\cos\alpha-u\sin\alpha) & -\beta u+c^{*}\sin\alpha & -c^{*}\cos\alpha-\beta v & \beta & -\beta & 0 \\ -k & 0 & 0 & 0 & 1 & 0 \\ -\epsilon & 0 & 0 & 0 & 0 & 1 \end{bmatrix}$$

$$\Lambda_B = \begin{bmatrix} v' & & & & & \\ & v' & & & & \\ & & v'+c\sec\alpha & & & \\ & & & v'-c\sec\alpha & & \\ & & & & v' & \\ & & & & & v' \end{bmatrix}$$

where $a = 0.5(u^2 + v^2)$, $\beta = \gamma - 1$, c is the sound speed and c^* is the sound speed based on the temperature calculated from effective pressure P_t. The matrices A, B, S_x^{-1}, S_y^{-1} can be found in Appendix A-4.

Then D_A and D_B are defined as

$$D_A = \begin{bmatrix} \lambda_{A1} & & & & & \\ & \lambda_{A2} & & & & \\ & & \lambda_{A3} & & & \\ & & & \lambda_{A4} & & \\ & & & & \lambda_{A5} & \\ & & & & & \lambda_{A6} \end{bmatrix} \tag{5.26}$$

$$D_B = \begin{bmatrix} \lambda_{B1} & & & & & \\ & \lambda_{B2} & & & & \\ & & \lambda_{B3} & & & \\ & & & \lambda_{B4} & & \\ & & & & \lambda_{B5} & \\ & & & & & \lambda_{B6} \end{bmatrix} \tag{5.27}$$

$$\text{and } \lambda_{Ai} = \text{Maximum} \left\{ |\Lambda_{Ai}| + \frac{2\nu}{\rho \Delta X} - \frac{1}{2}\frac{\Delta X}{\Delta t} , \quad 0.0 \right\} \tag{5.28}$$

$$\lambda_{Bi} = \text{Maximum} \left\{ |\Lambda_{Bi}| + \frac{2\nu}{\rho \Delta Y} - \frac{1}{2}\frac{\Delta Y}{\Delta t} , \quad 0.0 \right\} \tag{5.29}$$

Here, ν is an effective viscosity, which is determined as follows

$$\nu = \text{Maximum} \left\{ 4/3\ (\mu + \mu_t) , \quad \frac{\gamma}{\gamma - 1} \left(\frac{\mu}{Pr} + \frac{\mu_t}{Pr_t} \right) \right\} / Re_L \tag{5.30}$$

As λ_x, λ_y are constant and |A|, |B| can be expressed in the form of (5.23), the inversion of the left parts of equations of (5.14), (5.15), (5.19) and (5.20) will be quite simple. The calculation procedure is explained in Reference 20.

5.4.3. <u>The Treatment of the Source Term</u>.

Originally, MacCormack suggested that

$$\lambda_x \geq \text{Maximum} \left\{ \left| \frac{\partial H}{\partial U} \right| - H_o , \quad 0.0 \right\}$$

Unfortunately, as the source of the H contribution is much more complex than that of the inviscid parts of the flux vector F and G, it is almost impossible to derive the Jacobian matrix of H. From the fact that the deduction of MacCormack's implicit scheme is based on the weighted averaging concept[20], λ_x can be considered as a positive weighted constant value provided that the stability demanded in reference [20] can be assured. The stability of this scheme will be not affected. Thus, the implicit part for the treatment of the source term is composed of a diagonal matrix so that the original method of matrix inversion is held to retain the main advantage of MacCormack's scheme. For the present work, λ_x, λ_y are taken as

$$\lambda_x = \text{Maximum} \left\{ \frac{2\nu}{\rho\Delta X^2} - \frac{1}{2\Delta t}, \; 0.0 \right\} \tag{5.31}$$

$$\lambda_y = \text{Maximum} \left\{ \frac{2\nu}{\rho\Delta Y^2} - \frac{1}{2\Delta t}, \; 0.0 \right\} \tag{5.32}$$

The successful results from this computational scheme show that this treatment is feasible. It has furthermore been found that the restricting conditions used in other schemes for K-ϵ model are now unnecessary.

5.4.4. Additional Artificial Damping.

In a shock capture technique, the success of a numerical scheme lies in its ability to suppress nonlinear oscillations. Through the stability analysis the dissipative and dispersive properties of a numerical scheme can be assessed qualitatively as mentioned in section (3.1.6). This can provide an indication of the need for an additional artificial damping term. However the actual behaviour and the magnitude of this term, if it is necessary, will depend mainly on practical testing. Before starting the calculation, the ability to control the nonlinear oscillation of MacCormack's implicit scheme was investigated through the calculation of the flow field for a

supersonic flow over a sharp leading edged flat plate. The investigation included

1) Ways of controlling the nonlinear disturbance caused by the leading edge.

2) The behaviour of three different additional damping terms which are separately

   (a) A term, $T = \frac{| \delta P/C^2 - \delta\rho |}{\rho(\Delta t/\Delta Y)(\gamma-1)/\gamma}$ which is proportional to the change in entropy caused primarily by viscosity, added to the effective viscosity of the implicit part of the numerical scheme.

   (b) A fourth order product term is added to the explicit part of the scheme as follows,

   $$-C_x \frac{| P_{i+1} - 2P_i + P_{i-1} |}{P_{i+1} + 2P_i + P_{i-1}} (U_{i+1} - 2U_i + U_{i-1})$$

   (c) A fourth order derivation term added into the explicit part of the scheme, as follows: $-C_x (6U_i - 4U_{i+1} - 4U_{i-1} + U_{i+2} + U_{i-2})$

3) The behaviour of this scheme when a strong incident shock wave appears.

Here is presented the conclusion of this investigation the details of which are presented Appendix A-5. This investigation was carried out using the grid system described in Section (5.3). The present tests showed that the MacCormack's implicit scheme without any additional damping term is not able to suppress nonlinear oscillations in regions where the Courant number is much larger than 1 even when they are caused by a small disturbance such as a weak leading edge shock wave. The situation becomes worse when the Courant number increases (in other words when the mesh size in the Y direction decreases). The inclusion of the additional damping term (a) made

little improvement. The addition of term (b) could delay the appearance of the oscillation but did not provide an adequate solution. The term (c) could perfectly suppress the oscillation even for a small coefficient $C_x = 0.008$. It was also found that when the Courant number increases, the value of the coefficient should also increase. The analysis showed that the term (b) can smooth the shock wave while the term (c) can suppress the streamwise propagation of nonlinear oscillations in the region where the Courant number is large. Thus, in practise a combined form of damping term was used, namely

$$\text{Artificial damping term} = - C_{x_1} \frac{|P_{i+1}-2P_i+P_{i-1}|}{P_{i+1}+2P_i+P_{i-1}} (U_{i+1}-2U_i+U_{i-1}) - C_{x_2} (6U_i-4U_{i+1}-4U_{i-1}+U_{i+2}+U_{i-2}) \qquad (5.33)$$

In the calculation for a supersonic flow over a flat plate with a incident shock wave the C_{x_1} is taken as 0.5, and C_{x_2} close to 0.01. In the calculation for the ramp with the algebraic turbulence model, because a reasonable initial value is given, the term (c) is not necessary. In the calculation with the K-ϵ model, the term (c) is used to suppress the nonlinear oscillation caused by the large change of K and ϵ at the first steps then C_{x_2} decreases with time step Δt to reduce its effects.

The equation (5.33) can be expressed as

$$\Delta X^4 \left(C_1 \frac{\partial^2 P}{\partial X^2} \frac{\partial^2 U}{\partial X^2} + C_2 \frac{\partial^4 U}{\partial X^4} \right) + \text{higher order term},$$

When $\Delta X \to 0$, its value tends 0. Therefore, this term will not affect the accuracy and consistency of the MacCormack scheme.

5.5. Boundary Condition and Initial Data.

5.5.1. Explicit Boundary Condition.

All the conditions mentioned in Section 3.3 for $M > 1$ case are used. For the calculation using K-ϵ model the additional boundary

conditions for K, ϵ are as follows:

On the incoming flow boundary, the K, ϵ are specified.

On the outer boundary, $\frac{\partial K}{\partial \xi} = \frac{\partial \epsilon}{\partial \xi} = 0$.

On the upper boundary, $K = \epsilon = 0$.

On the solid wall, $K = 0$ and $\frac{\partial \epsilon}{\partial n} = 0$.

It is of note that in the approximating expression for the normal momentum equation on the wall for the high Reynolds number case, i.e. $\frac{\partial P}{\partial Y} = 0$, the P is static pressure rather than effective pressure P_t.

5.5.2 Implicit Boundary Condition.

On the incoming and upper boundary: because all the physical variables are specified in advance, $\delta U = 0$ is used.

On the downstream boundary: the mesh size is set large enough so that matrix $|A|$ vanishes and $\delta U = 0$ is used.

On the lower boundary: although several methods to deal with this implicit boundary condition have been proposed, it remains very difficult to give accurate implicit boundary conditions. Fortunately, only the steady state flow is under study and most of the flows on this boundary are viscous shear flow. Therefore implicit boundary conditions are less important than the explicit ones. Then two kinds of implicit boundary conditions are used: 1) if the lower boundary is a plane of symmetry, a reflecting boundary as mentioned in reference [20] is used. Namely, the results at $j = 2$ from the predictor step are saved to be used as a boundary condition for the corrector step that sweeps away from the wall; 2) if the lower boundary is a wall, $\delta U^{n+1} = 0$ is used.

5.5.3 Initial Value.

In the computational region, all the initial values are set to be equal to the value on the corresponding position of the incoming

boundary. At this boundary, the values of physical variables are easy to determine in the inviscid part. The field is a uniform flow field and the turbulent field variables K, ϵ are set to very small values. In the viscous flow region the mean field and K can be obtained from experimental data if available. Otherwise, we can use the following procedures:

For mean field flow

1) Select a C_{fw}.

2) Let P = constant = the value in the inviscid region.

3) Select a velocity profile such that for $Y^+ \leq 10$ 'the law of the wall' is used, and for $Y^+ > 10$ an exponential function is used.

4) The temperature distribution is determined by using

$$T = T_w + (T_{aw} - T_w)(u/u_e) + (T_\infty - T_{aw})(u/u_e)^2 \qquad (5.34)$$

where T_w is the temperature on the wall

T_{aw} is the adiabatic temperature and $T_{aw} = T_\infty(1+\sqrt[3]{Pr}\,\frac{\gamma-1}{2}\,M_\infty^2)$

5) The calculation of flat plate boundary layer flow with the initial values mentioned above is found by using the present programme in a smaller computational region.

6) By adjusting the values of C_{fw} and the power of the exponential function until the value of momentum thickness on one of the positions matches the experimental result.

The turbulent field variables K and ϵ, are obtained by integrating the equation some distance upstream, say $2\delta_0$, of the incoming flow boundary. At this position the distribution of K is assumed initially to be a triangular shape similar to the Klebanoff distribution. The peak value of K and its position in the η direction can be obtained from a number of trials. The turbulent dissipation can be determined from equation (4.17) since μ_t is known from the solution resulting

from the algebraic turbulence model and K is known from the above assumption. One can also first determine the turbulent length scale L_t from the Glushko length scale function. Then the relation $L_t = K^2/\epsilon$ can be used to obtain ϵ.

CHAPTER 6

THE COMPUTATIONAL RESULTS & DISCUSSION

Before discussing the computational results obtained by using the method discussed in Chapter 5, a simple reappraisal of the problem is appropriate.

It is clear that in the absence of viscosity, the intersection of a shock wave with a solid boundary would imply nothing more complicated than a discontinuity in surface pressure. In reality, of course, the fluid velocity decreases to zero at the wall through a laminar or a turbulent boundary layer and the shock wave will exist only in the supersonic part of flow. The result is that the disturbance propagates upstream through the subsonic region near the wall and the pressure at the wall is necessarily continuous. This results in a mutual interaction between the shock wave and boundary layer. The velocity profiles and the temperature profiles are thereby altered, as is the wave pattern in the external flow. The changes can be local if the shock wave is very weak but are observed on a large scale if the shock is strong enough to cause separation. The resulting flow field will be complicated as shown in Fig. 1.

The governing equations for this type of flow need effectively be the full N-S equations which are highly nonlinear and difficult to solve. Nevertheless, a considerable number of satisfactory solutions for laminar interaction, particularly for the 2-D case, have been achieved by using numerical methods. For turbulent interacting problems, the physical flow field is still governed by the N-S

equations but it is impossible to obtain the solution by directly solving the N-S equations as pointed out in Chapter 1. The Reynolds-averaged N-S equations, however, can accurately reflect the mean turbulent flow field, but its solutions will largely depend upon the quality of the turbulence model. The difficulty in obtaining accurate solutions is not only due to the requirement of finer mesh spacing and the increase of the degree of nonlinearity of the set of equations because of the addition of the turbulence model but are also due to the lack of accurate turbulence models for nonequilibrium boundary layers. Resulting from the lack of understanding of the mechanism of turbulent flow, the turbulence models widely used today have been developed from incompressible equilibrium boundary layer models with the addition of several empirical constants. Even though Morkovin had pointed out that the turbulence structure would not be expected to be affected by compressibility as long as Mach number fluctuations are much less than unity (so that the density fluctuations are small compared to the averaged values[87]), there remains a question of whether these models work well in a flow with a strong compression caused by a shock wave and in the resulting nonequilibrium boundary layer.

The present research work reflected in the results presented in this chapter and in Figs 5 to 9 was attempting to investigate the behaviour of three different turbulence models in an interacting flow caused by a supersonic turbulent flow over a ramp, by using the numerical solution of the Reynolds-averaged N-S equations. These models are, a) the Cebeci-Smith two-layer algebraic model (referred to as the C-S model), b) the C-S model with an upstream relaxation modification (referred to as the Relaxation model), c) the Jones and

Launder's K-ϵ two equations model (referred to as the K-ϵ model). Four flow regimes have been investigated, namely 1) an interaction between an oblique shock wave and a laminar boundary layer in supersonic flow, which is used for verifying the numerical scheme as it was not concerned with the turbulence modelling problem, 2) an interaction between an oblique shock wave and a turbulent boundary layer in supersonic flow, which is used to verify the implicit treatment of viscous stress in the calculation for turbulent flow, 3) the supersonic turbulent flow over an isothermal ramp, which case constitutes the main element of the validation of the method in which the behaviour of three different turbulent models and the effect of Reynolds number are investigated; 4) supersonic turbulent flow over an adiabatic ramp.

6.1. The Adjustment of Empirical Constant f_μ in K-ϵ Model

The Jones-Launder's K-ϵ model was developed from Hanjalic's model[45]. In order to provide predictions of the flow within the viscous layer adjacent to the wall, Jones and Launder made modifications in three ways. They are 1) viscous diffusion of K and ϵ must be included; 2) further terms must be added to account for the fact that the dissipation processes are not isotropic; and 3) the terms containing C_2 and C_μ will become dependent upon the local Reynolds number of turbulence. Based on their analyses the necessity and correctness for the first two modifications are obvious. These were not changed in this work. The third consideration leads to two additional Reynolds functions f_2 and f_μ which appear in equations (4.20) and (4.22). The function f_2 was chosen so that the model, when applied to the calculation of the decay of isotropic grid turbulence, accorded with experiment for both high and low turbulence intensities.

The function f_μ was obtained by equating the values of μ_t from equation (4.21) to those from the Van Driest form of the mixing length formula as applied in a calculation for a constant stress Couette flow. There exists, then, a logical reason to adjust these functions to obtain better results for different flow configurations. Coakley used different empirical constants in his calculations for transonic flow over an airfoil. These are $C_1 = 1.45$, $C_2 = 1.92$, $C = 0.09$, $C_{e1} = 2/9$, $C_{e2} = 36$, $f_\mu = \exp(-C_d/(1+0.02\ R_t)^2)$ and $C_d = 3.4$. His main modifications involved f_μ and f_2.

The present work is directed towards prediction of supersonic turbulent flow over an isothermal ramp. In order to examine the effect of further adjustments on f_μ and f_2, a series of investigations were carried out early on in the research programme using Case 3 - D. The final choice of adjustment was primarily made from a judgement upon obtaining consistent results between the calculations using the K-ϵ model and using the algebraic model and the experimental data in the part of the equilibrium boundary layer, and then from obtaining better results in and downstream of an interacting region. The initial test showed that the values of empirical constants used by Coakley produced better results than the original model but gave a larger values of C_f on the flat plate. Because the value of C_d would directly affect the eddy viscosity and the velocity profiles and to avoid complicated formulation, attention was concentrated on the modification of C_d. A further investigation indicated that a small value of C_d in the expression for f_μ overpredicts C_f and underpredicts the position of the separation point and the pressure propagation upstream, and vice versa. In Figs 11-1 and 11-2 are presented the results from two different values of C_d. The Model (1) implies C_d =

4.0 is used and the Model (2) indicates C_d = 3.6 is used. In the present calculations for Case 3, the value of 4.0 for C_d was used, but otherwise the remaining emprical constants as selected by Coakley were used. The computed results from this modification showed better predictions of velocity profiles were obtained close to the wall, which resulted in better C_f distribution even downstream of the attachment point.

In the calculation for adiabatic wall, the empirical constants given by Coakley were used.

6.2. Computed Results and Comparisons.

All the calculations were carried out on the Glasgow University ICL 2988 mainframe computer. The initial flow parameters for these calculations are shown in Table 2. The computational mesh used is that as described in Chapter 5 and as shown in Fig.2, i.e., in the X direction a uniform spacing is used and in the Y direction the grid is composed of a fine mesh and a coarse mesh. The height of computational region is roughly 4 times the thickness of the incoming boundary layer. All the mesh parameters are also listed in Table 2. The computational boundary conditions are those described in Chapter 3 for the explicit operator and in Chapter 5 for the implicit operator.

The convergence criterion has been chosen to be based on changes of wall parameters, because it has been reported and also been found in our calculations, that these parameters, particularly the skin friction coefficient C_f, are the most sensitive. If the ΔP indicates the maximum change of pressure on the wall between time $n\cdot\Delta t$ and $(n+1)\cdot\Delta t$, and ΔC_f expresses the maximum change of skin friction coefficient in the same time interval, the following joint criterion $|\Delta P| \leq 0.1\times10^{-4}$ and $|\Delta C_f| \leq 0.3\times10^{-7}$ are used to judge the convergence

of solutions.

6.2.1. Case - 1. An Interaction between an Oblique Shock Wave and a Laminar Boundary Layer in Supersonic Flow.

The computational region is a rectangular one as shown in Fig. 2-a. The flat plate is symmetrically placed between j = 1 and j = 2, and the leading edge is placed between i = 3 and i = 4. At the upper boundary, the parameters are set either to free stream values or the appropriate post-shock values thereby generating a shock towards the plate. All the results are shown in Figs 3-1 to 3-8.

Figs 3-1 and 3-2 present the distribution of wall pressure and skin friction coefficient. They show very good agreement between computational results and experimental data obtained by Hakkinen et al[84].

Figs 3-3 and 3-4 present velocity and pressure profiles within the flow field. Fig. 3-5 presents Mach number contours with an interval of 0.02, Fig. 3-6 shows the Mach number distribution and Fig. 3-7 provides pressure contours on the X-Y plane. These figures illustrate the effects of the leading edge and reflected shock wave system resulting from the separated region. The shock wave is spread over about 3 meshes in the x direction. These favourable results provide some verification of the numerical algorithm.

About 800 steps were needed to achieve a convergent solution, of which the first 400 steps Δt were taken as 0.018. Increased accuracy required a time step Δt gradually reducing to 0.005 or less for a further 400 steps to achieve the final convergent solution. The explicit scheme required over 5,600 steps[20] to achieve an acceptable level of convergence. Using the ICL 2988 computer, 0.32×10^{-2} sec/per point was required for the explicit algorithm to march one step whilst

0.4×10^{-2} sec/per point was required for the implicit algorithm. The gain in computational efficiency is evident.

6.2.2. Case - 2. An Interaction between an Oblique Shock Wave and a Turbulent Boundary Layer in Supersonic Flow.

This example is used to check the ability of the present scheme to calculate turbulent flow. The computed results of the wall pressure distribution, skin friction coefficient distribution and the velocity profiles are presented in Figs. 4-1 to 4-3. The simple comparison with Reference 17 which used MacCormack's hybrid scheme (1976), shows a good agreement between the computed values obtained by two different numerical schemes. This result further justifies the use of the simplified treatment of effective viscosity in turbulent flows.

Comparison with Example 1, demonstrates the differences between laminar and turbulent interactions. In turbulent flow, inherent flow fluctuations yield more momentum exchange between the outer layer and the inner layer of the boundary layer, which results in fuller velocity profiles than the laminar flow. Thus, a stronger interaction strength is needed to cause flow separation. In this demonstration case, there is no flow separation and the wall pressure distribution is similar to that obtained from an inviscid model.

The present method required roughly about 0.42×10^{-2} sec/per point and 1500 steps to achieve a convergent solution.

6.2.3. Case 3 - A to - D. Supersonic Turbulent Flow Over an Isothermal Ramp for a Reynolds Number, Re_∞/m, of $6.3\times10^7/m$.

For this flow, computations using the various turbulent models described in Chapter 4 are compared with experimental measurements of surface pressure, skin friction and velocity profiles. Also presented are comparisons of different computational results for eddy-viscosity

and the height of the separated flow region. Figs 5-1 to 5-10 present the results on an 8° ramp. Figs 6-1 to 6-9 are the results on a 16° ramp, Figs 7-1 to 7-11 the results on a 20° ramp and Figs 8-1 to 8-11 the results on a 24° ramp. The experimental data are taken from Reference 85.

Surface Parameter Predictions

Figure 5-1, 6-1, 7-1, 8-1 describe the wall pressure distributions for different ramp angles and the comparisons between computations and experimental results. It has been shown that when the pressure disturbance is so small that it will not cause flow to be separated, such as those caused by a ramp angle less than or equal to 16°, the three turbulent models can give excellent agreement with experimental results. If the ramp angle is increased further, flow separation appears and the computations employing different turbulent models present quite different behaviour. The computations using the C-S model can predict the overall pressure rise well but do not predict the location of initial pressure rise and the presence of a pressure "plateau". It underpredicts the upstream propagation of the pressure and overpredicts the value of the wall pressure in the region just behind the corner. The use of the C-S model with the relaxation modification gives , however, significant improvement. It detects a pressure "plateau" and the upstream propagation of the initial pressure rise in an acceptable way. The computations employing the K-ϵ model obviously give the best results in all respects, particularly in the situation where the pressure gradient is high, although the level of the pressure "plateau" is slightly overpredicted.

In Figs 5-2, 6-2, 7-2, 8-2, are presented the distribution of skin

friction coefficients. Generally, the computations employing any one of the three models can predict the separation point very well, although with the strengthening of interaction there do appear differences. At $\alpha = 24^{\circ}$ the results from using the C-S model predict a delayed position of the separation point whilst the results from using the relaxation modified model predict a slightly early position. The computations employing the K-ϵ model give very good agreement with experimental results. All the computations predict very well the distribution of skin friction coefficients in the region before the separation point, but they predict poorly the position of reattachment point and the skin friction coefficients in the region near and downstream of this point. The computations using K-ϵ model give comparatively much better results than the others and the computations employing the C-S model and the one using the modified C-S model give much worse results, between them there is little obvious difference.

Velocity Profile Predictions

Computed and measured velocity profiles throughout the flow field are shown in Figs 5-3, 6-3, 7-3, 8-3. It can been seen that in the region before the interaction or when the interaction is rather weak, such as that caused by an 8° ramp, the agreement between computed value and measured data and between computational results obtained by using different turbulent models is excellent. With the interaction strengthening, however, disagreement appears in the separated region and downstream. The computations employing the C-S model show a delayed response to the disturbance. In the vicinity of the separation region this computation overpredicts the velocity profile. Furthermore, in the region near and downstream of the reattachment

point it underpredicts them before undergoing a slow recovery to its equilibrium state. The use of the modified C-S model shows a considerable improvement in the prediction of the velocity profile in the region near the separation point, but it agrees with the results from the C-S model in the region near and downstream of reattachment point. In contrast, the computations employing the K-ϵ model show a fast reaction to a disturbance and a very quick recovery further downstream. Generally, the use of the K-ϵ model results in too large a retarded flow in the separated region in that part away from wall. In the vicinity of the wall, however, it gives much better results. For example in the region near and downstream of the separation point it can predit a larger negative velocity value, followed by more full velocity profiles further downstream. These results are consistent with the skin-friction coefficient distribution discussed earlier.

Figs 7-7, 7-8, 8-7 and 8-8 present respectively the computed height of the zero velocity line and the dividing stream line. It is seen that in the region before the corner the computed height of the separation bubble using the C - S model is smaller than the results from the other two models. This explains why the predictions of wall pressure distribution have differences.

The Mach Number & Density Contours

In Figs 5-7, 6-7, 7-9, 8-9-1 and 8-9-2, the Mach number contours are presented in intervals of 0.045 or 0.05. In Figs 5-8, 6-8, 7-10, 8-10-1 and 8-10-2, the density contours are presented in an interval of 0.02. These figures give a physical view of the computed flow field. Because the initial boundary layer is very thick, these figures mainly reflect the development of the flow field in the boundary layer. But it can be seen that with increasing ramp angle,

the position of the initial rise of density moves forward. After this rise in density there occurs a gradual compression followed by a more stronger one. Unfortunately, there were no interferograms available with which to compare these trends.

The Profiles of the Turbulent Kinetic Energy

Figs 5-5, 6-5, 7-5 and 8-5 show the profiles of the turbulent kinetic energy. These figures illustrate clearly an amplification of the turbulent kinetic energy after a shock wave as seen by the differences ocurring between $n/\delta_0 = -1.33$ and -0.44 in Fig. 8-5 for example.

The Heat Transfer Coefficient

Figs 5-9, 6-9, 7-11, 8-11 present the heat transfer coefficients, Ch, for 8°, 16°, 20° and 24° respectively, which is calculated from the formula $Ch = \mu_w \sec\alpha \frac{\partial T}{\partial Y} / [(Pr\ Re_{\infty L})(T_{o\infty} - T_w)]$[31].

The changes of Ch along the wall are generally consistent with the change of local skin friction coefficient C_f obtained by using the same turbulence model except that a pulse is found near the corner. At first, the amplitude of the pulse increases with ramp angle, then decreases rapidly after the appearance of the flow separation. It is difficult to explain this result physically. After a detailed survey, it was concluded that the pulse may be attributed to an inconsistency between the pressure gradient and the density gradient calculated from the computed results in the region adjacent to the corner. From Fig.5-10, it can be seen that just before the corner the rise of density is slightly greater than that of the pressure which trend is reversed after the corner. This results in an oscillation of the assessed temperature distribution. Furthermore, because the wall temperature is very near the stagnation temperature of the free

stream, a very small relative error, such as 0.004, is capable of contributing to this pulse. There are many reasons that could cause so small an error in such a region where parameters change rapidly. In fact, the cases examined are not good examples for studying heat transfer. Unfortunately, there is no experimental data suitable for comparison. Any differences that occur between the computed results from different models appear in the separation region and downstream. These again give weight to the observation that all of these models can well predict equilibrium turbulent boundary layers, but non-equilibrium ones less ably.

Eddy Viscosity Profile

Figs 5-6, 6-6, 7-6 and Figs 8-6 show the eddy viscosity profiles in different streamwise positions for 8°, 16°, 20° and 24° ramps. These illustrations help to understand why different turbulence models give different predictions. It is seen that at the position $X/\delta_0 = -0.246$ for the 16° ramp, $X/\delta_0 = 0.16$ for the 20° ramp and position $X/\delta_0 = -0.44$ for the 24° ramp the upstream relaxation process and the K-ϵ model reduce the value of the eddy-viscosity coefficient in the region away from the wall compared with the C-S model. This reduction leads to less turbulent mixing and less shear stress to balance the adverse pressure gradient, making the separation easier and allowing a larger upstream pressure rise. Furthermore in the region very close to the wall, use of the K-ϵ model usually predicts a larger value of μ_t and this reflects enhanced turbulence mixing leading to a fuller velocity profile in that region.

The Choice of Upstream Relaxation Parameters

In the last paragraph we have discussed the effects of the upstream relaxation process. Although no details were given to allow

comparison of the effect for different choices of relaxation parameters, the practical investigations showed that the use of different parameters will result in different results. In the calculations for the isothermal ramp at a Reynolds number of 6.3×10^{7}/m, the relaxation parameter λ chosen to be equal 1 is found suitable. A larger value of λ will produce too large a separation region and overpredicts the extent of upstream pressure influence. But in a later calculation for a 25° ramp with adiabatic wall and Reynolds number of 3.28×10^{7}/m it is found that $\lambda = 5$ is needed. The position X_0 is usually chosen at the place where the initial pressure rise starts.

Computational Efficieney

Usually, the computations using MacCormack's explicit scheme require at least 42,000 steps[20] to obtain a convergent solution for this type of flow. With the ICL 2988 computer, it needs 0.345×10^{-2} sec/per point to complete a step calculation for an explicit scheme using the C-S model, whereas, by using the present scheme it requires 0.42×10^{-2} sec/per point for the C-S model, 0.3×10^{-2} sec/per point for the modified C-S model and 0.64×10^{-2} sec/per point for the K—ϵ model to complete one step calculation and needs less than 2,500 steps to obtain an acceptable level of convergence. It is clear that the present implicit is much more efficient than the earlier explicit scheme.

Assessment of Turbulence Models

From the above comparisons, it is clearly seen that the K-ϵ model gives the best results among the three models, although it does not predict well the reattachment point and the skin coefficient distribution in the region near and downstream of this point.

However, it requires much more computing time to complete one step calculations and also it needs some extra additional procedures in the program to avoid the occasional occurrence that K or ϵ takes a negative value in the vicinity of the wall. The C-S model with the relaxation modification gives the worst results in predicting the position of reattachment and the downstream wall skin friction coefficient, but gives a very good prediction of the wall pressure distribution and the position of separation point. Because of its simplicity, this model is still a useful one for initial engineering evaluation, but the choice of relaxation parameter would be different depending on the configuration chosen. The C-S model gives the worst results except in its predicting the overall pressure rise. These results can be explained as follows.

The C-S model is based on the local equilibrium between mean-motion and turbulent motion, it can meet with great success in the calculation of the equilibrium boundary layer but fails to predict the non-equilibrium boundary layer with large adverse pressure gradients. The upstream relaxation modification takes turbulent flow history effects into account, particularly in the region near the separation point so that an improvement is achieved. The K-ϵ model considers the effects of the transport of turbulent flow field variables to provide, the best results, as compared to the application of the other two models. These eddy-viscosity models are generally based on the assumption that the turbulent stress responds immediately to changes in strain rate of mean motion and their deficiency is evident.

6.2.4. The Effects of Reynolds Number (Case - 4).

A comparative calculation for a 20° isothermal ramp with Reynolds

number of 3.1×10^8/m is carried out to investigate the effects of Reynolds number. Figs 9-1 to 9-10 present computational results. The present computations gives similiar results to those of Case 3 - C which is carried out at a Reynolds number of 6.3×10^7/m, but the present computations appear to give better agreement.

The comparisons between the two computations show that the rise of Reynolds number will cause the reduction in the extent of upstream pressure influence, the length of separation region, the distance between separation point and the corner, and the height of the separation region. The Table 3 shows the comparisons of the locations of separation point and reattachment point between the computed value and the measured value from Case 3 - C and Case - 4.

T A B L E 3

The Effects of Reynolds Number on Separation Region

Case No.	Turbulence Model	X_S mm	X_R mm
3 - C	Experimental Results	-11.2	4.1
3 - C	C-S	-10.88	14.76
3 - C	K-ϵ	-11.76	7.99
4	Experimental Results	-5.3	2.3
4	C-S	-6.08	8.09
4	K-ϵ	-7.14	6.49

where X_S is the position of the separation point.

X_R is the position of the reattachment point.

6.2.5. Case - 5. Supersonic Turbulent Flow over an Adiabatic Ramp for a Reynolds Number, Re_∞/m, of $3.28\times10^7/m$.

Figs 10-1 to 10-7 give the results from the calculations using the K-ϵ model and the C-S model with upstream relaxation modification (relaxation model) for a supersonic turbulent flow over a 25° adiabatic ramp. In the present calculations, all the empirical constants in the K-ϵ model are taken as the same value as used by Coakley however a larger value of relaxation parameter λ, for example 5, for the relaxation model is found necessary. The use of different values for these empirical constants for different flow cases may lead to the same conclusion that it would be unrealistic to expect that there is a universal turbulence model with a fixed set of universal constants. Fig. 10-1 and Fig. 10-2 present the distributions of the wall pressure and skin friction coefficient separately and the comparisons between the computed results using the two turbulence models and the experimental results which are from Reference 17. These comparisons again favour the choice of K-ϵ model. Fig. 10-3 and Fig. 10-4 show the velocity and density profiles. Fig. 10-5 presents the turbulent kinetic energy profiles. Fig. 10-6 and Fig. 10-7 give the separation region and the height of the zero velocity and dividing streamlines.

6.3. Computational Efficiency.

In Section 6.2, it is seen that the present numerical scheme is much more efficient than explicit schemes.

Compared with the Beam-Warming scheme, which is considered a typical implicit scheme in that it is required to invert a single

block tridiagonal system, the present scheme can be expected to be more efficient if the computational mesh is set up reasonably well. The investigation showed that the two block diagonal systems can be inverted about 10% more quickly than one block tridiagonal system, however the MacCormack's implicit scheme needs to calculate the Jacobians A and B and the explicit operator twice, so that the computing time needed for the two schemes is almost the same. The chief advantage arises because the present scheme allows the implicit step to be suppressed in regions where the explicit stability restriction is satisfied so that the computational efficiency is obtained. The test on a CDC 7600 for present the case indicated that the Beam-Warming scheme required 4.61×10^{-4} sec/per point, and the MacCormack's implicit scheme only needs 2.45×10^{-4} sec/per point. The additional calculation required for the artificial damping term in the present scheme only increases slightly the computing time. On the ICL 2988 it takes about 1.2×10^{-4} sec/per point.

The present method is slightly more efficient than MacCormack's hybrid scheme for lower Reynolds number calculations and, at most, twice as fast for the higher Reynolds number calculations[20].

During the calculations, it is found that MacCormack's scheme has a disagreeable defect in that the "steady state" solution is time dependent, particularly for the skin friction coefficient as seen in Figure 12. In order to decrease the dependence of the solution on Δt, the calculations at the first 1,000 ~ 1,500 steps are used to achieve an initial convergent solution using a large time step size Δt, then the time marching size Δt is successively reduced in a further approximately 1,000 steps to ensure the accuracy of the solution. Even then it is found that the residual of solution change will not

approach machine zero, but will oscillate arround it. This can be attributed to the approximation of factorization and the MacCormack's two step method. As it has been pointed in Chapter 5, the approximation of factorization will introduce an error when the C.F.L number is large. The MacCormack implicit scheme is used twice for this kind of approximation to achieve two block bidiagonal systems. The value of C_f is determined simply from flow field parameters near the wall where the C.F.L number is very large. The errors caused by large Δt are evident. Furthermore, the predictor and corrector steps of this scheme are of different type, usually one-side forward or backward difference operators. As a steady state solution is approached, if by chance one step satisfies the converged solution requirement, the other, using the same solution data but in a different manner, will most likely calculate a solution change of the order of the truncation error of the difference equations. Thus, a pseudo unsteady fluctuation of the numerical solution about the steady state solution is obtained. This is a nuisance and will produce a harmful effect on computational efficiency.

CHAPTER 7

CONCLUSIONS AND FUTURE WORK

7.1. Concluding Remarks.

Numerical solutions of the compressible Navier-Stokes equations for a complex flow caused by the interaction between a shock wave and a boundary layer have been obtained. For turbulent flow, three types of turbulence models are used. These models are the Cebeci-Smith (C-S) model, the C-S model with a relaxation modification and the two-equation K-ϵ model. These numerical solutions have been compared with the experimental measurements listed in References 84 and 85 respectively. Based on these results, the following specific conlusions can be made:

1. The original MacCormack's full implicit scheme (1981) with some new developments as outlined in Chapter 5 has been successfully developed using complex multi-equation turbulence models for use in calculations for those 2-D separated flows caused by interactions between shock waves and boundary layers. These new extensions retain the main advantages of the original scheme, such as second order accuracy, block bidiagonal form etc., but offer more ability to control nonlinear instability. The restricting conditions for values of K and ϵ, found necessary in other numerical schemes, have been removed. By using the same development further extension into the calculation for Reynolds stress models and 3-D flows is expected to be possible.

2. This scheme has three main advantages over conventional full

implicit methods. First, it only needs solution of block bidiagonal systems of algebraic equations, which are less costly to invert and more easy to program than the block tridiagonal systems found in conventional implicit schemes. Second, it employs effective viscous terms added to the Eulerian eigenvalues. This maintains the stability while avoiding the use of complete Jacobians for viscous stress and source terms, whose processing usually involves more computing time and in some cases leads to impossibility in derivation when using high order turbulence models. Finally, the algorithm allows the implicit step to be dropped automatically in regions where the explicit stability restriction is satisfied.

3. The present scheme is much more efficient than earlier explicit schemes as pointed at in Chapter 6. Compared with MacCormack's hybrid scheme, it is slightly more efficient than that scheme for lower Reynolds number calculations and, at most, twice as fast for the higher Reynolds number cases. Compared with Beam and Warming's scheme, it is easier to program and to be extended to calculations for complex turbulent models, although it is only a little more effcient. This is because it is possible to invert the two block diagonal systems required ten per cent more quickly than the single tridiagonal system in the former, and also some points in the field can be calculated explicitly in the latter.

4. Through comparisons with experiments, the scheme developed can very well predict laminar separated flow caused by the interaction of an incident oblique shock wave and a laminar boundary layer. For turbulent flows we can make the following general conclusions.

i) The most successful predictions obtained involve the wall pressure distribution. When the flow is near the equilibrium state,

all three turbulence models give excellent agreement with experimental results. When the interaction is strong, the computations employing the K-ϵ model and the C-S model with upstream relaxation modification give more accurate prediction than C-S model with the former model providing the best results.

ii) No single model correctly predicted surface skin friction downstream of the corner. However, the computations employing the K-ϵ model give a considerably better prediction than other two.

iii) The separation point is generally predicted to a reasonable accuracy. Although none of the three models predicted the locations of reattachment point, again results favoured the use of the K-ϵ model.

iv) The deficiency of the present computed results may be attributed to the assumption underlying eddy-viscosity models that the turbulent stress responds immediately to the local change in strain rate of mean motion. Use of a Reynolds-stress model or a full eddy simulation approach are expected to give more accurate prediction for these complex flows.

5. In spite of its advantages, the practical calculations showed that this scheme does have inherent defects. These are as follows.

First, although this scheme is unbounded in time marching step Δt, a limited time step Δt is used in practise in order to prevent errors caused by the factorization approximation.

Secondly, it has been found that the "steady state" numerical solutions resulting from this scheme are time step Δt dependent and the residual of the solution change will never reduce to machine zero. Because the finite difference operators of this scheme's predictor and corrector steps are of different type, usually one-side forward or

backward difference operators, as a steady state solution is approached, if by chance one step satisfies the converged solution requirement, the other, using the same solution data differently, will most likely calculate a solution change of the order of the truncation error of the difference equations. Thus, an unwelcome pseudo unsteady oscillation of the numerical solution about the steady state solution is obtained.

Further, in this scheme it is difficult to give a correct implicit boundary condition at the solid surface, unless the operator, which carries out the calculation to move away from this boundary, is revised locally. But this revision will destroy the block bidiagonal form of the operator. As has been pointed our in Appendix 5, the incorrect implicit boundary will increase the number of computational steps required to approach a convergent solution and in the extreme it might cause computational instability.

These shortcomings are the price to be paid for using a second-order accurate implicit scheme which only needs the inversion of a block bidiagonal matrix. The last two defects might be the fatal weakness of this scheme.

7.2. Future Work.

7.2.1. Further Improvement in Numerical Scheme.

Although the present algorithm is much more efficient than the explicit algorithm and it also possesses some advantages over other popular implicit algorithms, there do exist some aspects to be improved. These include:

1) Further enhancement of the convergent rate.
2) Removal of the character of the dependence of the steady state solution on time step Δt.

3) Introduction of a correct implicit boundary condition.

4) Reduction of the error caused by the approximate factorization.

5) Improvement of the ability for self control of nonlinear oscillations.

One way to improve problems from 2 to 4 listed above is to directly resolve the set of equations (3.15) of the implicit scheme, rather than to use approximate factorization or MacCormack's block bidiagonal method. This requires the inversion of a block pentadiagonal matrix in two-dimensional flow and a block septadiagonal matrix in three-dimensional flow. These manipulations are much more difficult than that of a block tridiagonal or block bidiagonal matrix. But, an indirect iterative procedure can be used for inversion in the expectation that only a few iterations will be required for each time step. Although, it will take more computer time in one marching step, the large size of the time step could make up for this loss so that an enhancement in convergent rate would be expected.

Recently, Mulder and Leer[86] proposed a method in which they used Newton's method to construct an implicit algorithm to speed the convergent rate. In one-dimensional linear problems, it only needs less than twenty steps to obtain excellent results. It would be profitable to extend this method to multidimensional and nonlinear problems, particularly for turbulent flow. Furthermore, the behaviour of this numerical scheme using the flux splitting approach in complex flow situations whose advantage is that additional artificial damping term is usually not required, should be investigated.

7.2.2. Turbulence Modelling.

The present investigation is only restricted to supersonic flows. In order to obtain a complete picture of the behaviouer of the types

of turbulent model, examined, the study should be extended into transonic and hypersonic flows.

The failure of prediction in the region downstream of the separation point, however, has shown the deficiency of the eddy-viscosity model and the need for examination of Reynolds stress models or the large eddy simulation method.

TABLE 1.

Author	Flow State	Problem	Initial Conditions & Turbulence Model	Numerical Method
J.E.Carter [13]1972 [47]1973	Laminar 2-D	1	Plane flow past a compression corner a) M_∞=3 α=10° $Re_\infty=1.68\times10^4$ b) M_∞=6.06 α=10.25° $Re_\infty=1.5\times10^5$ c) M_∞=4 α=10° $Re_\infty=6.8\times10^4$	Brailovskaya's scheme grid (77x28) (129x36) (121x36)
R.W.MacCormack [48]1971	Laminar 2-D	2	M_∞=2 P_f/P_∞=1.4 $Re_{\infty L}=2.84\times10^5$	MacCormack's scheme with time-splitting
M.Hanin etal [49]1974	Laminar 2-D	2	M_∞=2 P_f/P_∞=1.4 $Re_{\infty L}=2.96\times10^5$ P_f/P_∞=1.91 $Re_{\infty L}=3.29\times10^5$	Brailovskaya's scheme grid (20x50)
G.S.Deiwert [50]1974	Turbulence 2-D	3	M_∞=0.775 $Re_{\infty C}=(1,2,4\&10)\times10^6$ simple mixing length model	MacCormack's scheme with time-splitting grid (50x38)
D.C.Wilcox [51]1973	Turbulence 2-D	2	M_∞=2.96 P_f/P_∞=5.10 $Re_{\infty\delta}=2.5\times10^5$ & 10^6 P_f/P_∞=5.1 or P_f/P_∞=3.72 $Re_\delta=2.5\times10^5$	AFTON 2 PT code grid (1007~3885) mesh points)
D.C.Wilcox [52]1974	Turbulence 2-D	1	M_∞=2.96 α=20°, 26° $Re_{\infty\delta}=2.5\times10^5$~$10^6$ Saffman turbulence model eqs.	AFTON 2 PT code grid (1007~3000 points)
R.W.MacCormack B.S.Baldwin [53]1974	Turbulence 2-D	2	M_∞=8.47 P_f/P_∞=83 $Re_{\infty L}=22.5\times10^6$ C-S & Saffman-Wilcox's turbulence model eqs.	MacCormack's explicit scheme with time-splitting 4 mesh system in Y total grid (40x32)
R.W.MacCormack B.S.Baldwin [54]1975	Laminar	2	M_∞=2 P_f/P_∞=1.2 $Re_{\infty L}=2.84\times10^5$ P_f/P_∞=1.4 $Re_{\infty L}=2.96\times10^5$	MacCormack's scheme with time splitting grid (34x32)
C.M.Hung R.W.MacCormack [55]1975	Laminar 2-D	1	a) α=10° M_∞=3 $Re_{\infty L}=1.68\times10^4$ b) α=15°,18° & 24° M_∞=14.1 $Re_{\infty L}=1.04\times10^5$	MacCormack's explicit scheme with time-splitting a) grid (86x28) b) grid (90x30)

J.S.Shang W.L.Hankey [56]1975	Turbulence 2-D	1	M_∞=2.96 α=15°~25° $Re_{\infty L}=10^7$ C-S model with relaxation modification	MacCormack's explicit scheme with time-splitting grid (64x22)
J.S.Shang W.L.Hankey [57]1975	Turbulence 2-D	1	M_∞=2.96 $Re_{\infty L}=10^7$ C-S model with relaxation modification	MacCormack's explicit scheme with time-splitting grid (64x22)
C.C.Horstman et al. [58]1975	Turbulence 2-D	2	M_∞=6.7 $Re_\delta=2.3\times10^5$ modified C-S model	MacCormack's explicit scheme with time-splitting grid (48x78)
R.W.MacCormack [17]1976	Laminar Turbulence 2-D	2	M_∞=2.0 $Re_L=2.96\times10^5$ (Laminar) $Re_L=2.96\times10^6$ (Turbulene)	MacCormack's hybrid-scheme
J.S.Shang W.L.Hankey C.H.Law [59]1976	Turbulence 2-D	2	M_∞=2.96 $Re_L=1.2\times10^7$ θ_{shock}=7.93°~12.17° C-S model with relaxation modification	MacCormack's explicit scheme with time-splitting grid (64x30)
C.M.Hung R.W.MacCormack [60]1976	Turbulence 2-D	1	a) M_∞=2.96 $Re_L=10^7$ α=25° δ_0=0.01403 b) M_∞=8.66 $Re_L=2.2\times10^7$ α=27° T_w=298.33°K C-S model with relaxation modification	MacCormack's explicit scheme with time-splitting grid (63x31)
G.G.Mateer A.Brosh J.R.Viegas [61]1976	Turbulence Axisymmetric	4	M_∞=2.85 $Re_{/m}=6.3\times10^7$/m C-S model C-S model with relaxation modification a) global relaxation b) local relaxation	MacCormack's explicit scheme with time-splitting
J.R.Viegas T.J.Coakley [62]1977	Turbulence Axisymmetric 2-D	a)4 b)5	a) M_∞=1.44 $Re_{x0}=3.67\times10^7$ T_∞=200.3°K P_∞=5.94psia b) M_∞=6.85 $Re_{x0}=1.3\times10^7$ θ_{shock}=15° C-S model one-equation model	MacCormack's hybrid scheme
C.C.Horstman G.S.Settles I.E.Vas S.M.Bogdonoff C.M.Hung [63]1977	Turbulence 2-D	1	M_∞=2.85 $Re_{/m}=6.3\times10^7$/m α=20°, 24° δ_0=23.9mm C-S model C-S model with Pressure gradient correction C-S model with relaxation modification Kinetic Energy model (one-equation)	MacCormack's explicit Scheme with time-splitting
J.S.Shang [16]1977	Laminar 2-D	2	M_∞=2.0 $Re_L=2.96\times10^5$	Shang's hybrid scheme

T.J.Coakley J.R.Viegas C.C.Horstman [64]1977 [65]1977	Turbulence 2-D	a)1 b)4 c)5	a) M_∞=2.8 $T_w/T_t \cong 1$ α=20° $Re_{\delta o}=1.65\times10^6$ α=24° $Re_{\delta o}=1.33\times10^6$ b) M_∞=1.44 T_∞=200.3°K $Re_{xo}=3.67\times10^7$ c) M_∞=6.85 $Re_{xo}=1.3\times10^7$ C-S model one-equation model K-ϵ(Jones-Launder) model	MacCormack's hybrid scheme
R.M.Beam R.F.Warming [19]1977	Laminar 2-D	2	M_∞=2.0 $Re_L=2.96\times10^5$	Beam & Warming's implicit scheme
J.S.Shang W.L.Hankey [66]1977	Laminar 3-D	7	M_∞=12.5 $Re=1.21\times10^6$ wedge angle	MacCormack's explicit scheme grid (8x12x20) (8x20x28) (8x32x36)
B.S.Baldwin H.Lomax [67]1978	Turbulence 2-D	a)1 b)2	a) M_∞=2.85 α=24° $Re_{\delta o}=1.33\times10^6$ b) M_∞=3 $Re_{\delta o}=10^6$ Baldwin-Lomax algebraic model	Steger's implicit scheme grid (64x36)
J.R.Viegas C.C.Horstman [68]1978	Turbulence 2-D	a)1 b)2 c)4 d)6	a) M_∞=2.8 α=10°~24° $Re_{\delta o}=0.5\sim8.0\times10^6$ δ_0=2.5cm $T_w/T_t \cong 1$ b) M_∞=2.9 $Re_{\delta o}=1\times10^6$ θ_{shock}=7°,10°,13° c) M_∞=1.44 δ_0=2.5cm $Re_{\delta o}=0.5\times10^6$ d) M_∞=1.47 δ_0=0.4cm $Re_{\delta o}=0.5\times10^5$ C-S model one-equation model K-ϵ model (Jones-Launder) K-ω^2 (Wilcox-Rubesin)	MacCormack's hybrid scheme
C.M.Hung R.W.MacCormack [69]1978	Turbulence 3-D	7	M_∞=5.9 α=6°,12° T_w=297.2°K $Re_{/m}=0.3281\times10^6$ Escudier's Algebraic model	MacCormack's hybrid scheme grid (21x36x32)
J.S.Shang W.L.Hankey J.S.Petty [70]1978	Turbulence 3-D	8	M_∞=3.0 α=9.480 $Re_\infty=0.4\sim1.1\times10^6$ C-S type model	MacCormack's explicit scheme with time-splitting grid (17x33x33)
C.C.Horstman C.M.Hung [71]1979	Turbulence 3-D	7	M_∞=2.0~4.0 α=3.75~16° Algebraic model	MacCormack's hybrid scheme
C.M.Hung [72]1979	Laminar 3-D	9	M_∞=2.8 θ=15° attack angle α=0°~4°	MacCormack's hybrid scheme grid (45x34x20)

D.A.Johnson C.C.Horstman W.D.Bachalo [73]1980	Turbulence 2-D	12	M_∞=0.875 $Re_{/m}$=13.6x10^6/m C-S model K-ω^2 model (Wilcox-Rubesin model)	MacCormack's hybrid scheme
M.I.Kussoy J.R.Viegas C.C.Horstman [74]1980	Turbulence 3-D	10	M_∞=2.2 $Re_{/m}$=1.2x10^6 C-S model	MacCormack's hybrid scheme
C.M.Hung D.S.Chaussee [75]1980	Turbulence 3-D	11	M_∞=2.0 α=0°,4°,8° Θ=23° $Re_{\infty/m}$=11.42x10^6/m Baldwin-Lomax Algebraic model	Beam and Warming's implicit scheme MacCormack's hybrid scheme
D.S.Chausse T.H.Pulliam [76]1981	Laminar 2-D	13	M_∞=2.0 Re=10^4/ft	Steger's implicit methods
R.W.MacCormack [20]1981	Laminar 2-D	1	M_∞=2.9 Re_L=2.96x10^5	MacCormack's implicit scheme
Ajay Kumar [77]1981	Laminar 2-D	14	M_∞=5 P_∞=0.1013 Mpa T_∞=293°K Re_L=11x10^6	MacCormack's implicit scheme
T.J.Coakley [78]1981	Laminar 2-D	3	M_∞=0.786 Re_L=11x10^6	Coakley's implicit scheme grid (81x61)
E.Von Lavante W.T.Thompkins [79]1981	Laminar 2-D	15	M_∞=0.75 Re_∞=2.3x10^3	MacCormack's implicit scheme
D.Om M.E.Childs J.R.Viegas [80]1982	Turbulence 2-D	4	M_∞=1.28~1.48 $Re_{/m}$=4.92x10^6 K-ω^2 model (Wilcox-Rubesin model)	MacCormack's hybrid scheme grid (40x30)
T.J.Coakley [81]1983	Turbulence 2-D	3	M_∞=0.73 Re_∞=6.5x10^6 C-S model K-ϵ (Chien) model K-ω^2 (Wilcox-Rubesin) model Q-ω model	Coakley's modified flux splitting method grid (160x50)
M.Visbal D.Knight [82]1983	Turbulence 2-D	1	M_∞=2.9 $Re_{\delta o}$=0.76~7.7x10^6 α=8°,16°,20°,24° Baldwin-Lomax Algebraic model	Beam and Warming's implicit approximate factorization algorithm
C.M.Hung W.Kordulla [83]1983	Turbulence 3-D	16	M_∞=2.95 $Re_{/m}$=6.3x10^7/m C-S model	MacCormack's implicit scheme with time-splitting grid (40x32x32)

Problem 1 Supersonic flow over a ramp

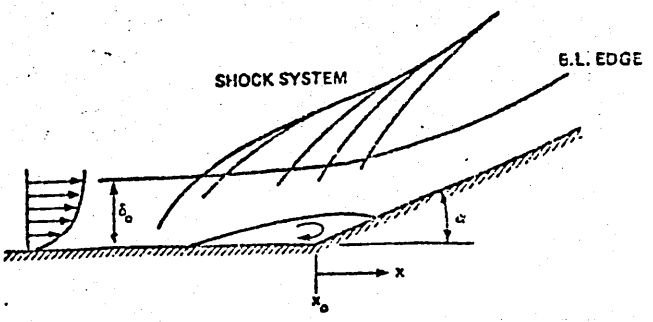

Problem 2 An incident shock wave on a flat plate

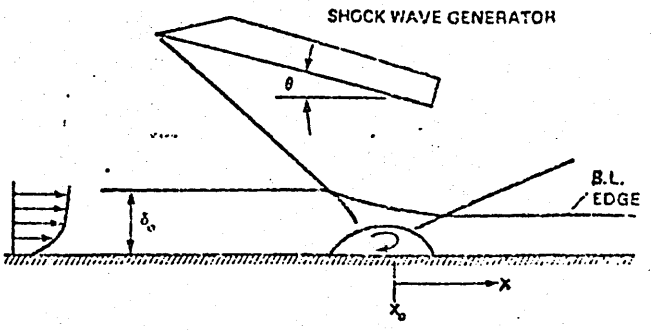

Problem 3 Transonic flow over an airfoil

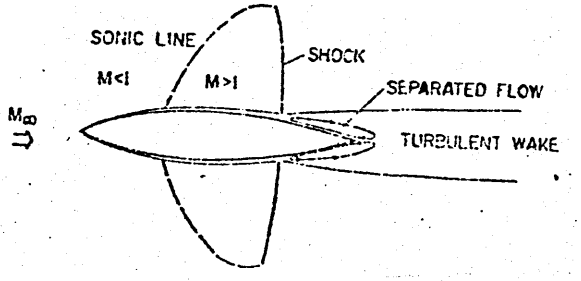

Problem 4 Axisymmetric, transonic, normal shock-wave boundary-layer interaction

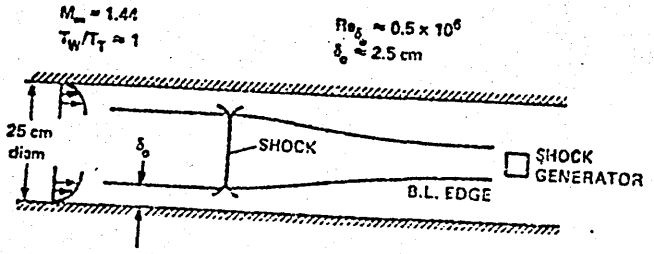

Problem 5 Hypersonic oblique boundary-layer interaction

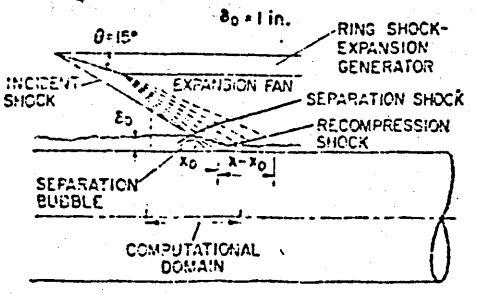

Problem 6 2 - D transonic, normal shock-wave boundary-layer interaction

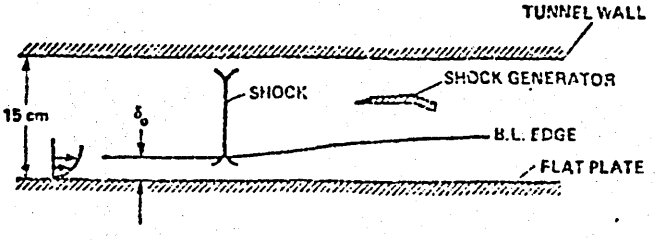

Problem 7 Supersonic flow over 3-D corner

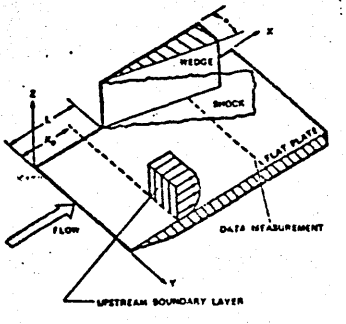

Problem 8 Supersonic flow over 3-D wedge

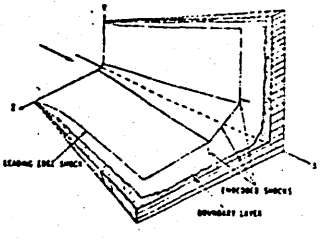

Problem 9 Supersonic flow over a incilined body of Revolution

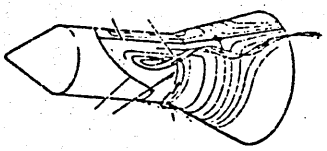

Problem 10 Supersonic 3-D interaction

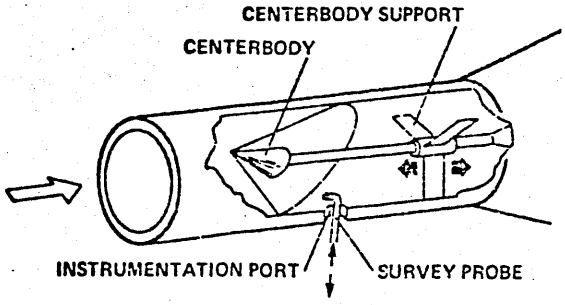

Problem 11 Supersonic turbulent flow over an inclined Ogive-Cylinder-Flare

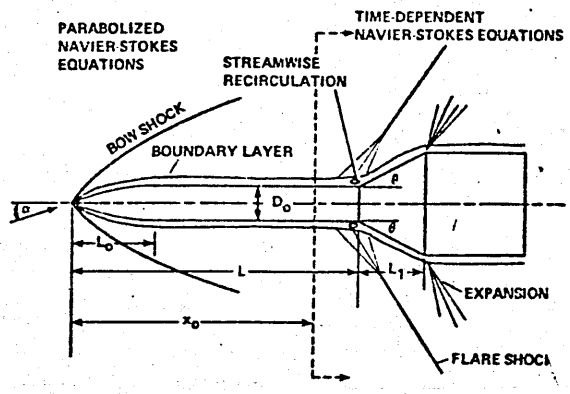

problem 12 Transonic flow over an axisymmetric "bump"

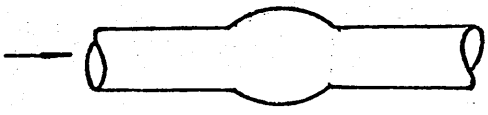

Problem 13 Supersonic laminar flow over a 2-D wedge inlet configuration

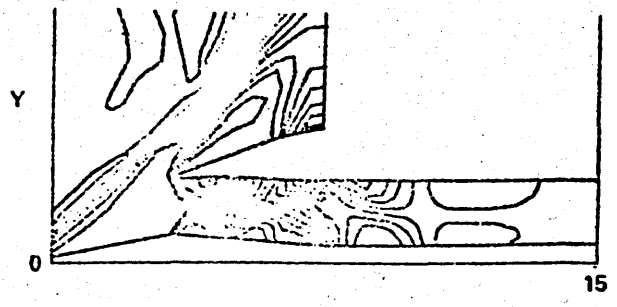

Problem 14 Supersonic flow over a 2-D inlet

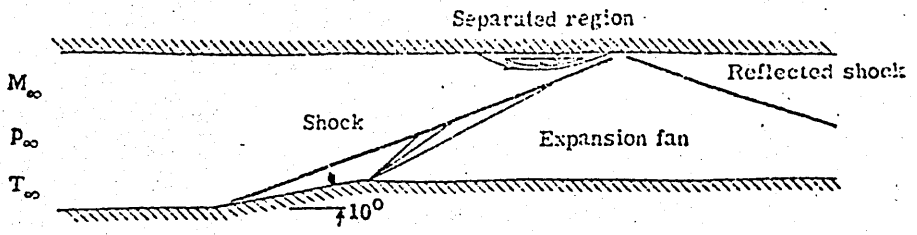

Problem 15 Supersonic diffuser

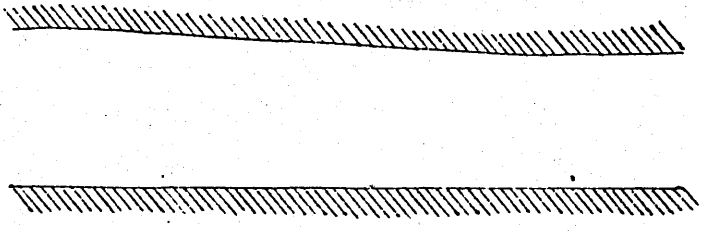

Problem 16 Supersonic flow over a blunt fin on a flat plate

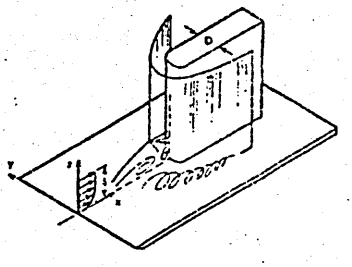

TABLE 2.

Computational Examples

Parameters \ Case	1	2	3 - A	3 - B
α	0°	0°	8°	16°
Re_{∞} /m	6.07×10^{6}	6.07×10^{7}	6.3×10^{7}	6.3×10^{7}
M_{∞}	2.0	2.0	2.87	2.85
$T_{0\infty}$ $^{\circ}K$	290	290	280	268
T_{∞} $^{\circ}K$	161.11	161.11	106	102
T_{w} $^{\circ}K$	Adiabatic wall	Adiabatic wall	291	282
P_{∞} N/m^2			2.3×10^{4}	2.4×10^{4}
δ_0 cm			2.6	2.6
δ_0^* cm			0.67	0.63
θ_{shk}	32.59	32.59		
Turbulence Model	Laminar	C-S model	1) C-S model 2) K-ϵ model	1) C-S model 2) C-S model with relaxation modification 3) K-ϵ model
Experimental Data	[84]		[85]	[85]
Computational Region and Grid Spacing (mm)	II = 36 JJ = 38 J_1 = 30 R_L = 48.77 ΔX = 2.68 ΔY_{min}=0.0427 ΔY_{max}=1.56	II = 36 JJ = 40 J_1 = 30 R_L = 48.77 ΔX = 2.68 ΔY_{min}=0.0055 ΔY_{max}=1.12 Y^{+}_{min}=2.45	II = 50 JJ = 34 J_1 = 26 I_{con} = 23 R_L = 26 ΔX=2.2414 ΔY_{min}=0.0061 ΔY_{max}=0.0427 Y^{+}_{min}=2.06	II = 50 JJ = 34 J_1 = 26 I_{con} = 20 R_L = 26 ΔX = 2.3091 ΔY_{min}=0.0061 ΔY_{max}=6.27 Y^{+}_{min}=2.10

T A B L E 2.

(Continuance)

Case / Parameters	3 - C	3 - D	4	5
α	20°	24°	20°	25°
Re_{∞} /m	6.3×10^{7}	6.3×10^{7}	3.1×10^{8}	3.28×10^{7}
M_{∞}	2.79	2.84	2.90	2.96
$T_{0\infty}$ $^{\circ}K$	258	262	275	270.4
T_{∞} $^{\circ}K$	101	100	103	98.333
T_{W} $^{\circ}K$	274	276	289	Adiabatic Wall
P_{∞} N/m^2	2.6×10^{4}	2.4×10^{4}	1.1×10^{5}	
δ_0 cm	2.5	2.3	1.8	0.4276
δ_0^* cm	0.66	0.61	0.46	
Turbulence Model	1) C-S model 2) C-S model with relaxation modification 3) K-ϵ model	1) C-S model 2) C-S model with relaxation modification 3) K-ϵ model	1) C-S model with relaxation modification 2) K-ϵ model	1) C-S model with relaxation modification 2) K-ϵ model
Experimertal Data	[8s]	[8s]	[8s]	[17]
Computational Region and Grid Spacing (mm)	II = 50 JJ = 34 J_1 = 26 I_{con}= 20 R_L = 25 ΔX=2.4581 ΔY_{min}=0.0061 ΔY_{max}=6.27 Y^{+}_{min}=2.22	II = 50 JJ = 34 J_1 = 26 I_{con}= 23 R_L = 23 ΔX=2.9143 ΔY_{min}=0.0061 ΔY_{max}=6.27 Y^{+}_{min}=2.28 for K-ϵ model II = 52 JJ = 35 J_1 = 37 ΔY_{min}=0.0017 Y^{+}_{min}= 0.635	II = 50 JJ = 34 J_1 = 26 I_{con}= 20 R_L = 18 ΔX=2.4581 ΔY_{min}=0.0012 ΔY_{max}=5.88 Y^{+}_{min}=1.998	II = 52 JJ = 34 J_1 = 26 I_{con}= 25 R_L = 4.27 ΔX=2.9143 ΔY_{min}=0.00486 ΔY_{max}=1.478

REFERENCE

[1] D.R. Chapman "Computational Aerodynamics Development and Outlook"
AIAA Journal Vol.17, No.12, pp.1293-1313
Dec. 1979
AIAA Paper 79-0129, 1979

[2] P. Kutler "A Perspective of Theoretical and Applied Computational Fluid Dynamics"
AIAA Paper 83-0037, 1983

[3] J.S. Shang "An Assessment of Numerical Solution of the Compressible Navier-Stokes Equations"
J. Aircraft Vol.22, No.5, pp.353-370, 1985
AIAA Paper 84-1549, 1984

[4] H.H. Pearcey "Shock-Induced Separation and Its Prevention by Design and Boundary-Layer Control"
In Boundary Layer and Flow Control,
ed. G.V. Lachmann, Vol.2, pp. 1166-1344
New York: Pergamon 1961

[5] J.E. Green "Interactions between Shock Waves and Turbulent Boundary layers"
Prg. in Aerospace, Sci. 11: 235-340, 1970

[6] W.L. Hankey
M. S. Holden "Two-dimensional Shock-Wave Boundary layer Interaction in High Speed Flows"
AGARDograph No.203 1975

[7] R.W. MacCormack
H. Lomax "Numerical Solution of Compressible Viscous Flows"
Ann. Review Fluid Mechanics 11: 289-316, 1979

[8] T.C. Adamson
A.F. Messiter "Analysis of Two Dimensional Interactions Between Shock Waves and Boundary Layers"
Ann. Review Fluid Mechanics 12: 103-138, 1980

[9] Dany D. Vandromme
H. Ha Minh "Solution of the Compressible Navier-Stokes Equations: Application To Complex Turbulent Flows"
VKI-LS-1984-04 'Computational Fluid Dynamics', 1984

[10] J.C. Le Balleur
H. Viviand
R. Peyret "Numerical Studies in High Reynolds Number Aerodynamics"
Computers and Fluids Vol.8. pp. 1-30, 1980

[11] F. Thomasset "Implementation of Finite Element Methods for Navier-Stokes Equations"

Springer-Verlag, Berlin, 1981

[12] R.W. MacCormack "The Effect of Viscosity in Hypervelocity Impact Cratering"
AIAA Paper 69-354, 1969

[13] J.E. Carter "Numerical Solution of the Navier-Stokes Equations for Supersonic Laminar Flow over a Two-Dimensional Compression Corner"
NASA TR R. 385 July 1972

[14] I.Yu.Brailovskaya "Calculation of Viscous Compressible Gas Flow Past a Corner"
Fluid Dynamics, Vol.2, No.3, pp. 49-55, 1967

[15] P. Peyret, H. Viviand "Computation of Viscous Compressible Flows Based on the Navier-Stokes Equations"
AGARDograph No.212 1975

[16] J.S. Shang "Implicit-Explicit Method for Solving the Navier-Stokes Equations"
AIAA Journal Vol.16, No.5, May 1977
AIAA Paper 77-646, 1977

[17] R.W. MacCormack "An Efficient Numerical Method for Solving the Time Dependent Compressibe Navier-Stokes Equations at High Reynolds Number"
NASA-TM-X-73129, 1976

[18] W.R. Briley, H. McDonald "Solution of the Multidimensional Compressible Navier-Stokes Equations by a Generalized Implicit Method"
Journal of Computational Physics
24: 372-397, 1977

[19] R.M. Beam, R.F. Warming "An Implicit Factored Scheme for the Compressible Navier-Stokes Equations"
AIAA J. Vol.16, No.4, April 1978
AIAA Paper 77-645, 1977

[20] R.W. MacCormack "A Numerical Method for Solving the Equation of Compressible Viscous Flow"
AIAA Paper 81-0110, AIAA Journal Vol.20, No.9, September 1982

[21] J. Douglas, J.E. Gunn "A General Formulation of Alternating Direction Methods, Part I. Parabolic and Hyperbolic Problems"
Numerical Mathematics 6: 428-453, 1964

[22] T.H. Pulliam, D.C. Chaussee "A Diagonal Form of an Implicit Approximate-Factorization Algorithm"
Journal of Computational Physics 39: 347-363, 1981

[23] M.D. Salas "Shock Fitting Method for Complicated

Two-Dimensional Supersonic Flows"
AIAA Vol.14, No. 5, May 1976

[24] J.A. Harten "High Resolution Schemes for Hyperbolic Conservation Laws"
J. of Comput. Phys. 49: 357-393, 1983

[25] H.C. Yee
R.F. Warming "Implicit Total Variation Diminishing (TVD) Schemes for Steady-State Calculatons"
Journal of Computational Physics 57: 327-360, 1983

[26] H. Schlichting "Boundary-Layer Theory" 7th Edition
McGraw-Hill, New York, 1979

[27] W.E. Langlois "Slow Viscous Flow" MacMillan, New York, 1964

[28] S. Chapman
T.G. Cowling "The Mathematical Theory of Non-Uniform Gases"
Cambidge Univ. Press., 1960

[29] T. Cebeci
A.M.O. Smith "The Analysis of Turbulent Boundary Layer"
Academic Press, New York, 1974

[30] P.J. Roach "Computational Fluid Dynamics"
Hermesa Publishers, Albuquerque, 1972

[31] S.L. Lawrence
J.C. Tannehill
D.S. Chaussee "Application of the Implicit MacCormack Scheme to the Parabolized Navier-Stokes Equations"
AIAA J. Vol. 22, No. 12, pp. 1755-1763
Dec. 1984
AIAA Paper 83-1956, 1983

[32] R.D. Richtmeyer
K.W. Morton "Difference Methods for Initial-Value Problems"
2nd Edition Interscience Publishers 1967

[33] G. Degrez "Implicit Time Dependent Methods for Inviscid and Viscous Compressible Flows"
VKI-LS-1985-01 'Introduction to Computational Fluid Dynamics', 1985

[34] R.F. Warming
R.M. Beam "On the Construction and Application of Implicit Factored Schemes for Conservation laws"
SIAM-AMS Proceeding, Vol.11, pp. 85-129, 1978

[35] J.L. Steger
R.F. Warming "Flux-Vector Splitting of the Inviscid Gas Dynamics Equations with Application To Finite Difference Methods"
J. Computational Physics, Vol.40, No.2
pp. 262-293, 1981

[36] J.F. Thompson
C.T. Frank
C.W. Mastin "Automatic Numerical Generation of Body-Fitted Curvilinear Coordinate System for Field Containing Any Number of Arbitrary Two-Dimensional Bodies"
J. of Computational Physics, Vol.15,

pp. 299-319, 1974

[37] J.H. Ferziger "Large Eddy Numerical Simulations of Turbulent Flows"
AIAA Journal Vol.15, No.9, Sep. 1977

[38] B.E. Launder
D.B. Spalding "Lectures in Mathematical Models of Turbulence"
Academic Press, New York, 1972

[39] W.C. Reynolds "Computation of Turbulent Flow"
Ann. Review Fluid Mechanics 8: 183-208, 1976

[40] P. Bradshaw
T. Cebeci
T. Whitelaw "Engineering Calculation Methods for Turbulent Flow" Academic Press, New York, 1981

[41] J.G. Marvin "Turbulence Modeling for Computationcal Aerodynamics"
AIAA J. Vol.21, No.7, July 1983 pp. 941-955
AIAA Paper 82-0164, 1982

[42] P. Bradshaw "An Introduction to Turbulence and Its Measurement"
Pergamon Press, Oxford, 1971

[43] P. Bradshaw
etal "Calculation of Boundary-Layer Development Using the Turbulent Energy Equation"
J. Fluid Mech. Vol.28, Part 3, pp. 593-616, 1967

[44] P. Bradshaw
D.H. Ferriss "Calculation of Boundary-Layer Development Using the Turbulent Energy Equation Compressible Flow on Adiabatic Walls"
J. Fluid Mech, Vol.46, Part 1, pp. 83-11, 1971

[45] W.P. Jones
B.E. Launder "The Prediction of Laminarization with A Two-Equation Model of Turbulence"
J. Heat Transfer, Vol.15, pp. 301-314, 1972

[46] R.W. MacCormack "Numerical Solution of the Equations of Compressible Viscous Flow"
'Transonic, Shock and Multidimensional Flow, Advances in Scientific Computing', Academic Press 1982

[47] J.E. Carter "Numerical Solution of the Supersonic Laminar Flow over a Two-Dimensional Compression Corner"
Lecture Notes in Physics Vol.19,
Springer Verlag, Berlin, 1973

[48] R.W. MacCormack "Numerical Solution of the Interaction of a Shock Wave with a Laminar Boundary Layer"
Lecture Notes in Physics, Vol.8, pp.151-163,
Springer Verlag, Berlin, 1971

[49] M. Hanin "Numerical Solution of Navier-Stokes Equations

M. Wolfshtein
U.E. Landau
for Interaction of Shock Wave with Laminar Boundary Layer"
ICAS Paper No. 74-17, Aug. 1974

[50] C.S. Deiwert
"Numerical Simulation of High Reynolds Number Transonic Flows"
AIAA Paper No. 74-603
AIAA Journal, Vol.13, No.10, 1975

[51] D.C. Wilcox
"Calculation of Turbulent Boundary-Layer Shock-Wave Interaction"
AIAA J., Vol.11, No.11, 1973

[52] D.C. Wilcox
"Numerical Study of Separated Turbulent Flows"
AIAA Paper 74-584, June 1974

[53] B.S. Baldwin
R.W. MacCormack
"Numerical Solution of the Interaction of a Strong Shock Wave with a Hypersonic Turbulent Boundary Layer"
AIAA Paper 74-558, June 1974

[54] R.W. MacCormack
B.S. Baldwin
"A Numerical Method for Solving the Navier-Stokes Equations with Application to Shock-Boundary Layer Interactions"
AIAA Paper 75-1, Jan. 1975

[55] C.M. Hung
R.W. MacCormack
"Numerical Solutions of Supersonic and Hypersonic Laminar Flows over a Two-Dimensional Compression Corner"
AIAA Paper 75-2, Jan. 1975

[56] J.S. Shang
W.L.Jr. Hankey
"Numerical Solutions of the Navier-Stokes Equations for Supersonic Turbulent Flow over a Compression Corner"
AIAA Paper 75-3, Jan. 1975

[57] J.S. Shang
W.L.Jr. Hankey
"Supersonic Turbulent Separated Flows Utilizing the Navier-Stokes Equations"
AGARD CP-168, May 1975

[58] C.C. Horstman
M.I. Kussoy
T.J. Coakley
M.W. Rubesin
J.G. Marvin
"Shock Wave Induced Turbulent Boundary Layer Separation at Hypersonic Speeds"
AIAA Paper 75-4, Jan. 1975

[59] J.S. Shang
W.L.Jr. Hankey
C.H. Law
"Numerical Simulation of Shock Wave-Turbulent Boundary-Layer Interaction"
AIAA Journal Vol.14, No.10, October 1976
AIAA Paper 76-95

[60] C.M. Hung
R.W. MacCormack
"Numerical Simulation of Supersonic and Hypersonic Turbulent Compression Corner Flows"
AIAA Journal Vol.15, No.3, March 1977
AIAA Paper 76-410

[61] G. Mateer, A. Brosh, J.R. Viegas — "A Normal Shock-Wave Turbulent Boundary-Layer Interaction at Transonic Speeds" AIAA Paper 76-161, 1976

[62] J.R. Viegas, T.J. Coakley — "Numerical Investigation of Turbulence Models for Shock-Separated Boundary-Layer Flows" AIAA Journal Vol.16, No.4, April 1978 AIAA Paper 77-44

[63] C.C. Horstman, G.S. Settles, I.E. Vas, S.M. Bogdonoff, C.M. Hung — "Reynolds Number Effects on Shock-Wave Turbulent Boundary-Layer Interactions" AIAA Paper 77-42 AIAA Journal Vol.15, No.8, August 1977

[64] T.J. Coakley, J.R. Viegas — "Turbulence Modeling of Shock Separated Boundary-Layer Flows" Presented at the Symposium on Turbulent Shear Flow, University Park, Penn., April 1977

[65] T.J. Coakley, J.R. Viegas, C.C. Horstman — "Evaluation of Turbulence Models for Three Primary Types of Shock Separated Boundary-Layers" AIAA Paper 77-692, 1977

[66] J.S. Shang, W.L. Hankey — "Numerical Solution of the Navier-Stokes Equations for a Three-Dimensional Corner" AIAA Paper 77-169 AIAA Journal Vol.15, No.11, Nov. 1977

[67] B.S. Baldwin, H. Lomax — "Thin Layer Approximation and Algebraic Model for Separated Turbulent Flows" AIAA Paper 78-257, 1978

[68] J.R. Viegas, C.C. Horstman — "Comparison of Multiequation Turbulence Models for Several Shock Separated Boundary-Layer Interaction Flows" AIAA Paper 78-1165, 1978

[69] C.M. Hung, R.W. MacCormack — "Numerical Solution of Three-Dimensional Shock Wave and Turbulent Boundary-Layer Interaction" AIAA Paper 78-161 AIAA J. Vol.16, No.10, Oct. 1978

[70] J.S. Shang, W.L. Hankey, J.S. Petty — "Three-Dimensional Supersonic Interacting Turbulent Flow Along a Corner" AIAA Paper 78-1210 AIAA J. Vol.17, No.7, July 1978

[71] C.C. Horstman, C.M. Hung — "Computations of Three Dimensional Turbulent Separated Flows at Supersonic Speeds" AIAA Paper 79-0002

[72] C.M. Hung — "Numerical Solution of Supersonic Laminar Flow over a Inclined Body of Revolution" AIAA Paper 79-1547 AIAA J. Vol.18, No.8, Aug. 1980

[73] D.A. Johnson, C.C. Horstman, W.D. Bachalo "A Comprehensive Comparison Between Experiment and Prediction for Transonic Turbulent Separated Flow" AIAA Paper 80-1407, 1980

[74] M.I. Kussoy, J.R. Viegas, C.C. Horstman "Investigation of a Three-Dimensional Shock Wave Separated Turbulent Boundary-Layer" AIAA Paper 80-0002 AIAA J. Vol.18, No.2, December 1980

[75] C.M. Hung, D.S. Chaussee "Computation of Supersonic Turbulent Flow over an Inclined Ogive-Cylinder-Flare" AIAA Paper 80-1410 AIAA J. Vol.19, No.9, Sept. 1981

[76] C.S. Chaussee, T.H. Pulliam "Two-Dimensional Inlet Simulation Using a Diagonal Implicit Algorithm" AIAA Joural Vol.19, No.2, February 1981

[77] Ajay Kumar "Some Observations on a New Numerical Method for Solving the Navier-Stokes Equations" NASA TP-1934-1981, 1981

[78] T.J. Coakley "Numerical Method for Gas Dynamics Combining Characteristic and Conservation Concepts" AIAA Paper 81-1257, 1981

[79] E.Von Lavante, W.T. Thompkins "An Implicit Bi-Diagonal Numerical Method for Solving the Navier-Stokes Equations" AIAA Paper 82-0063, 1982

[80] D. Om, M.E. Childs, J.R. Viegas "An Experimental Investigation and a Numerical Prediction of a Transonic Normal Shock Wave Turbulent Boundary-Layer Interaction" AIAA Paper 82-0990, 1982

[81] T.J. Coakley "Turbulence Modeling Methods for the Compressible Navier-Stokes Equations" AIAA Paper 83-1693, 1983

[82] M. Visbal, D. Knight "Evaluation of the Baldwin-Lomax Turbulence Model for Two-Dimensional Shock Wave Boundary-Layer Interactions" AIAA Paper 83-1697, 1983

[83] C.M. Hung, W. Kordulla "A Time-Split Finite-Volume Algorithm for Three-Dimensional Flow Field Simulation" AIAA Paper 83-1957, 1983

[84] R.J. Hakkinen, I. Greber, L. Trilling, S.S. Abarbanel "The Interaction of An Oblique Shock Wave with A Laminar Boundary Layer" NASA MEMO 2-18-59W, 1959

[85] G.S. Settles "Data Compilation for Shock Wave Turbulent

R.B. Gilbert
S.M. Bogdonoff
Boundary Layer Interaction Experiments on Two-Dimensional Compression Corners" Princeton University Report MAE-1489, 1980

[86] W.A. Mulder
B.V. Leer
"Experiments with Implicit Upwind Methods for the Euler Equations" Journal of Computational physics 59, 232-246 1985

[87] P. Bradshaw
"Compressible Turbulent Shear Layers" Annual Review Fluid Mechanics 9: 33-54, 1977

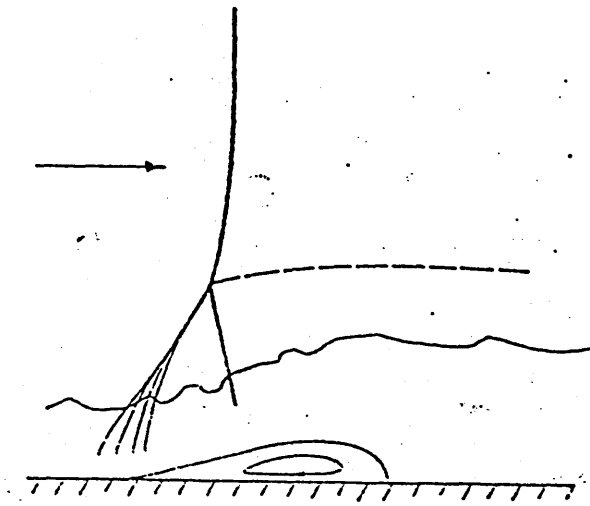

a. NORMAL SHOCK WAVE

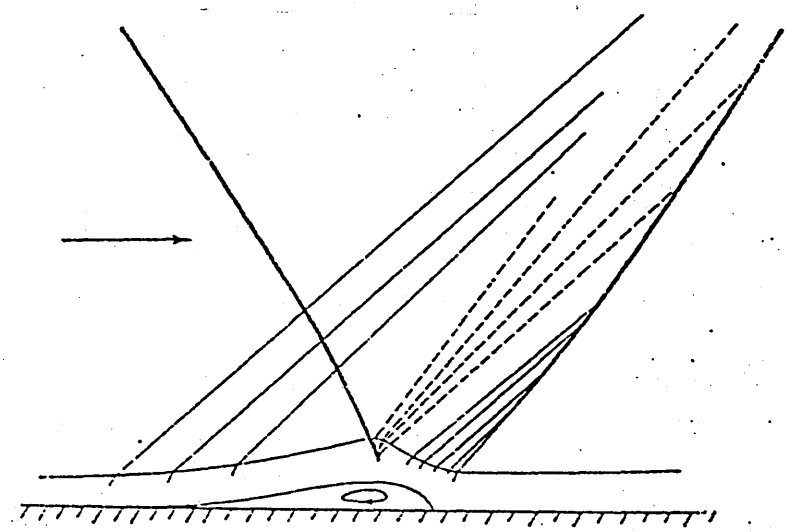

b. INCIDENT OBLIQUE SHOCK WAVE

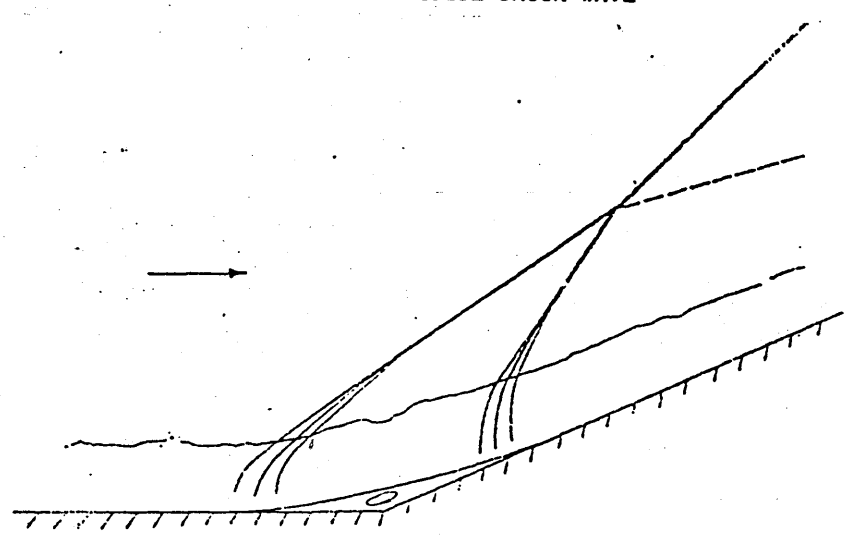

c. COMPRESSION RAMP OR CORNER

Figure 1. TYPICAL INTERACTIONS BETWEEN SHOCK WAVE AND BOUNDARY LAYER

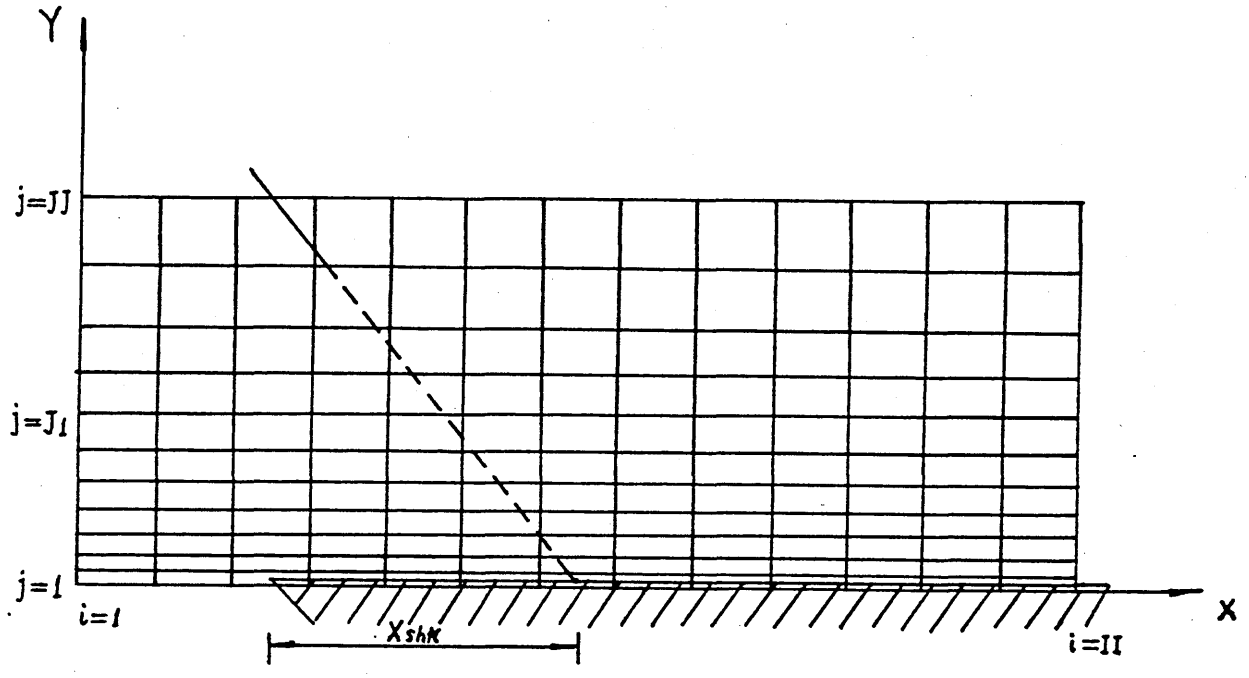

a. COMPUTATIONAL GRID FOR FLAT PLATE

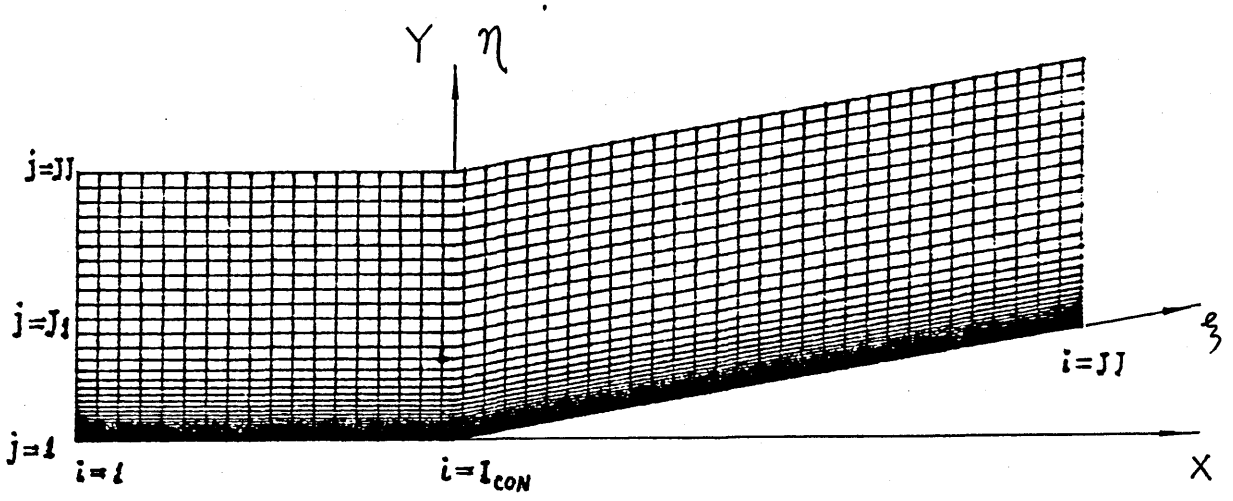

b. COMPUTATIONAL GRID FOR COMPRESSION RAMP

Figure. 2. COMPUTATIONAL MESH

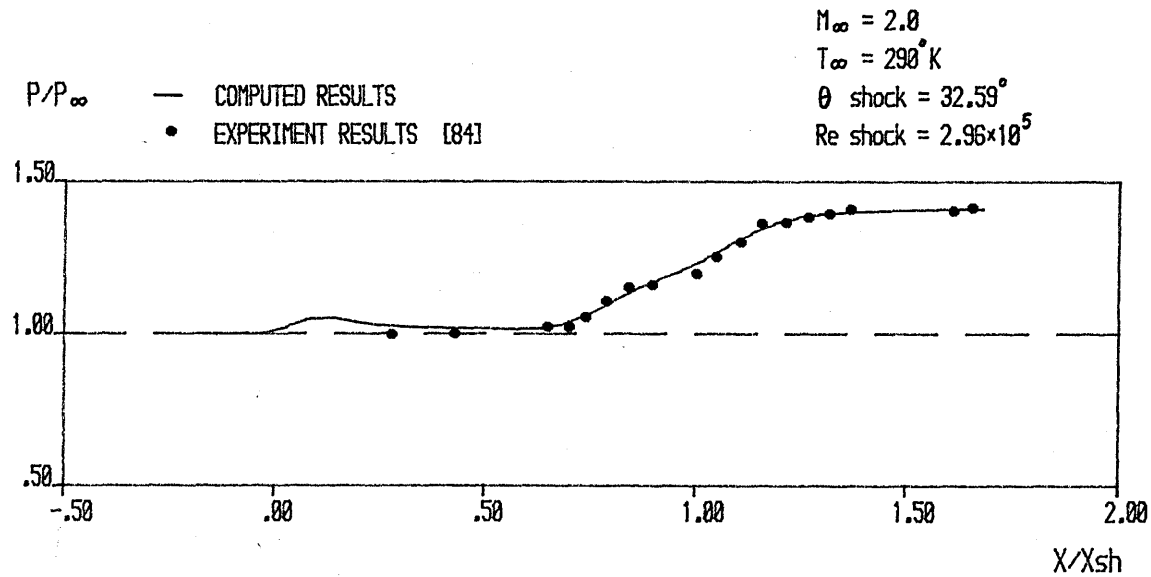

Figure 3-1. THE WALL PRESSURE DISTRIBUTION
(CASE - 1) LAMINAR

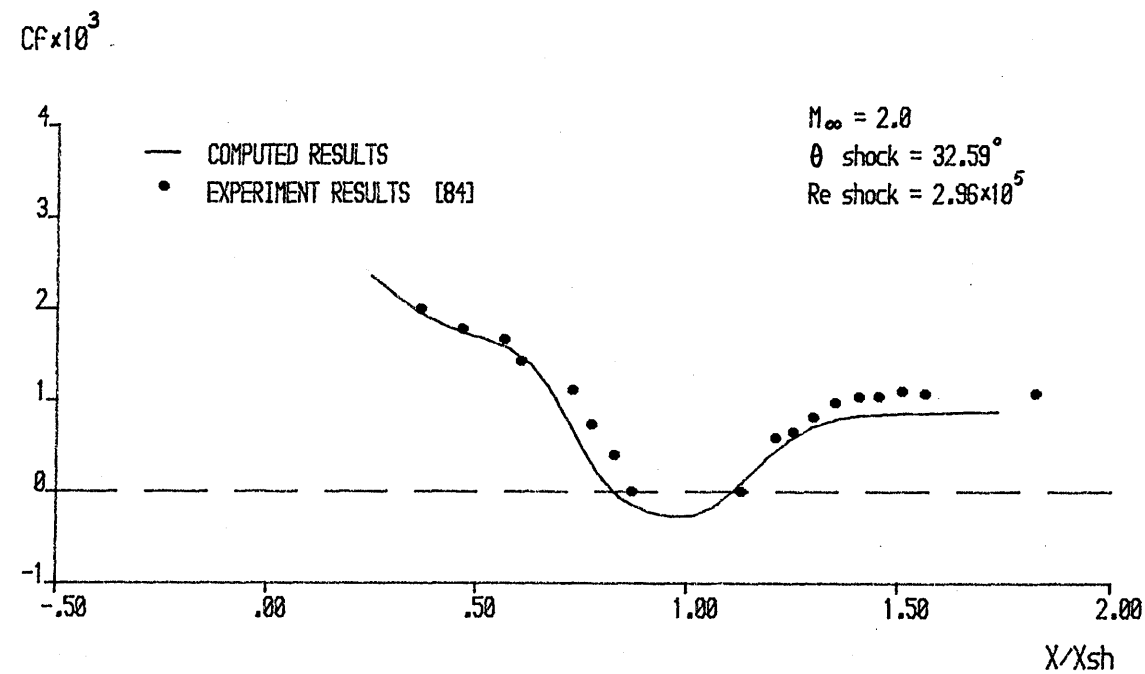

Figure 3-2. SKIN FRICTION COEFFICIENT
(CASE - 1) LAMINAR

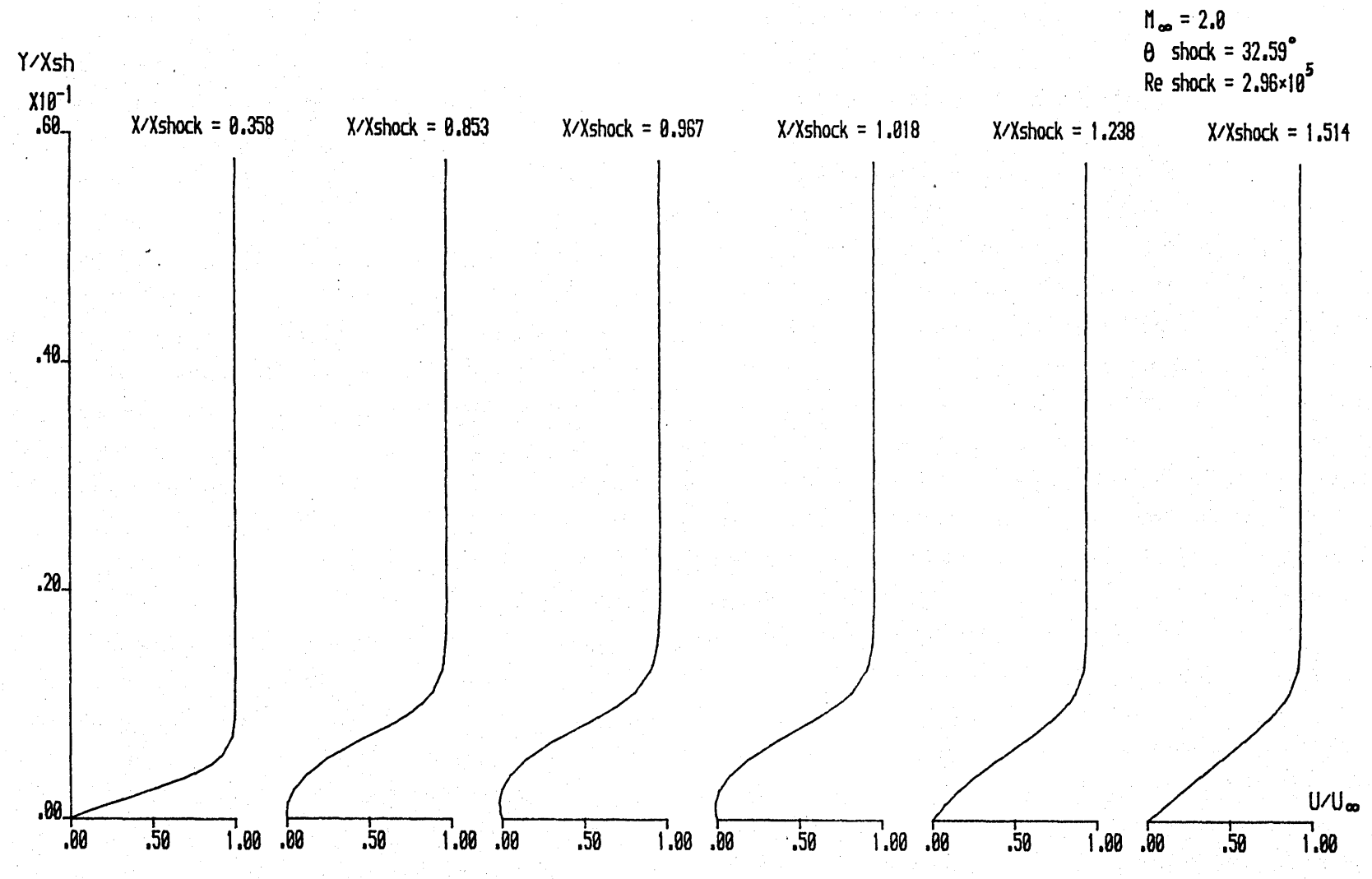

Figure 3-3. VELOCITY PROFILE (CASE - 1)
LAMINAR

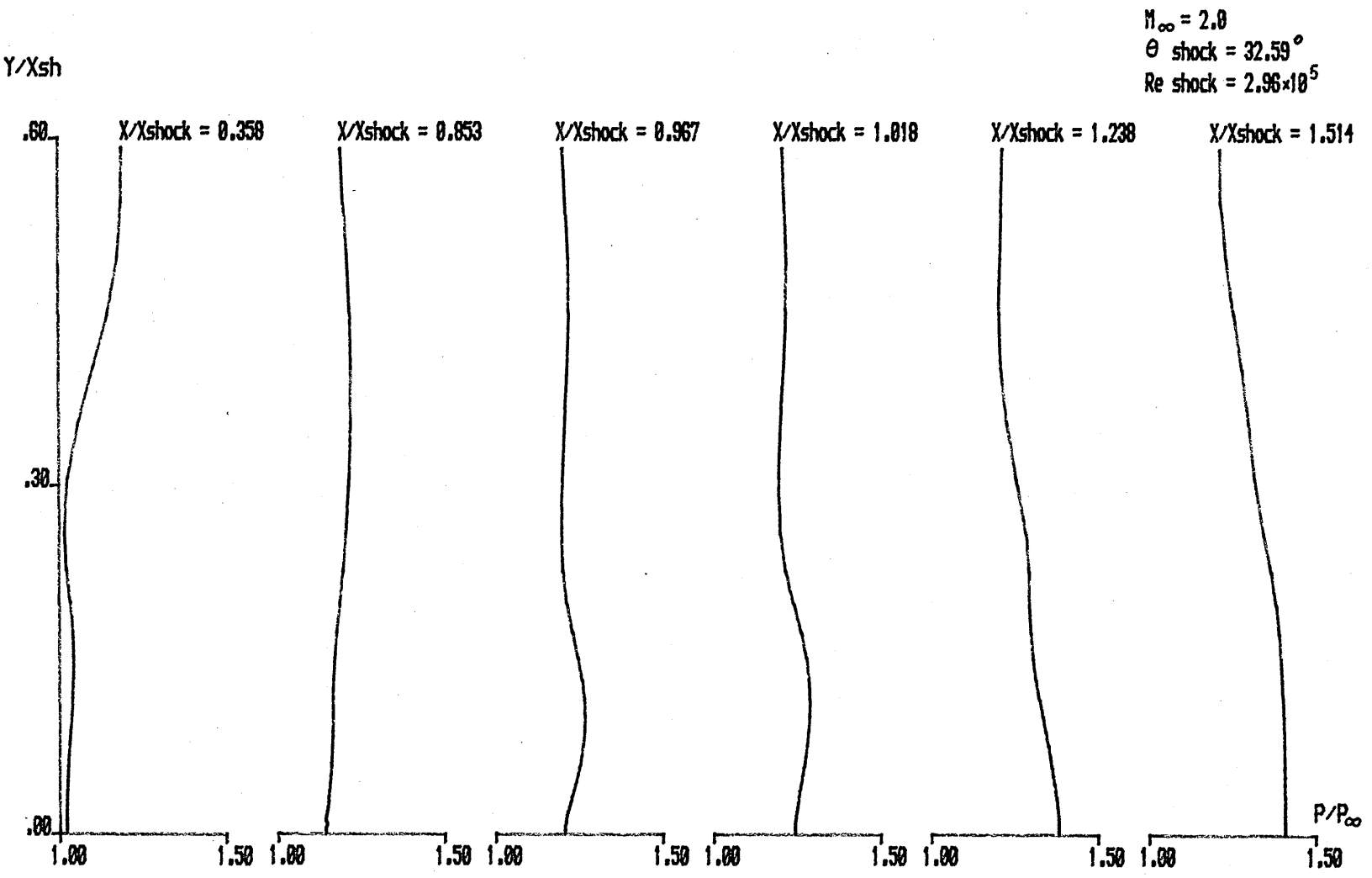

Figure 3-4. PRESSURE PROFILE (CASE - 1)
LAMINAR

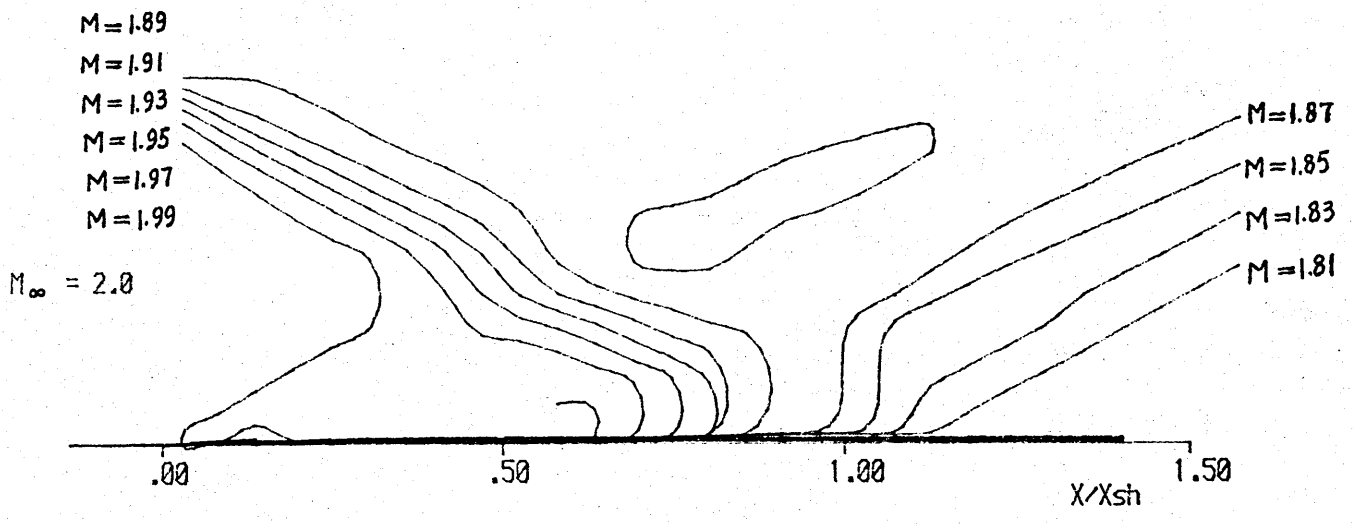

Figure 3-5. MACH NUMBER CONTOURS
(CASE - 1) LAMINAR

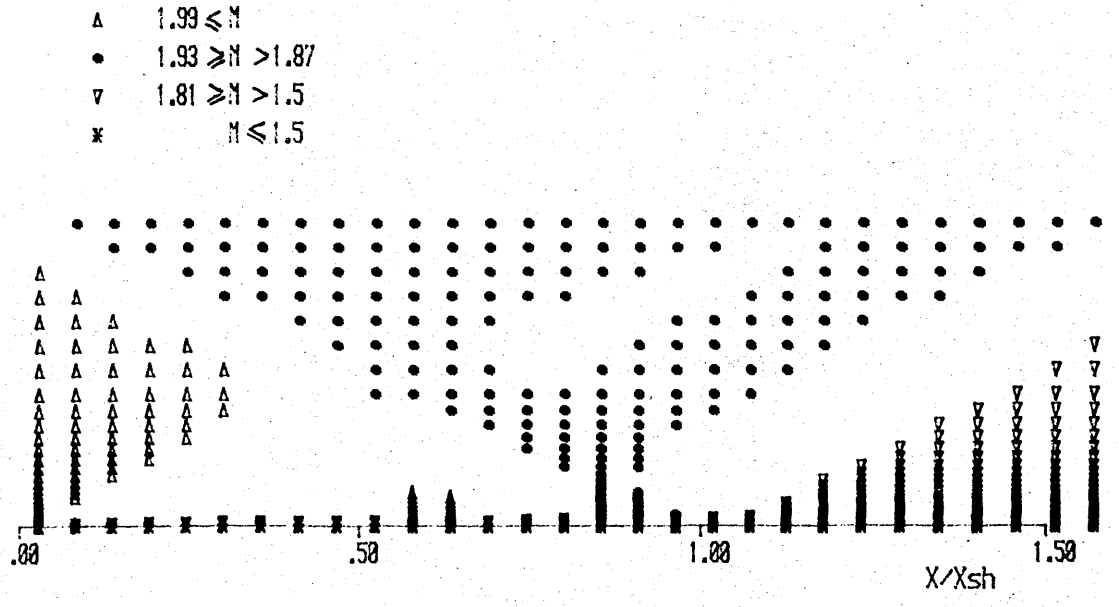

Figure 3-6. MACH NUMBER DISTRIBUTION
(CASE - 1) LAMINAR

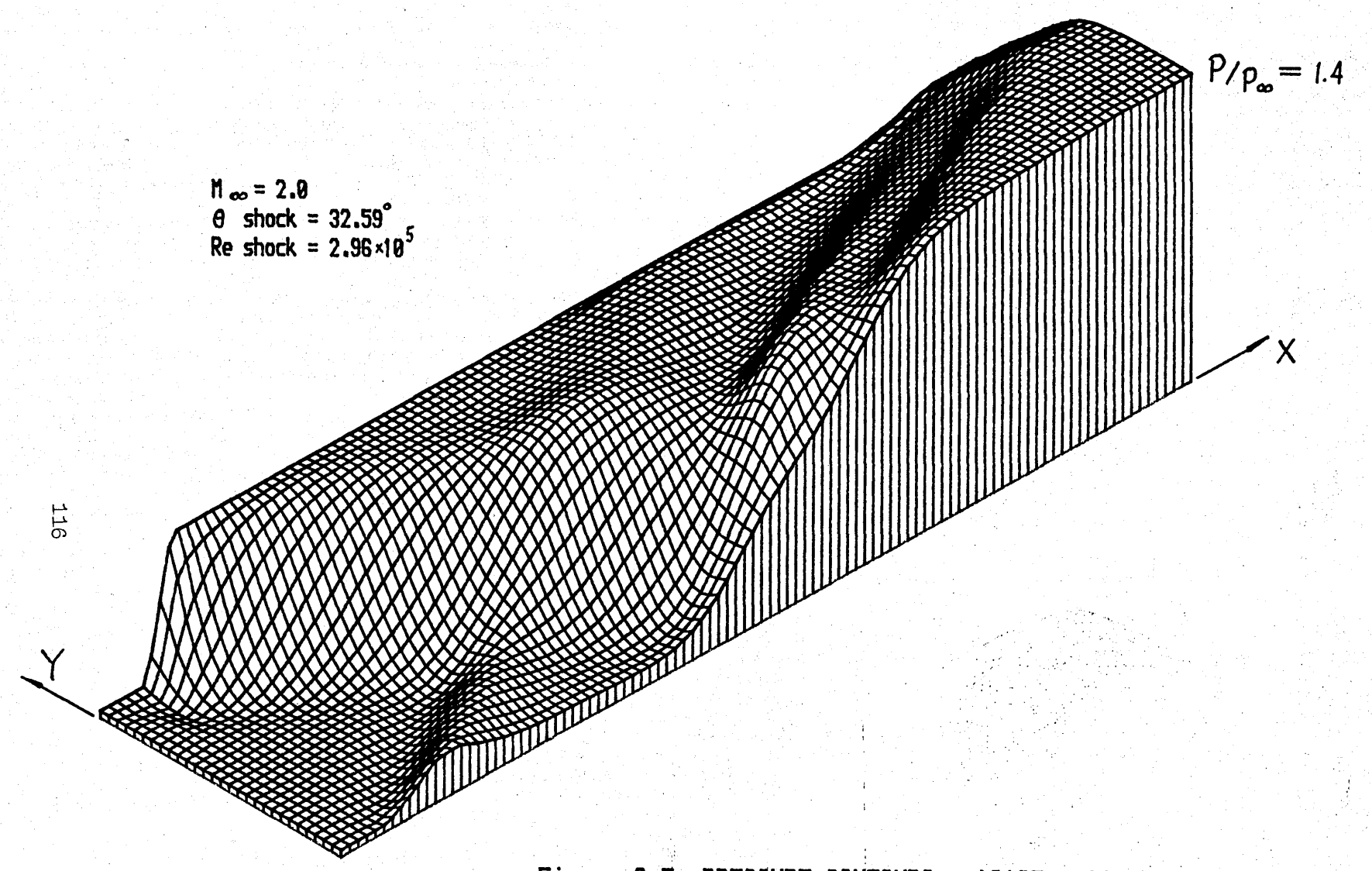

Figure 3-7. PRESSURE CONTOURS (CASE - 1) LAMINAR

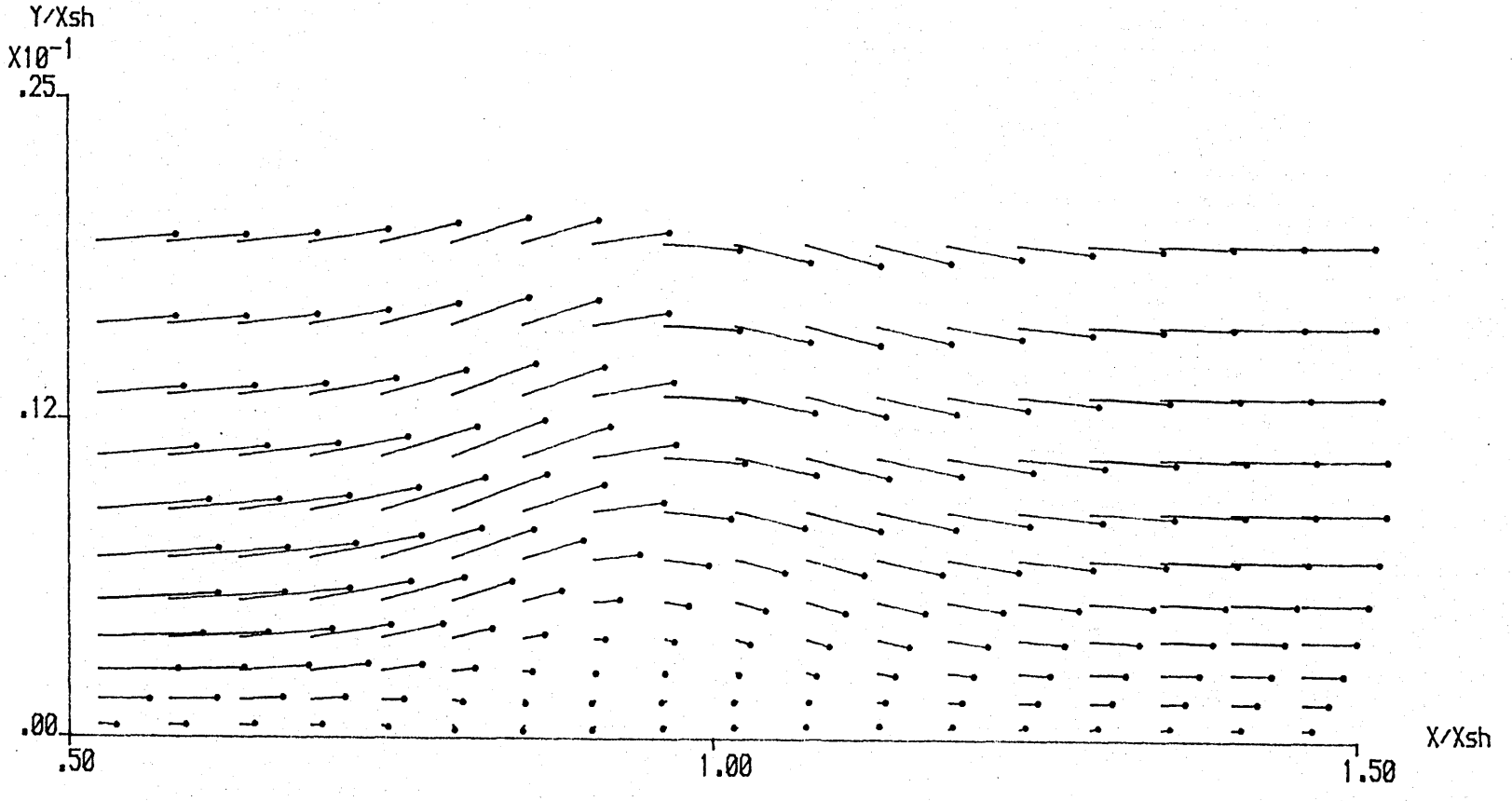

Figure 3-8. THE VEOCITY VECTOR NEAR THE WALL
(CASE - 1) LAMINAR

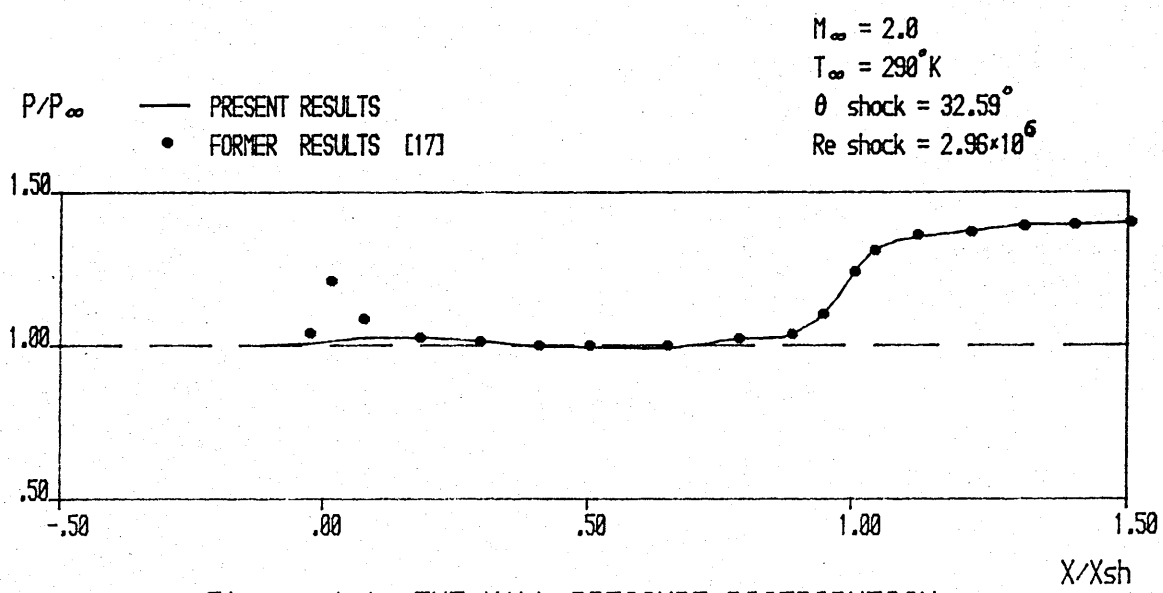

Figure 4-1. THE WALL PRESSURE DISTRIBUTION
(CASE - 2) TURBULENT

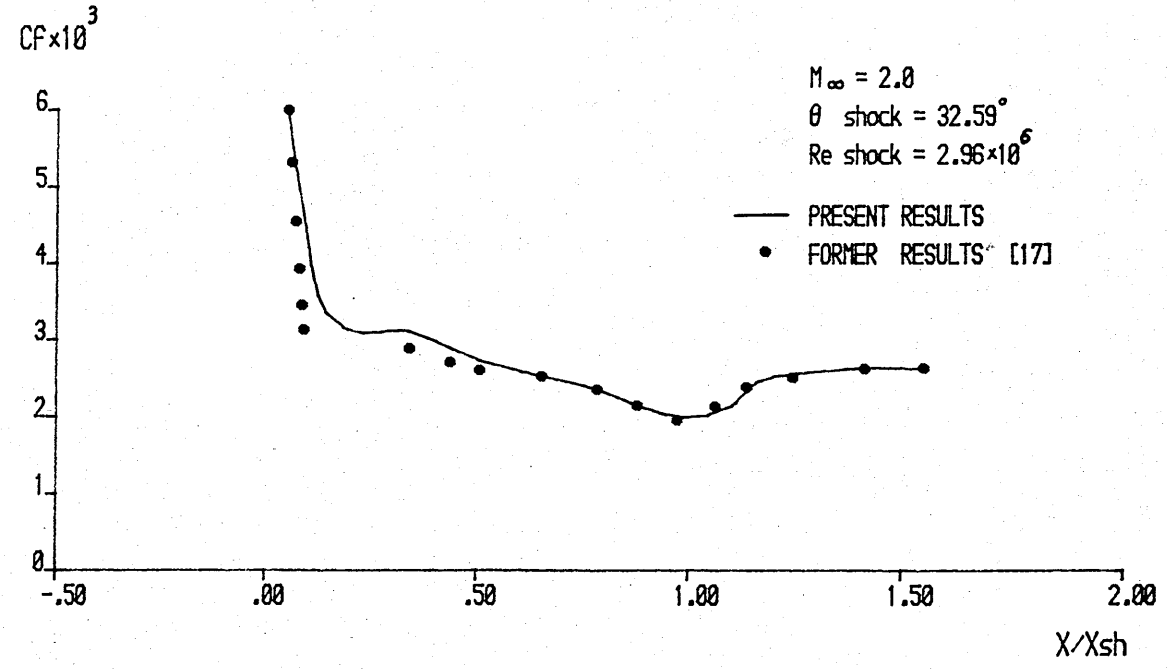

Figure 4-2. SKIN FRICTION COEFFICIENT
(CASE - 2) TURBULENT

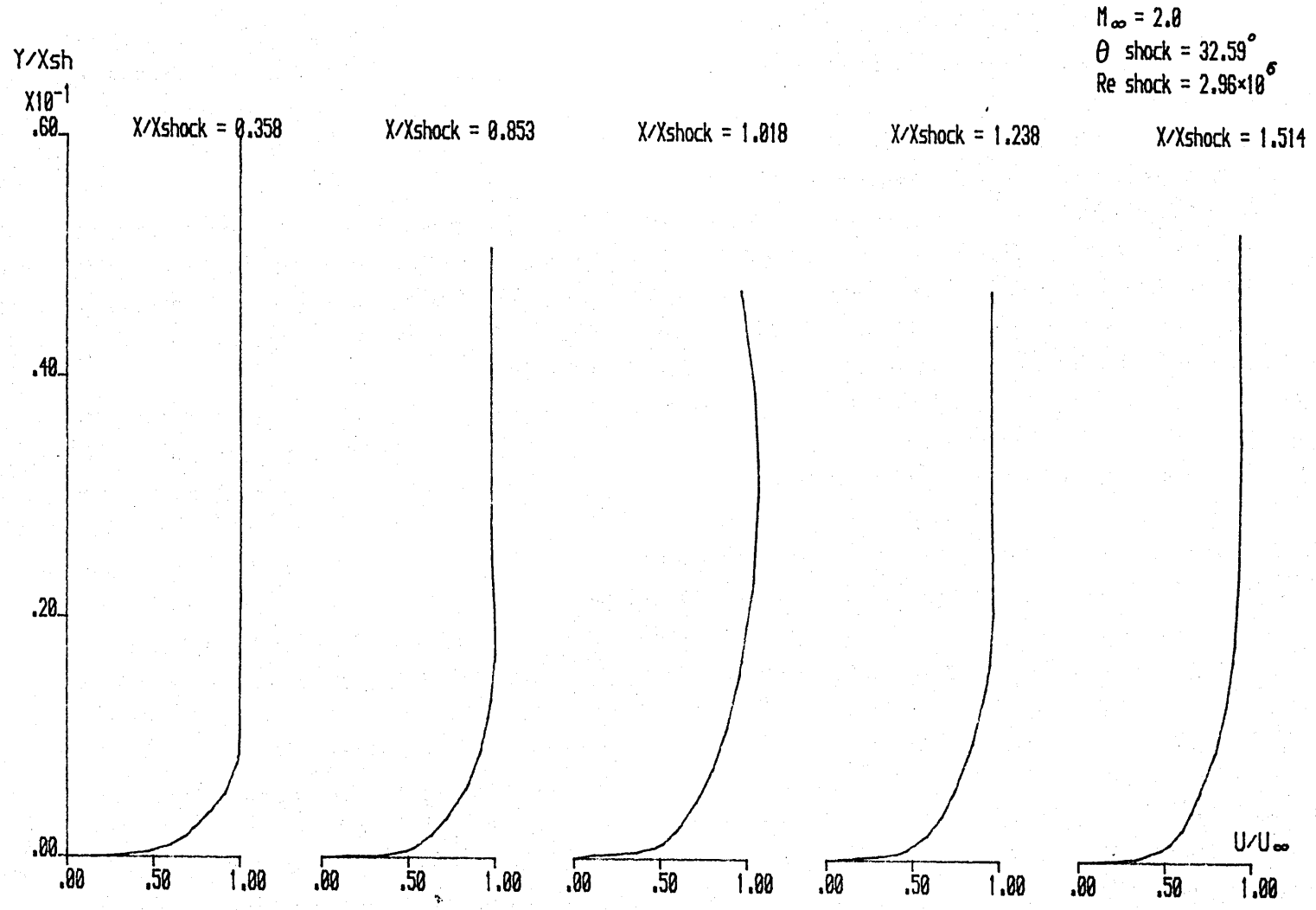

Figure 4-3. VELOCITY PROFILE (CASE - 2)
TURBULENT

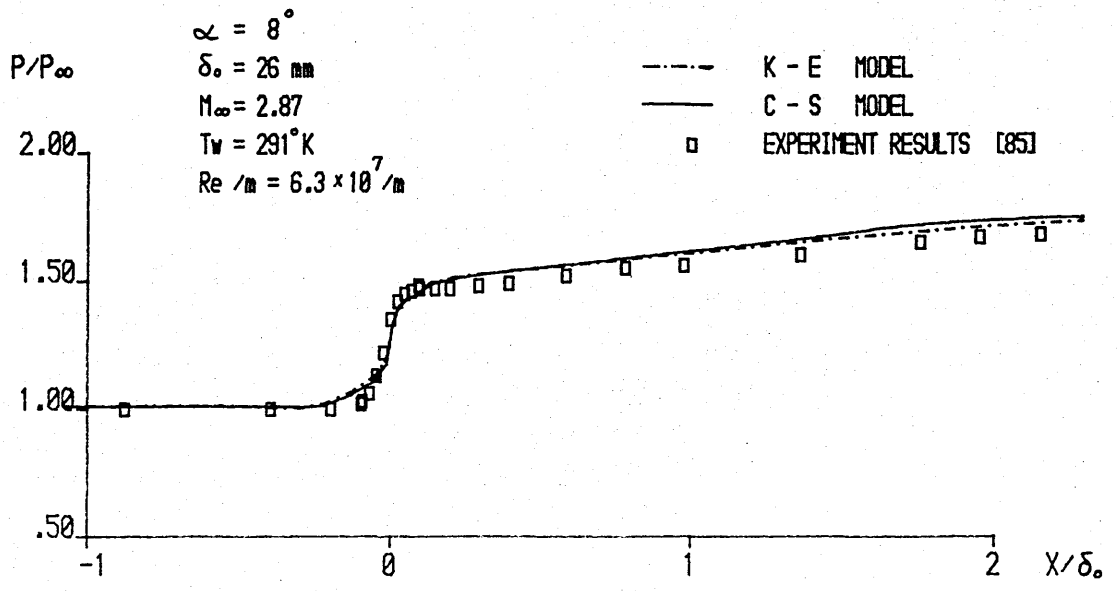

Figure 5-1. THE DISTRIBUTION OF THE WALL PRESSURE
(CASE - 3 - A)

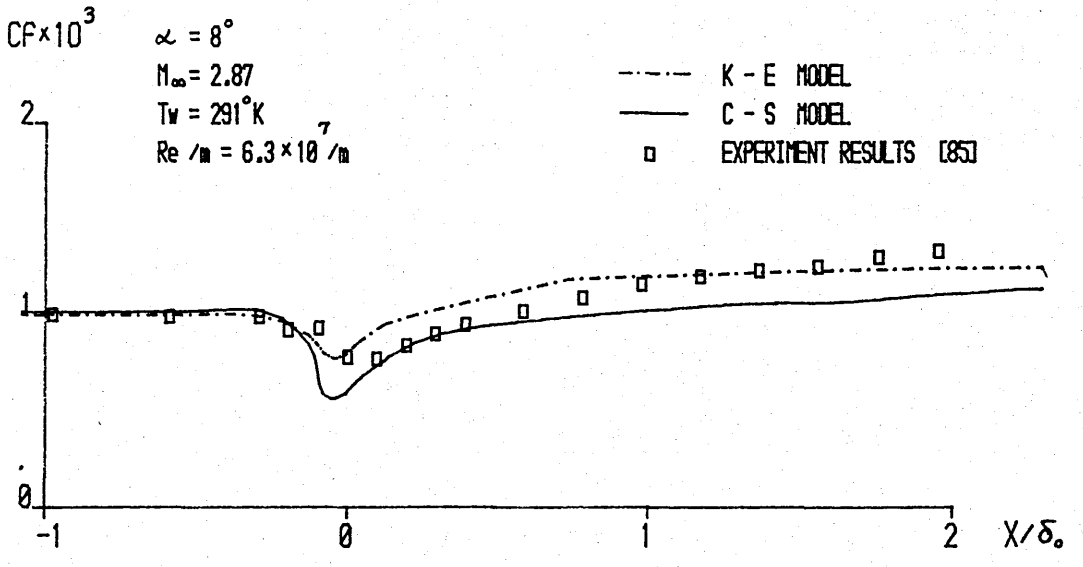

Figure 5-2. SKIN FRICTION COEFFICIENT
(CASE - 3 - A)

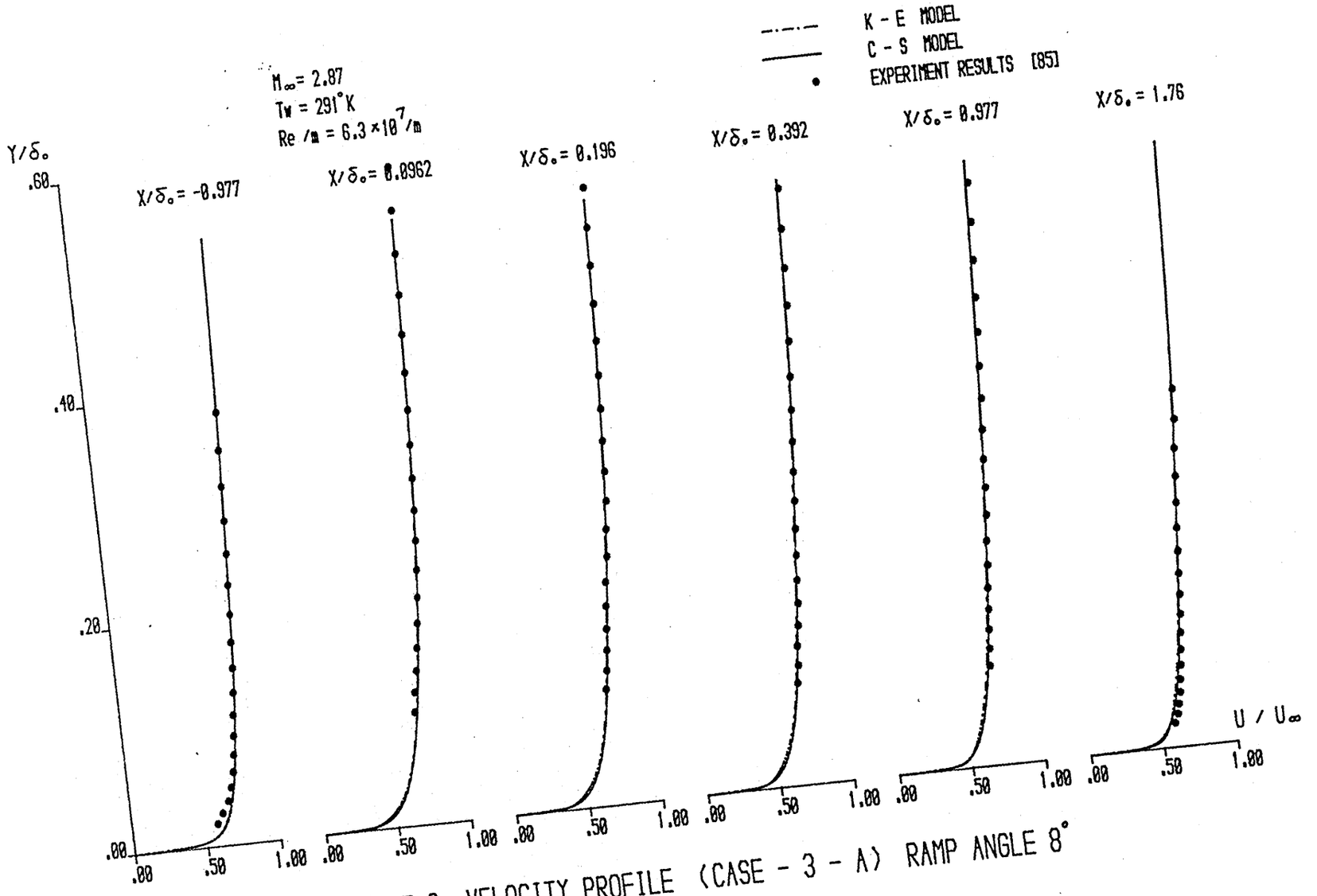

Figure 5-3. VELOCITY PROFILE (CASE - 3 - A) RAMP ANGLE 8°

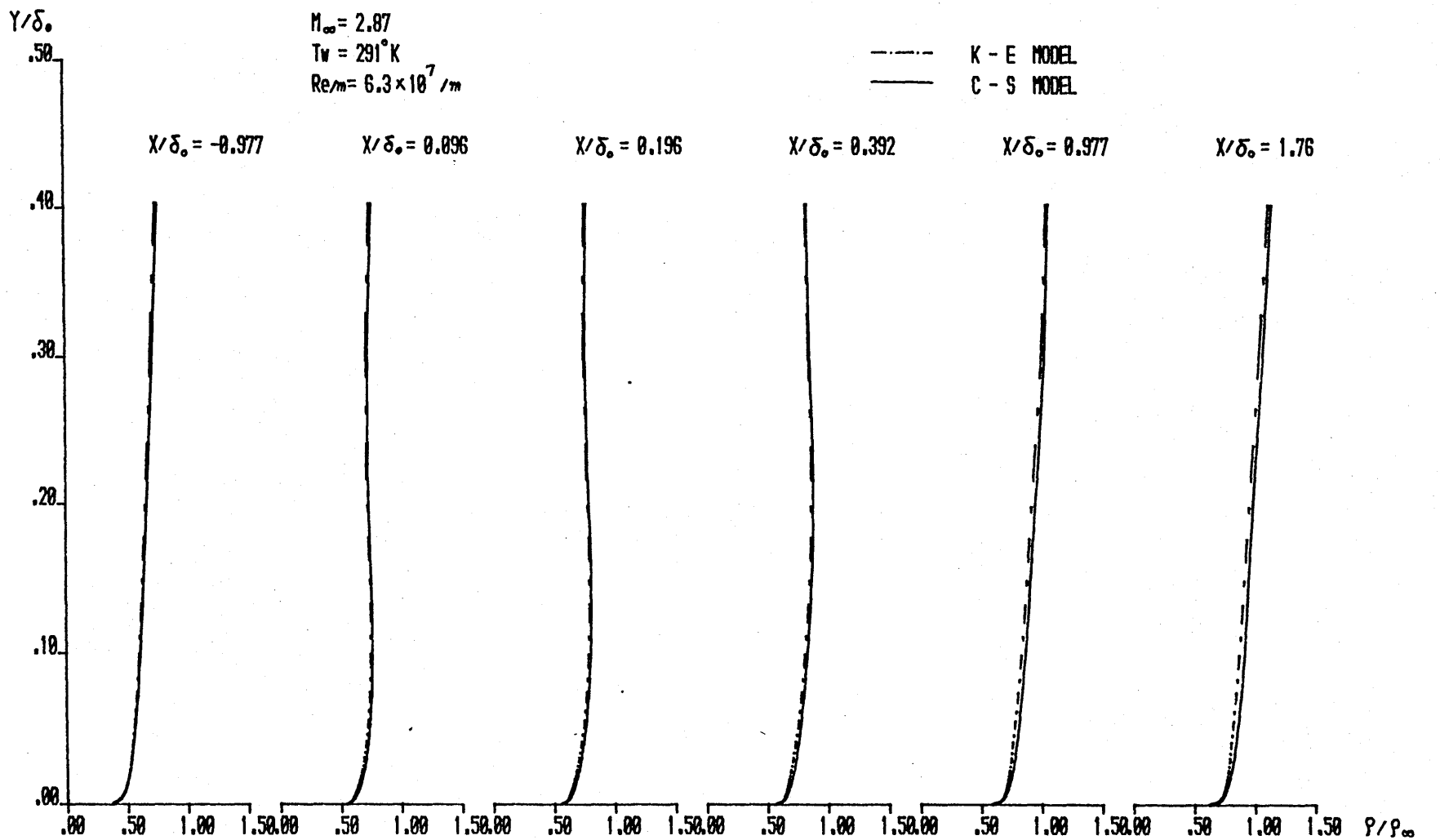

Figure 5-4. DENSITY PROFILE (CASE - 3 - A) RAMP ANGLE 8°

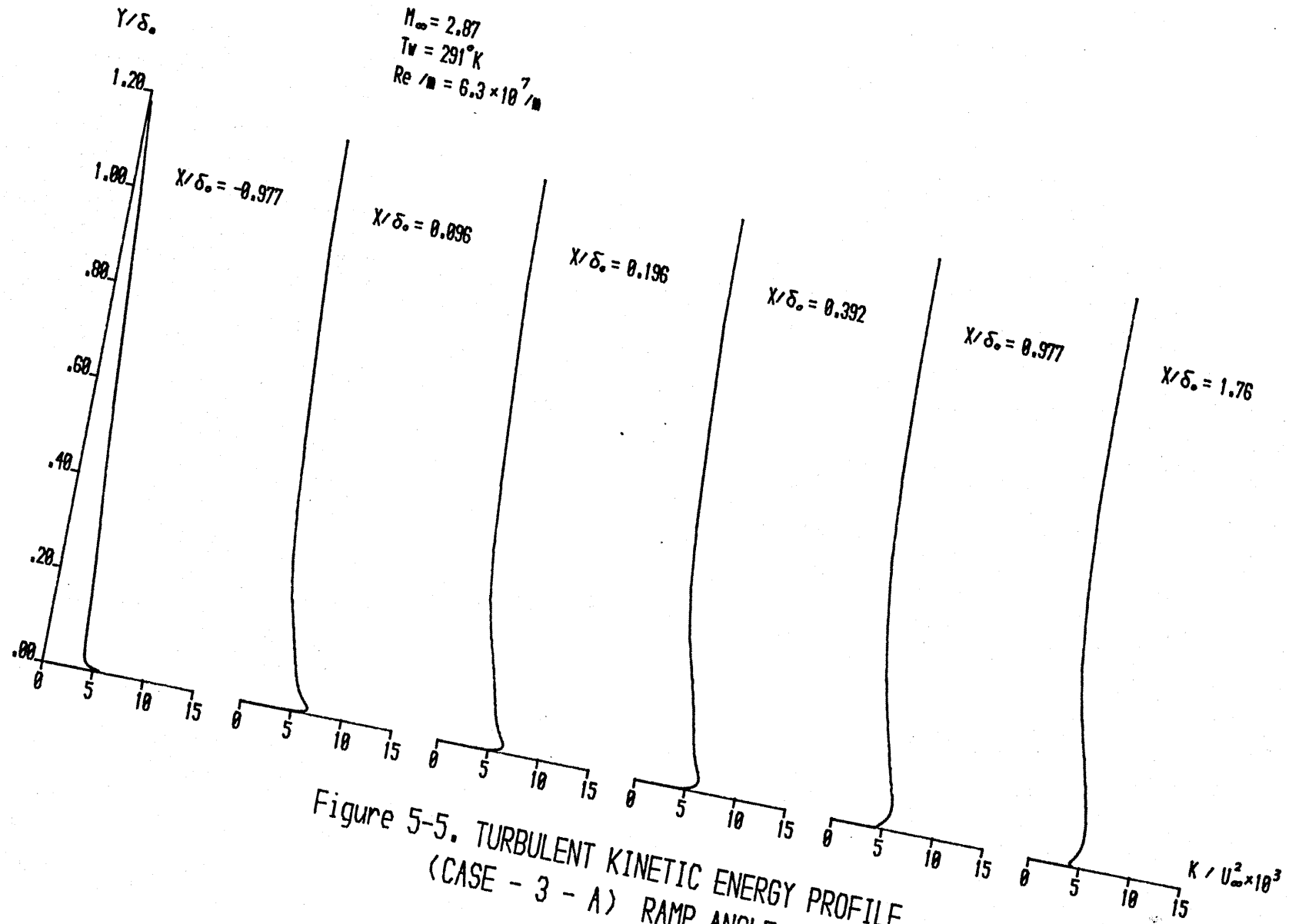

Figure 5-5. TURBULENT KINETIC ENERGY PROFILE
(CASE - 3 - A) RAMP ANGLE 8°

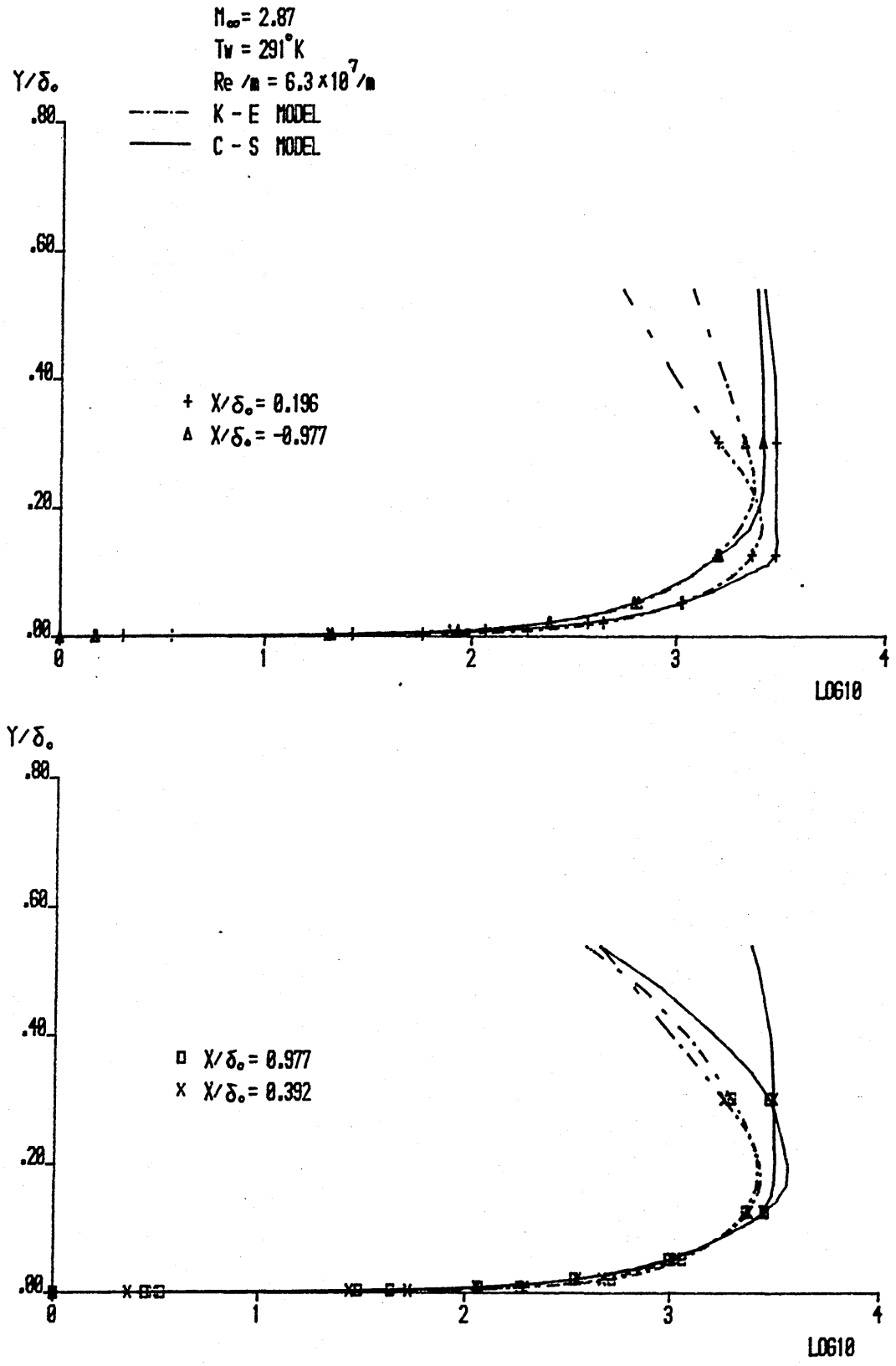

Figure 5-6. EDDY VISCOSITY PROFILE
(CASE - 3 - A) RAMP ANGLE 8°

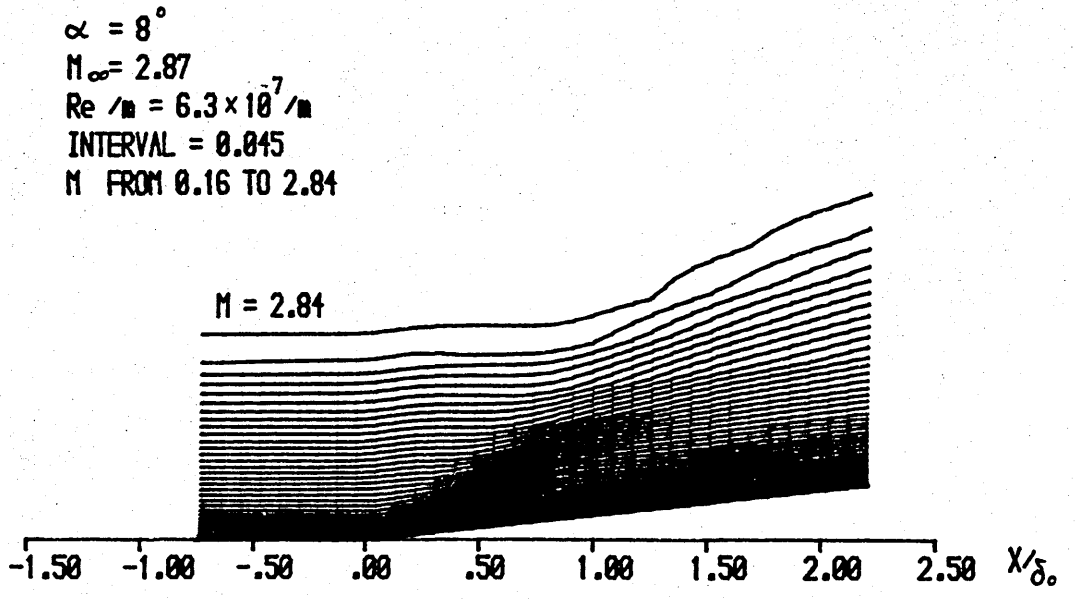

Figure 5-7. MACH NUMBER CONTOURS
K - E MODEL
(CASE - 3 - A)

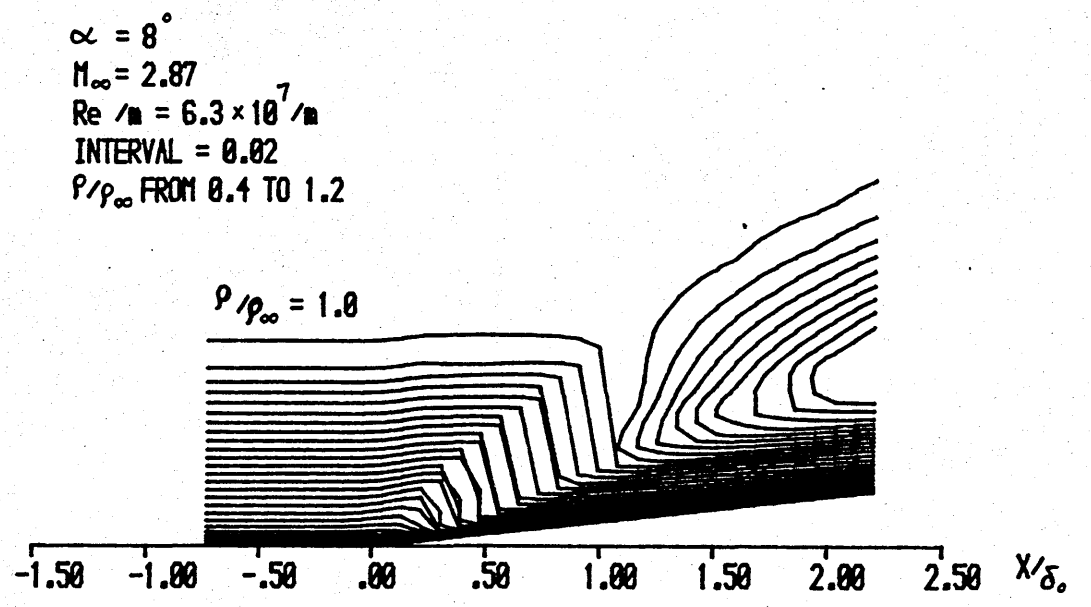

Figure 5-8. DENSITY CONTOURS
K - E MODEL
(CASE - 3 - A)

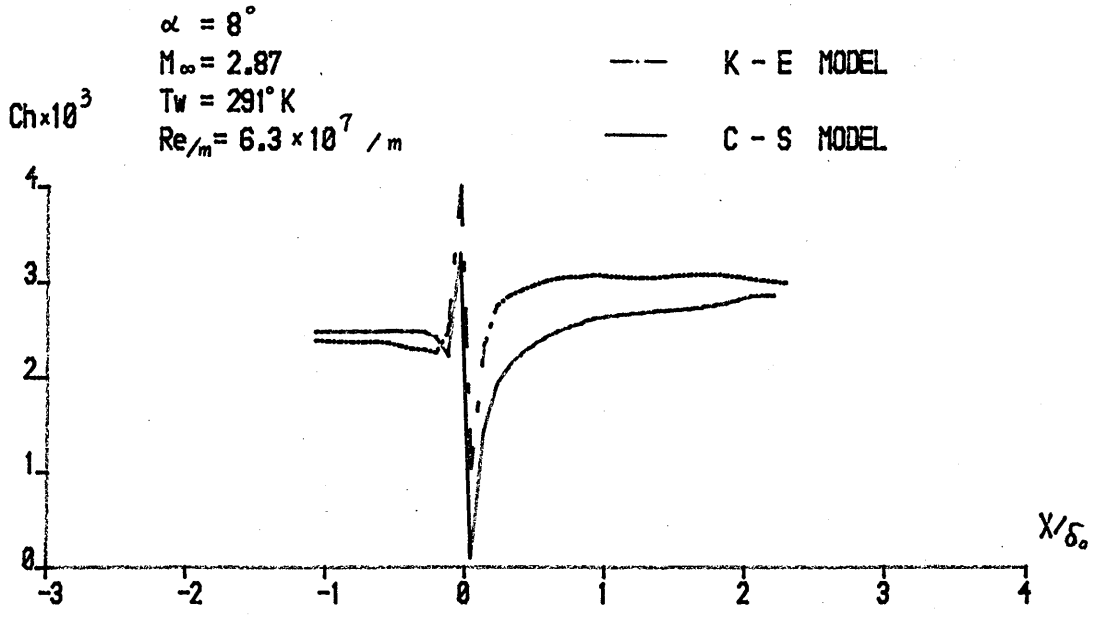

Figure 5-9. THE HEAT TRANSFER COEFFICIENT
(CASE - 3 - A)

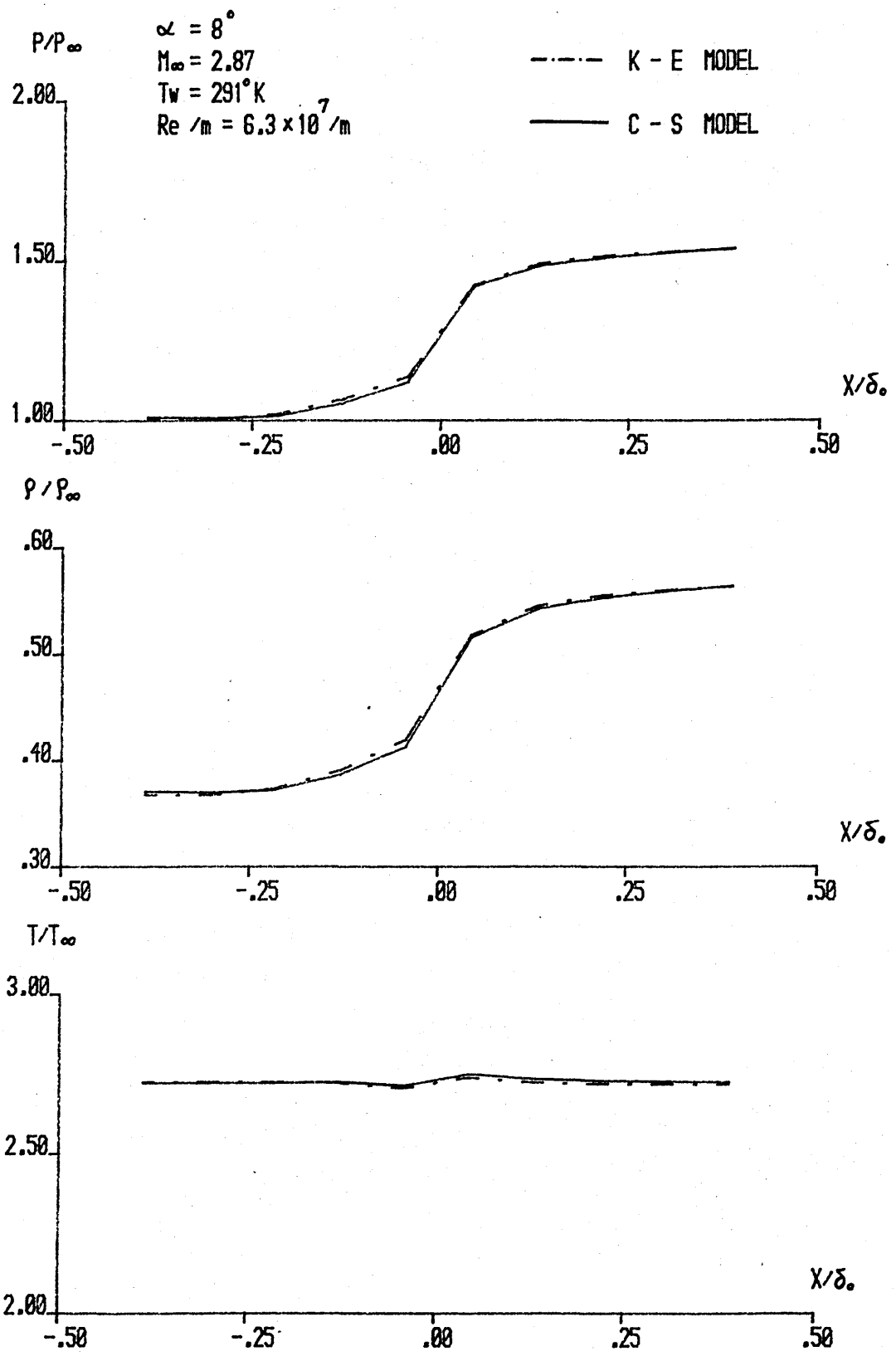

Figure 5-10. P/P_∞ , ρ/ρ_∞ , T/T_∞ AT J = 2 VIS $X/\delta_\circ$

(CASE - 3 - A)

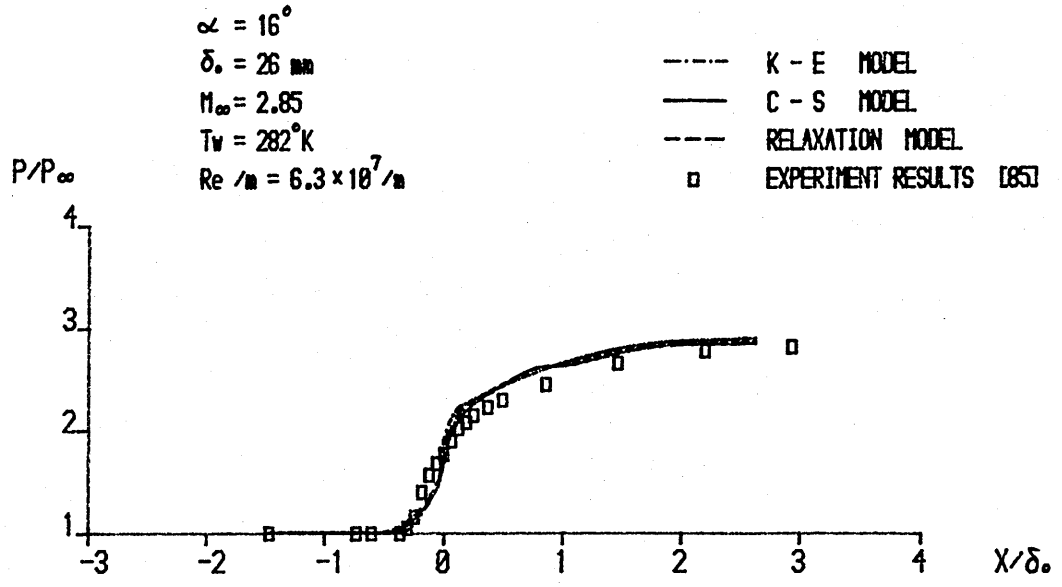

Figure 6-1. THE DISTRIBUTION OF THE WALL PRESSURE
(CASE - 3 - B)

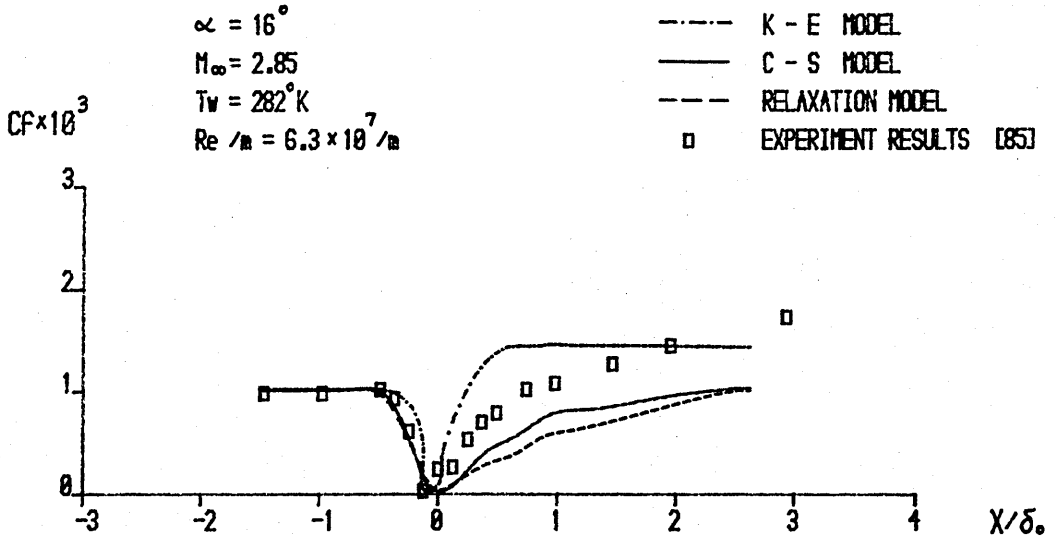

Figure 6-2. SKIN FRICTION COEFFICIENT
(CASE - 3 - B)

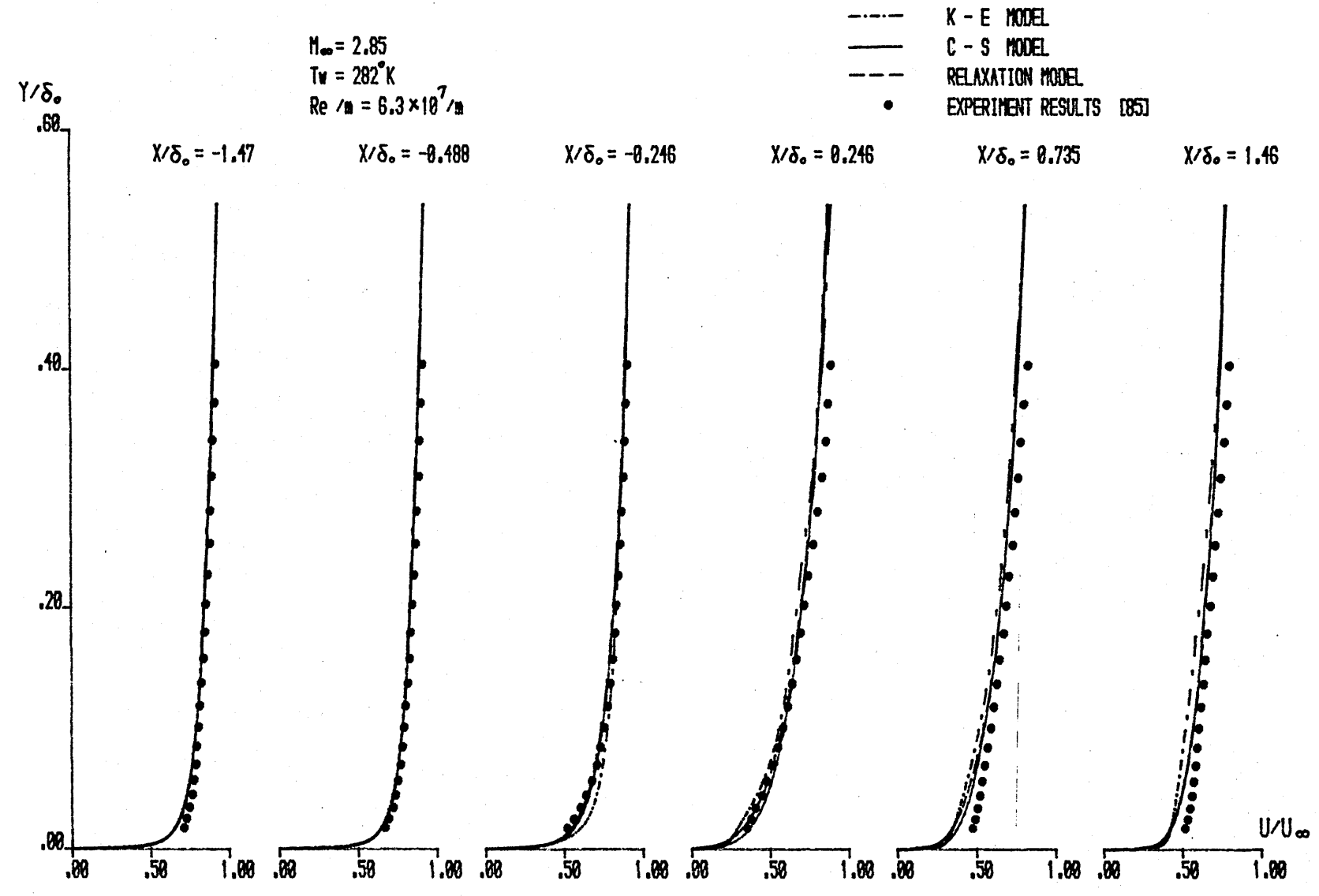

Figure 6-3. VELOCITY PROFILE (CASE - 3 - B) RAMP ANGLE 16°

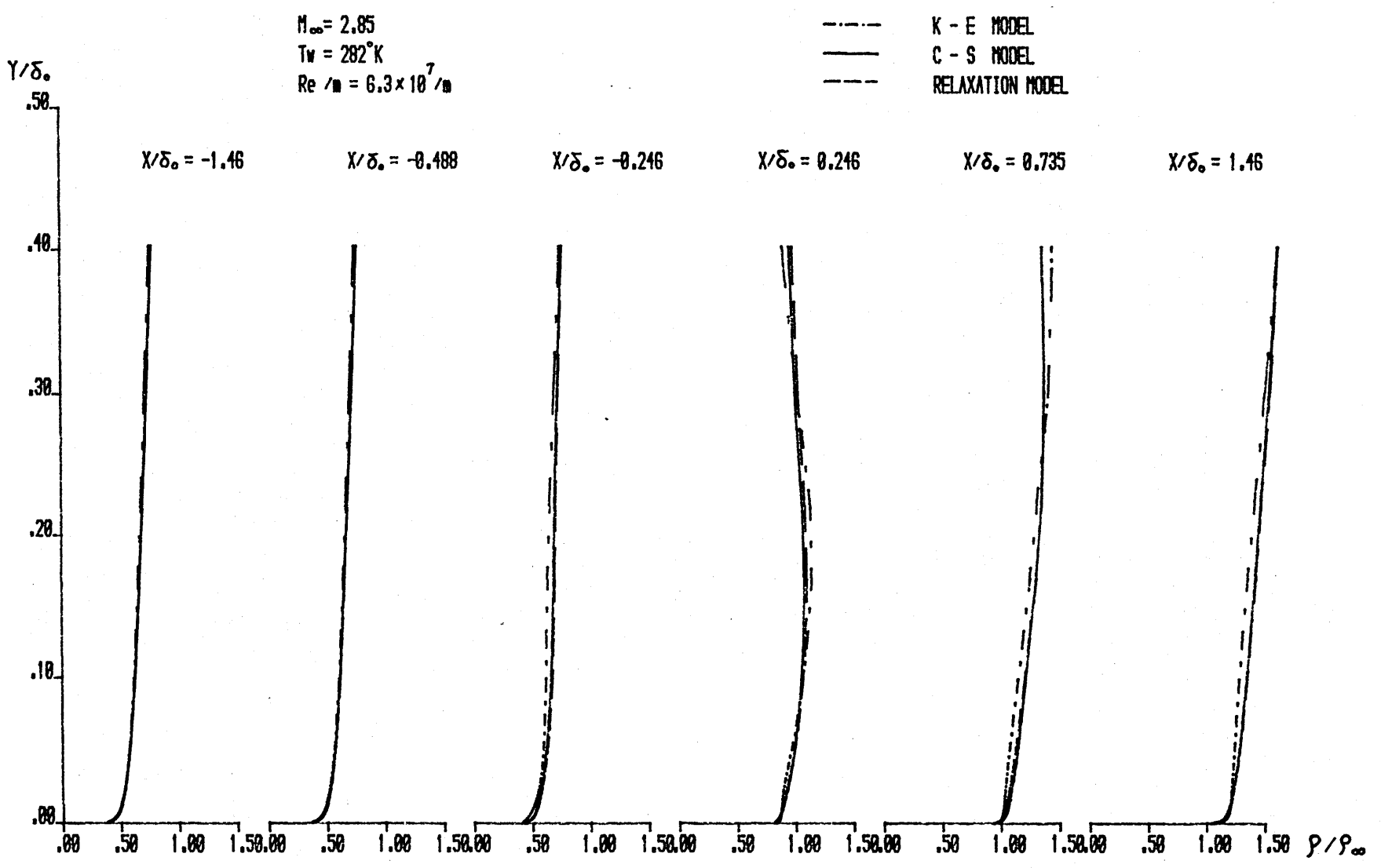

Figure 6-4. DENSITY PROFILE (CASE - 3 - B) RAMP ANGLE 16°

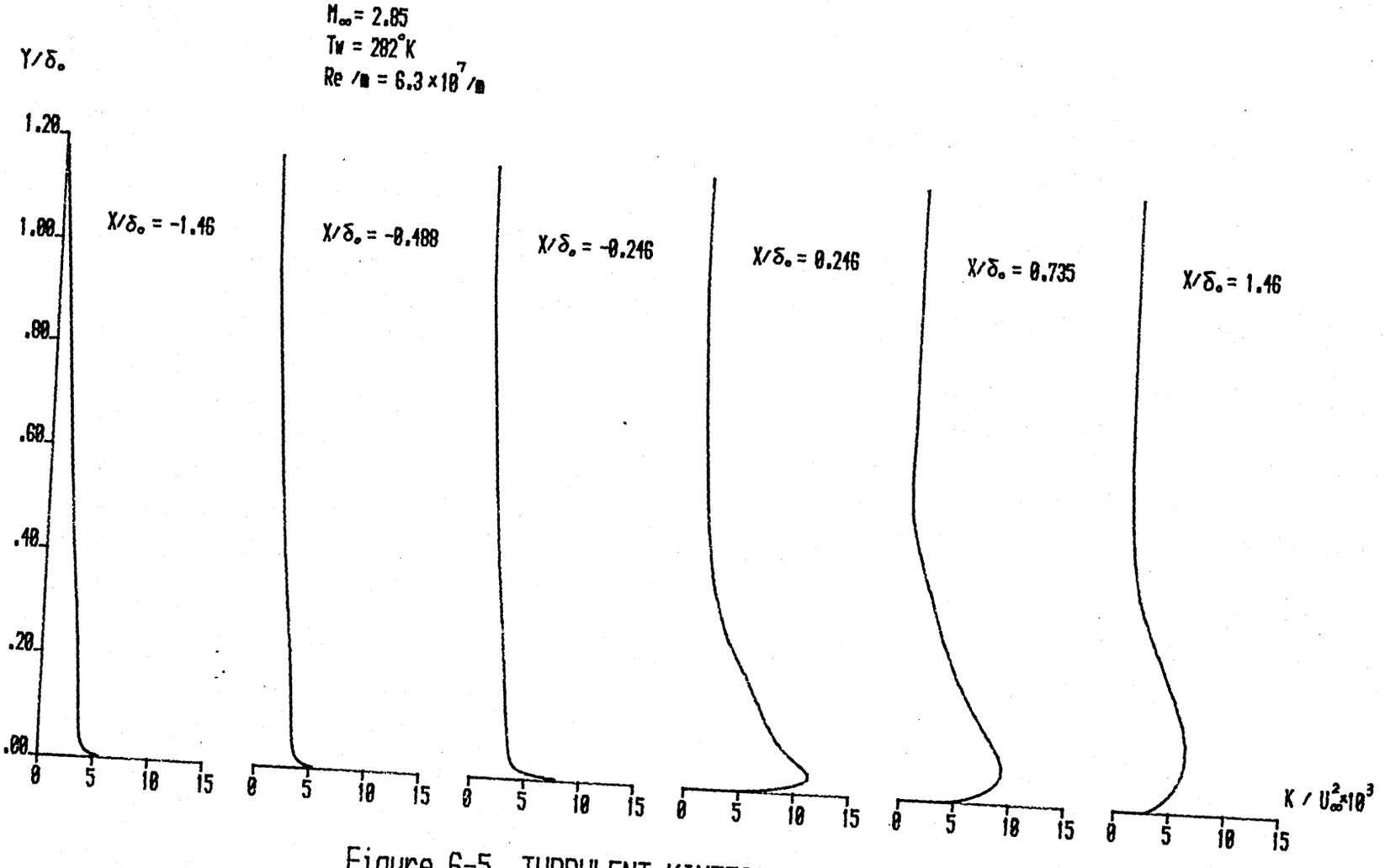

Figure 6-5. TURBULENT KINETIC ENERGY PROFILE
(CASE - 3 - B) RAMP ANGLE 16°

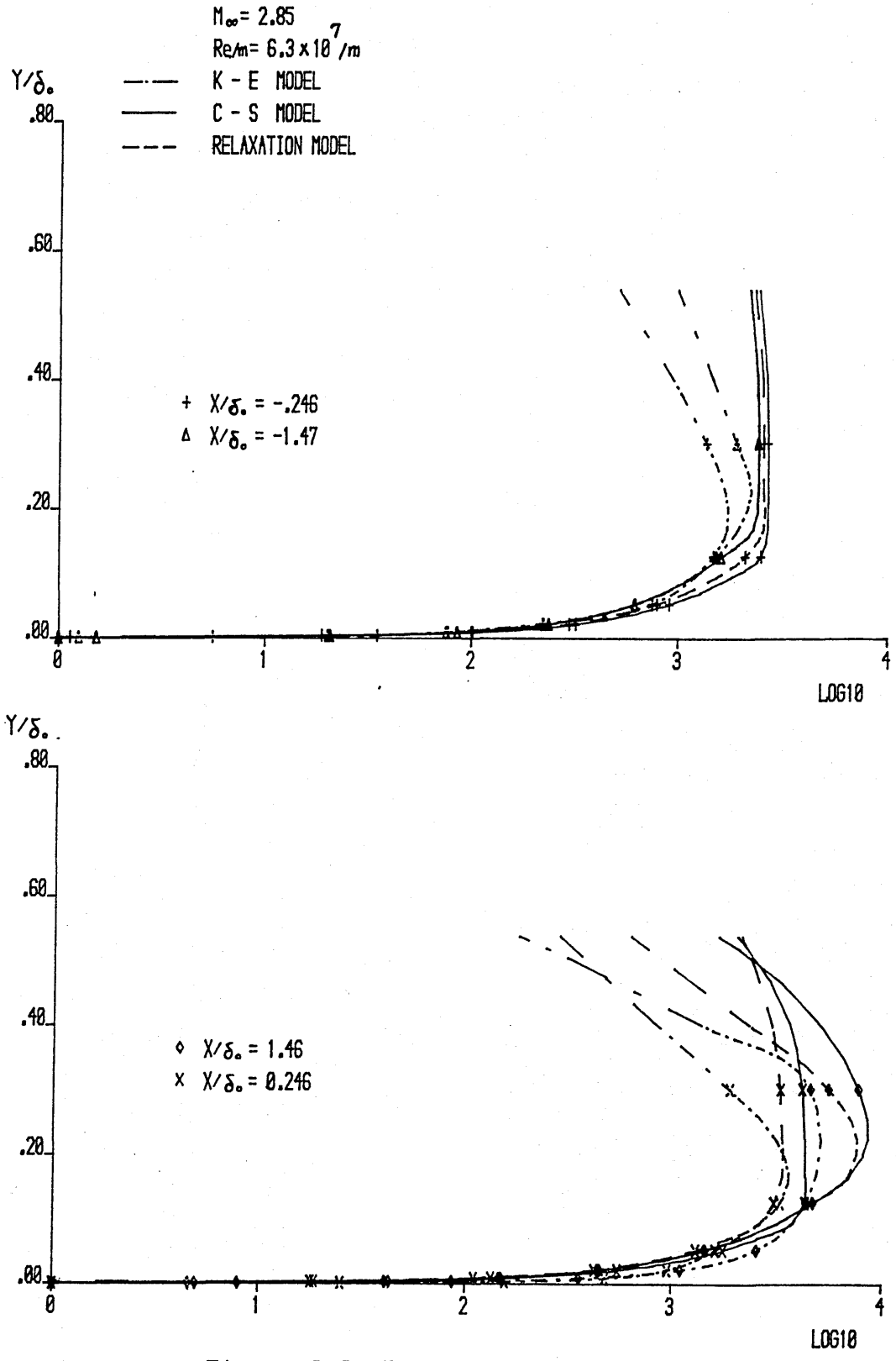

Figure 6-6. EDDY VISCOSITY PROFILE
(CASE - 3 - B) RAMP ANGLE 16°

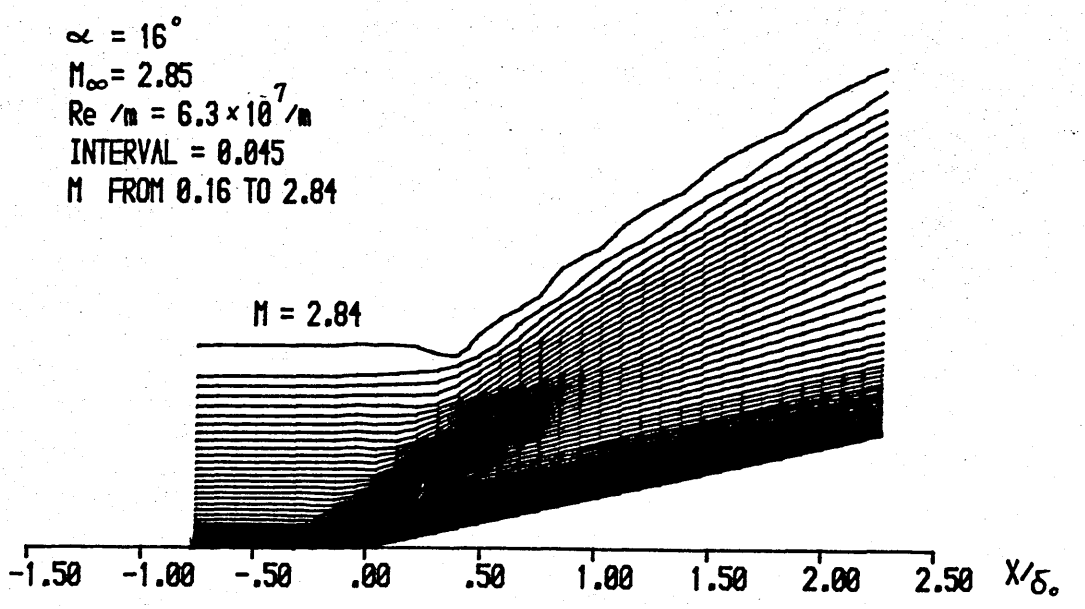

Figure 6-7. MACH NUMBER CONTOURS
K - E MODEL
(CASE - 3 - B)

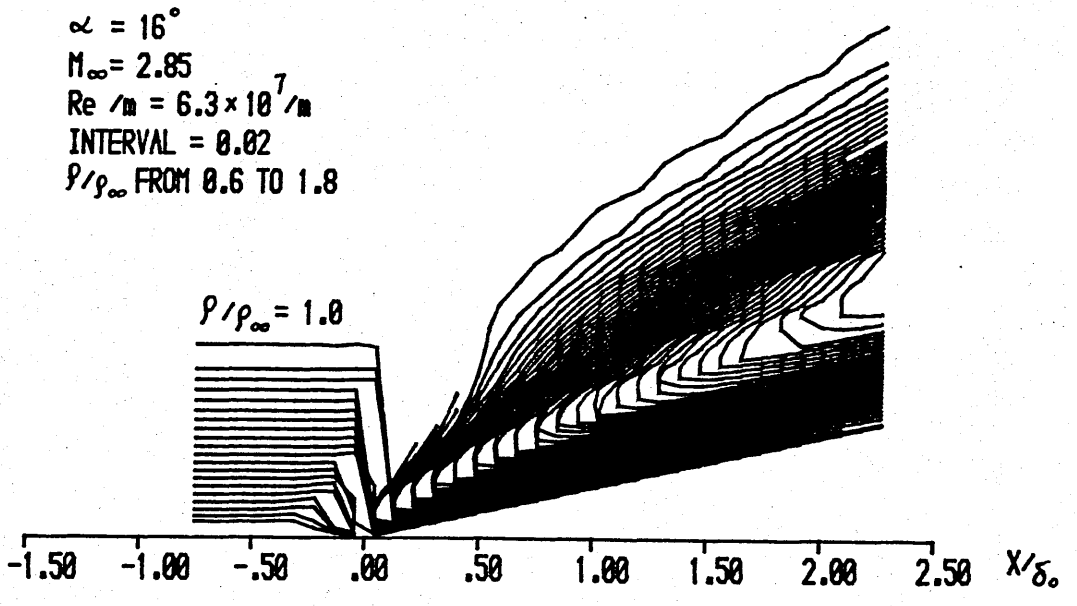

Figure 6-8. DENSITY CONTOURS
K - E MODEL
(CASE - 3 - B)

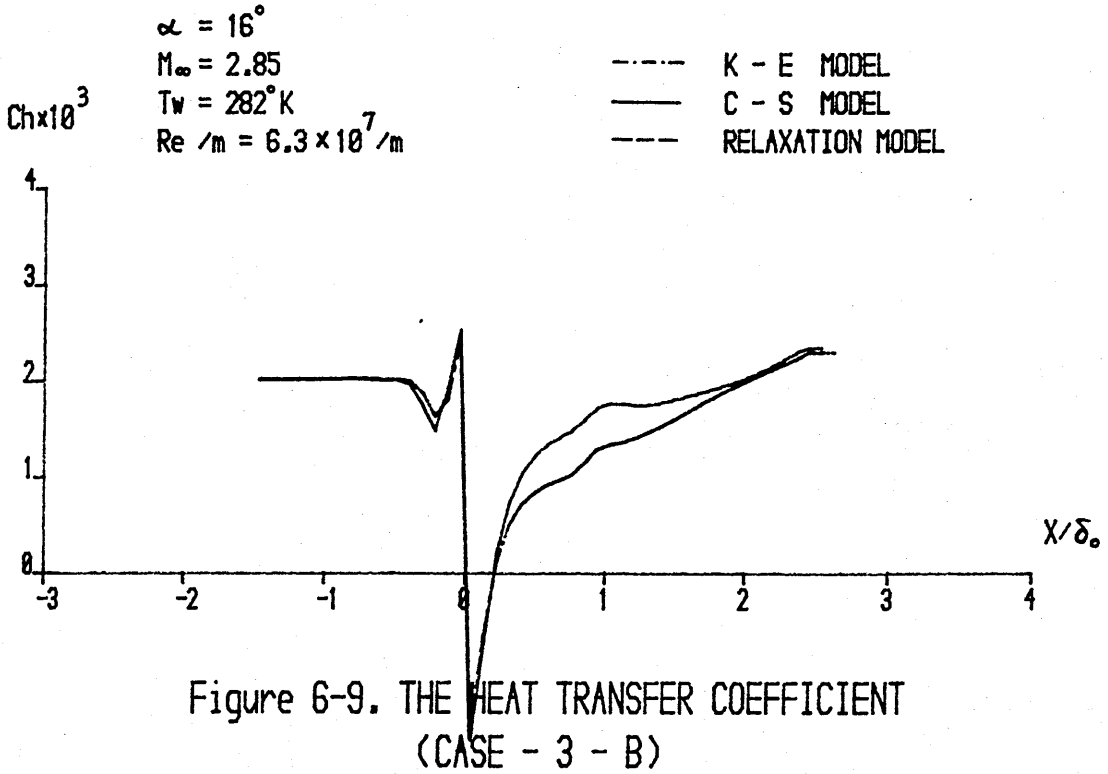

Figure 6-9. THE HEAT TRANSFER COEFFICIENT
(CASE - 3 - B)

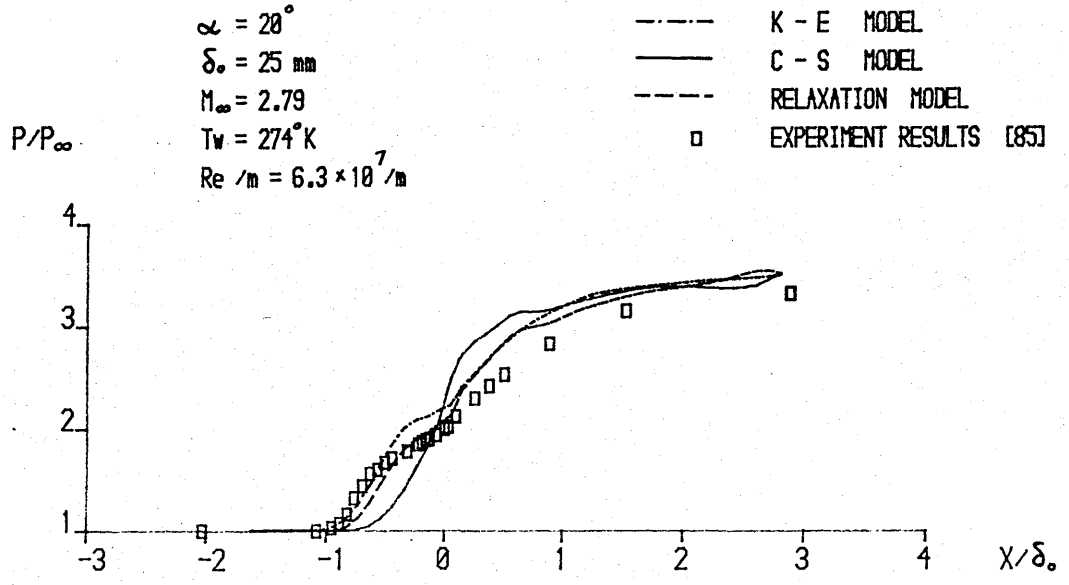

Figure 7-1. THE DISTRIBUTION OF THE WALL PRESSURE
(CASE - 3 - C)

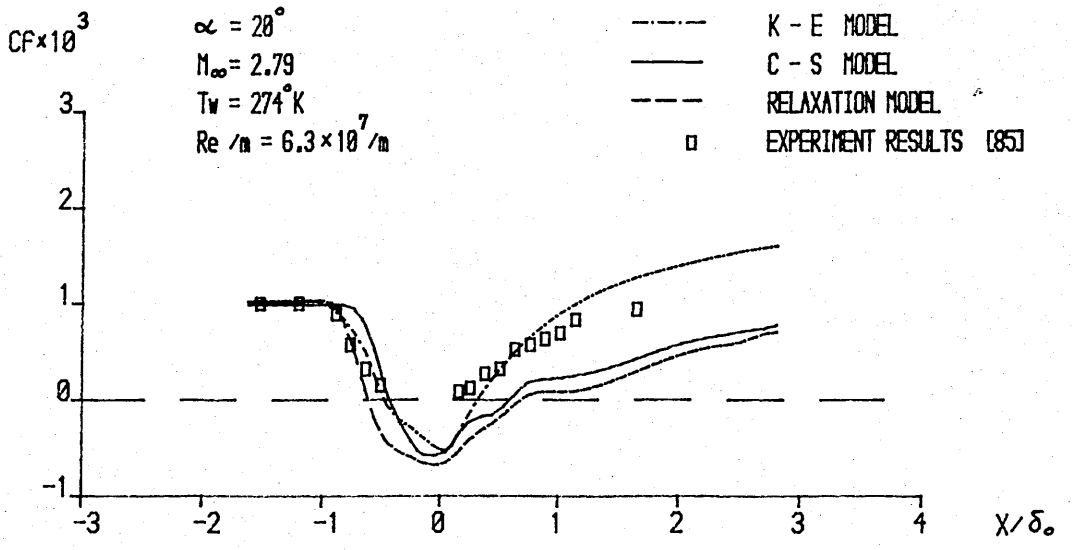

Figure 7-2. SKIN FRICTION COEFFICIENT
(CASE - 3 - C)

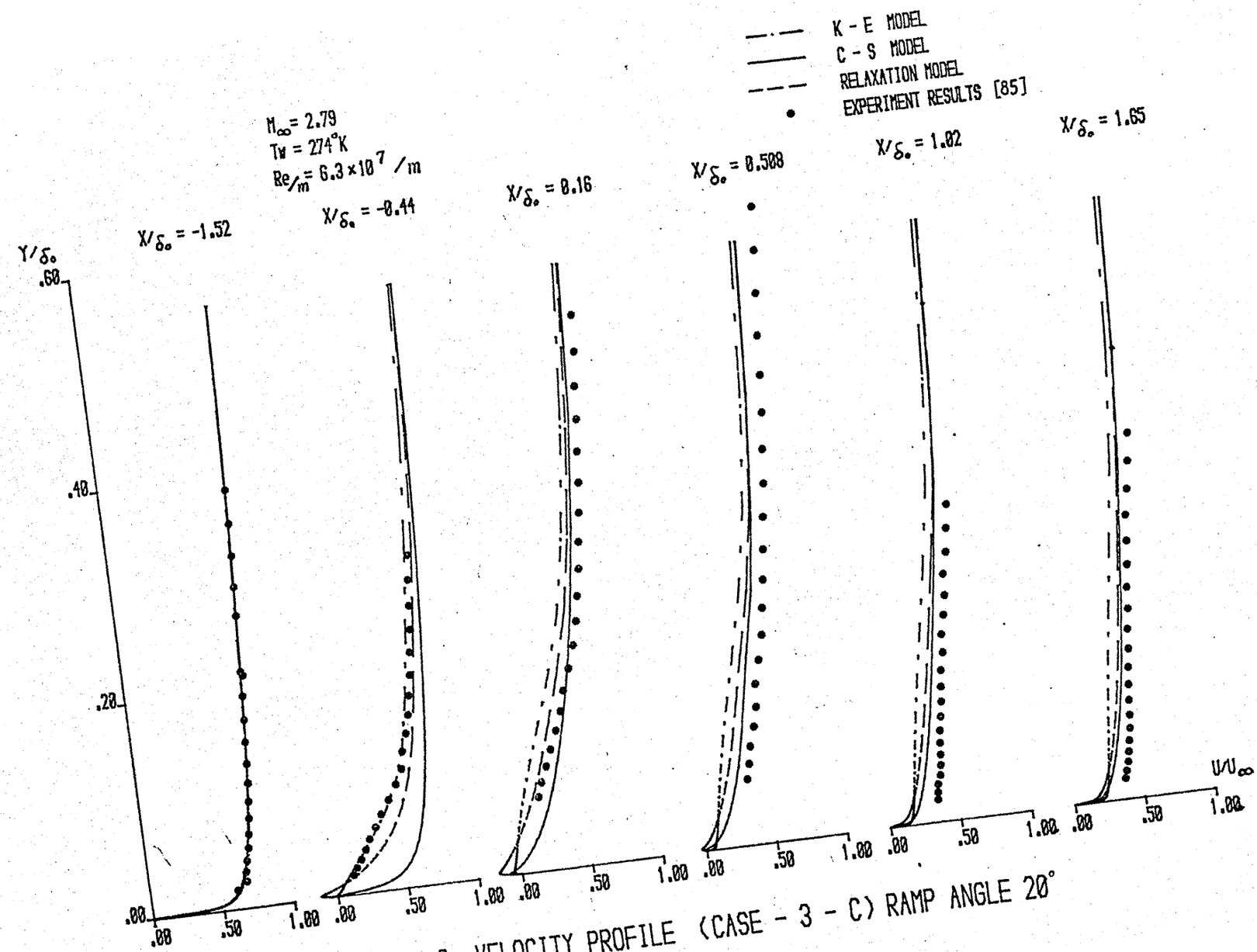

Figure 7-3. VELOCITY PROFILE (CASE - 3 - C) RAMP ANGLE 20°

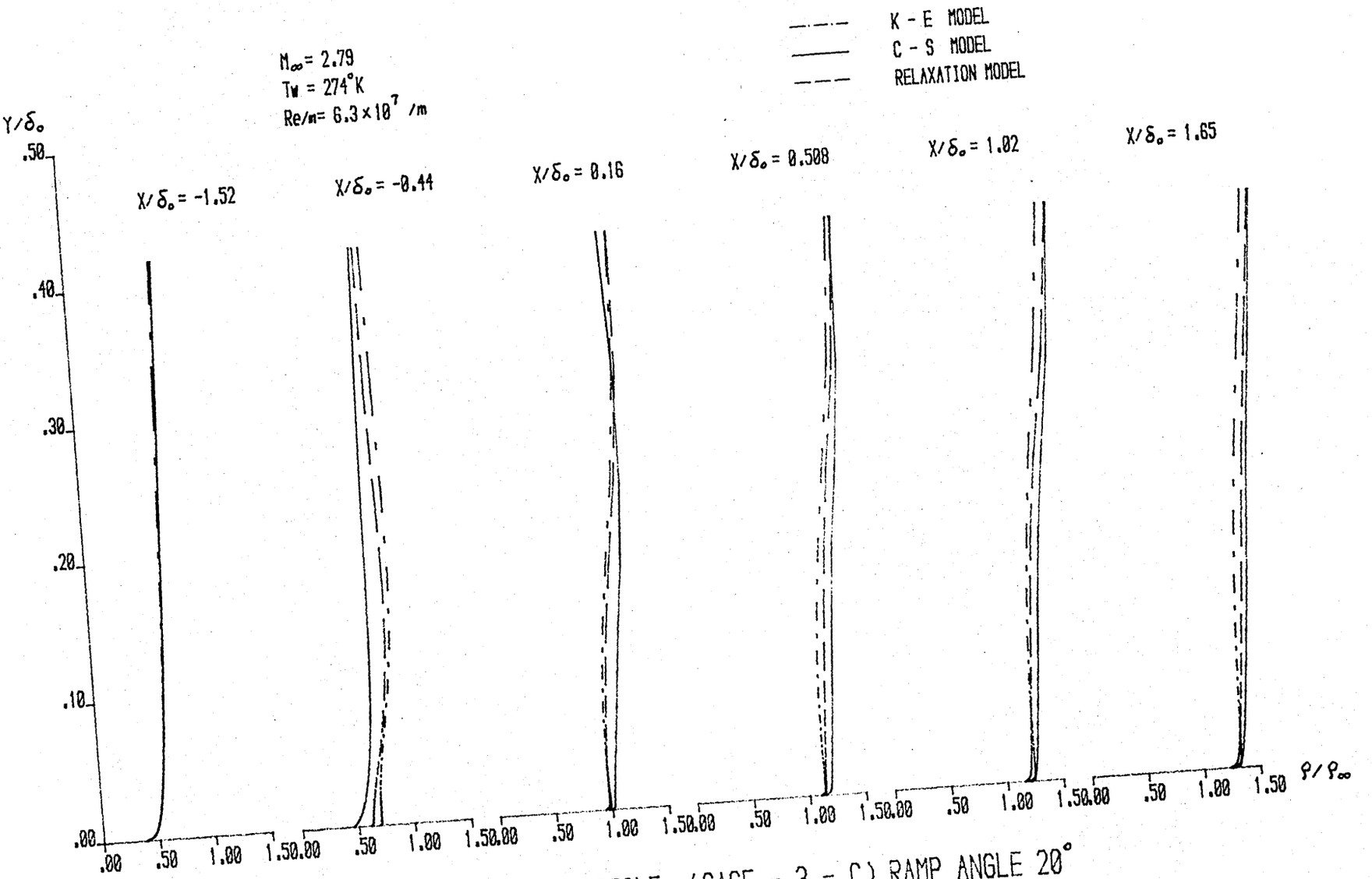

Figure 7-4. DENSITY PROFILE (CASE - 3 - C) RAMP ANGLE 20°

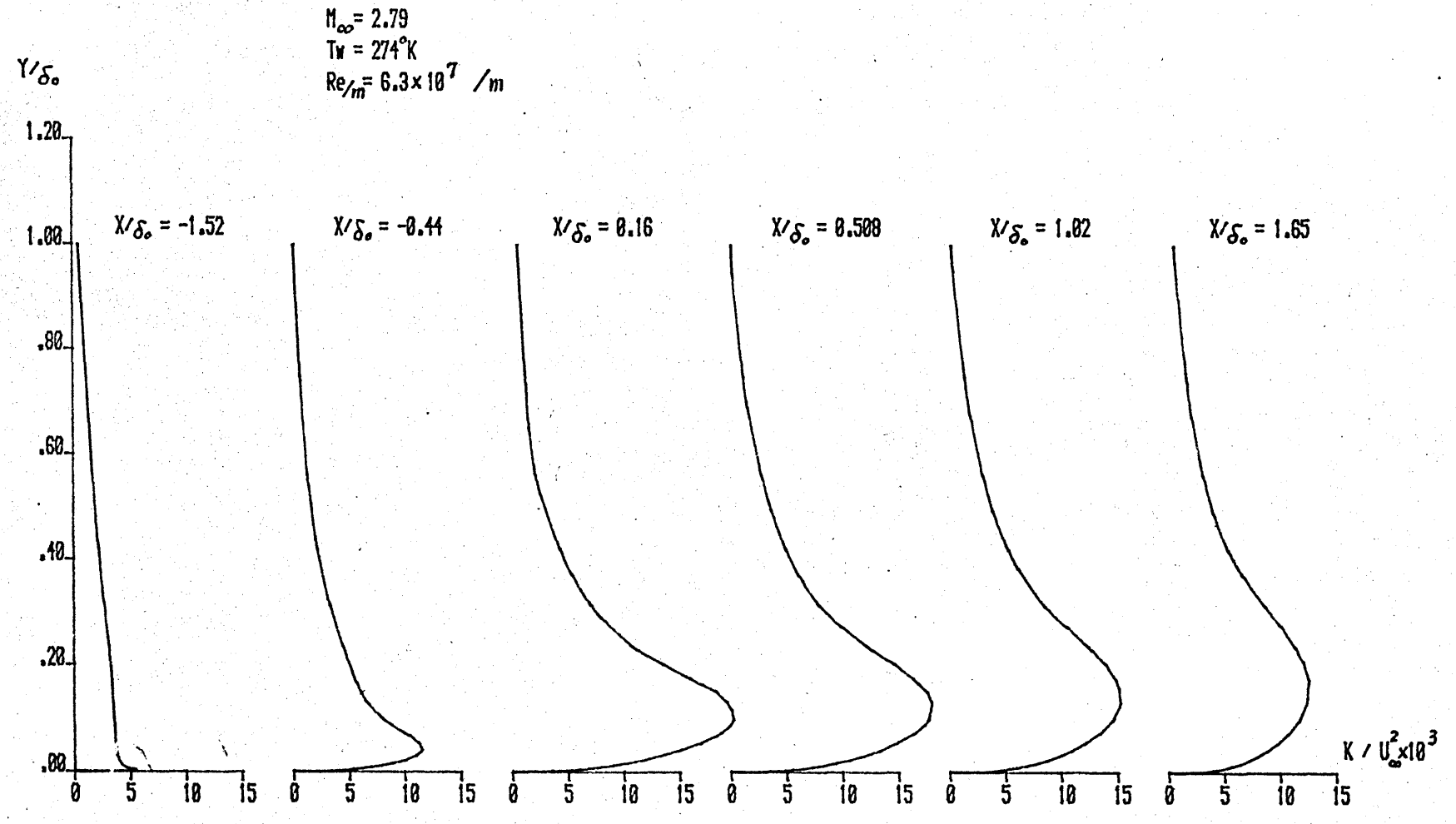

Figure 7-5. TURBULENT KINETIC ENERGY PROFILE
(CASE - 3 - C) RAMP ANGLE 20°

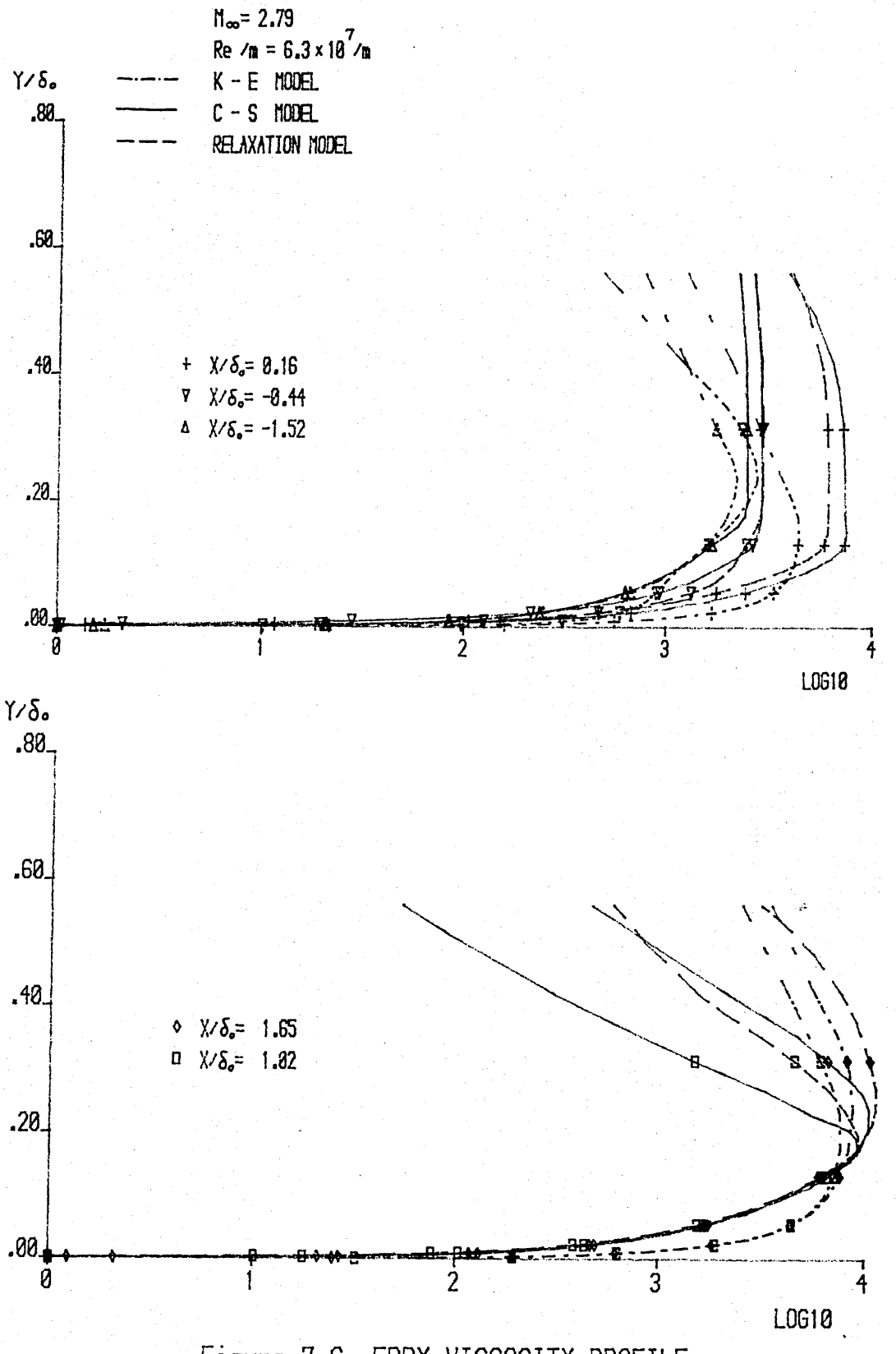

Figure 7-6. EDDY VISCOSITY PROFILE
(CASE - 3 - C) RAMP ANGLE 20°

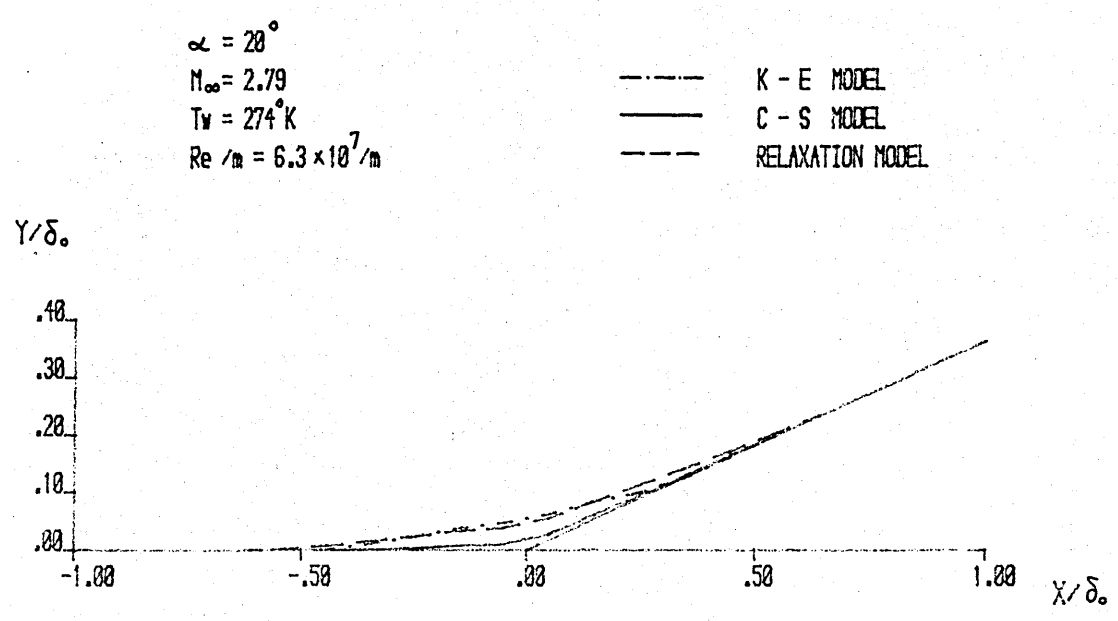

Figure 7-7. THE HEIGHT OF ZERO VELOCITY LINE
(CASE - 3 - C)

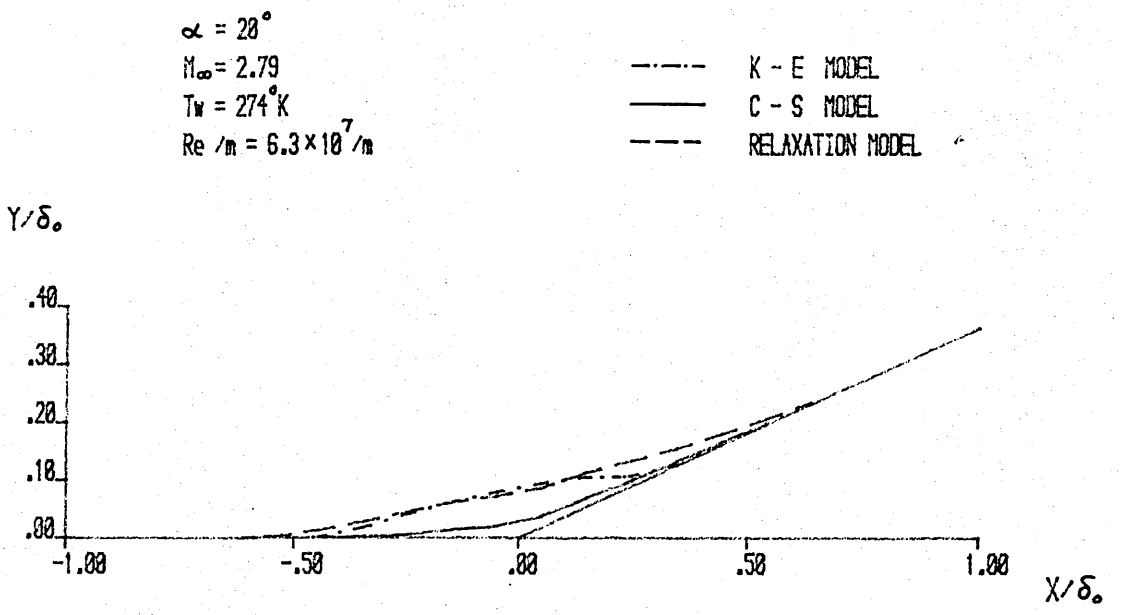

Figure 7-8. THE HEIGHT OF DIVIDING STREAM
(CASE - 3 - C)

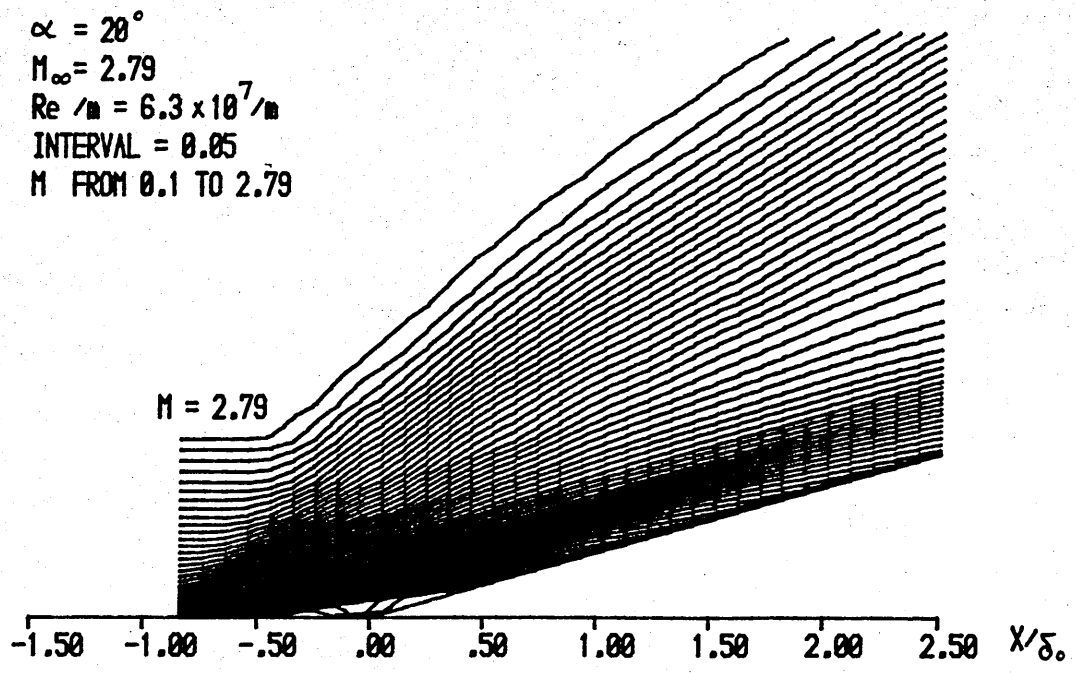

Figure 7-9. MACH NUMBER CONTOURS
K - E MODEL
(CASE - 3 - C)

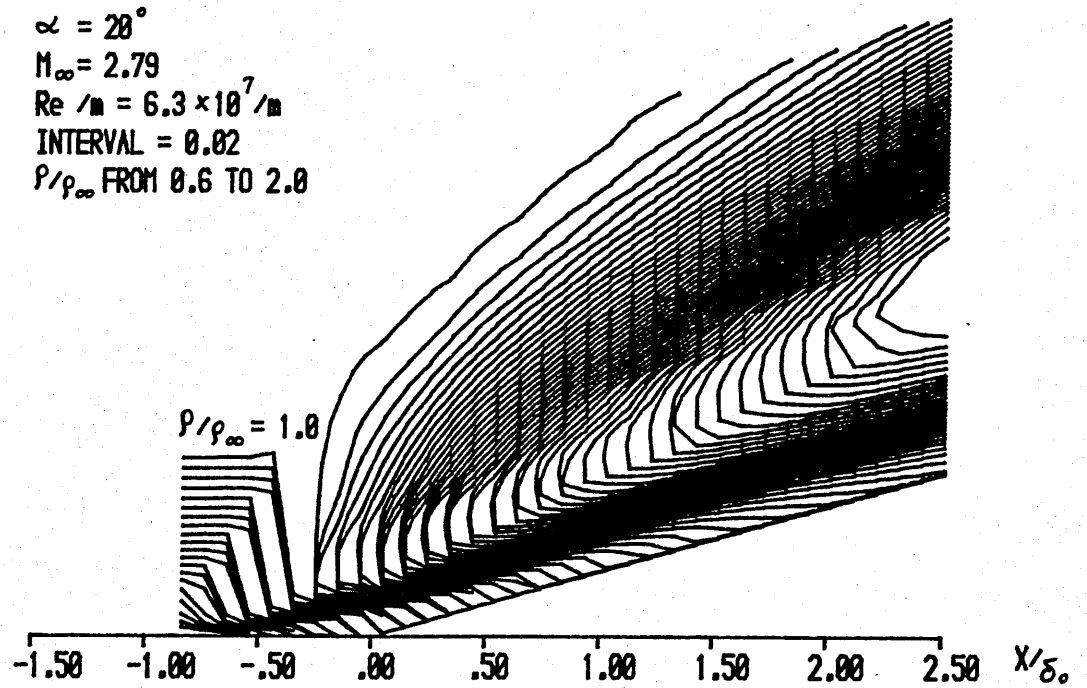

Figure 7-10. DENSITY CONTOURS
K - E MODEL
(CASE - 3 - C)

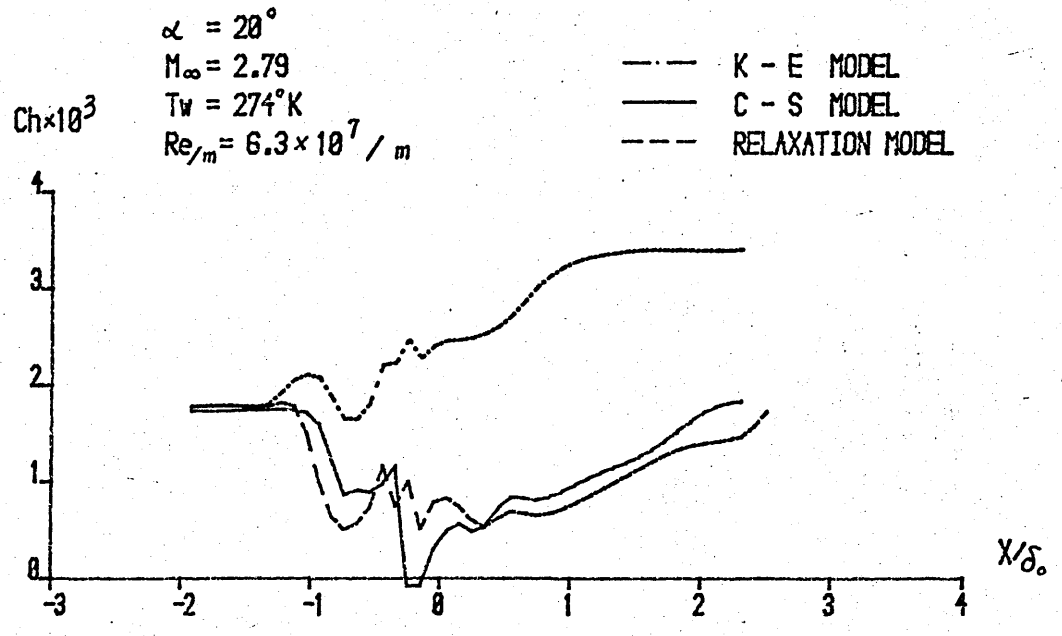

Figure 7-11. THE HEAT TRANSFER COEFFICIENT (CASE - 3 - C)

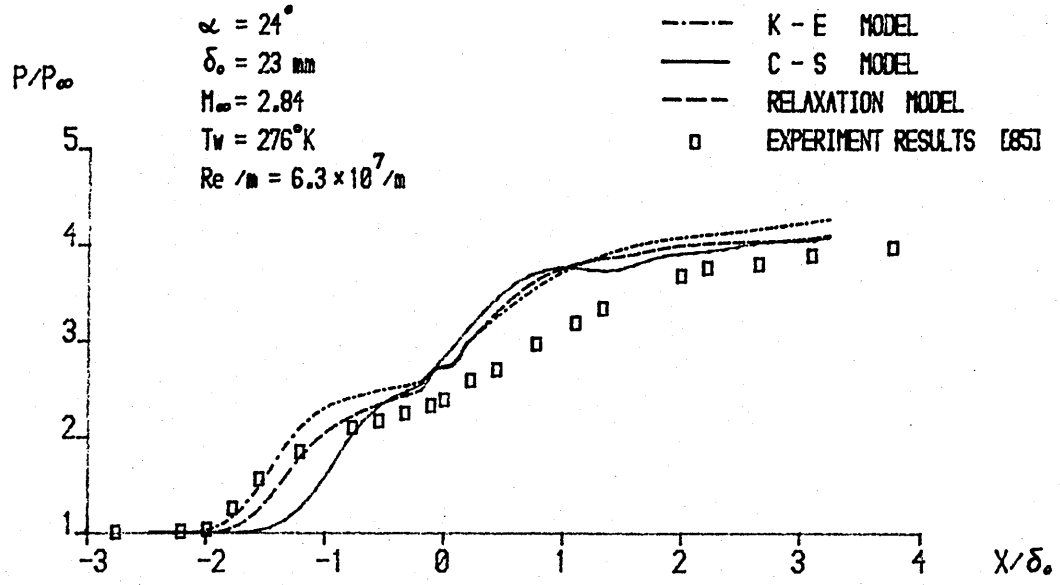

Figure 8-1. THE DISTRIBUTION OF THE WALL PRESSURE
(CASE - 3 - D)

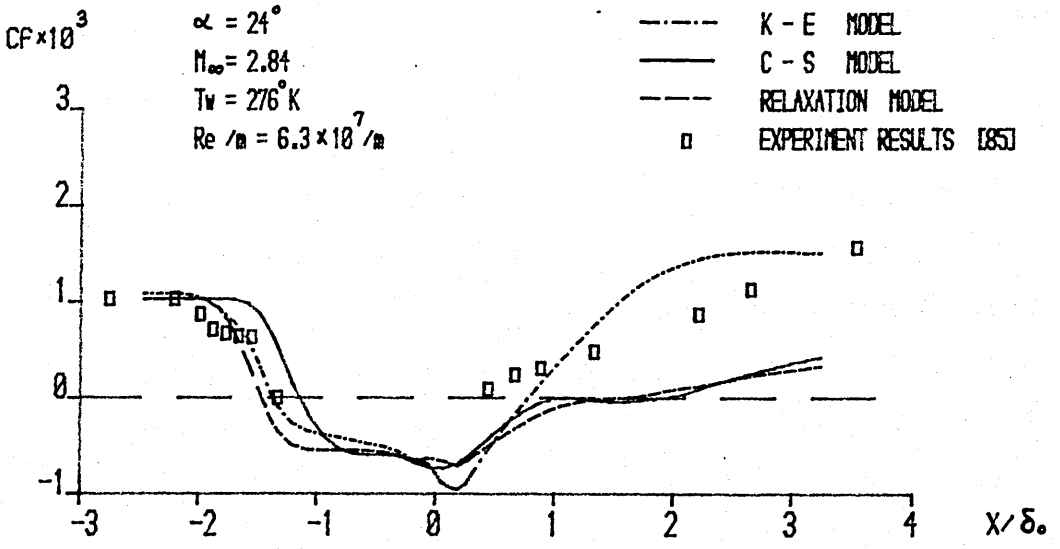

Figure 8-2. SKIN FRICTION COEFFICIENT
(CASE - 3 - D)

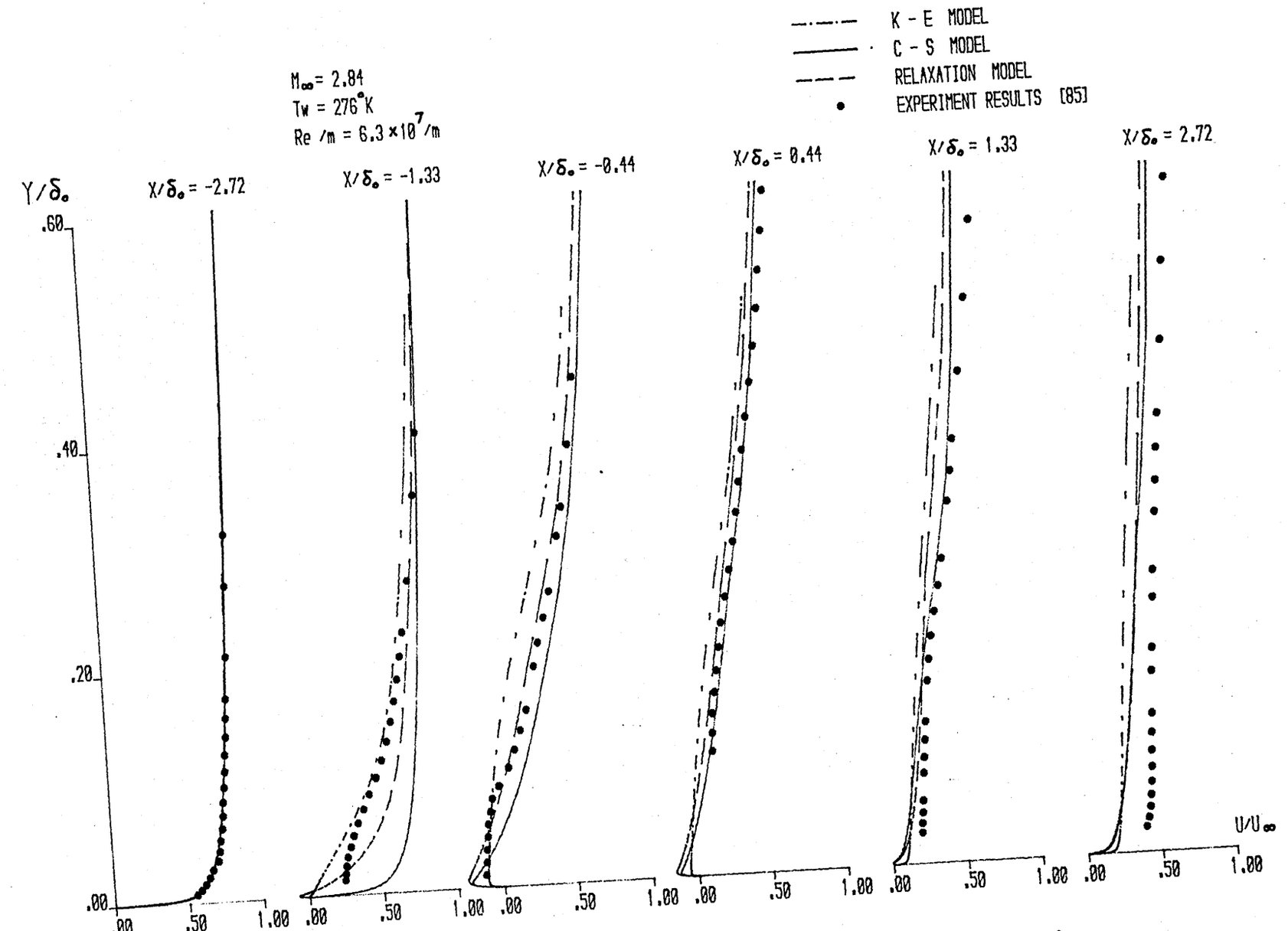

Figure 8-3. VELOCITY PROFILE (CASE - 3 - D) RAMP ANGLE 24°

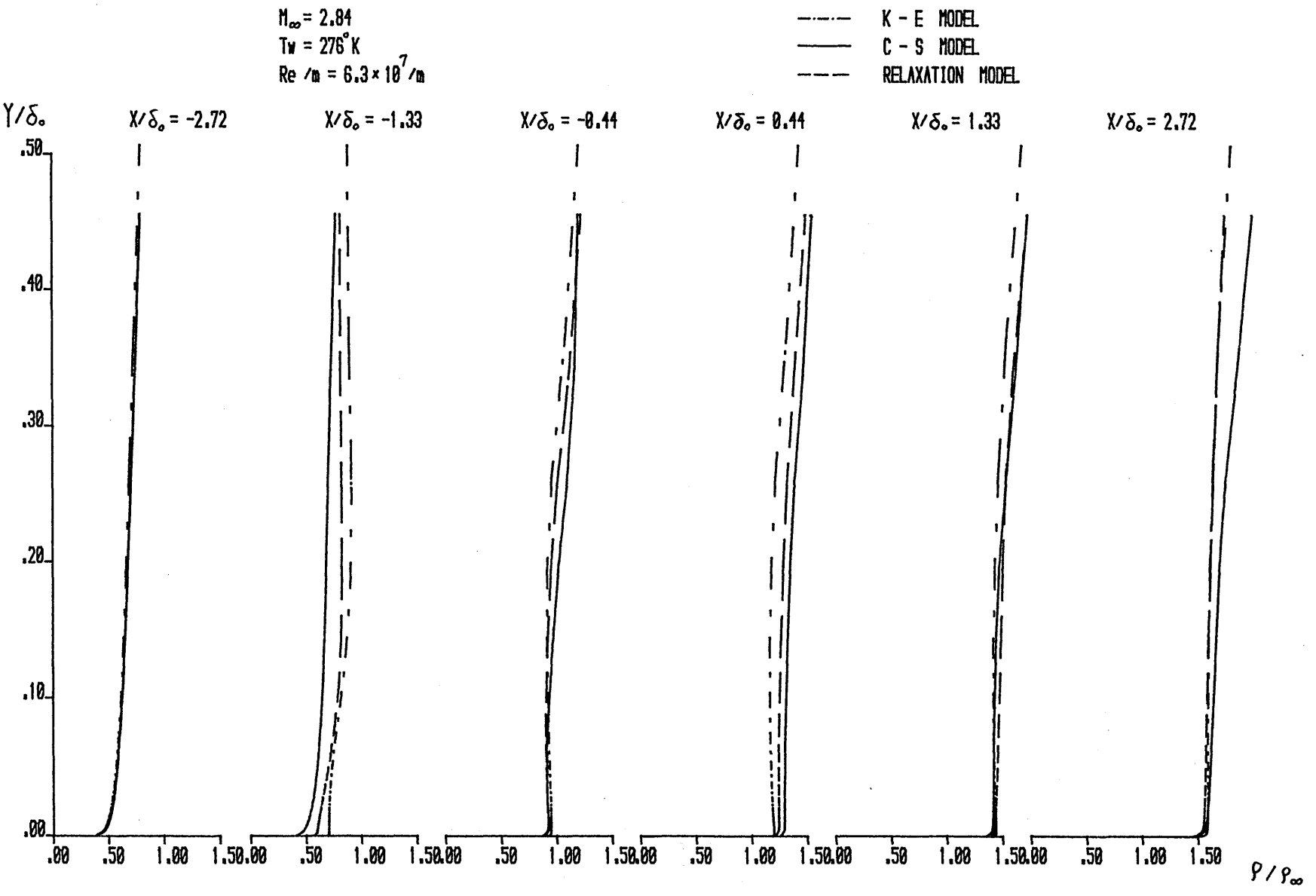

Figure 8-4. DENSITY PROFILE (CASE - 3 - D) RAMP ANGLE 24°

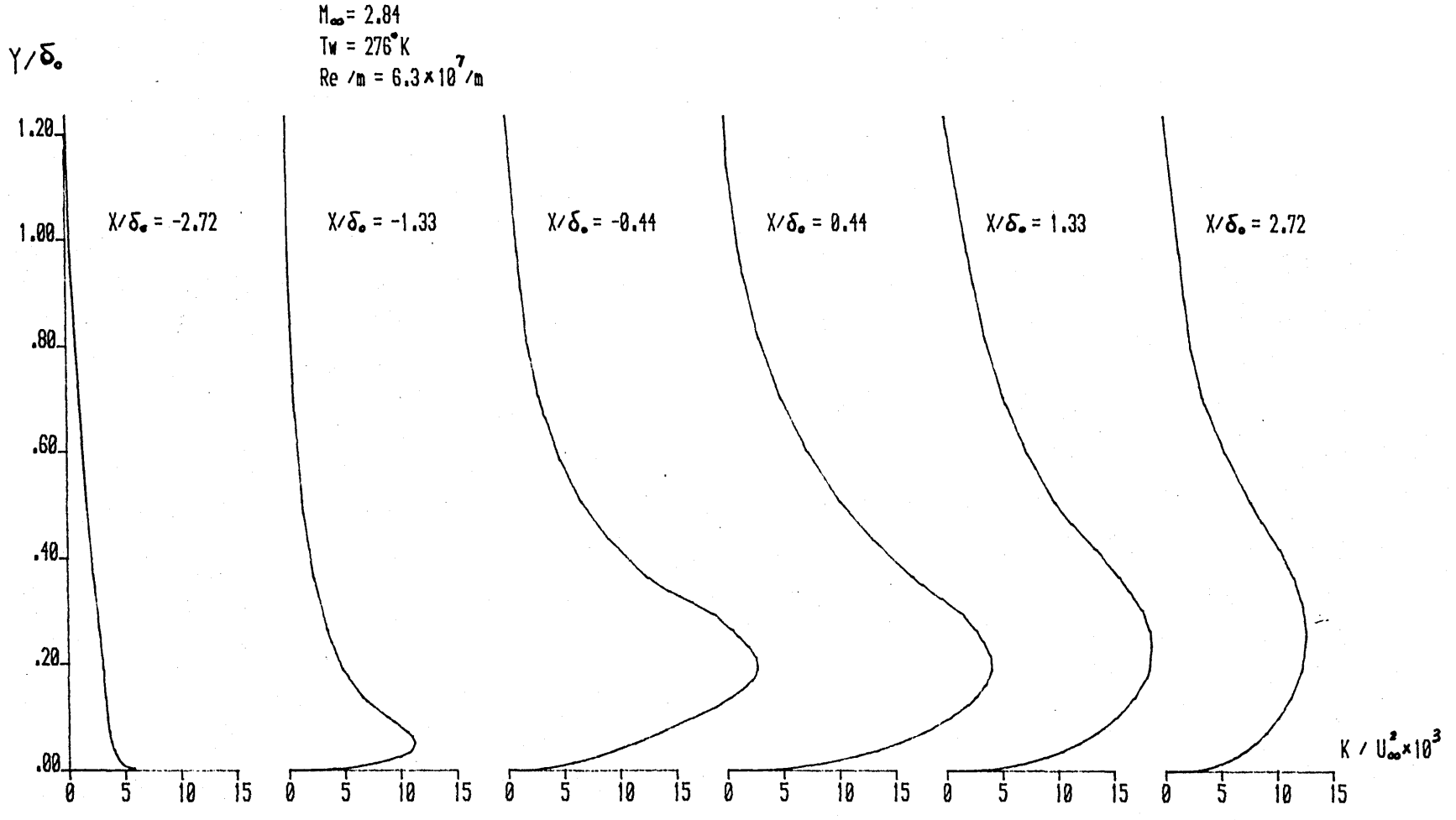

Figure 8-5. TURBULENT KINETIC ENERGY PROFILE
(CASE - 3 - D) RAMP ANGLE 24°

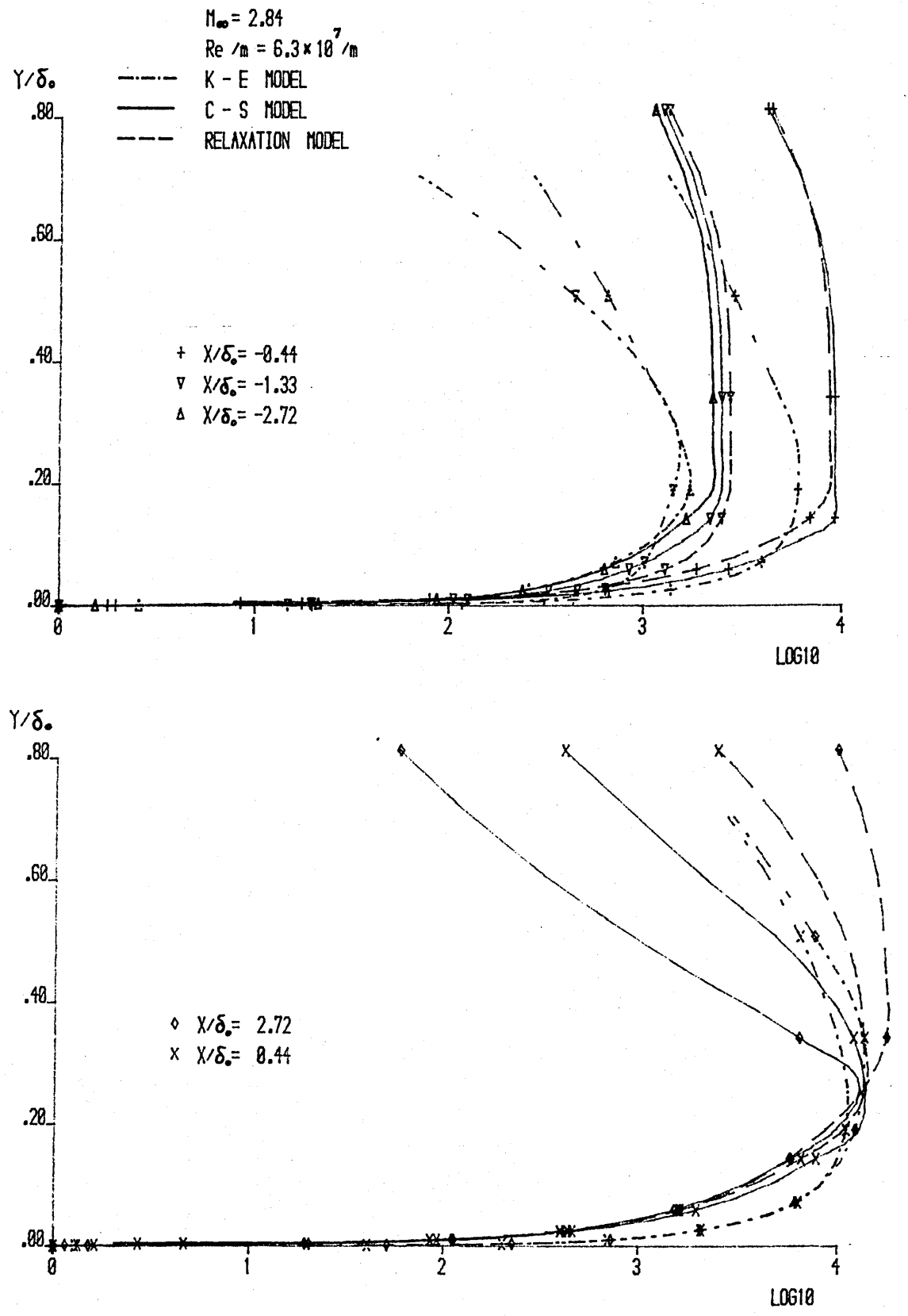

Figure 8-6. EDDY VISCOSITY PROFILE
(CASE - 3 - D) RAMP ANGLE 24°

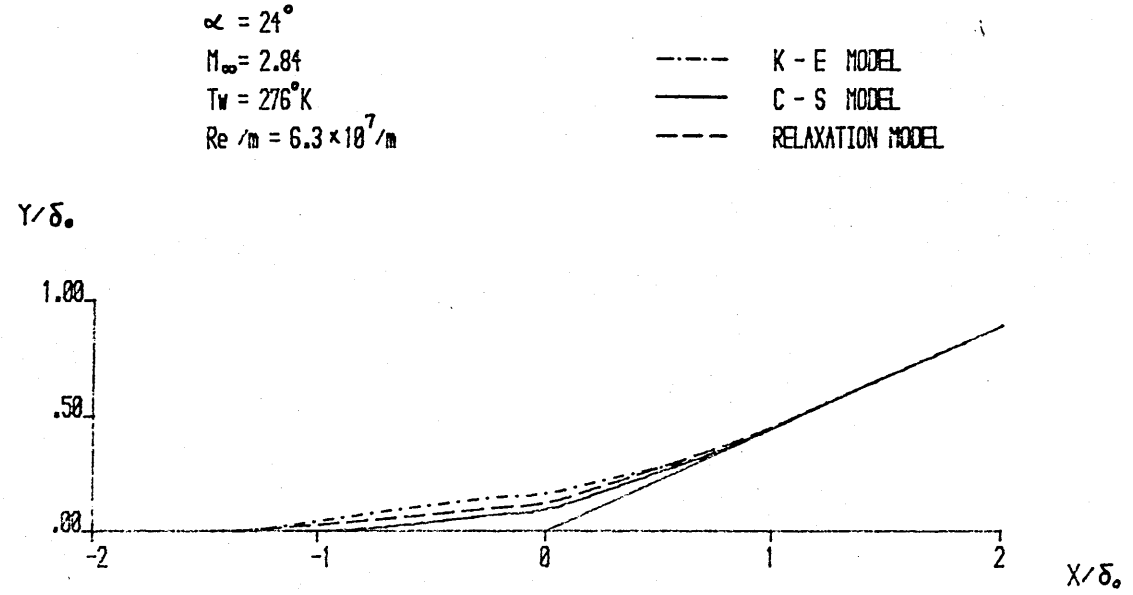

Figure 8-7. THE HEIGHT OF ZERO VELOCITY LINE
(CASE - 3 - D)

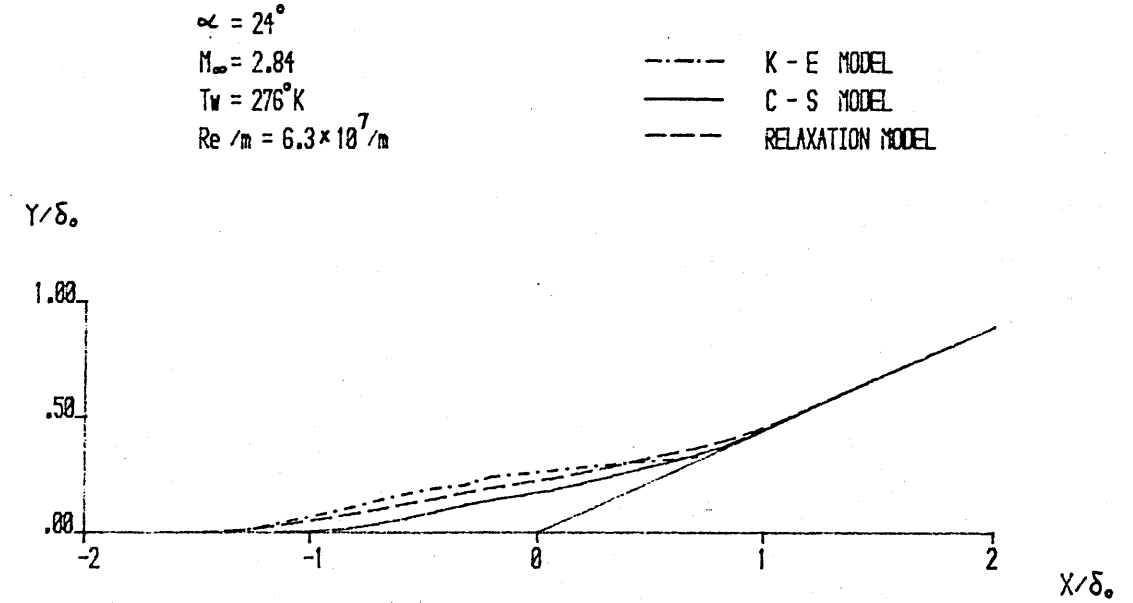

Figure 8-8. THE HEIGHT OF DIVIDING STREAM
(CASE - 3 - D)

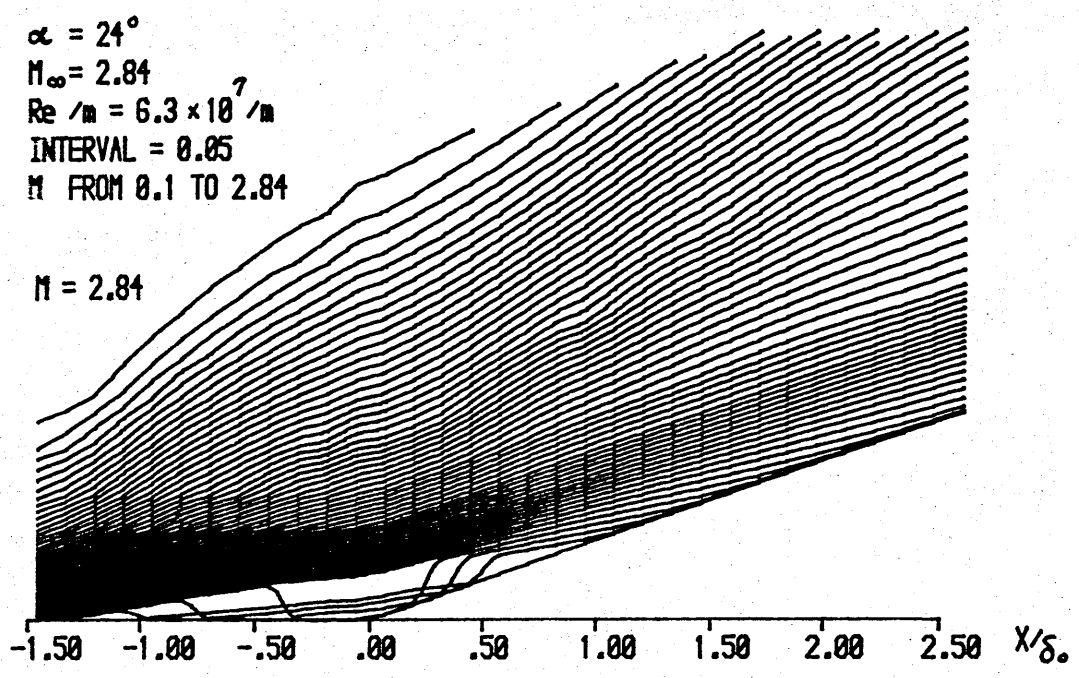

Figure 8-9-1. MACH NUMBER CONTOURS
K - E MODEL
(CASE - 3 - D)

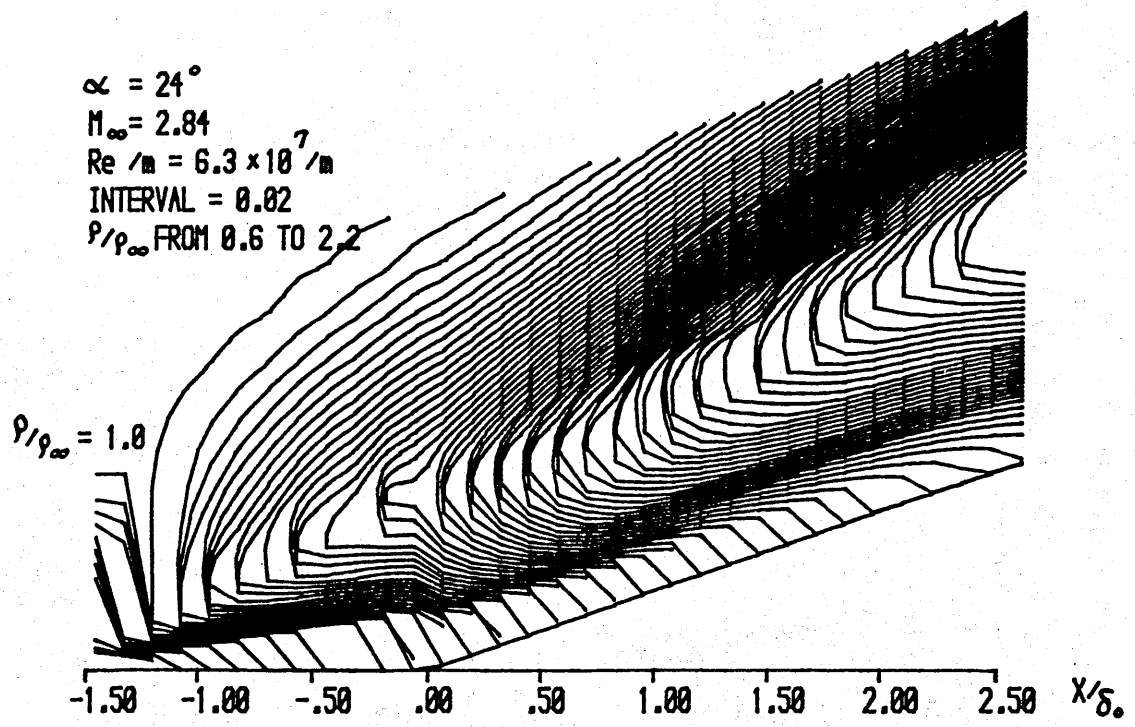

Figure 8-10-1. DENSITY CONTOURS
K - E MODEL
(CASE - 3 - D)

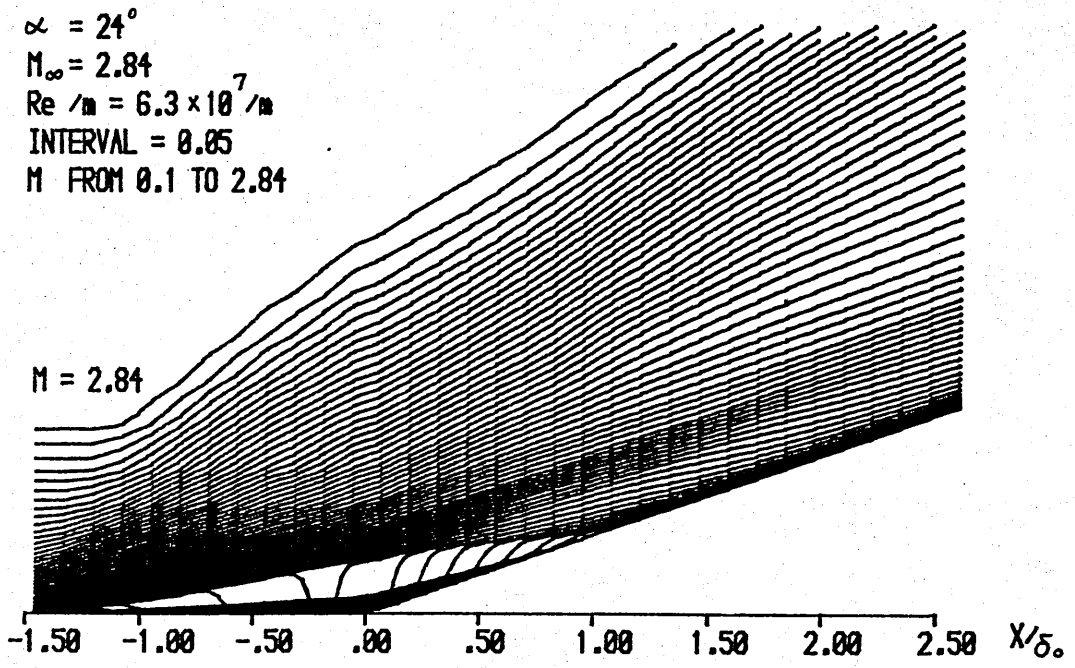

Figure 8-9-2. MACH NUMBER CONTOURS
UPSTREAM RELAXATION
(CASE - 3 - D)

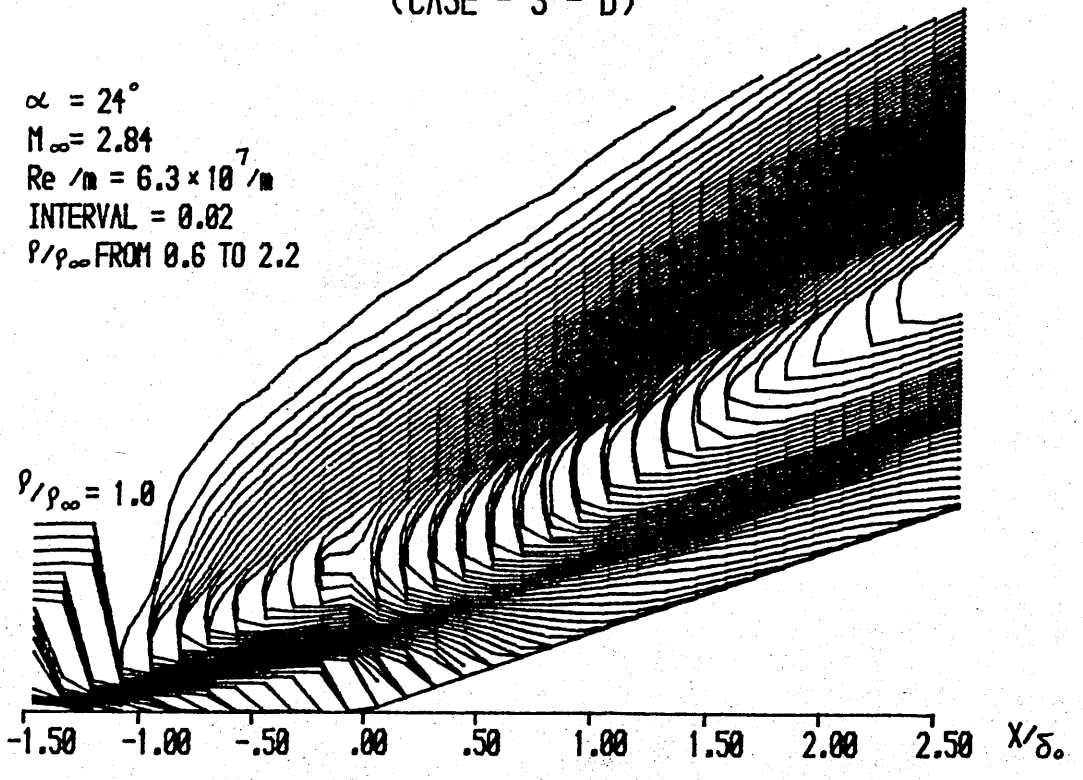

Figure 8-10-2. DENSITY CONTOURS
UPSTREAM RELAXATION
(CASE - 3 - D)

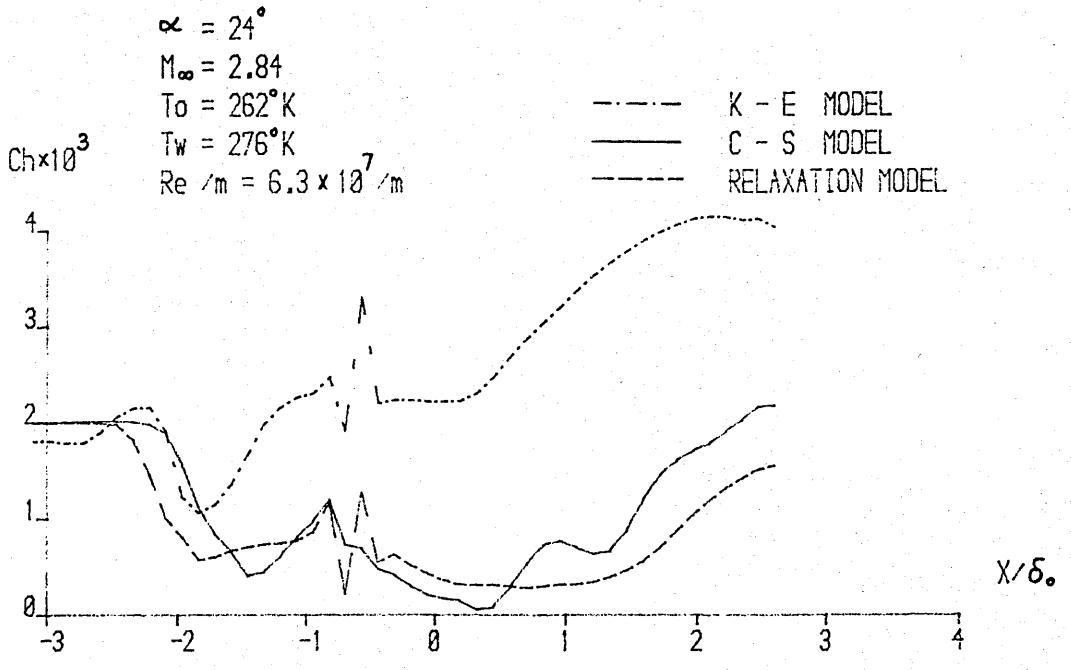

Figure 8-11. THE HEAT TRANSFER COEFFICIENT
(CASE - 3 - D)

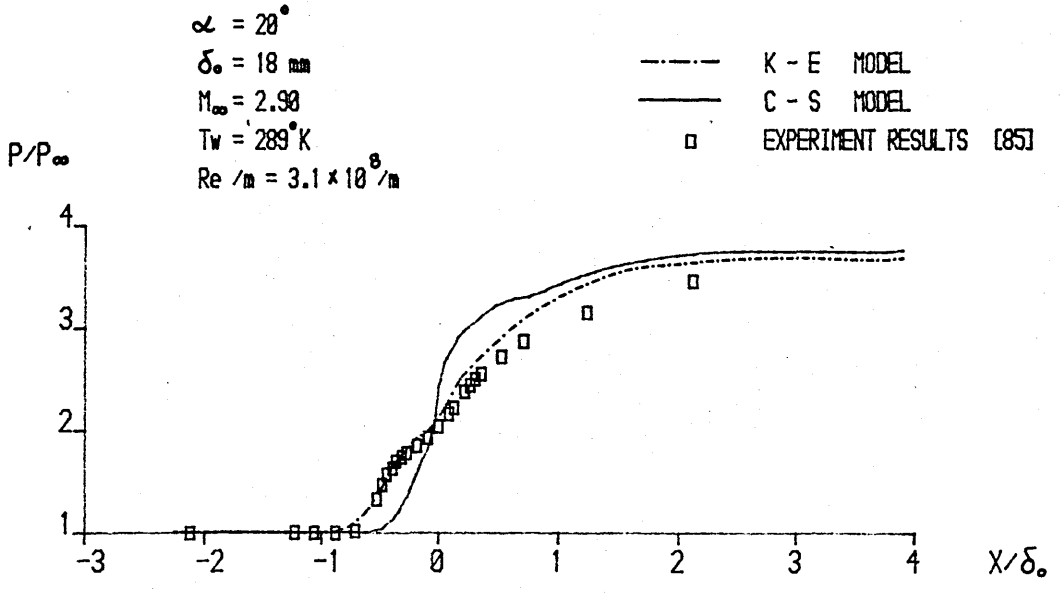

Figure 9-1. THE DISTRIBUTION OF THE WALL PRESSURE (CASE - 4)

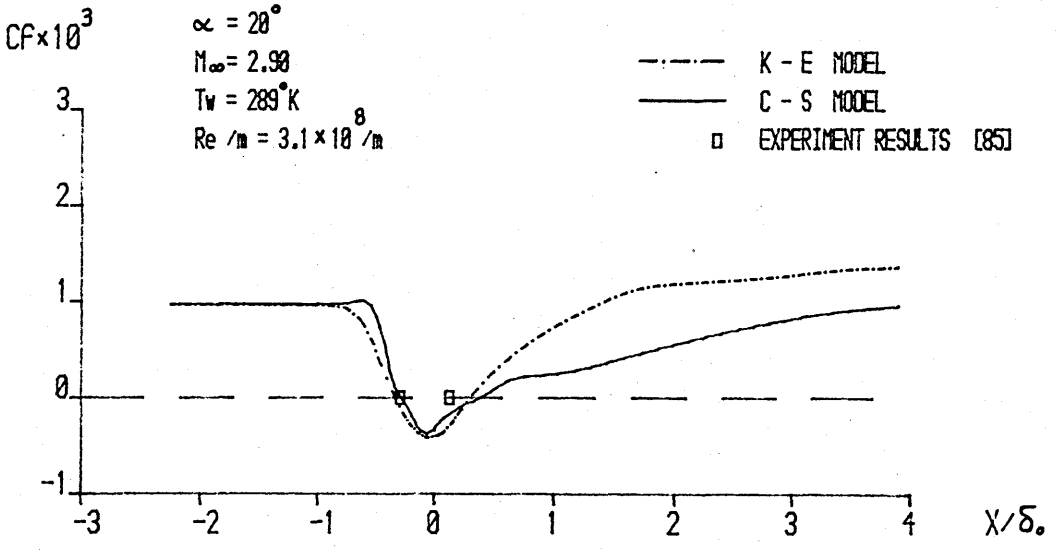

Figure 9-2. SKIN FRICTION COEFFICIENT (CASE - 4)

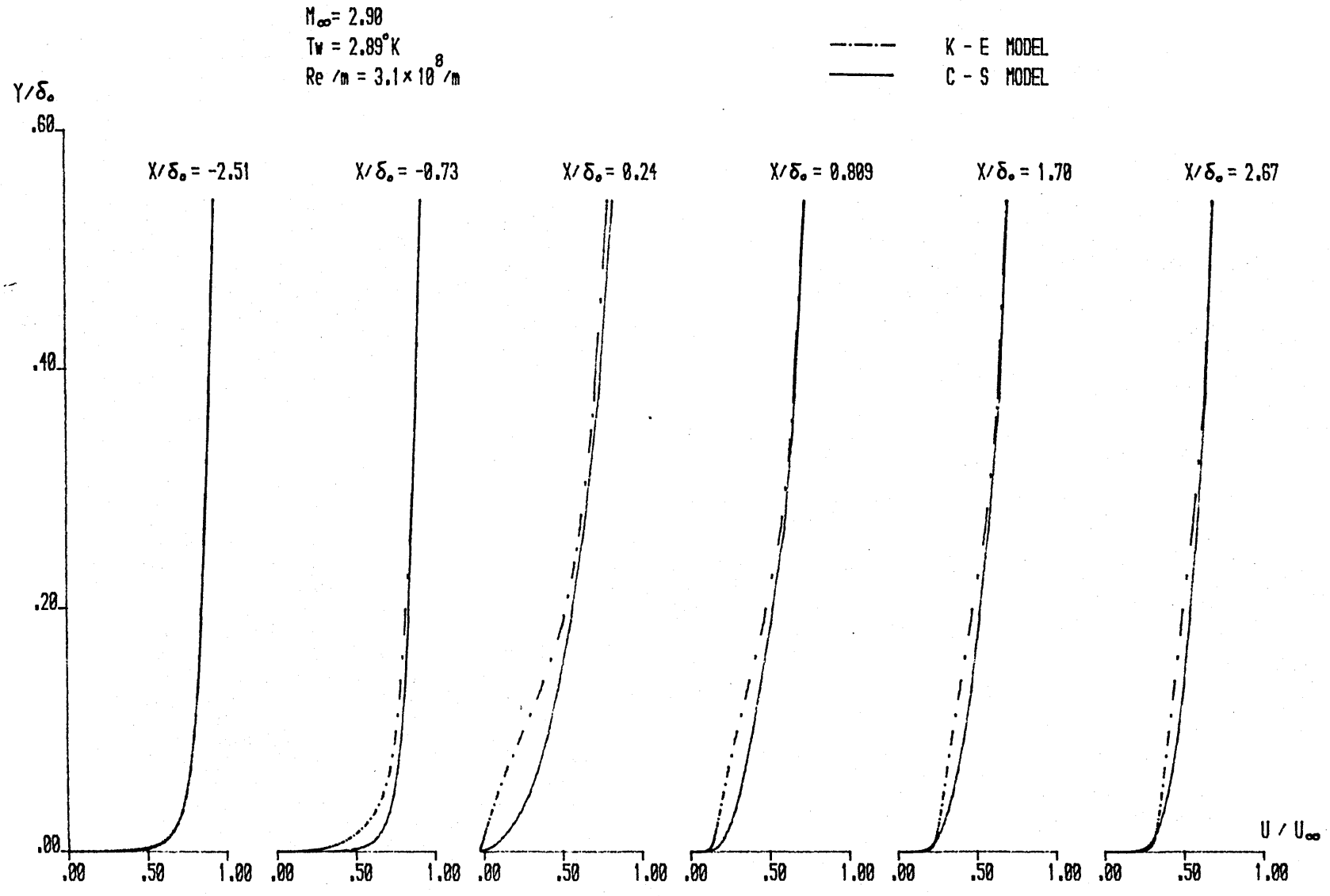

Figure 9-3. VELOCITY PROFILE (CASE - 4) RAMP ANGLE 20°

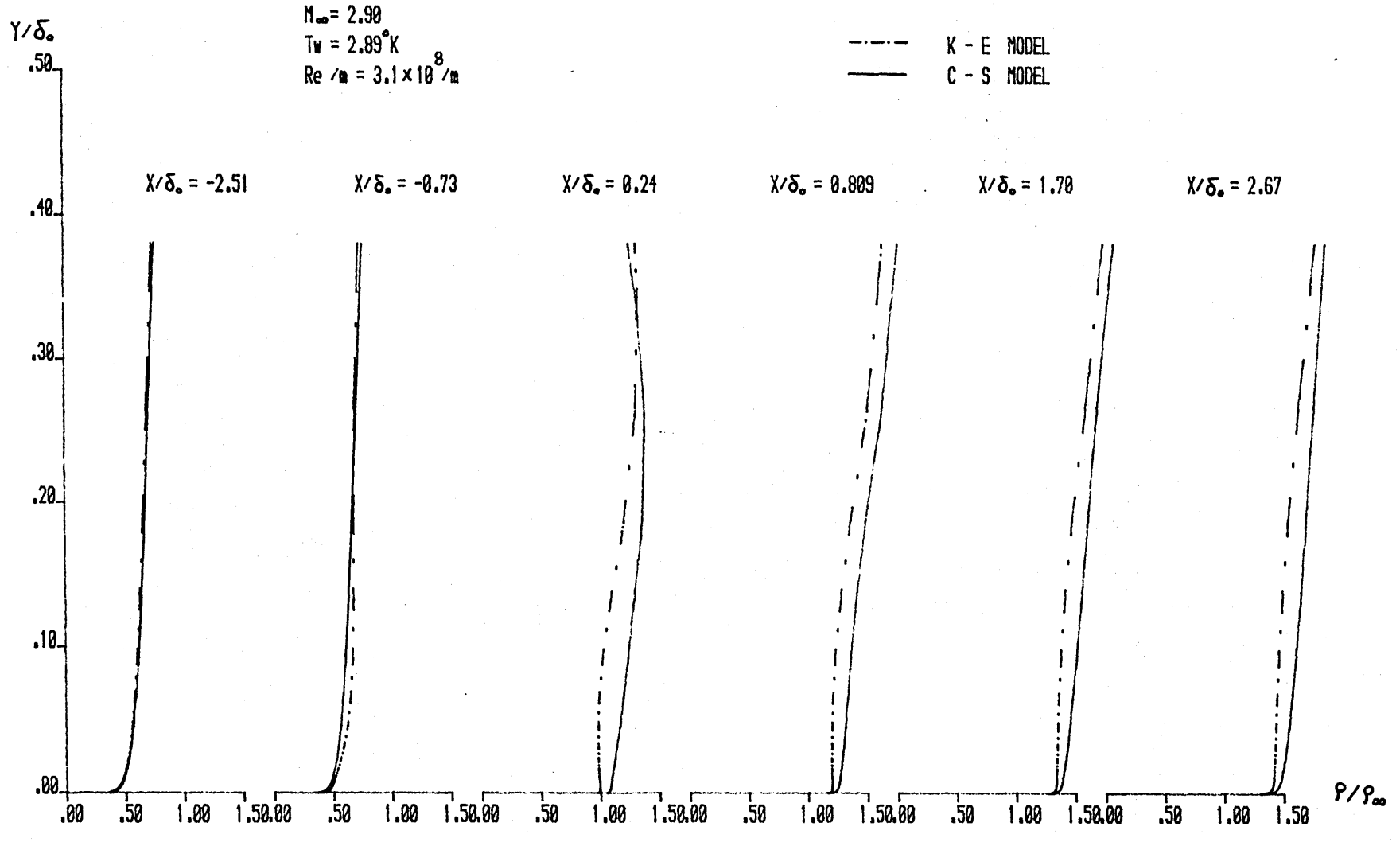

Figure 9-4. DENSITY PROFILE (CASE - 4) RAMP ANGLE 20°

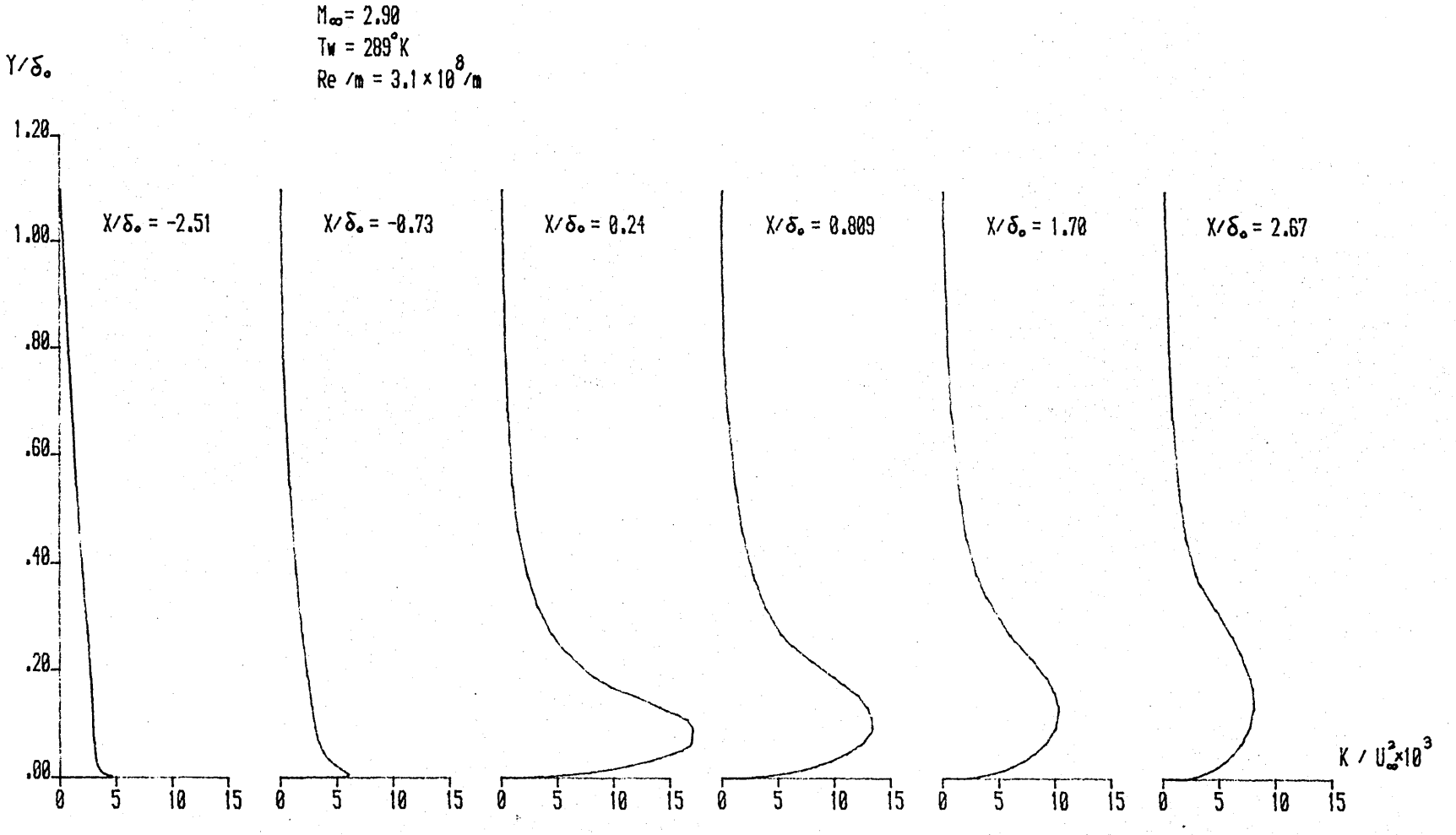

Figure 9-5. TURBULENT KINETIC ENERGY PROFILE
(CASE - 4) RAMP ANGLE 20°

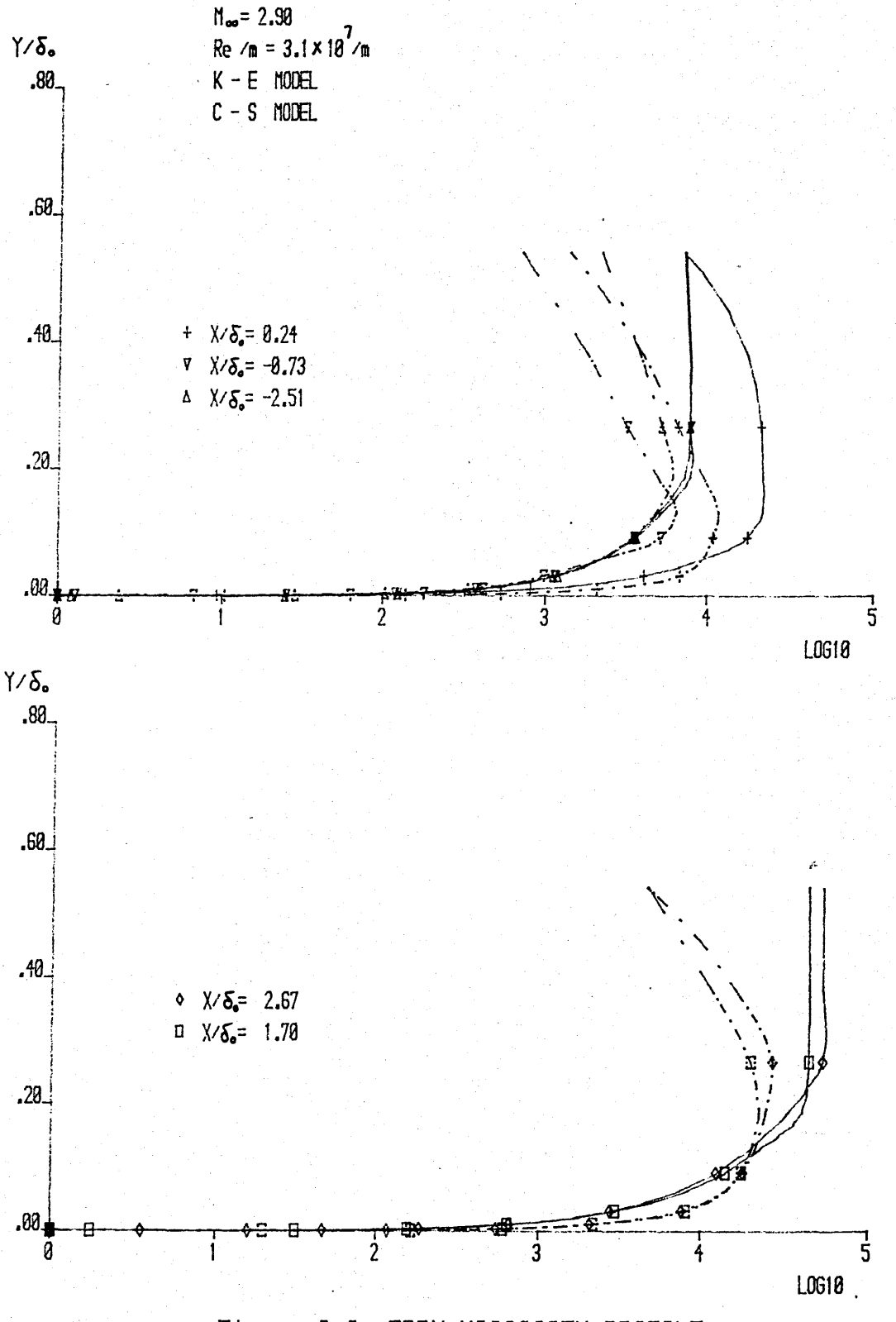

Figure 9-6. EDDY VISCOSITY PROFILE
(CASE - 4) RAMP ANGLE 20°

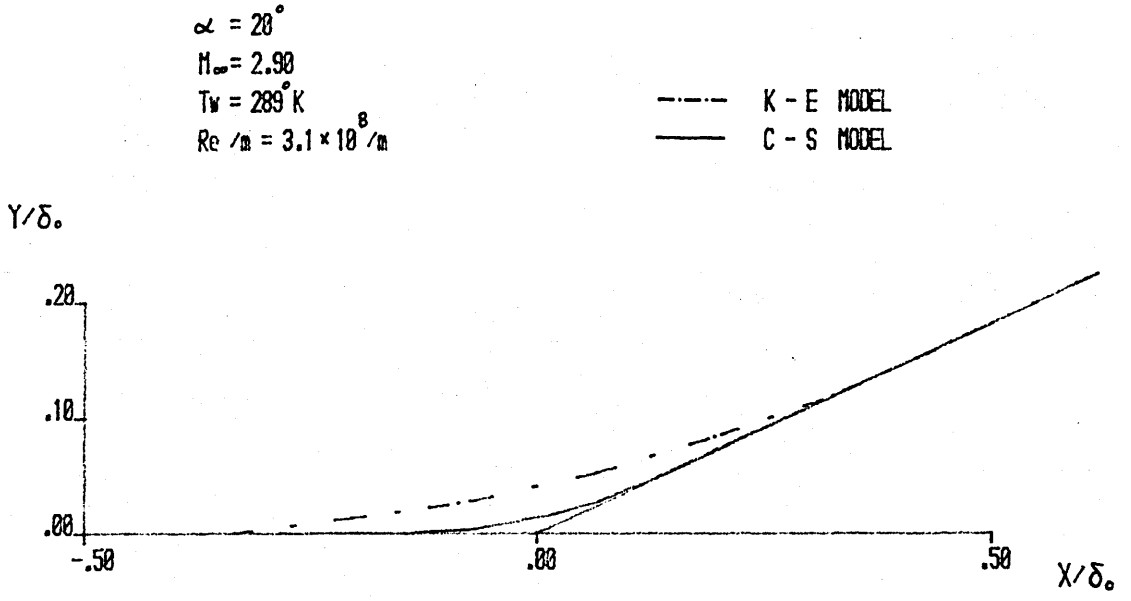

Figure 9-7. THE HEIGHT OF ZERO VELOCITY LINE
(CASE - 4)

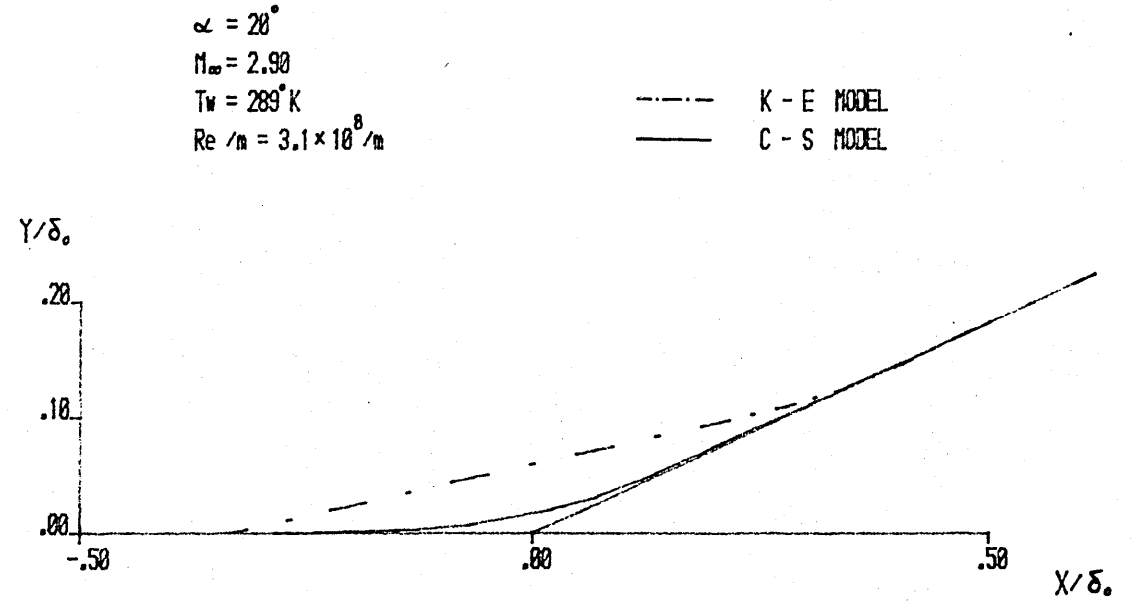

Figure 9-8. THE HEIGHT OF DIVIDING STREAM
(CASE - 4)

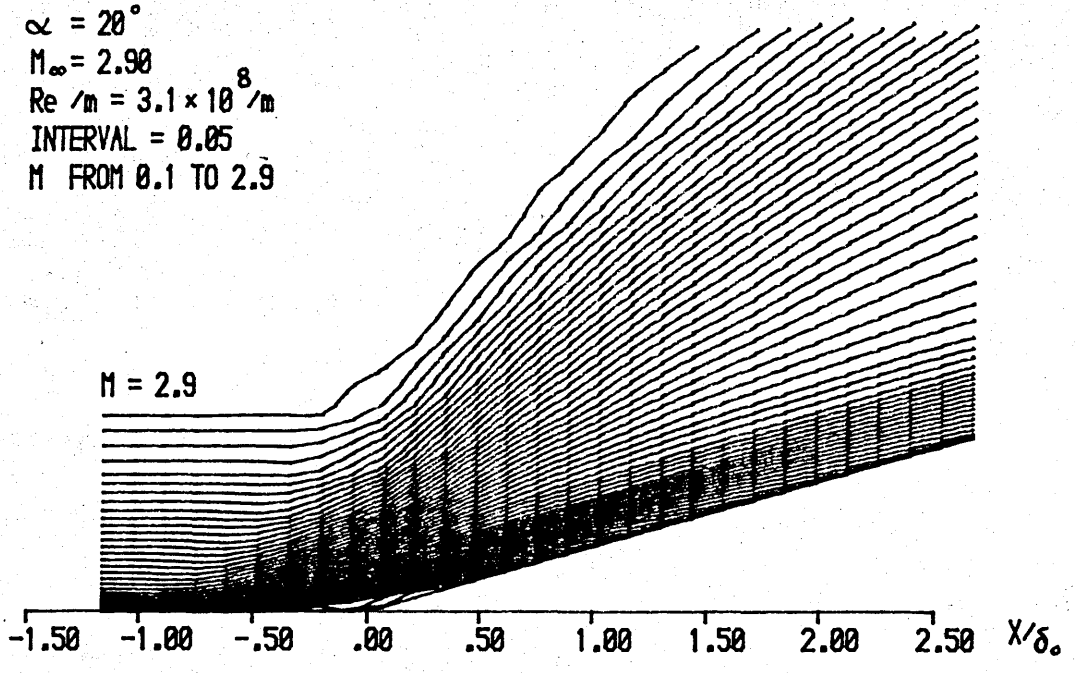

Figure 9-9. MACH NUMBER CONTOURS
K - E MODEL
(CASE - 4)

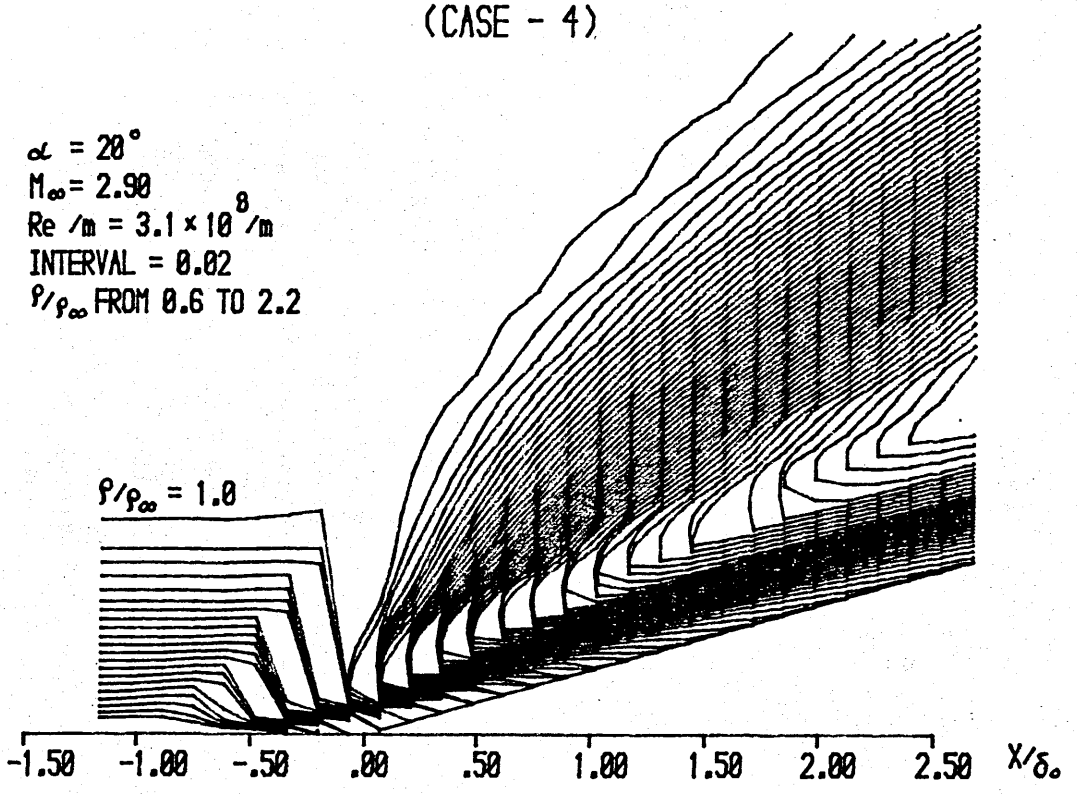

Figure 9-10. DENSITY CONTOURS
K - E MODEL
(CASE - 4)

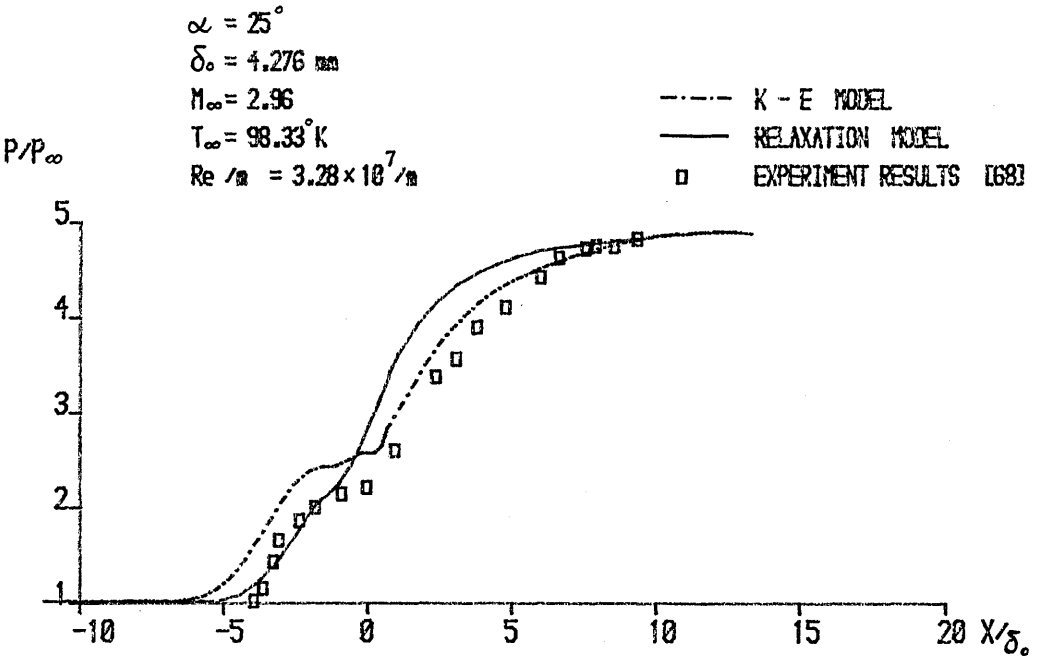

Figure 10-1. THE DISTRIBUTION OF THE WALL PRESSURE (CASE - 5)

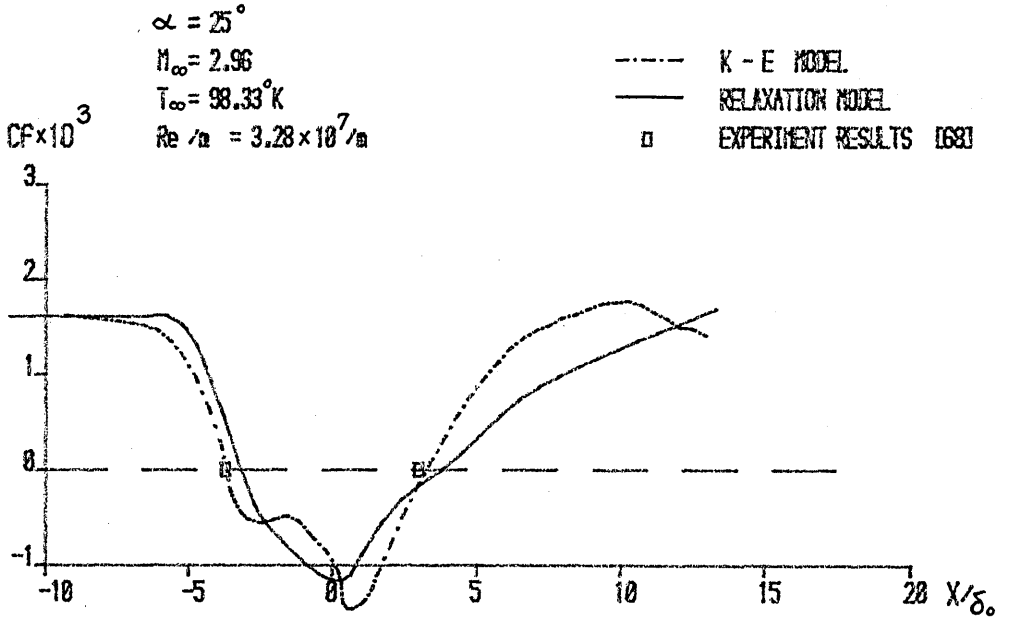

Figure 10-2. SKIN FRICTION COEFFICIENT (CASE - 5)

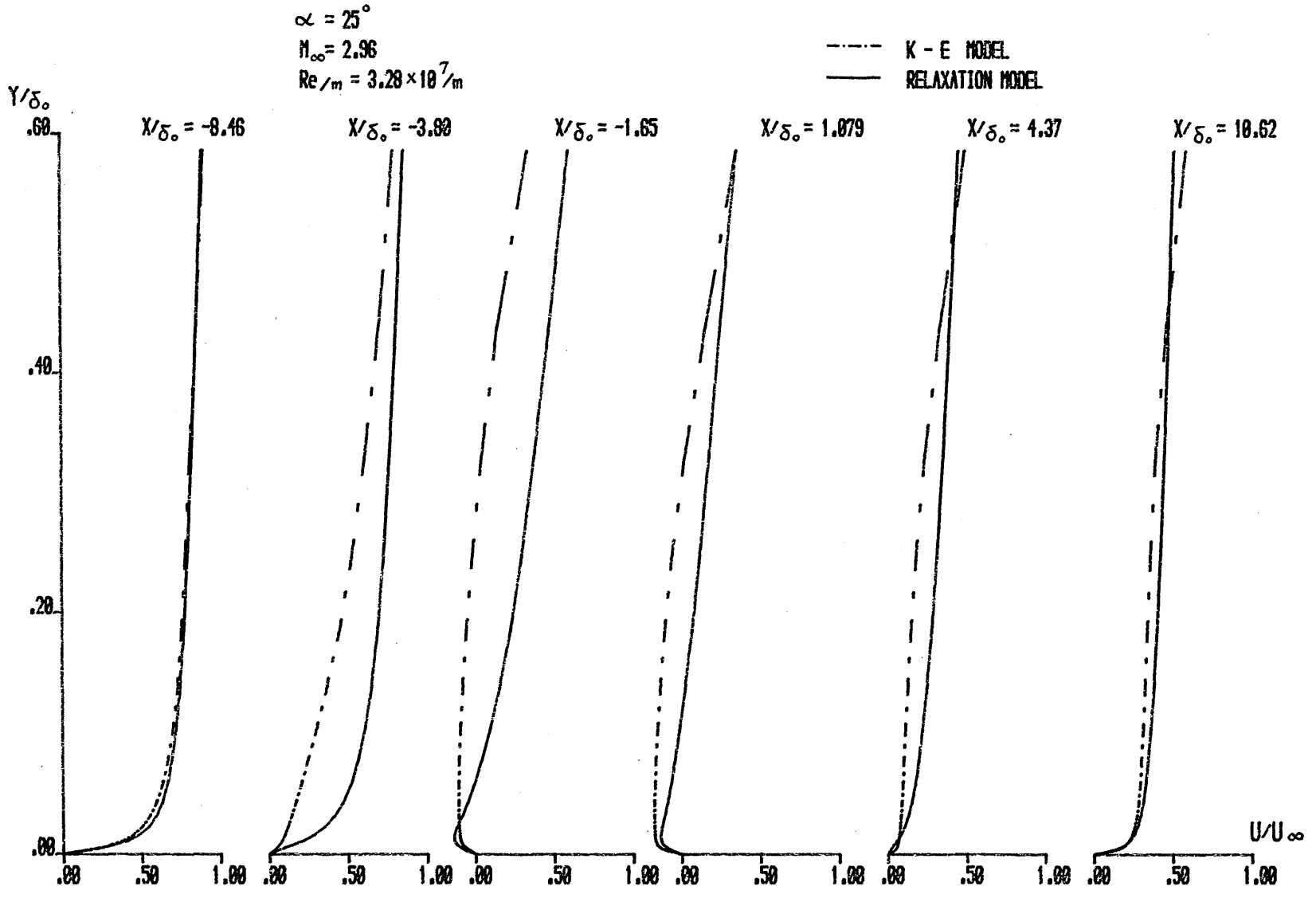

Figure 10-3. VELOCITY PROFILE (CASE - 5) ADIABATIC WALL

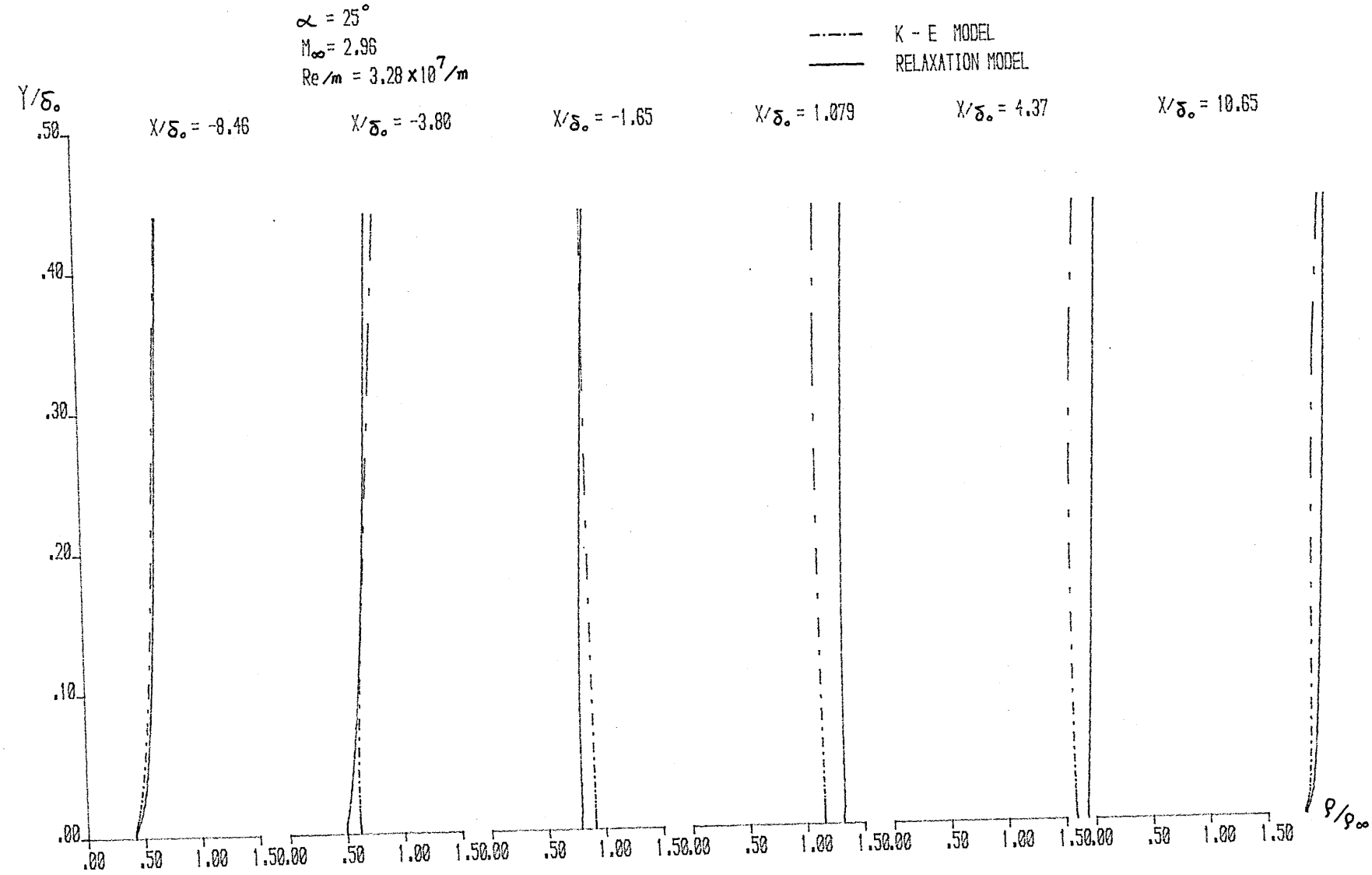

Figure 10-4. DENSITY PROFILE (CASE - 5) ADIABATIC WALL

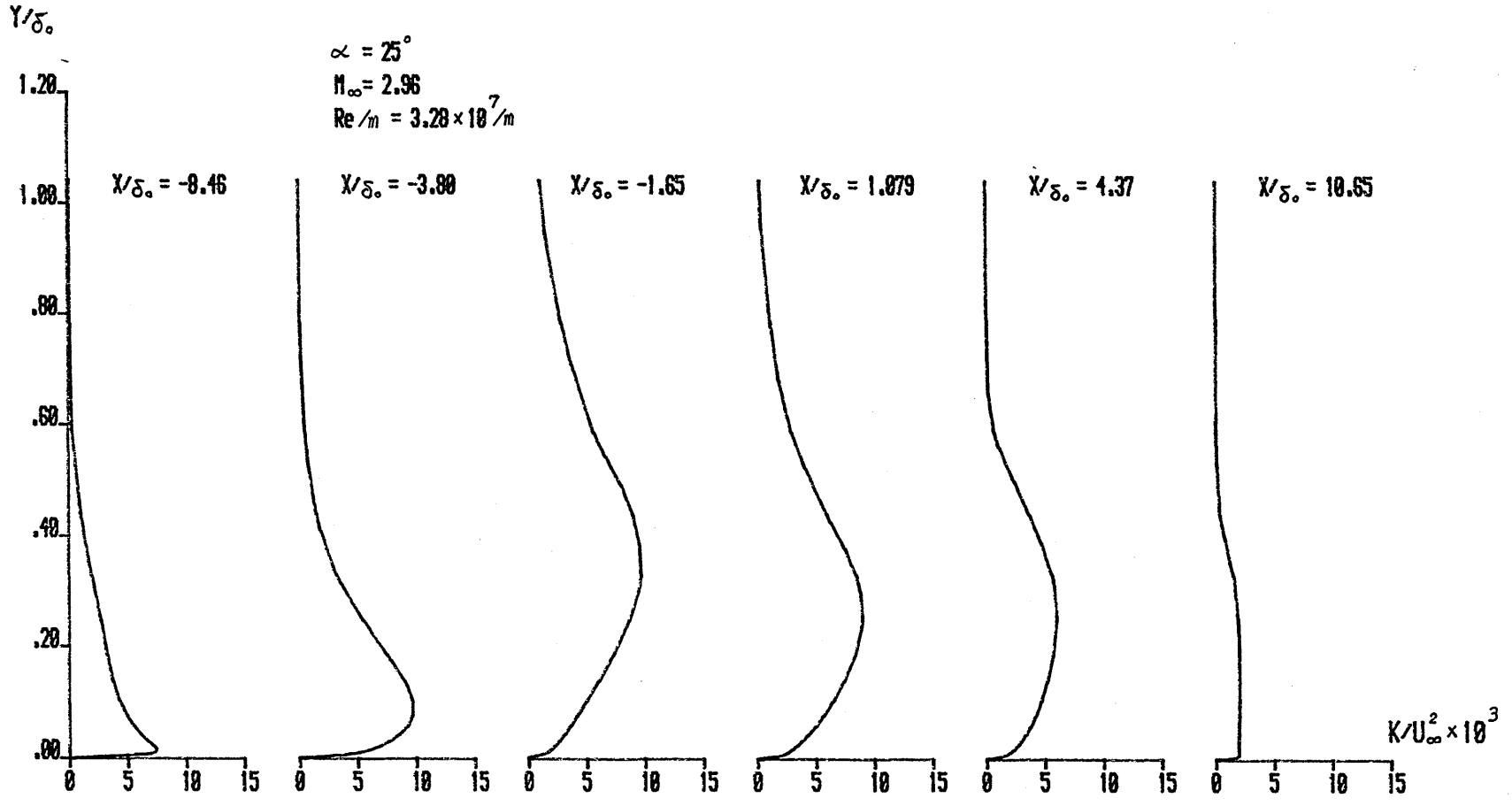

Figure 10-5. TURBULENT KINETIC ENERGY PROFILE
(CASE - 5) ADIABATIC WALL

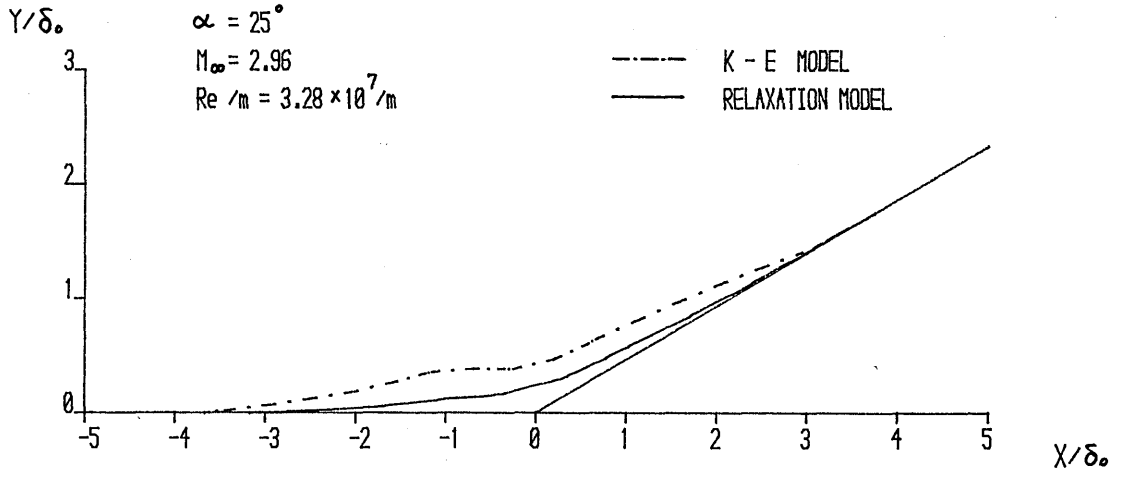

Figure 10-6. THE HEIGHT OF ZERO VELOCITY LINE
(CASE - 5)

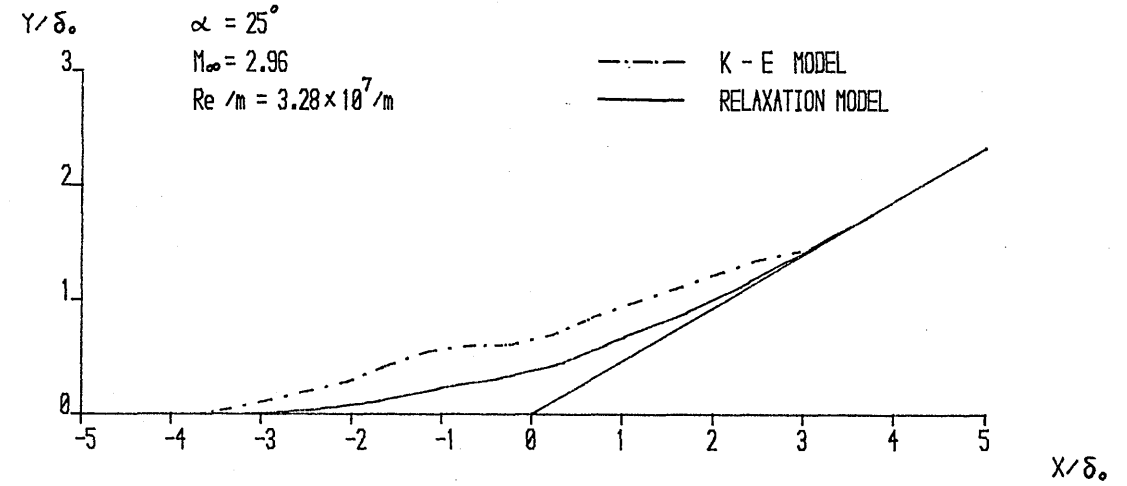

Figure 10-7. THE HEIGHT OF DIVIDING STREAM
(CASE - 5)

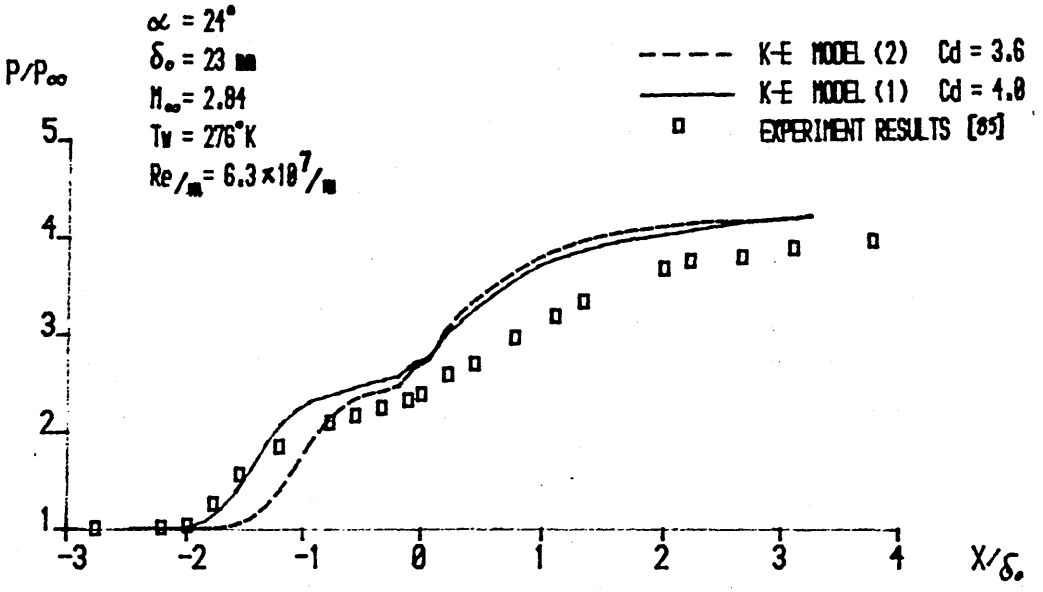

Figure 11-1. THE DISTRIBUTION OF THE WALL PRESSURE (CASE 3 - D)

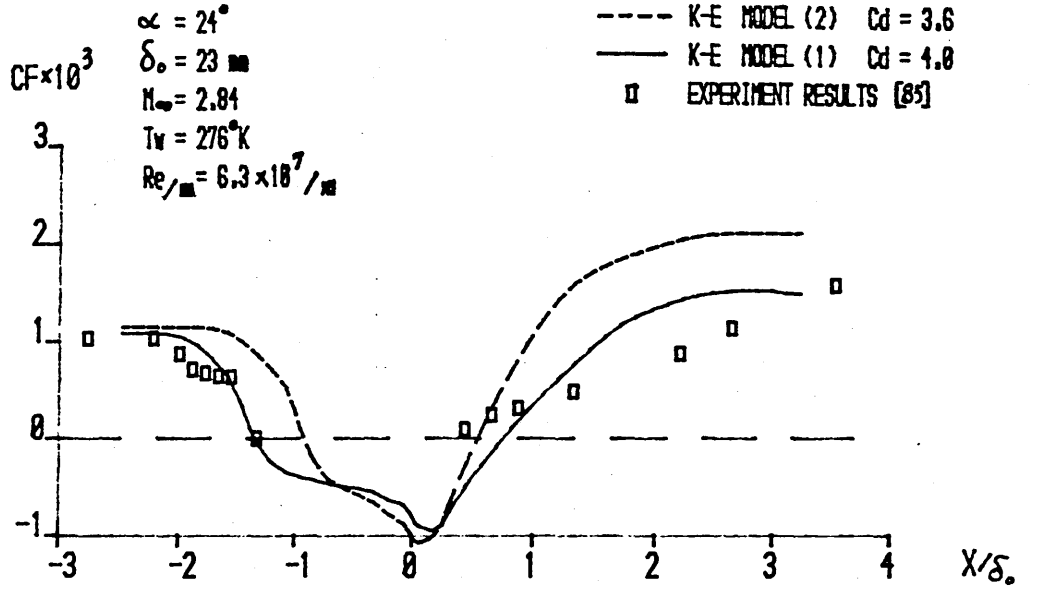

Figure 11-2. SKIN FRICTION COEFFICIENT (CASE 3 - D)

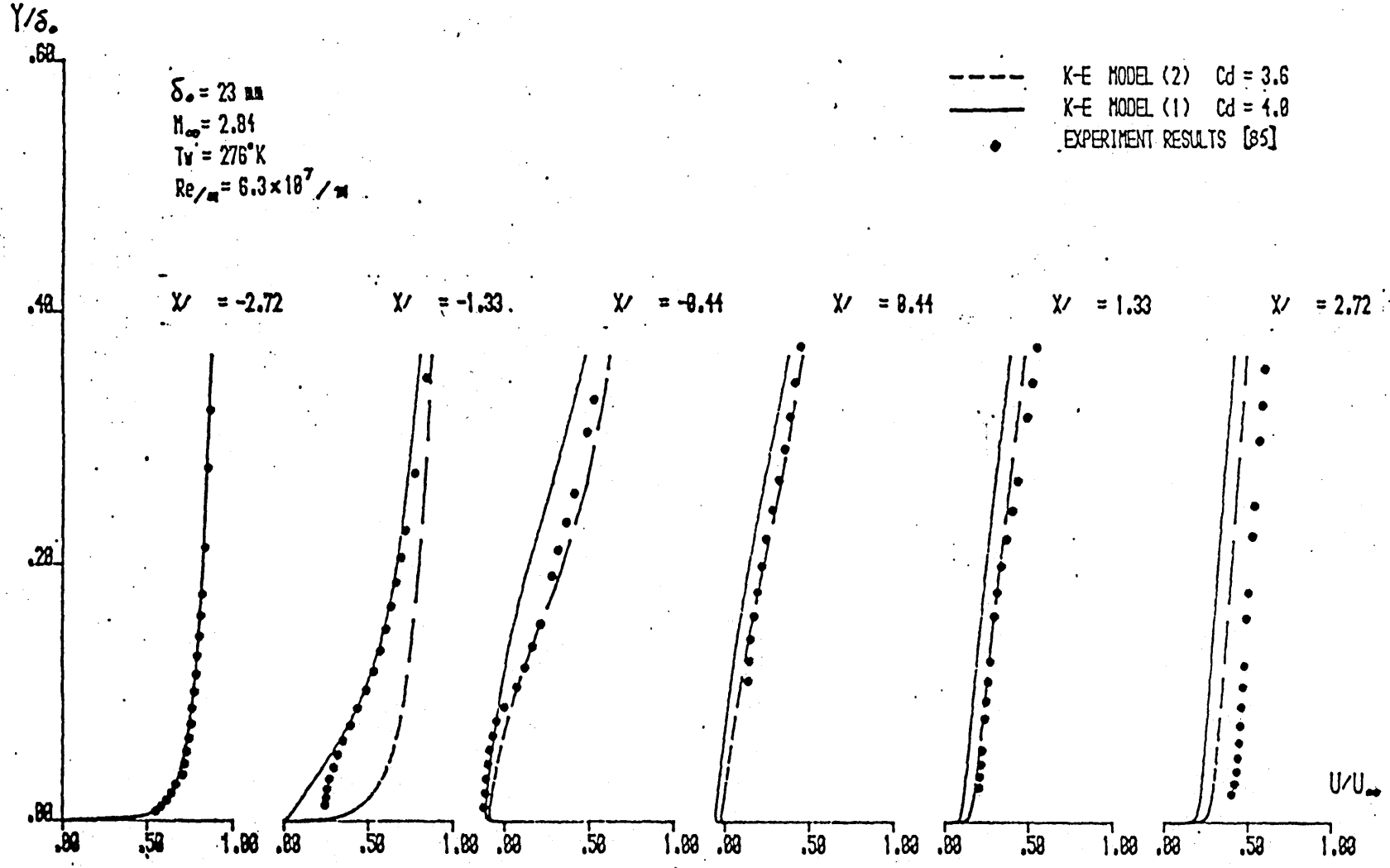

Figure 11-3. VELOCITY PROFILE (CASE - 3 - D) RAMP ANGLE 24°

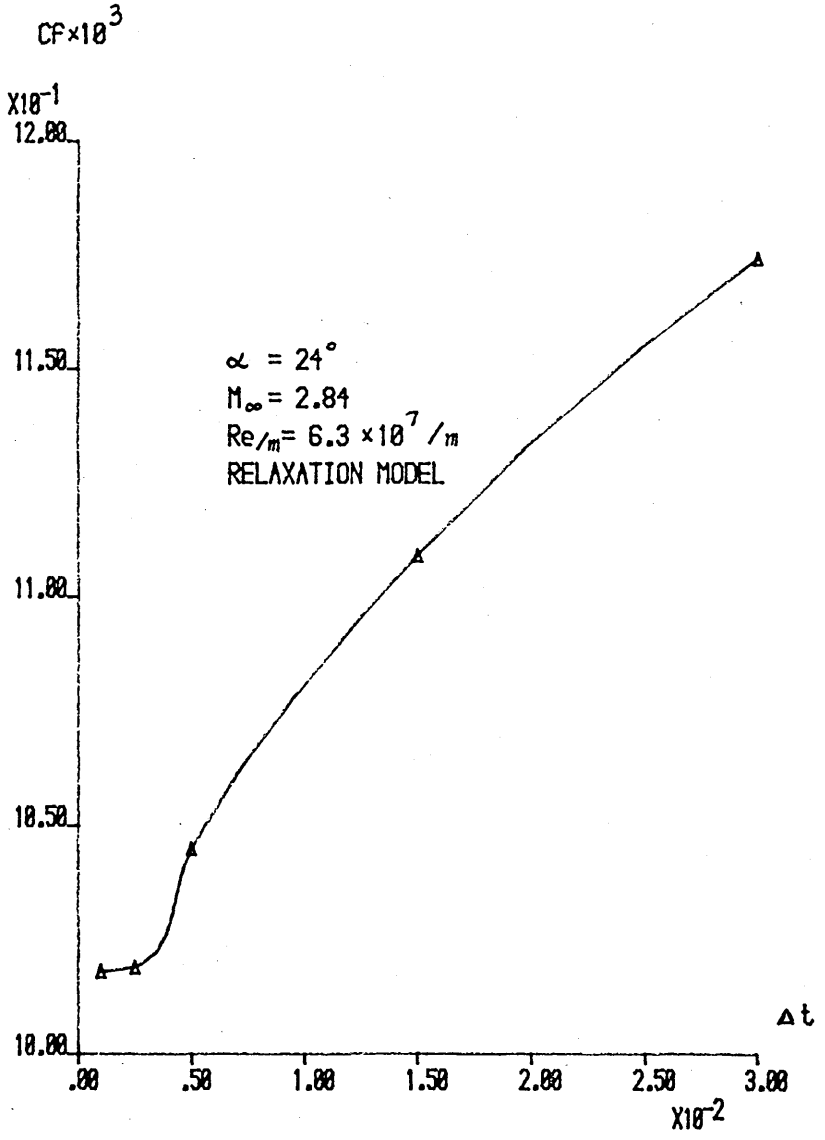

Figure 12. THE CHANGE OF CF VIS Δt
(CASE - 3 - D)

APPENDIX A-1

The General Form of N-S Equations in Coordinates (ξ, η, ζ).

Subject to the general transformation:

$$X = X(\xi, \eta, \zeta), \quad Y = Y(\xi, \eta, \zeta), \quad Z = Z(\xi, \eta, \zeta) \qquad \text{(A-1-1)}$$

The general form of equation (2.17) under the new coordinate system is

$$\frac{\partial U}{\partial t} + \frac{\partial F}{\partial \xi} + \frac{\partial G}{\partial \eta} + \frac{\partial W}{\partial \zeta} = 0 \qquad \text{(A-1-2)}$$

where

$$U = U/J$$
$$F = (\xi_x F + \xi_y G + \xi_z W)/J$$
$$G = (\eta_x F + \eta_y G + \eta_z W)/J$$
$$W = (\zeta_x F + \zeta_y G + \zeta_z H)/J$$

J is the transformation Jacobian and

$$J = \begin{vmatrix} \partial\xi/\partial x & \partial\xi/\partial y & \partial\xi/\partial z \\ \partial\eta/\partial x & \partial\eta/\partial y & \partial\eta/\partial z \\ \partial\zeta/\partial x & \partial\zeta/\partial y & \partial\zeta/\partial z \end{vmatrix}$$

APPENDIX A-2

An Example of Difference Scheme Stability.

For simplicity, a one-dimensional heat conduction along a rod, at the ends of which the temperatures are fixed, is examined. The differential equation of one-dimensional conduction is

$$\frac{\partial T}{\partial t} = \alpha \frac{\partial^2 T}{\partial X^2} \qquad \text{(A-2-1)}$$

The equation is a parabolic partial differential equation similar to the N-S equations.

If the time derivative is approximated by a forward difference, and the space derivative is approximated by central difference, the difference equation approximating (A-2-1) is

$$T_j^{n+1} - T_j^n = S\,(T_{j-1}^n - 2\,T_j^n + T_{j+1}^n)$$

or $$T_j^{n+1} = S\,(T_{j-1}^n + T_{j+1}^n) + (1 - 2\,S)\,T_j^n \qquad \text{(A-2-2)}$$

where $S = \alpha\,\Delta t / \Delta X^2$

Assuming that $\alpha = 0.01$, $\Delta X = 0.1$, $j = 0, 1, \cdots\cdots, 10$, and the initial and boundary values are $T(0) = T(1) = 100$, $T(j) = 0$, $j = 2, \cdots\cdots, 9$. The solutions of (A-2-2) for $S = 1/2$ and $S = 1$ at first 5 steps are given in Table 4. It is seen that for $S = 1/2$, the solution is converging and for $S = 1$ the solution diverges. Therefore, when $S = 1$ the difference scheme is unstable. This conclusion is in agreement with the Von Neumann's stability analysis.

T A B L E 4

The Solution of (A-2-2), for S = 1/2

nΔt \ jΔt	0	0.1	0.2	0.3	0.4	0.5	0.6	0.7	0.8	0.9	1.0
0	100	0	0	0	0	0	0	0	0	0	100
0.5	100	50	0	0	0	0	0	0	0	50	100
1.0	100	50	25	0	0	0	0	0	25	50	100
1.5	100	62.5	25	12.5	0	0	0	12.5	25	62.5	100
2.0	100	62.5	37.5	12.5	6.25	0	6.25	12.5	37.5	62.5	100
2.5	100	68.5	37.5	21.875	6.25	6.25	6.25	21.875	37.5	68.75	100

The Solution of (A-2-2), for S = 1

nΔt \ jΔt	0	0.1	0.2	0.3	0.4	0.5	0.6	0.7	0.8	0.9	1.0
0	100	0	0	0	0	0	0	0	0	0	100
1	100	100	0	0	0	0	0	0	0	100	100
2	100	0	100	0	0	0	0	0	100	0	100
3	100	200	-100	100	0	0	0	100	-100	200	100
4	100	-200	400	-200	100	0	100	-200	400	-200	100
5	100	700	-800	700	-300	200	-300	700	-800	700	100

A P P E N D I X A-3

Reynolds stress Transport Equation.

The derivation of the Reynolds stress transport Equation is carried out in reference [29]. The resulting formula is here presented

$$
\begin{aligned}
\frac{D}{Dt}\,\overline{\rho u_i'' u_j''} \equiv\ & \frac{\partial}{\partial t}\,\overline{\rho u_i'' u_j''} + \frac{\partial}{\partial X_k}\,\tilde{u}_k\,\overline{\rho u_i'' u_j''} && \text{I}\\
=\ & -\overline{\rho u_i'' u_j''}\,\frac{\partial \tilde{u}_j}{\partial X_k} - \overline{\rho u_j'' u_k''}\,\frac{\partial \tilde{u}_i}{\partial X_k} && \text{II}\\
& - \tau_{ik}\,\frac{\partial u_j''}{\partial X_k} - \tau_{jk}\,\frac{\partial u_i''}{\partial X_k} && \text{III}\\
& - \frac{\partial}{\partial X_k}\,\overline{u_j'' \tau_{ik}} + \frac{\partial}{\partial X_k}\,\overline{u_i'' \tau_{jk}} \\
& - \frac{\partial}{\partial X_k}\,\overline{u_k'' \rho u_i'' u_j''} && \text{IV}\\
& - \frac{\partial}{\partial X_i}\,\overline{u_j'' P} - \frac{\partial}{\partial X_j}\,\overline{u_i'' P} \\
& + P\left(\frac{\partial u_j''}{\partial X_i} + \frac{\partial u_i''}{\partial X_j}\right) && \text{V}
\end{aligned}
\qquad \text{(A-3-1)}
$$

where k expresses the coordinate axis on which the derivative is taken, and the Roman numerals express the different meaning of terms which will be explained as follows

I represents the local rate of change and the transport of Reynolds-stress,

II represents the production of Reynolds stress,

III is the dissipation term,

IV represents the diffusion caused separately by viscous forces, velocity fluctuation and the pressure,

and V represents the redistribution by pressure.

When i = j, equation (A-3-1) becomes the turbulent kinetic energy equation.

A P P E N D I X A-4

The Jacobian Matrix of Flux Vectors & Their Diagonalization.

The Jacobian Matrix $A = \frac{\partial F_{inviscid}}{\partial U}$ and $B = \frac{\partial G_{inviscid}}{\partial U}$ can be deduced in the following form:

$$A = \begin{bmatrix} 0 & 1 & 0 & 0 & 0 & 0 \\ a\beta-u^2 & (3-\gamma)u & -\beta v & \beta & -\beta & 0 \\ -uv & v & u & 0 & 0 & 0 \\ (-\frac{\gamma E}{\rho}+2a\beta+\beta K)u & \frac{\gamma E}{\rho}-\frac{\beta}{2}(3u^2+v^2+2K) & -\beta uv & \gamma u & -\beta u & 0 \\ -uK & K & 0 & 0 & u & 0 \\ -u\epsilon & \epsilon & 0 & 0 & 0 & u \end{bmatrix}$$

$$B = \begin{bmatrix} 0 & -\tan\alpha & 1 & 0 & 0 & 0 \\ -a\beta\tan\alpha-uv' & v'+(\gamma-2)u\tan\alpha & u+\beta v\tan\alpha & -\beta\tan\alpha & \beta\tan\alpha & 0 \\ a\beta-vv' & -v\tan\alpha-\beta u & -u\tan\alpha-(\gamma-3)v & \beta & -\beta & 0 \\ (\frac{-\gamma E}{\rho}+2a\beta+\beta K)v' & -(\frac{\gamma E}{\rho}-a\beta-\beta K)\tan\alpha-\beta uv' & \frac{\gamma E}{\rho}-a\beta-\beta K-\beta vv' & \gamma v' & -\beta v' & 0 \\ -v'K & -K\tan\alpha & K & 0 & v' & 0 \\ -v'\epsilon & -\epsilon\tan\alpha & \epsilon & 0 & 0 & v' \end{bmatrix}$$

$$A = S_X^{-1} \Lambda_A S_X$$

$$S_X^{-1} = \begin{bmatrix} 1 & 0 & \frac{1}{2C^{*2}} & \frac{1}{2C^{*2}} & 0 & 0 \\ u & 0 & \frac{u+C^*}{2C^{*2}} & \frac{u-C^*}{2C^{*2}} & 0 & 0 \\ v & 1 & \frac{v}{2C^{*2}} & \frac{v}{2C^{*2}} & 0 & 0 \\ a+K & v & \frac{1}{2C^{*2}}(a+K+uC)+\frac{1}{2\beta} & \frac{a+K}{2C^{*2}}-\frac{u}{2C^{*2}}+\frac{1}{2\beta} & 1 & 0 \\ K & 0 & \frac{K}{2C^{*2}} & \frac{K}{2C^{*2}} & 1 & 0 \\ \epsilon & 0 & \frac{\epsilon}{2C^{*2}} & \frac{\epsilon}{2C^{*2}} & 0 & 1 \end{bmatrix}$$

$$B = S_y^{-1} \Lambda_B S_y$$

$$S_y^{-1} = \begin{bmatrix} 1 & 0 & \frac{1}{2C^{*2}} & \frac{1}{2C^{*2}} & 0 & 0 \\ u & \cos\alpha & \frac{u-C^*\sin\alpha}{2C^{*2}} & \frac{u+C^*\sin\alpha}{2C^{*2}} & 0 & 0 \\ v & \sin\alpha & \frac{v+C^*\cos\alpha}{2C^{*2}} & \frac{v-C^*\cos\alpha}{2C^{*2}} & 0 & 0 \\ a+K & u\cos\alpha+v\sin\alpha & \frac{a+K+C^*v^*}{2C^{*2}} + \frac{1}{2\beta} & \frac{a+K-C^*v^*}{2C^{*2}} + \frac{1}{2\beta} & 1 & 0 \\ K & 0 & \frac{K}{2C^{*2}} & \frac{K}{2C^{*2}} & 1 & 0 \\ \epsilon & 0 & \frac{\epsilon}{2C^{*2}} & \frac{\epsilon}{2C^{*2}} & 0 & 1 \end{bmatrix}$$

where $v' = v - u \tan \alpha$

$$a = \frac{1}{2}(u^2 + v^2)$$

$\beta = \gamma - 1$

$v^* = v\cos\alpha - u\sin\alpha$

C^* is an effective sound speed which is correspounding to an effective pessure P_t.

A P P E N D I X A-5

In order to check the ability of MacCormack's implicit scheme to suppress nonlinear oscillations a series of tests have been carried out. The tests made are listed in Table 5. The notation used in this table has the following meaning:

A expresses that an artificial damping term is used. The subscript 2 indicates a MacCormack's Fourth-order product term is used, i.e., $CX_2 \frac{|P_{i+1} - 2P_i + P_{i-1}|}{P_{i+1} + 2P_i + P_{i-1}} (U_{i+1} - 2U_i + U_{i-1})$ and 4 indicates a fourth-order derivation term i.e., $CX_4 (6U_i - 4U_{i+1} - 4U_{i-1} + U_{i+2} + U_{i-2})$ is used.

B indicates the implicit boundary condition. The subscript 0 means $\delta U=0$ and 1, the reflecting boundary condition is used.

S indicates that a strong incident shock wave exists in the computational region.

E expresses that a term related to the change of entropy is added into the effective viscosity of the implicit operator part.

F indicates a finer mesh spacing near the wall is used.

The computational grid used is the same as that shown in Fig. 2. The plate is placed between j = 1 and j = 2 and the leading edge is placed between I = 3 and I = 4. The results of testing can been discussed in two respects, one concerns the effects of artificial damping and the other, the effect of choice of boundary condition. From testing 1 and 2, it can been seen that apparently when a steep gradient appears a nonlinear oscillation develops first in the region near the wall where the CFL number can be very large and then propagates gradually into the whole flow field. The MacCormack's implicit scheme does not offer

any ability to control the nonlinear oscillation at such large CFL numbers. In that situation the additional term E which is suggested by MacCormack to take the change of entropy into account is no longer helpful. From the results of tests 4 to 12 , we can see that the addition of a fourth product term can make some improvement and smooth the shock wave but it cannot suppress the nonlinear oscillation throughout the region. A fourth-order derivation term with small coefficient can perfectly control the nonlinear oscillation, however, it also smears the solution if the coefficient CX_4 is too large. In a practical calculation, the CFL number was kept at a value around 400, the fourth-order product term was used to smooth the shock wave and the fourth-order derivation term with small coefficient used to suppress nonlinear oscillations.

Comparing the results of two different kinds of boundary condition, it is easy to find that an unsuitable boundary condition will cause further computational instability. Using the present mesh system for a flat plate calculation, a reflecting condition is recommended.

TABLE 5

Test Calculation
(Supersonic Laminar Flow over a Flat Plate)

Test No.	State	Δt	CFL Number	CX_2	CX_4
1	B_0E	0.015	373	0	0
2	$B_1$1	0.015	373	0	0
3	B_0A_2E	0.015	373	0.5	0
4	B_1A_2E	0.015	373	0.5	0
5	B_0A_4	0.015	373	0	0.008
6	B_1A_4	0.015	373	0	0.008
7	B_1A_4F	0.015	2577	0	0.008
8	B_0A_4S	0.015	373	0	0.008
9	B_1A_4S	0.015	373	0	0.008
10	B_1A_4SF	0.012	2061	0	0.012
11	B_1A_4SF	0.012	2061	0	0.025
12	$B_1A_2A_4SF$	0.012	2061	0.5	0.025

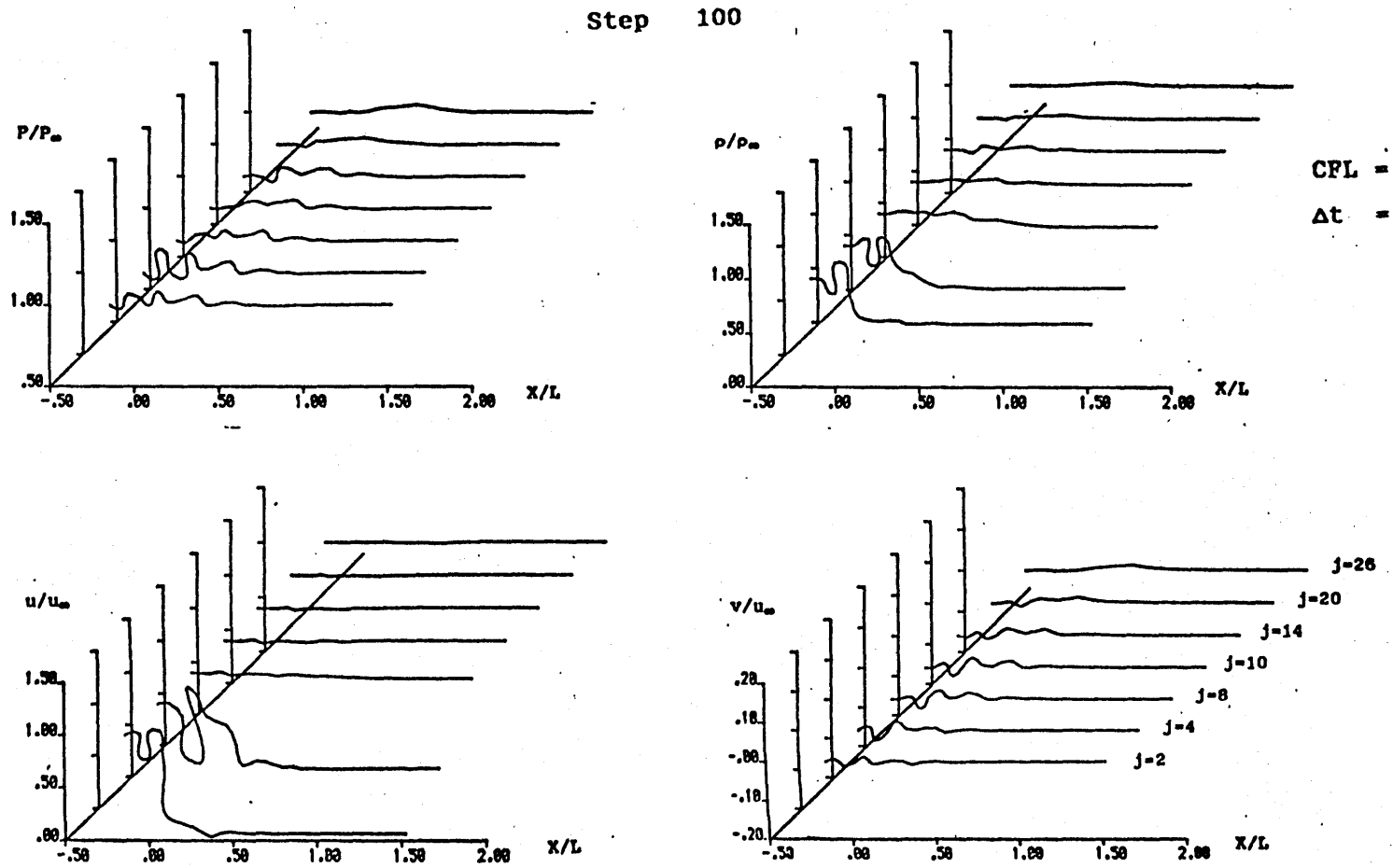

Figure A - 5 - 1 Test 1 (B_0 E)

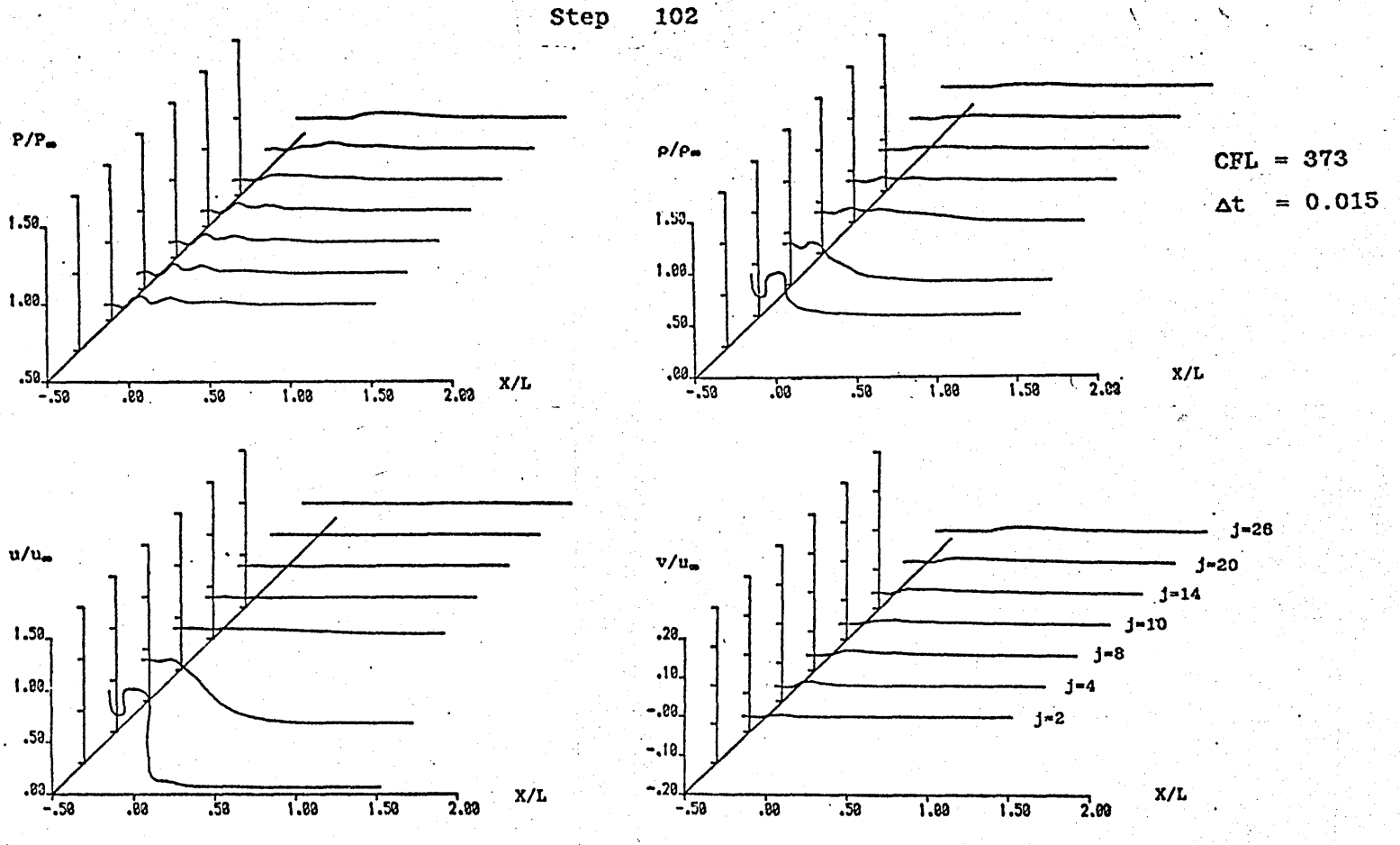

Figure A - 5 - 2 Test 2 (B_1 E)

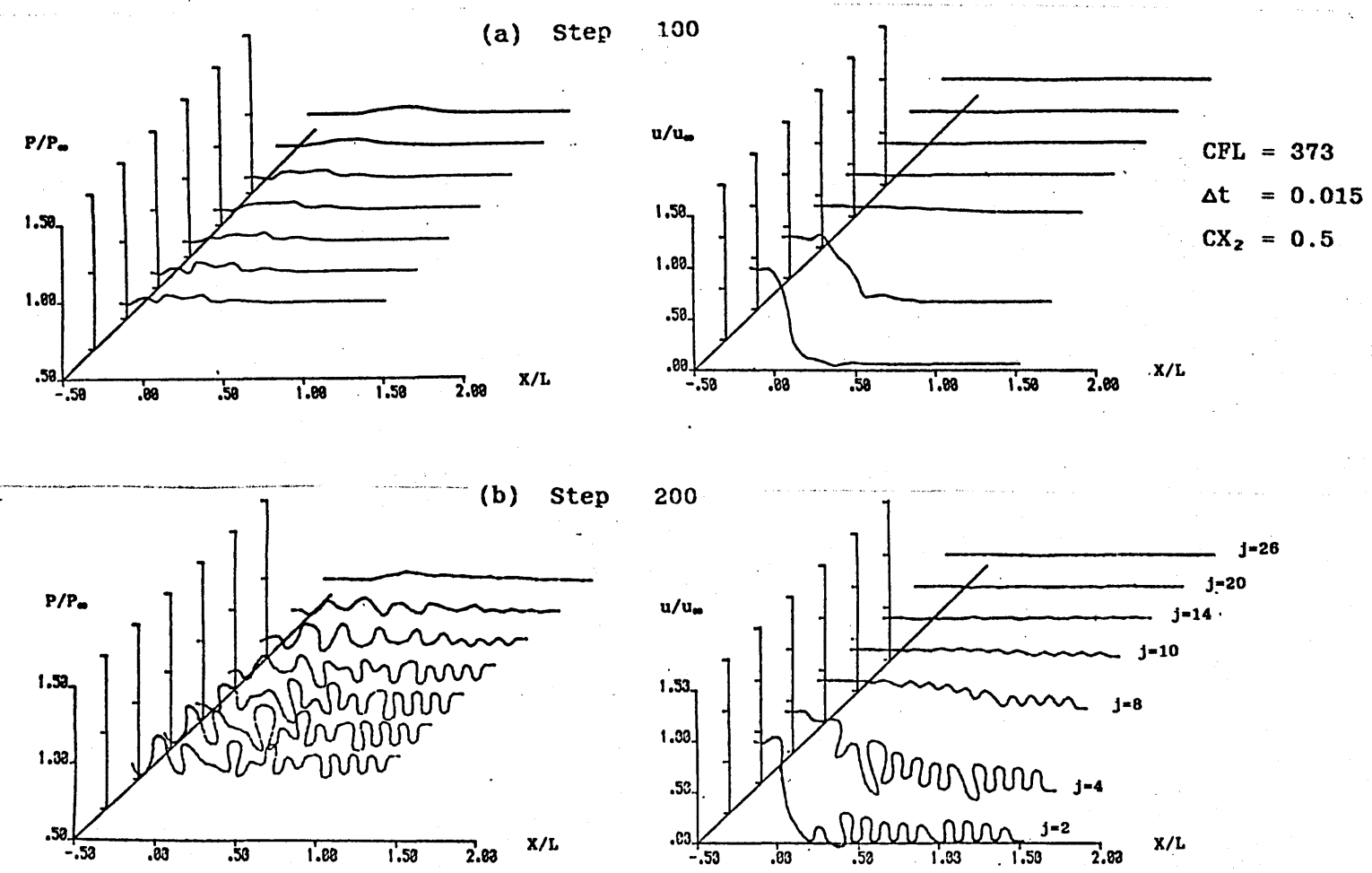

Figure A - 5 - 3 Test 3 (B_0 A_2 E)

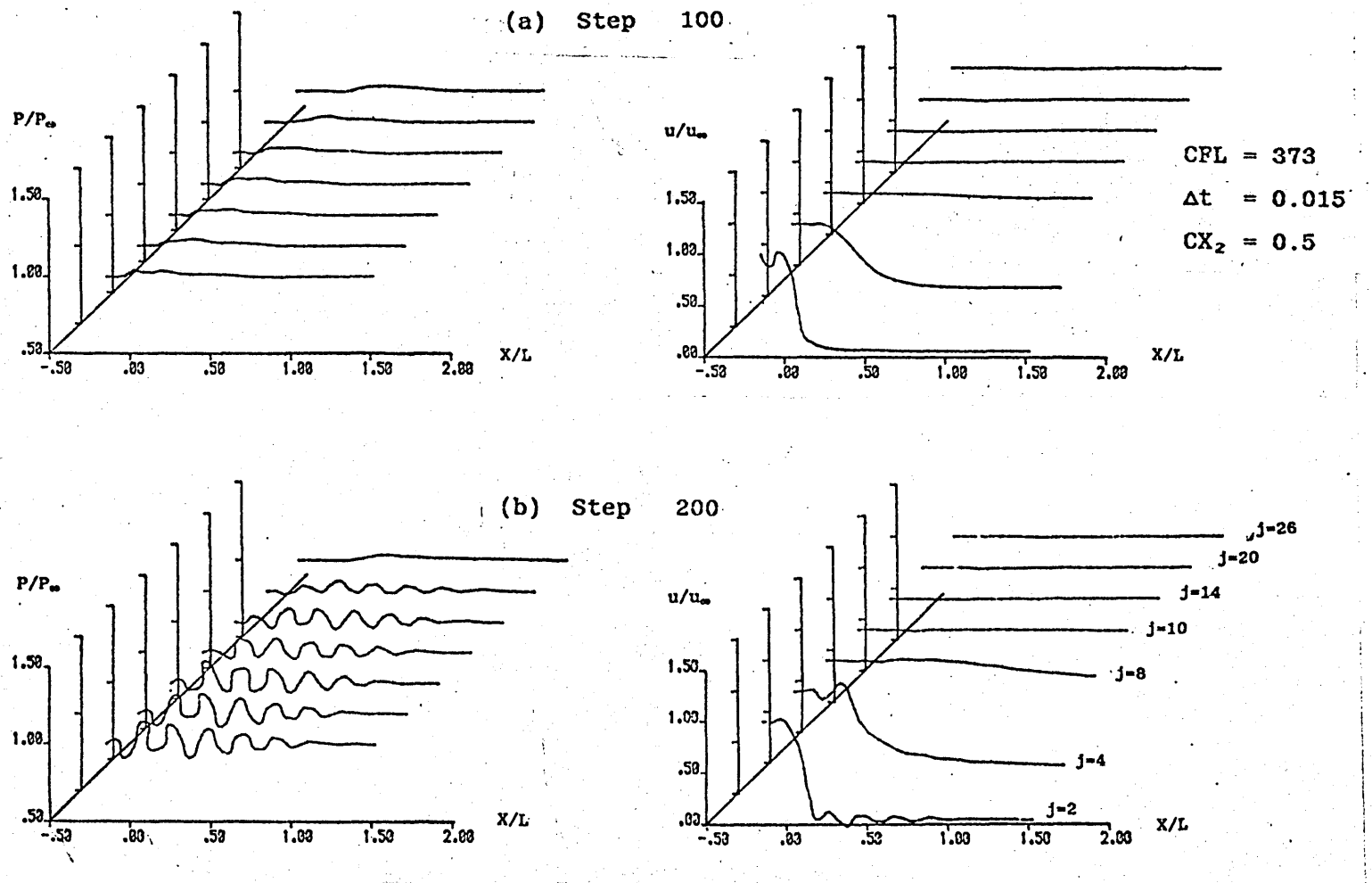

Figure A - 5 - 4 Test : 4 (B_1 A_2 E)

(a) Step 100

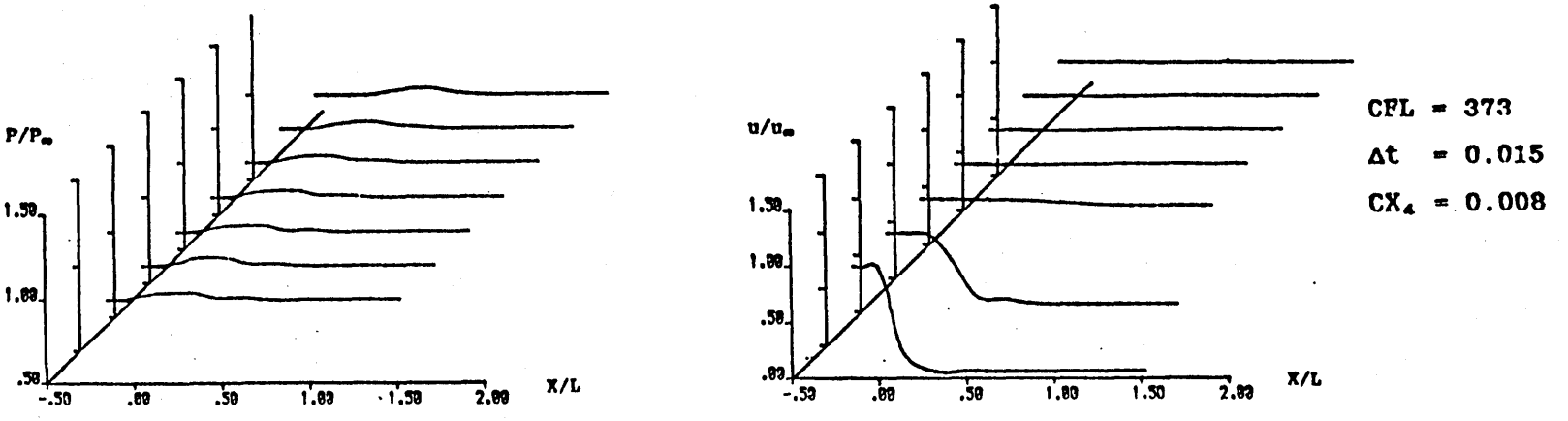

(b) Step 200

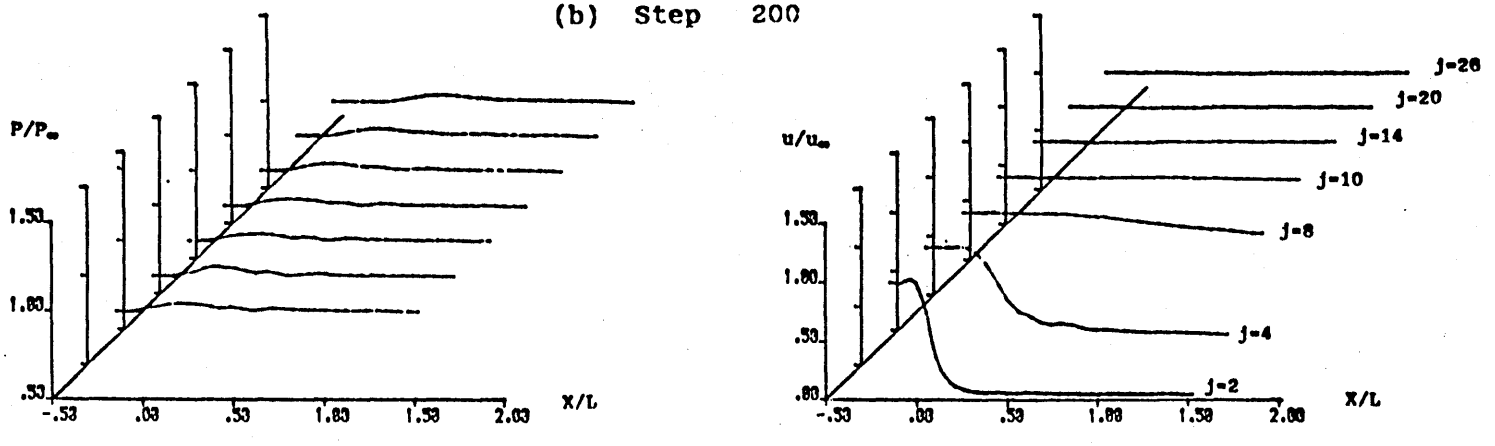

Figure A - 5 - 5 Test 5 (B_0 A_4)

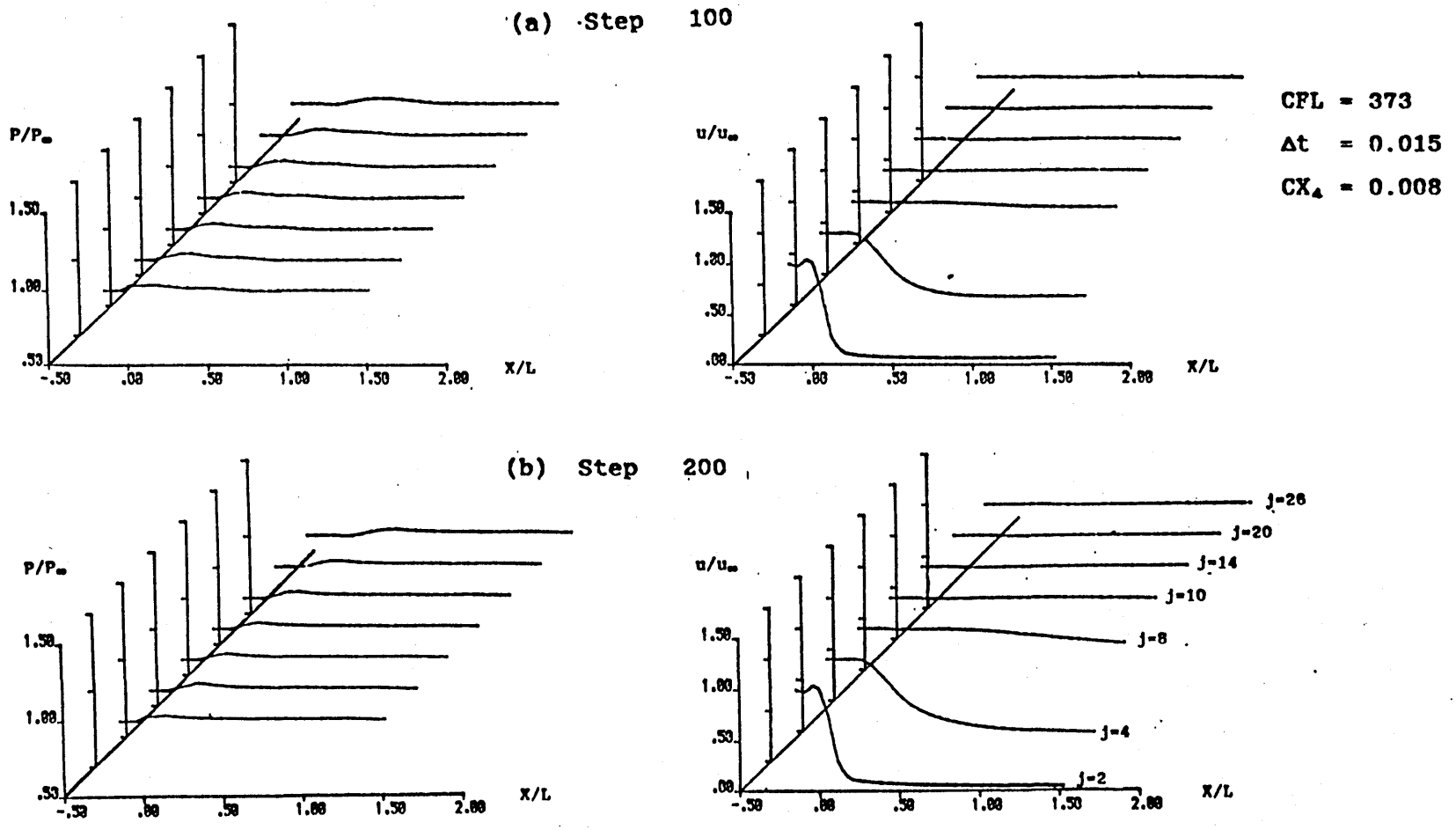

Figure A - 5 - 6 Test 6 (B_1 A_4)

Step 150

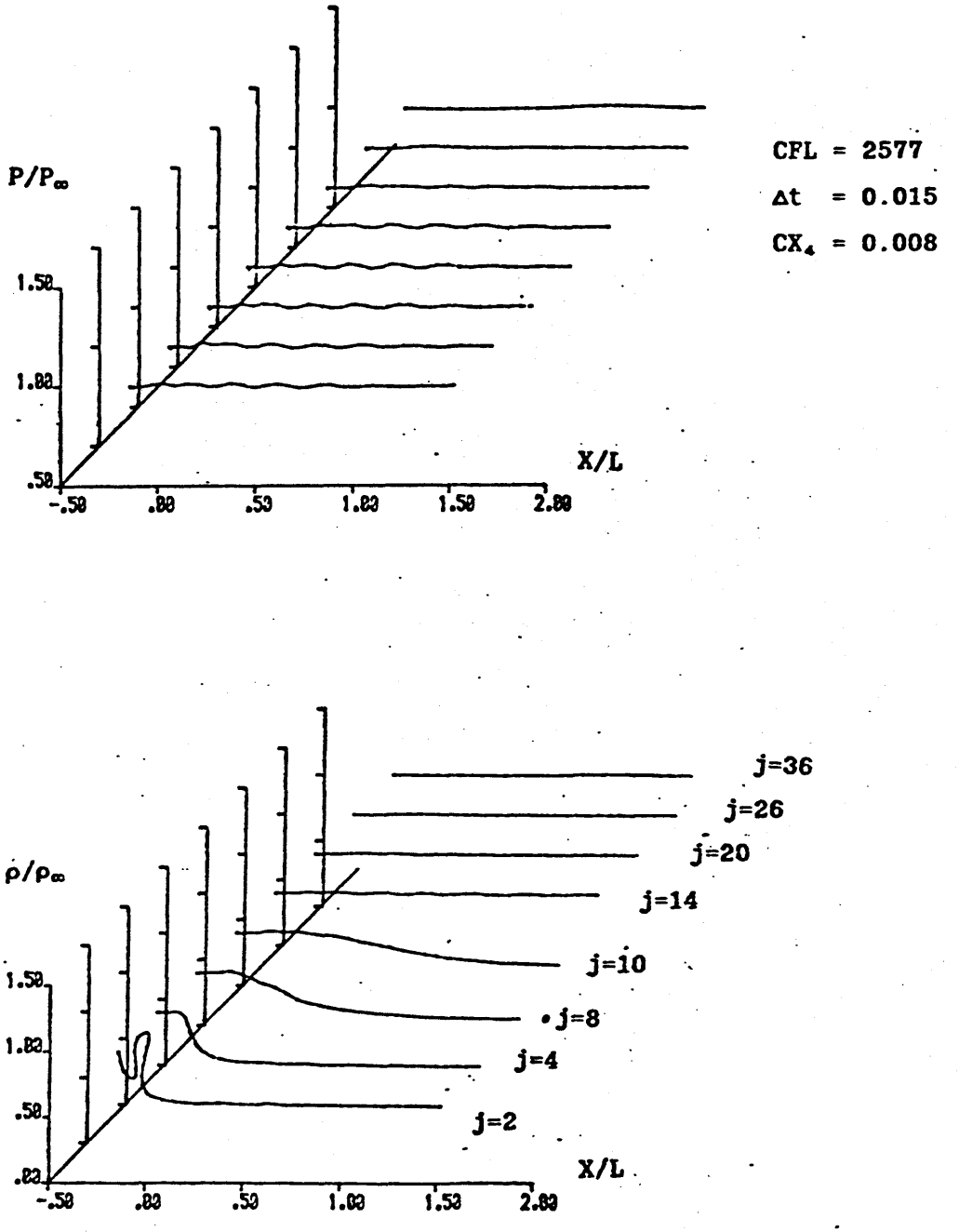

Figure A - 5 - 7 Test 7 (B_1 A_4 F)

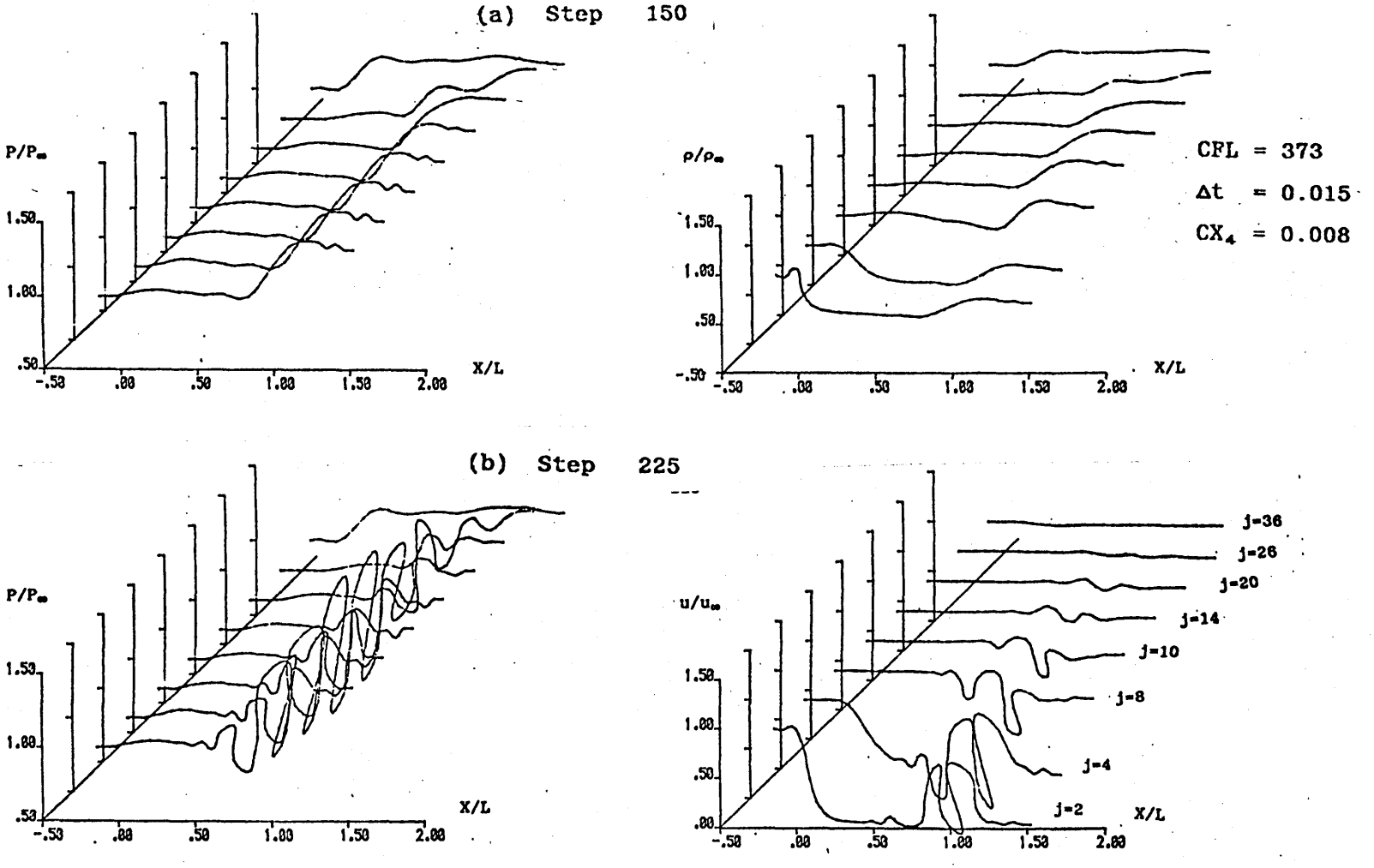

Figure A - 5 - 8 Test 3 (B_0 A_4 E S)

(a) Step 200

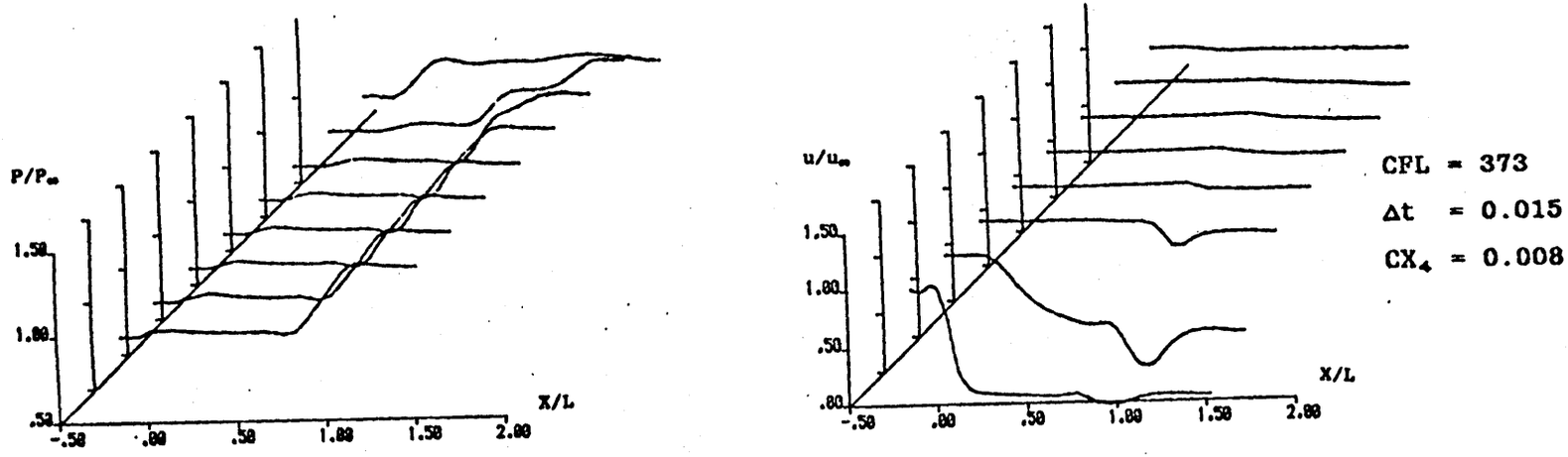

(b) Step 400

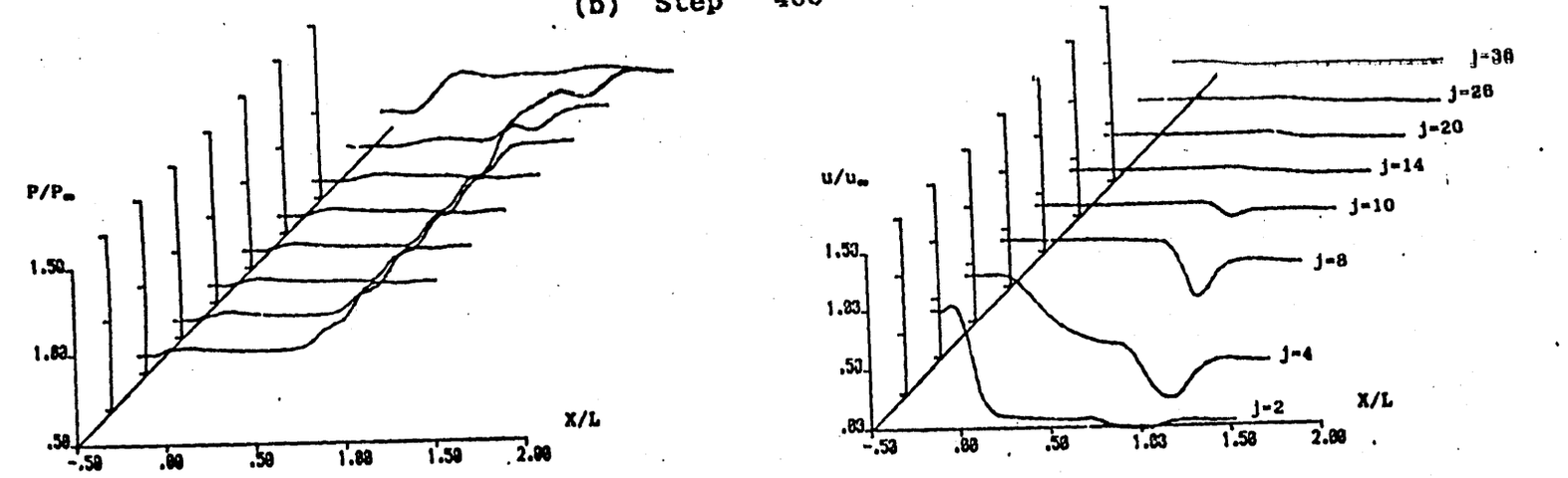

Figure A - 5 - 9 Test 9 (B_1 A_4 E S)

(a) Step 200

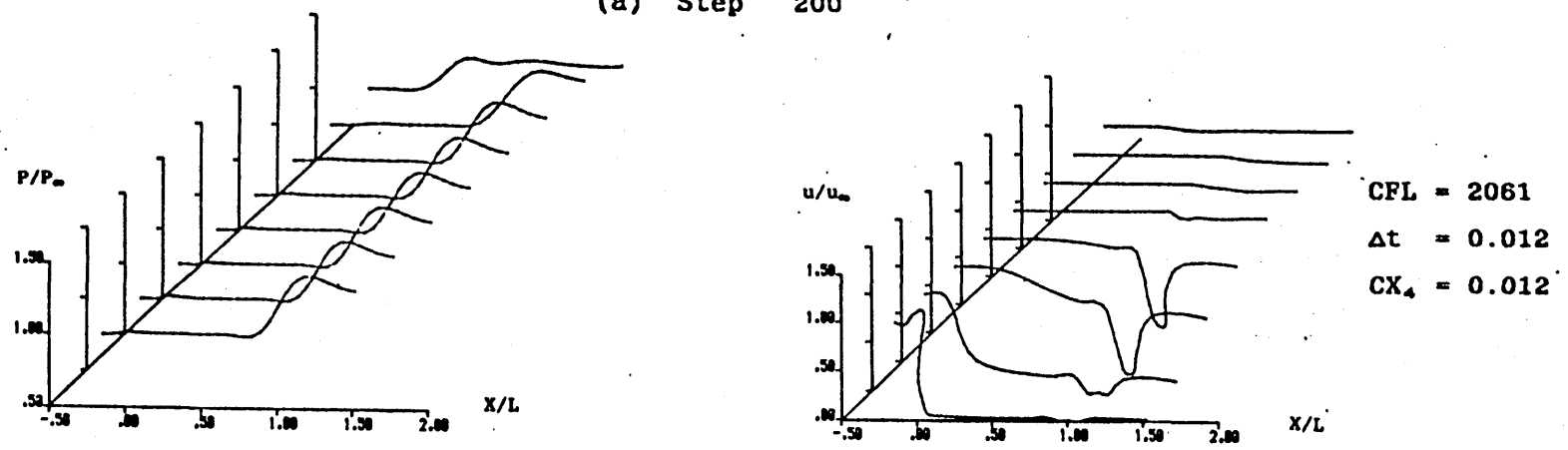

(b) Step 400

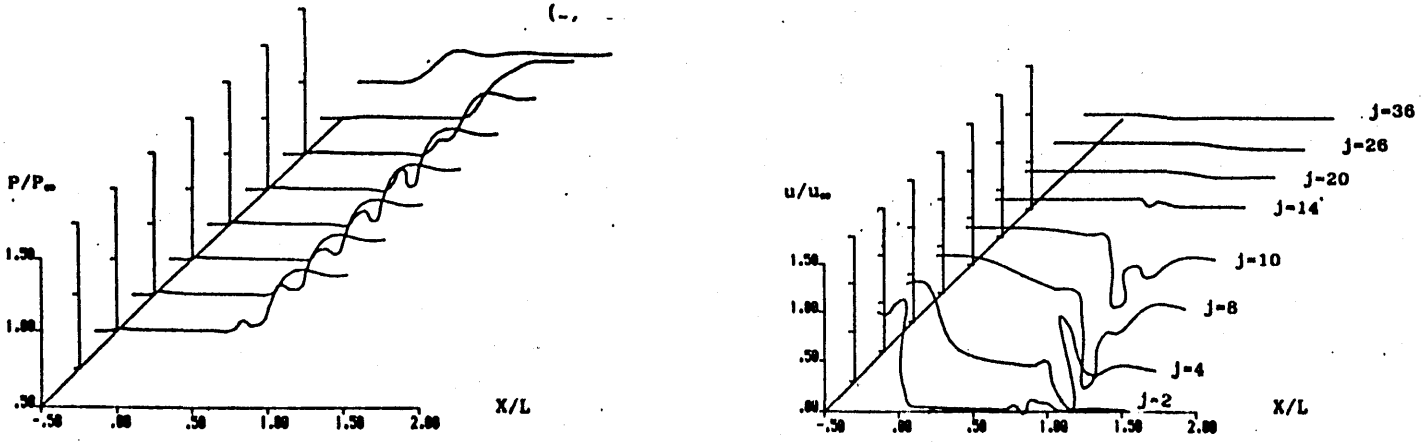

Figure A - 5 - 10 Test 10 (B_1 A_4 S F)

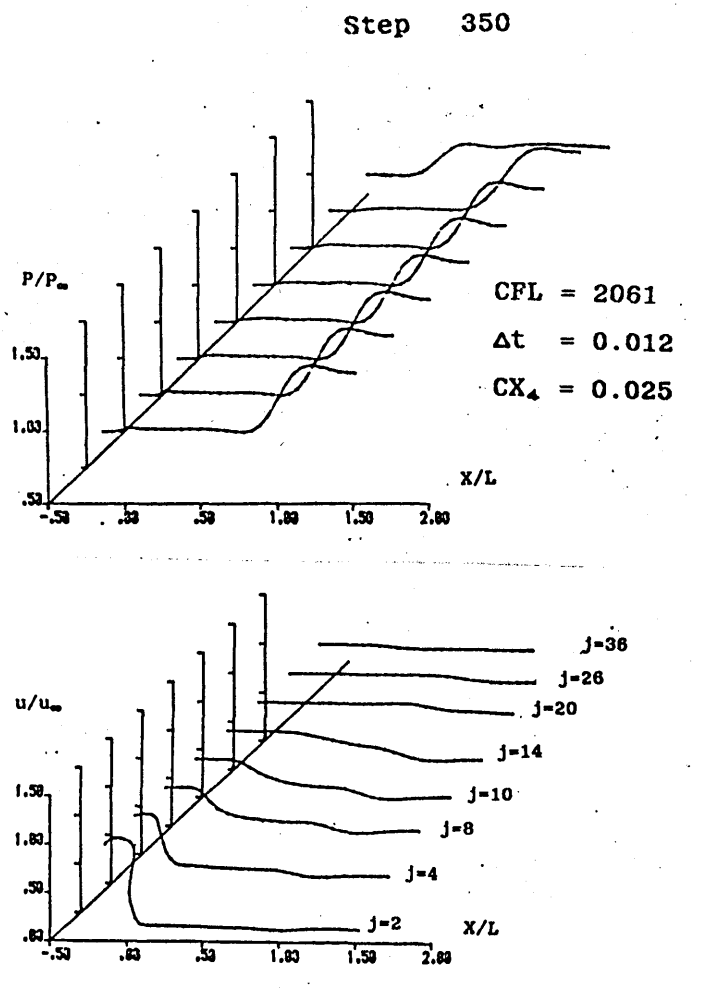

Figure A - 5 - 11 Test 11 (B_1 A_4 S F)

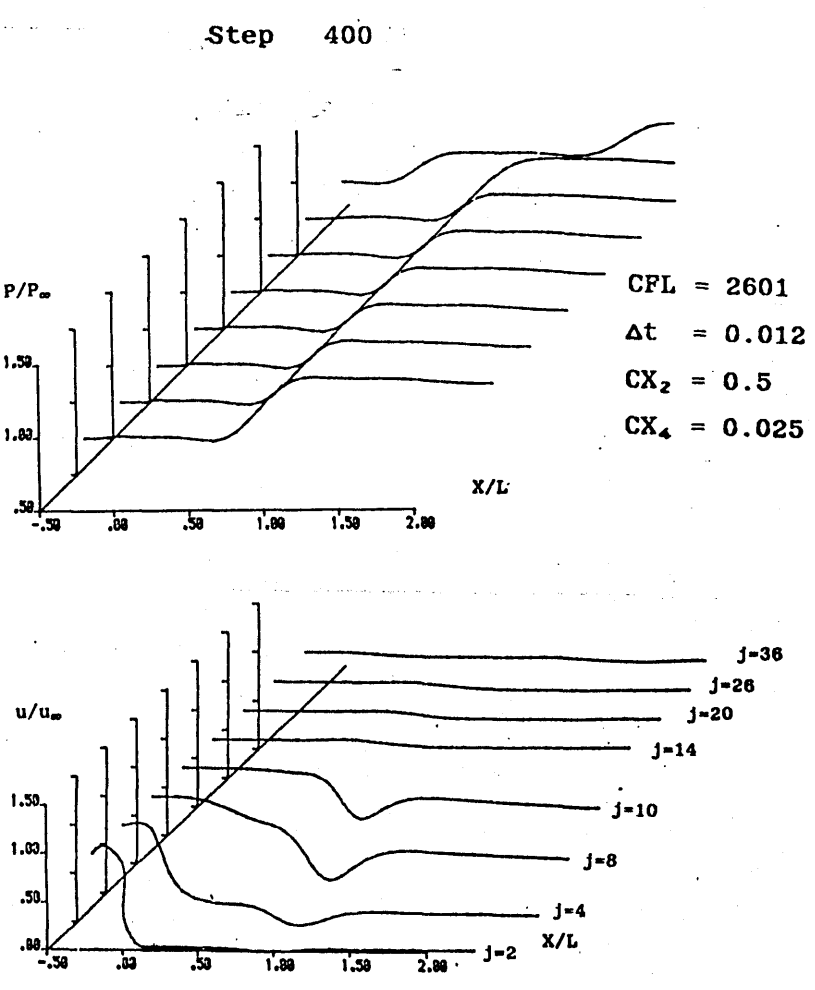

Figure A - 5 - 12 Test 12(B_1 A_4 S F)